Compression Mode Characterizations of Magnetorheological Elastomers

Hossein Vatandoost

A Thesis
in the Department of
Mechanical, Industrial, and Aerospace Engineering

Presented in Partial Fulfilment of the Requirements
for the Degree of

Doctor of Philosophy (Mechanical Engineering) at

Concordia University
Montreal, Quebec, Canada

July 2020

CONCORDIA UNIVERSITY

SCHOOL OF GRADUATE STUDIES

This is to certify that the thesis prepared

By: Hossein Vatandoost

Entitled: Compression Mode Characterizations of Magnetorheological Elastomers

and submitted in partial fulfillment of the requirements for the degree of

Doctor Of Philosophy (Mechanical, Industrial, and Aerospace Engineering)

complies with the regulations of the University and meets the accepted standards with respect to originality and quality.

Signed by the final examining committee:

_____ Chair
Dr. Anjan Bhowmick

_____ External Examiner
Dr. Jean-Sébastien Plante

_____ External to Program
Dr. Ali Nazemi

_____ Examiner
Dr. Muthukumaran Packirisamy

_____ Examiner
Dr. Ayhan Ince

_____ Thesis Co-Supervisor
Dr. Ramin Sedaghati

_____ Thesis Co-Supervisor
Dr. Subhash Rakheja

Approved by _____
Dr. Ivan Contreras, Graduate Program Director

September 17, 2020

_____

Dr. Mourad Debbabi, Dean
Gina Cody School of Engineering and Computer Science

ABSTRACT

Compression Mode Characterizations of Magnetorheological Elastomers

Hossein Vatandoost, Ph.D.
Concordia University, 2020.

Magnetorheological (MR) elastomers (MREs) with controllable stiffness and damping properties offer significant potential for fail-safe semi-active and active control of vibration in many engineering applications. While the properties of MREs in the shear mode have been widely characterized, the compression mode properties of the MREs have been addressed in fewer studies. Unlike the shear mode, the compression mode characterization necessitates compensation for the magnetic force developed by the electromagnet in order to extract viscoelastic force from the measured force. In this dissertation research, a systematic methodology and a mathematical model are developed for compensating for the magnetic force for extracting the viscoelastic component of the force attributed to compression mode viscoelasticity of the MRE. For this purpose, an optimal design of a UI-shaped electromagnet was realized with minimum mass and magnetic flux density up to 1 Tesla. An experiment was designed to apply magnetic field in the direction of mechanical loading and to facilitate measurement of magneto-mechanical force. Results revealed peak errors in equivalent stiffness and damping constants of the MRE in the orders of 90% and 163%, respectively, in the absence of magnetic force compensation. The proposed compensation methodology provided a framework for accurate compression mode characterizations of the MREs as functions of the volume fraction and anisotropy of iron particles, and shape factor apart from the magnetic flux density, pre-strain and strain amplitude and strain rate excitations.

MREs typically experience large static pre-strain in many applications in order to support the machine/structure weight, which can alter the distances among the magnetizable particles and thus the MR effect. The dynamic compression mode properties of isotropic and anisotropic MREs with 30% volume fraction of iron-particles and nominal shape factor (SF) of 0.56 were experimentally characterized under broad ranges of strain amplitude (2.5–20%) superimposed on a large static pre-strain of 21%, excitation frequency (0.1–50 Hz) and magnetic flux density (0–750 mT). Subsequently, the experiments were designed to evaluate the effects of the shape factor (SF), pre-strain and particle volume fraction (PVF) on compression mode properties of the isotropic and anisotropic MREs under broad ranges of excitations and magnetic flux density. The measured data

were analyzed to evaluate compression mode properties in terms of stress-strain characteristics, relative MR effect, equivalent stiffness, equivalent damping, and elastic and loss moduli as functions of the design factors (pre-strain, PVF, SF and anisotropy) and operating factors (strain amplitude, strain rate and the magnetic flux density). The results invariably, revealed hysteretic stress-strain characteristics with strongly nonlinear and coupled dependence on the various design and operating factors. Among the design factors considered, the PVF revealed greatest effects on the stiffening and dampening behaviors of the MREs. Increasing the SF and PVF generally resulted in substantially higher MR effect in view of the elastic modulus of the MREs. The relative MR effect, however, decreased with increase in the pre-strain.

The influences of various design and operating factors on the compression mode properties of are thoroughly analyzed and discussed, which would serve as design guidance for the MREs in different engineering applications. Phenomenological models with only a few unknown parameters were further formulated to predict the SF-, pre-strain-, and PVF-dependent compression elastic and loss moduli of both types of MREs. The effectiveness of the models is demonstrated by comparing the model-predicted properties with the measured data over broad ranges of design and operating conditions.

Dedication

This Ph.D. dissertation is dedicated to my beloved parents and brother

for their endless love, support, and encouragement.

Acknowledgment

Firstly, I would also like to express my deepest sense of gratitude to my co-supervisors, Prof. Ramin Sedaghati and Prof. Subhash Rakheja for providing such an unparalleled opportunity for me to be a part of their research group, and for their patience, motivation, crucial guidance, support, and immense knowledge. This thesis would have not been possible without their continuous support and encouragement. Their guidance and critiques have helped me to do more in-depth research, write a better research article, and showed me how I could improve my work.

I would like to thank Dr. Masoud Hemmatian for his valuable comments, participation, and assistance during the experimental stages of this work. I gratefully acknowledge Mr. Alex Macpherson, Mr. Robert Oliver, Mr. Gilles Huard, and Mr. Jose Esteves from MIAE, for their assistance with instrumentation of the experiments. Financial support from the Natural Sciences and Engineering Research Council of Canada is also gratefully acknowledged.

I sincerely acknowledge the truthful advice and enriching discussions from Prof. Faramarz Gordaninejad and Prof. Norman Wereley. I would like to thank my former advisor, Dr. Masoud Sajjadi, for introducing me to the field of smart materials, and for his every guidance since 2012. I would like to thank Dr. Hamid Taghavifar, for his support, mentorship, and taking time out of his busy schedule to help me with everything.

I would like to acknowledge all the administrative staff in MIAE, especially the graduate program coordinator, Leslie Hosein, for all her assistance with the administrative matters. A very heartfelt thank you to all my labmates and friends for their support and friendship. Last but certainly not least, I would like to extend my thanks and appreciation to my parents and my brother, Ashkan, for their continued love, support, and encouragement throughout this very exciting Ph.D. journey.

Table of Contents

List of Figures..... x

List of Tables..... xv

Nomenclature..... xvi

INTRODUCTION AND SCOPE OF THE THESIS 1

1.1 Literature review 2
1.2 Motivations and Objectives 7
1.3 Organization of the Dissertation 8

MAGNETIC FORCE COMPENSATION OF AN OPTIMALLY DESIGNED ELECTROMAGNET 13

2.1 Introduction 13
2.2 Design of a UI-shaped electromagnet 15
2.2.1 Design specifications and constraints 18
2.2.2 Design Optimization 18
2.3 Experimental methods 20
2.3.1 Static magnetic force and flux measurements 20
2.3.2 Dynamic magnetic force measurements 23
2.3.3 Compression mode characterization of MRE 24
2.4 Compensation for the magnetic force 25
2.4.1 Estimation of static magnetic force 25
2.4.2 Estimations of dynamic magnetic force characteristics 28
2.5 Conclusions 35

DYNAMIC COMPRESSION MODE CHARACTERIZATION 36

3.1 Introduction 36
3.2 Experimental Methods 37
3.2.1 MRE Samples 37
3.2.2 Electromagnet design 38
3.2.3 Experimental setup and methods 38
3.3 Results and discussion 42
3.3.1 Strain amplitude effect 43
3.3.2 Magnetic field effect 47

3.3.3 Strain-rate effect 49
3.3.4 Storage modulus and loss factor 51
3.4 Conclusion 59

SHAPE FACTOR EFFECTS 61

4.1 Introduction 61
4.2 Experimental setup and methods 62
4.2.1 MRE samples 62
4.2.2 Test setup and methods 63
4.2.3 Data analysis 64
4.3 Compression mode stress-strain characteristics 66
4.3.1 Effect of shape factor on stress-strain characteristics 66
4.3.2 Effect of shape factor on the compression moduli and loss factor 71
4.3.3 Influence of shape factor on the relative MR effect 78
4.4 Model development for predicting the compression moduli 81
4.5 Conclusion 86

PRE-STRAIN EFFECTS 88

5.1 Introduction 88
5.2 Experimental Methods 89
5.2.1 MRE samples 89
5.2.2 Test rig 91
5.2.3 Data analysis 94
5.3 Experimental Results 96
5.3.1 Effect of pre-strain on stress-strain characteristics 96
5.3.2 Effect of pre-strain on the compression moduli and loss factor 103
5.3.3 Influence of pre-strain on the relative MR effect 108
5.4 Model Development 112
5.4.1 The compression elastic and loss moduli 112
5.4.2 Stress-strain hysteresis characteristics 117
5.5 Conclusion 120

VOLUME FRACTION EFFECTS 122

6.1 Introduction 122
6.2 Experimental setup and methods 124

6.2.1 MRE samples 124
6.2.2 Experimental test setup 125
6.2.3 Data analysis 127
6.3 Results and discussions 129
6.3.1 Effects of particles volume fraction on stress-strain properties 129
6.3.2 Effects of particle volume fraction on the compression moduli 134
6.3.3 Influence of particle volume fraction on the relative MR effect 138
6.4 Model development for predicting the compression moduli 142
6.5 Conclusion 147

CONCLUSIONS AND RECOMMENDATIONS 149

7.1 Major contributions 149
7.2 Major Conclusions 150
7.3 Recommendations for future works 153

REFERENCES 155

APPENDIX A 163

APPENDIX B 167

LIST OF FIGURES

Figure 2.1 UI-shaped electromagnet: (a) schematic, (b) 3D view, (c) leakage and fringing flux permeance paths, and (d) EMC model. 16

Figure 2.2 Dependency of the magnetic flux density within air gap of an optimal solution on the total mass and working time. 20

Figure 2.3 Schematic illustration of the experimental set up for measurements of air gap flux density and total force in the compression mode (a); placement of rubber samples (or MRE) in the air gap with the Gauss probe (b). 21

Figure 2.4 Variations in (a) air gap magnetic flux density, and (b) magnetic force as functions of coil current and gap length, (c) correlation between air gap magnetic force and flux density, and (d) variations in the magnetic flux density measured within the isotropic MRE as functions of gap length and applied current. 22

Figure 2.5 Variations in magnetic force under 0.4 mm amplitude harmonic displacement at 1 Hz (flux density= 450 mT). 23

Figure 2.6 FEMM simulation model of the electromagnet (a), magnetic flux density distribution under 3 A current and gap length of 8 mm (b), and distribution of magnetic flux density in the air gap (c). 27

Figure 2.7 Comparisons of the magnetic flux density (a, b) and the magnetic force (c, d) predicted from the analytical, phenomenological and finite element models with the measured data for two different gap lengths ($lg = 5$ and 8 mm). 28

Figure 2.8 Comparison of static and dynamic magnetic force at frequency of 1 Hz and displacement amplitude of 0.8 mm: (a) B=300 mT; and (b) B=600 mT. 29

Figure 2.9 Effects of frequency (left column) and magnetic flux density (right column) on the magnitude ratio M and phase lag ϕ under displacement amplitudes of 0.8 mm and 1.6 mm. 30

Figure 2.10 Comparisons of time-histories (left-column) and magnetic force-displacement characteristics (right-column) obtained from the phenomenological models with the measured data for lg= 1.6 mm, Bg= 600 mT, and: (a) f= 0.1 Hz; (b) f= 1 Hz; and (c) f= 10 Hz. 33

Figure 2.11 Measured force-displacement characteristics of MRE (a), Dynamic magnetic force-displacement characteristics obtained from the model (b) and Viscoelastic (compensated) force displacement characteristics of MRE (0.8 mm excitation at 1 Hz, and magnetic flux density of 450 mT) (c). 35

Figure 3.1 Schematic of the UI-shaped electromagnet with upper and lower mounts and MRE specimens. 38

Figure 3.2 Pictorial views of electromagnet with upper and lower mounts, and MRE specimens in the gaps (a), and uniaxial compression test setup (b). 39

Figure 3.3 Influence of gap length and coil current on the air gap magnetic flux density: (a, b) without MRE specimens; (c) with isotropic MRE specimens; and (d) with anisotropic MRE specimen. 40

Figure 3.4 Effect of strain amplitude on the stress-strain characteristics of MREs at different excitation frequencies (a) isotropic, 0.1 Hz; (b) isotropic, 1 Hz; (c) anisotropic, 0.1 Hz; (d) anisotropic, 1 Hz (magnetic flux density, B=0). 44

Figure 3.5 Effect of strain amplitude on the stress-strain characteristics of MREs at different excitation frequencies (a) isotropic, 0.1 Hz; (b) isotropic, 1 Hz; (c) anisotropic, 0.1 Hz; (d) anisotropic, 1 Hz (magnetic flux density, *B*=750 mT). 45

Figure 3.6 Effect of anisotropy on the stress-strain characteristics of the MRE under different strain amplitudes (ε) at a frequency of 1 Hz in the absence of magnetic field: (a) ε=2.5%; (b) ε=10%. 46

Figure 3.7 Effect of anisotropy on the stress-strain characteristics of the MREs under different strain amplitudes (ε) at a frequency of 1 Hz and magnetic flux density of 750 mT: (a) ε=10%; (b) ε=20%. 47

Figure 3.8 Effect of magnetic flux density on the stress-strain characteristics of the MREs under different strain amplitude excitations (a) isotropic, f=1 Hz, ε=5%; (b) isotropic, *f*=20 Hz, ε=10%; (c) anisotropic, *f*=1 Hz, ε=5%; (d) anisotropic, *f*=20 Hz, ε=10%. 48

Figure 3.9 Effect of anisotropy on the stress-strain characteristics of MREs subject to 5% strain and different magnetic flux density: (a) B = 300 mT; and (b) B = 600 mT (f = 10Hz). 49

Figure 3.10 Effect of loading frequency on the stress-*strain* characteristics of MREs under strain amplitude of 10%: (a) isotropic, B = 300 mT; (b) isotropic, B = 750 mT; (c) anisotropic, B = 300 mT; (d) anisotropic, B = 750 mT. 50

Figure 3.11 Effect of anisotropy on the stress-strain characteristics of MREs subject to 300 mT magnetic flux density and 5% strain at different frequencies: (a) f= 1 Hz; and (b) f= 30 Hz. 51

Figure 3.12 Effects of (a) strain amplitude ε (B = 300 mT; f = 1 Hz); (b) frequency f (B = 750 mT; ε = 2.5%); and (c) magnetic flux density B (f= 0.1 Hz; ε = 5%) on the storage modulus and loss factor of the isotropic and anisotropic MREs. 52

Figure 3.13 Relative MR effect in view of storage moduli ($RMRSB$) of the isotropic (left column) and anisotropic (right column) MREs subject to magnetic flux density of: (a) 300 mT; (b) 450 mT; and (c) 750 mT. 55

Figure 3.14 Relative MR effect in view of loss factor ($RMRLB$) of the isotropic (left column) and anisotropic (right column) MREs subject to magnetic flux density of: (a) 300 mT; (b) 450 mT; and (c) 750 mT. 57

Figure 4.1 Schematic of the test setup for compression mode characterization of the MRE. 63

Figure 4.2 Effect of shape factor on stress-strain characteristics of isotropic (left column) and anisotropic (right column) MREs under two different strain amplitudes: (a) 5%; and (b) 10% (B=0; f=0.1 Hz). 67

Figure 4.3 Effect of shape factor on stress-strain characteristics of isotropic (left column) and anisotropic (right column) MREs under different strain amplitudes: (a) 5%; and (b) 10% (B=450 mT; f=0.1 Hz). 68

Figure 4.4 Effect of shape factor on stress-strain characteristics of the isotropic (left column) and anisotropic (right column) MREs under higher magnetic flux density (B=750 mT) and 10% strain amplitude at 0.1 Hz. 69

Figure 4.5 Effect of shape factor on stress-strain characteristics of isotropic (left column) and anisotropic (right column) MREs subject to %5 peak strain at different frequencies: (a) f= 1 Hz, (b) f= 10 Hz. (B=300 mT). 70

Figure 4.6 Effect of shape factor on the compression mode elastic modulus (a), loss modulus (b) and loss factor (c) of the isotropic (left column) and anisotropic (right column) MREs for different strain amplitudes (f=1 Hz, and B=450 mT). 72

Figure 4.7 Effect of shape factor on the compression mode elastic modulus (a), loss modulus (b) and loss factor (c) of the isotropic (left column) and anisotropic (right column) MREs under different excitation frequencies (strain amplitude=5%, and B=600 mT). 74

Figure 4.8 Effect of shape factor on the compression mode elastic modulus (a), loss modulus (b) and loss factor (c) of isotropic and anisotropic MREs under different levels of magnetic flux density (strain amplitude =2.5%, f=1 Hz). 76

Figure 4.9 Dependency of relative MR effect in view of elastic modulus (a) and loss factor (b) on the shape factor of the isotropic (left column) and anisotropic (right column) MREs under different strain amplitudes (B= 600 mT; f=1 Hz). 79

Figure 4.10 Dependency of relative MR effect on shape factor of the isotropic and anisotropic MREs at magnetic flux density of 600 mT under strain amplitude 10%: compression elastic modulus (a) and loss factor (b). 80

Figure 4.11 Effects of SF, magnetic flux density, frequency and strain on the compression elastic modulus of the isotropic and anisotropic MREs. 82

Figure 4.12 Comparisons of the SF-dependent compression elastic modulus predicted from the proposed model with those derived from the Payne's model [60] and the measured data for the isotropic (left column) and anisotropic (right column) MREs subject to 5% strain at 1 Hz: (a) $B = 0\ mT$ and (b) $B = 450\ mT$. 85

Figure 4.13 Comparisons of the SF-dependent loss modulus predicted from the proposed model with those derived from the Payne's model [99] and the measured data for the isotropic (left column) and anisotropic (right column) MREs subject to 2.5% strain at 10 Hz: (a) $B = 0\ mT$ and (b) $B = 150\ mT$. 86

Figure 5.1 Pictorial illustration of the test setup for compression mode characterization of the MRE. 90

Figure 5.2 The effect of pre-strain on the strain-stress characteristics of the isotropic (left column) and anisotropic (right column) MREs with different particle volume fractions: (a) 15%, (b) 30%, and (c) 45% (ε= 2.5%, f= 1 Hz, and B= 0 mT). 98

Figure 5.3 The effect of pre-strain on the strain-stress characteristics of the isotropic (left column) and anisotropic (right column) MREs with different particle volume fractions: (a) 15%, (b) 30%, and (c) 45% (ε=2.5%, f= 1 Hz, and B= 450 mT). 100

Figure 5.4 Effect of pre-strain on stress-strain characteristics of the isotropic (left column) and anisotropic (right column) MREs with 30% volume fraction under magnetic flux density of 300 mT subject to %2.5 peak strain at different frequencies: (a) f= 1 Hz, (b) f= 10 Hz. 102

Figure 5.5 Effect of pre-strain on the compression mod e elastic modulus (a), and loss modulus (b) of the isotropic (left column) and anisotropic (right column) MREs with volume fraction of 30% under different excitation frequencies (ε=2.5%, and B=150 mT). 105

Figure 5.6 Effect of pre-strain on the compression mode elastic modulus (a),and loss modulus (b) of isotropic (left column) and anisotropic (right column) MREs with volume fraction of 30% under different levels of magnetic flux density (ε=2.5%, f=1 Hz). 107

Figure 5.7 The effects of the pre-strain on the relative MR effect in view of elastic (a) and loss factor (b) of the isotropic (left column) and anisotropic (right column) MREs with 30% volume fraction under different excitation frequencies (ε=2.5%, and B= 600 mT). 110

Figure 5.8 Comparisons of the pre-strain dependent compression elastic (a) and loss moduli (b) predicted from the proposed model with the measured data for the isotropic (left column) and anisotropic (right column) MREs with different volume fractions (ε=2.5%, f=1 Hz, B=300 mT). 116

Figure 5.9 Comparisons of the pre-strain dependent compression elastic (a) and loss moduli (b) predicted from the proposed model with the measured data for the isotropic (left column) and anisotropic (right column) MREs with different volume fractions (ε=2.5%, f=10 Hz, B=450 mT). 117

Figure 5.10 Nonlinear viscoelastic model for MREs. 118

Figure 5.11 Comparisons of the stress-strain hysteresis characteristics predicted from the proposed model with the measured data for the isotropic (a, c, and d), anisotropic (b) MREs subject to different level of pre-strain and excitation conditions. 119

Figure 6.1 Schematic (a) and pictorial (b) illustrations of test setup for characterization of compression mode properties of MREs [9]. 126

Figure 6.2 Effect of particle volume fraction on stress-strain characteristics of isotropic (left column) and anisotropic (right column) MREs under two different strain amplitudes: (a) ε= 2.5%; and (b) ε = 10% (B=0; f=1 Hz). 130

Figure 6.3 Effect of particle volume fraction on stress-strain characteristics of isotropic (left column) and anisotropic (right column) MREs under two different strain amplitudes: (a) ε= 2.5%; and (b) ε= 10% (B=600 mT; f=1 Hz). 131

Figure 6.4 Effect of volume fraction on stress-strain characteristics of isotropic (left column) and anisotropic (right column) MREs subject to 10% peak strain at different frequencies: (a) f= 1 Hz, (b) f= 10 Hz. (B=150 mT). 133

Figure 6.5 Effect of volume fraction on the compression mode elastic modulus (a), and loss modulus (b) of the isotropic (left column) and anisotropic (right column) MREs for different strain amplitudes (f=1 Hz, and B=300 mT). 135

Figure 6.6 Effect of volume fraction on the compression mode elastic modulus (a), and loss modulus (b) of the isotropic (left column) and anisotropic (right column) MREs under different excitation frequencies (ε=10%, and B=600 mT). 136

Figure 6.7 Effect of volume fraction on the compression mode elastic modulus (a), and loss modulus (b) of isotropic and anisotropic MREs under different levels of magnetic flux density (strain amplitude =2.5%, f=1 Hz). 137

Figure 6.8 Dependency of relative MR effect in view of elastic modulus on the volume fraction of the isotropic (left column) and anisotropic (right column) MREs under different strain amplitudes when B was increased from 0 to 600 mT: (a) f=1 Hz, (b) f=10 Hz, and (c) f=30 Hz). 139

Figure 6.9 Comparisons of the volume fraction dependent compression elastic (a) and loss (b) moduli of the isotropic (left column) and anisotropic (right column) MREs predicted from the proposed model with the measured data under magnetic flux density of 450 mT and loading condition of ε= 5%, and f= 10 Hz. 145

Figure 6.10 Dependency of relative MR effect in view of loss modulus on the volume fraction of the isotropic (left column) and anisotropic (right column) MREs under different strain amplitudes when B was increased from 0 to 750 mT: (a) f=1 Hz, (b) f=10 Hz. 141

Figure 6.11 Comparisons of the volume fraction dependent compression elastic moduli of the isotropic (left column) and anisotropic (right column) MREs predicted from the proposed model with the measured data under (a) B=450 mT, f=1 Hz, ε=5%, and (b) B=750 mT, f=10 Hz, ε=5%. 145

Figure 6.12 Comparisons of the volume fraction dependent compression elastic moduli of the isotropic (left column) and anisotropic (right column) MREs predicted from the proposed model with the measured data under (a) B=450 mT, f=1 Hz, ε=5%, and (b) B=750 mT, f=10 Hz, ε=5% 146

LIST OF TABLES

Table 2.1	Identified coefficients of the magnetic force and flux models.	26
Table 2.2	Identified parameters of proposed relations for predicting the magnitude ratio M and phase lag ϕ.	31
Table 4.1	Identified coefficients of the proposed phenomenological model for predicting the elastic and loss moduli of the isotropic and anisotropic MREs.	84
Table 5.1	Identified coefficients of the proposed model for estimating the elastic modulus of both kinds of MREs	115
Table 5.2	Identified coefficients of the proposed model for estimating the loss modulus of both kinds of MREs	115
Table 6.1	Identified coefficients of the presented simple phenomenological model for estimating the elastic and loss moduli of the isotropic and anisotropic MREs.	144

NOMENCLATURE

A	Cross section area of the core (m^2)	PVF	Particle volume fraction
a	Height of I-shaped core (mm)	$\mathcal{P}$	Permeance ($WbA^{-1}T^{-1}$)
A_c	Surface area of winding (mm^2)	$RSF_{\acute{E}}$	Relative SF effect in view of the elastic modulus
A_g	Cross-section area of the air gap (mm^2)	RSF_{η}	Relative SF effect in view of the loss factor
B_g	Air gap magnetic flux density (Tesla)	$RMRS_B$	Relative MR effect in view of storage modulus
B_{St}	Saturation magnetic flux density (Tesla)	$RMRL_B$	Relative MR effect in view of loss factor
B	Magnetic flux density (Tesla)	r	Radius of cylindrical MRE sample
C_{eq}	Equivalent damping (Nsm^{-1})	$\mathcal{R}$	Reluctance ($Wb^{-1}AT$)
d	Bare conductor diameter (mm)	$\mathcal{R}_{bf}$	Reluctance of back-side fringing flux ($Wb^{-1}AT$)
D	Diameter of MRE sample	$\mathcal{R}_{ff}$	Reluctance of front-side fringing flux ($Wb^{-1}AT$)
E	Compression modulus	$\mathcal{R}_g$	Air gap reluctance ($Wb^{-1}AT$)
E_c	Effective compression modulus	$\mathcal{R}_I$	Core reluctances between nodes 3-1 ($Wb^{-1}AT$)
E'	Compression elastic modulus	$\mathcal{R}_{lf}$	Reluctance of left-side fringing flux ($Wb^{-1}AT$)
E''	Compression loss modulus	$\mathcal{R}_{rg}$	Reluctance of right-side fringing flux ($Wb^{-1}AT$)
E_0	Young's modulus of unfilled rubbers	$\mathcal{R}_{tf}$	Reluctance of total fringing flux ($Wb^{-1}AT$)
E^*	Complex compression modulus	$\mathcal{R}_{tg}$	Total gap reluctance ($Wb^{-1}AT$)
E_m	Measured compression or loss modulus	$\mathcal{R}_{U_1}$	Core reluctances between nodes 1-2 ($Wb^{-1}AT$)
$E^{\varepsilon_{p_{min}}}$	Elastic moduli corresponding to the minimum pre-strain	$\mathcal{R}_{U_2}$	Core reluctances between nodes 2-3 ($Wb^{-1}AT$)
$E^{\varepsilon_{p_{max}}}$	Elastic moduli corresponding to the maximum pre-strain	SF	Shape factor
$E'_{SF_{max}}$	Elastic moduli corresponding to the minimum shape factor	W_D	Energy dissipation per cycle (Nm)
$E'_{SF_{min}}$	Elastic moduli corresponding to the maximum shape factor	WT	Continuous working time (s)
f	Frequency (Hz)	WT_a	allowable working time (s)
F_g	Magnetic force in absence of MRE in the gap (N)	X_1	Width of lower winding of U-shaped core (mm)
F_g^M	Magnetic force in presence of MRE in the gap (N)	X_2	Width of upper winding of I-shaped core (mm)
F_I	I- core magnetomotive force (AT)	Y_1	Height of lower winding of U- core (mm)
F_{MRE}	Field-dependent viscoelastic force of MRE (N)	Y_2	Height of upper winding of I- core (mm)
F_T	Total load cell force (N)	Y_c	U-shaped core leg length (mm)
F_U	U-shaped core magnetomotive force (A.T)	ε	Strain (displacement) amplitude % (mm)

h_c	Natural convection heat transfer coefficient (Wm-2K-1)	ε^*	Complex strain
h	Height of MRE sample	ε_p	Pre-strain (%)
I	Current (A)	ε_x	Horizontal clearance (mm)
J	Cost function	ε_y	Vertical clearance (mm)
K_{ai}	Air and conductor insulation factor	ϕ	Phase between static and dynamic magnetic forces (Rad)
K_b	Bobbin factor	ϕ_g	Magnetic flux in the air gap (Wb)
K_{ed}	Edge factor	φ	Particle volume fraction
K_{eq}	Equivalent stiffness (Nm^{-1})	ρ_c	Mass density of the conductor (kgm^{-3})
K_s	Lamination stacking factor	ρ_{mc}	Mass density of core (kgm^{-3})
K_{wu}	Window utilization factor	μ_0	Magnetic permeability of vacuum (Hm^{-1})
l_c	Total core length (mm)	μ_r	Relative magnetic permeability of core
l_g	Gap length (mm)	θ_∞	Ambient temperature (°K)
$\bar{l_g}$	Variation in the gap length (mm)	θ_{max}	Maximum allowable temperature (°K)
l_0	Static gap length (mm)	θ_{ss}	Steady-state winding temperature (°K)
l_{tw}	Total conductor length (mm)	η	Loss factor
M	Ratio of static and dynamic magnetic force amplitudes	$\eta_{SF_{min}}$	Loss factor corresponding to the minimum shape factor
MMF	Magnetomotive force (AT)	$\eta_{SF_{max}}$	Loss factor corresponding to the maximum shape factor
M_T	Total electromagnet mass (Kg)	β	Shape coefficient
MR_η	Relative MR effect in view of loss factor	σ_{MRE}	Compression output stress of MRE
$MR_{\acute{E}}$	Relative MR effect in view of compression elastic modulus	σ^*	Complex output stress
N_I	Number of turns of I- core winding	δ	Loss angle
N_U	Number of turns of two windings of the U- core	ζ	Viscosity

CHAPTER 1

INTRODUCTION AND SCOPE OF THE THESIS

Magnetorheological elastomers (MREs) are a class of "smart materials" that exhibit controllable mechanical properties in response to an external magnetic field. The "smart material" terminology appeared in the 20th century, which referred to a class of materials that can adjust their properties in a controllable manner with an external stimulus such as deformation, temperature, moisture, electrical and magnetic field. The piezo-electric materials are, indeed, the most widely-known smart materials, which cause mechanical stress in response to an electrical field, and vice-versa. Magnetorheological (MR) materials have emerged as a smart material during the past few decades, which exhibit considerable and reversible variations in their mechanical properties in response to an externally applied magnetic field. MR elastomers (MREs) and MR fluids (MRFs) are the two main MR materials that can be easily fabricated by embedding micron size magnetizable particles into a solid- and fluid-like host matrix, respectively.

Although the MR material was firstly introduced by Jacob Rabinow in 1948, the developments in MR fluids and MR elastomers for varied engineering applications have emerged only during the past few decades [1]. Both the MR fluids and MREs exhibit rapid response time in the order of a few milliseconds, while the response time of MREs is generally lower than their fluid counterparts [2]. In contrast to the MR fluids, which generally provide controllable damping, MREs can significantly change both the stiffness and damping properties under application of an external magnetic field. Moreover, the performance of MR fluids is known to deteriorate due to sedimentation of iron particles, environmental contamination and leakage, which are not of concern in case of MREs.

Owing to their rapid response, simple fabrication process, and controllable and reversible mechanical properties, MREs offer meritorious potentials for many engineering applications, particularly in developing adjustable vibration isolators [3] and adaptive vibration absorbers [4]. In order to gain better understanding of their performance potentials and to seek guidance on their fabrication and design for diverse applications, mechanical properties of MREs have been widely characterized in recent years in different operational modes, namely, shear, compression, and combined shear and compression. The stress-strain characteristics of MREs in the shear [5] and

the compression [6] modes have been widely investigated experimentally considering widely different design configurations and excitation conditions. These have shown that shear and elastic moduli of MREs are related to many design factors in a highly complex manner, apart from the mechanical loading conditions and intensity of the magnetic field. It has been shown that the MREs exhibit greater MR effects in the compression mode compared to the shear mode. Despite this, the vast majority of the reported studies have been limited only to the shear mode characterizations. This is mostly attributed to two major design challenges. Firstly, unlike the shear mode, the compression mode characterizations necessitate application of the magnetic field in the direction of mechanical loading, which poses difficult design issues. Secondly, the force developed during compression of the MRE is generally dominated by magnetic force caused by the applied magnetic field, which makes it difficult to extract the viscoelastic force of the MRE.

This dissertation research is focused on a systematic methodology for characterizing compression mode properties of MREs through development of a magnetic force compensation strategy. The methodology is applied to obtain compression mode characteristics of MREs as functions of the primary design factors, namely, the volume fraction and anisotropy of iron particles within the matrix, shape factor and pre-strain coupled with broad variations in the operating or excitation conditions, namely, the strain amplitude and rate, and magnetic flux density. Phenomenological models are formulated to predict compression mode elastic and loss moduli of the MREs as functions of the design and operating factors.

1.1 Literature review

The reported studies related to the characterization of MREs are briefly discussed in this section to illustrate essential knowledge gaps and to formulate the scope of the dissertation research. The reported studies relevant to specific design factors are further summarized in the subsequent chapters.

The reported studies have generally focused on identifications of storage and loss moduli of MREs as functions of the magnetic field, strain amplitude and excitation frequency or the strain rate [7-9], although these have employed different experimental methods and MREs with different volume fractions of iron particles (PVF). These have, invariably, shown that the storage and loss moduli of MREs can be enhanced substantially by increasing the magnetic flux density, irrespective of the mode of deformation [10]. Gong et al. [11] reported nearly 60% increase in the

shear modulus of the isotropic MREs, when subjected to 1.0 T magnetic flux density. The effect of magnetic flux density on the properties of MRE is also expressed in terms of the MR effect, defined as the relative change in the MRE modulus under the application of the maximum available magnetic flux density with respect to that of the passive MRE [12, 13].

Although MREs can be employed in different deformation modes, the majority of the reported studies have focused on their properties in the shear mode, where the MR effect tends to subside under higher shear deformations due to increasing distance between the magnetic particles [14-16]. Relatively fewer studies have investigated the properties of MREs in the compression mode, even though MREs exhibit considerably higher MR effect during compression partly due to reduced particle distances [17-19]. Gordaninejad et al. [19] reported considerably higher MR effect in compression (99%) compared to that in the shear mode (68%). Furthermore, Kallio [6] investigated dynamic properties of unaligned and anisotropic MREs, and obtained MR effects of 39% and 60%, respectively, in the shear and compression modes. Besides, Lerner and Cunefare [4] developed MRE-based vibration absorbers that showed natural frequency shifts up to 507% and 470% in the compression and shear modes, respectively.

The limited efforts reported on characterizations of MREs in the compression mode may be partly due to complexities associated with the experimental setup. Unlike the shear mode, the compression mode measurements require applications of the mechanical loading and the magnetic field in the same direction, which poses a considerable design complexity for the laboratory fixtures. A few studies have attempted to circumvent this difficulty by employing permanent magnets [20-22], which do not permit controllable magnetic field. Although many electromagnets have been designed, including the air core [17, 23], the open path magnetic circuit [6, 24-26] and the closed path magnetic circuit [27, 28], to achieve controllable magnetic field. The size and weight of the electromagnet continues to be the primary challenge for compression mode characterizations of MREs.

Secondly, the compression mode characterization requires compression of the MRE specimen positioned within the gap between two magnetic poles. This causes variations in the magnetic field and thus the magnetic force attributed to pull between the two magnetic poles of the electromagnet. The force measured during the experiments is thus the sum of the magnetic force developed by the electromagnet and the viscoelastic force attributed to the MRE. The magnetic force may be

substantially higher compared to the viscoelastic force, especially under low deformations of the MRE and high magnetic field intensities. The compression mode characterizations thus involve compensation for the magnetic force, which is not of concern in the shear mode since the viscoelastic and magnetic forces occur in the orthogonal directions. In the reported studies, the contribution of the magnetic force has been either neglected [10, 17] or measured as a function of the air gap in the absence of the MRE specimen. The latter approach, however, can yield considerable errors in the induced magnetic force, since the presence of MRE within the air gap can significantly alter the magnetic flux density and thus the magnetic force due to magnetization of iron particles within the MRE [29, 30].

Considering reported studies that have addressed characterization of MRE in the compression mode, summarized in Tables A1 and A2, a comprehensive compression mode characterization of both isotropic and anisotropic MREs under relatively wide ranges of excitation frequency, strain amplitude, and magnetic flux density, superimposed on a relatively large static pre-strain, has not been investigated. However, in many applications involving compression of the MRE, the MRE will likely undergo large static strain due to weight of the supported structures. The MRE vibration isolators and absorbers are some example applications. The large static strain can considerably alter the MR effect due to decrease in the distance between the magnetizable particles. Despite its important significance, the dynamic compression characterization of MREs superimposed on large static pre-strain has not been reported, to the best of our knowledge. Furthermore, the reported studies have employed either isotropic or anisotropic MREs.

Additionally, the important design factors that can dramatically affect the MR effect or properties of MREs in the compression mode, are the MREs' shape factor (SF), level of pre-strain (or pre-load) imposed on the MRE prior to an input excitation, and particle volume fraction (PVF), apart from the size, geometry, anisotropy and spatial distribution of the magnetic particles. While the SF [31], pre-strain [32], and volume fraction [33, 34] effects on zero-field properties of an MRE are relatively similar to that of a passive filled-elastomer, the dynamic properties of the MRE may exhibit significant SF, pre-strain, and volume fraction effects in the presence of a magnetic field. Diguet [35] showed that increasing the SF from 0.35 to 1.2 resulted in nearly 300% increase in the axial force generated by the cylindrical MRE in the static regime. Kalina et al. [36] numerically investigated the effect of mechanical pre-load on deformation dependent properties

of MREs and they showed that the interaction of particles in wavy chains depending on the level of pre-load, is predominately responsible for magnetostriction strain. Kim et al. [37] showed that saturation magnetization of an isotropic MRE composites linearly increases from 229 to 915 mT, when volume fraction increased from 11% to 53%.

Despite the considerable importance of the SF, pre-strain, and volume fraction factors, reported studies have not experimentally investigated the effect of these factors on the compression mode properties of MREs under wide ranges of magnetic and mechanical loading conditions. The reported compression mode characterization of MRE together with the observed MR effect in each study are summarized in Tables A1 and A2, respectively, in Appendix A. From these tables, it is evident that only a few studies have considered the effects of shape factor (SF), although the objectives of the studies differed. These have shown somewhat contradictory findings on the SF effects. Schrittesser et al. [38] realized three different values of SF of the MRE by varying its thickness for the purpose of varying the gap between the permanent magnets and thereby the magnetic flux density. Gordaninejad et al. [17] investigated compression behavior of MREs under static condition considering four different SFs and concluded that compression modulus in the static regime is independent of the SF. Ubaidillah et al. [39] characterized the properties of MRE samples with three different SFs under 1 to 10% strain excitation at 1 Hz. Each MRE sample, however, contained different iron particle volume fraction. Sapouna [40] investigated the effect of SF on the zero-field dynamic stiffness and MR effect of an isotropic MRE under a low strain amplitude of 0.5% at a frequency of 5 Hz and concluded insignificant effect of the sample size and shape on the MR effect. Many other studies, however, have shown that the MR effect of MREs is strongly affected by sample dimensions even in the static regime [41-43].

Moreover, further examination of studies summarized in Tables A1 and A2 suggests that the vast majority of the studies have neither reported nor assessed the effect of pre-strain (or pre-stress) on dynamic behavior of the MREs. However, in many applications involving compression of the MRE such as vibration isolators and absorbers, the MRE will likely undergo comprehensive static strain due to weight of the supported structures. The static pre-strain can considerably alter the MR effect due to decrease in the distance between the magnetizable particles. Despite its important significance, only limited efforts are evident with regard to the effect of pre-strain on viscoelastic and hysteresis behavior of the MREs. Koo et al. [20], Martins et al. [44] and Vatandoost et al. [21]

have characterized properties of MREs under specified constant pre-strains of 5%, 6.5% and 0%, respectively. Lee et al. [26] characterized compression mode properties of an anisotropic MRE in the static regime and showed that lower level of pre-strain in the specimen resulted in relatively higher stress change upon application of the magnetic field of 300 mT. Sapouna [40] experimentally assessed the effect of pre-strain on dynamic behavior of MREs at a constant frequency of 5 Hz and obtained 50% and 30% increases in the storage and loss modulus of the anisotropic MRE, respectively, when the pre-strain was increased from 2% to 10%. The corresponding increases for the isotropic MRE were reported as 25% and 5%. The effects of pre-strain on the compression mode properties under broad ranges of dynamic deformations (strain amplitude and frequency) and higher levels of magnetic flux density have not been investigated.

The reported studies, summarized in Tables A1 and A2, also suggest that the important effects of particle volume fraction (PVF) on the mechanical properties of MRE have not been adequately studies with simultaneous variations in the loading conditions (strain amplitude, strain rate and magnetic flux density). These have investigated the PVF effects under either static regime [17, 26, 45] or at a constant excitation frequency [46], or under constant strain amplitude [47], and/or at relatively low levels of the magnetic flux density [23]. The study by Fuchs et al. [48] constitutes the only exception, which characterized MRE samples with different particle volume fractions while considering relatively wide ranges of excitation frequency, strain amplitude and magnetic flux density. The maximum volume fraction (or weight fraction) of magnetic particles, however, was limited to 24% (or 70% by weight). Although, the MREs with relatively higher PVF exhibit enhance relative and absolute MR effects in shear [5] and mixed shear-compression modes [49], the reported studies have been mostly limited to a maximum of 33% particle volume fraction. Furthermore, Lerner [50] stated that the MREs employed in vibration absorbers may fail under the weight of the absorber, when PVF is less than 30%. The MREs with relatively higher PVF were thus recommended for designing MRE-based adaptive vibration absorbers. The dynamic properties of MREs are, thus, expected to depend on the SF, pre-strain, and volume fraction while studies reporting experimental characterizations and analytical models of MREs generally neglect potential contributions of the SF, pre-strain and volume fraction. A better understanding and modeling of these effects are, hence, desired for optimally designing MRE-based devices.

1.2 Motivations and Objectives

The compression mode characterization of MREs have been, invariably, obtained using either permanent magnets [20-22] and bulky electromagnets [27, 28], which raise many concerns on practical applications of the MREs. Besides, the contribution of the magnetic force has been either neglected [10, 17] or measured as a function of the air gap in the absence of the MRE specimen. Both the approaches yield considerable errors in the stress-strain properties of the MREs in the compression mode [29, 30]. Development of a systematic methodology for identifying the viscoelastic force by compensating for the magnetic force is thus vital for accurate characterizations of compression mode properties of MREs. The review of relevant reported studies indicated only limited knowledge on the effects of the SF, pre-strain, and anisotropy and volume fraction of magnetic particles on the dynamic compression mode properties of the MREs. Building essential knowledge on the roles of important design and operation factors is vital for establishing design guidance for MREs in different applications.

The overall goal of this dissertation research was thus formulated to develop a systematic methodology for accurately characterizing compression mode properties of MREs, and facilitate the analyses of effects of essential design and operating factors. The specific goals of this research dissertation are summarized below:

a) Obtain an optimal design of a UI-shaped electromagnet and present a general systematic methodology for compensating for the magnetic force, and its applications to accurately characterize the viscoelastic force of the MRE;

b) Develop an experimental set up for compression mode characterizations of isotropic and anisotropic MREs with nominal shape factor of 0.56, and volume fraction of 30% under relatively large static pre-strain;

c) Investigate the effect of important design factors, namely, shape factor, pre-strain, and particle volume fraction on the dynamic compression properties of both types of MREs under broad ranges of loading conditions;

d) Formulate phenomenological models for estimating compression elastic and loss moduli of the MREs as function of the design factors and loading conditions.

1.3 Organization of the Dissertation

This manuscript-based dissertation has been compiled on the basis of requirements described in "Thesis Preparation and Thesis Examination Regulation" booklet of the School of graduate Studies at Concordia University. This dissertation research is organized in 7 chapters, which address the research goals mentioned above, including the Introduction and Literature Review chapter (Chapter 1) and the concluding chapter (Chapter 7). Chapter 2 describes the optimal design of the electromagnet and presents a systematic methodology for compensating for the magnetic force, and its applications for accurate characterizations of compression mode properties of MREs (goal *a*).

Chapter 3 presents the design of the experimental setup to characterize compression mode properties of isotropic and anisotropic MREs with constant particle volume fraction and shape factor superimposed on large static pre-strain (goal b). Chapter 3 also describes the measurement and data analyses methods used to characterize MREs, considering wide range of variations in operating factors, including strain amplitude, loading frequency, and magnetic flux density (goal *b*). The effects of essential design factors, namely, shape factor, pre-strain and particle volume fraction on dynamic compression mode properties of isotropic and anisotropic MREs are presented in Chapters 4 to 6, respectively, (goal *c*). These chapters also present the shape factor, pre-strain and particle volume fraction-dependent models of the MREs (goal *d*). The highlights of the manuscripts, presented in Chapters 2 to 6, are further summarized below:

Chapter 2 presents the following article accepted for publication in the *IEEE Transactions on Magnetics* subject to only minor revisions.

H. Vatandoost, S. Rakheja, R. Sedaghati, M. Hemmatian. "Compensation of Magnetic Force of an Electromagnet for Compression Mode Characterization of Magnetorheological Elastomers", IEEE Transactions on Magnetics, 2020.

This paper presents a general systematic methodology for compensating for the magnetic force by performing different series of magnetic force and flux measurements with the isotropic and anisotropic MREs. The paper describes the design and fabrication of an optimal UI-shaped

electromagnet to facilitate measurements of the force under controlled magnetic flux density of up to 1 T. Results revealed notable phase and magnitude differences between the measured static and dynamic magnetic forces. The observed differences were dependent on the magnetic flux density and the excitation frequency in a nonlinear manner. A compensation model was proposed to accurately predict the magnetic force for the entire ranges of flux density and excitation conditions considered in the study. The validity of the proposed model was illustrated using the measured data. The model was employed to identify viscoelastic force of an isotropic MRE. Results revealed peak errors in the equivalent stiffness and damping constants of the MRE in the orders of 90% and 163%, respectively, without the magnetic force compensation. The proposed methodology provided an efficient framework for accurate characterization of MREs in the compression mode.

Chapter 3 presents the following article published in the *Composites Journal, Part B*:

H. Vatandoost, M. Hemmatian, R. Sedaghati, S. Rakheja. "Dynamic Characterization of Isotropic and Anisotropic Magnetorheological Elastomers in the Oscillatory Squeeze Mode Superimposed on Large Static Pre-strain", Composites Part B: Engineering, 2020, 182:107648.

In this article, a methodology is presented for experimental characterizations of dynamic compression mode properties of isotropic and anisotropic MREs under broad ranges of excitation and magnetic flux density. The isotropic as well as anisotropic MREs samples with 30% volume fraction of iron-particles were fabricated in the laboratory. An experimental set-up integrating the electro-magnet was designed for characterizing compression mode properties of the isotropic and anisotropic MRE samples. The experiments were designed to obtain force-deflection (stress-strain) characteristics of the samples subject to pre-strain (21%) and compression under broad ranges of strain amplitude (2.5–20%), excitation frequency (0.1–50 Hz), and magnetic flux density (0–750 mT). The measured data were analyzed to evaluate samples' properties in terms of stress-strain characteristics, relative MR effect, storage moduli and loss factor as functions of the anisotropy, strain amplitude, strain rate and the magnetic flux density considering the correction for the magnetic force generated between the poles of the electromagnet. Results revealed maximum increases in the storage moduli of the isotropic and anisotropic MRE specimens of 340.47% and 206.47%, respectively, which occurred under the low strain amplitude of 2.5% at frequencies of 10 and 30 Hz. The measured data obtained for 20% strain revealed maximum changes in the loss factors of 188.32% and 216.24% for the isotropic and anisotropic MREs, respectively, which occurred under excitation frequency of 0.1 Hz. The observed broad changes

in the compression mode storage and loss moduli suggest unique potentials of MREs for vibration and noise control in load-bearing type applications.

Chapter 4 presents the following article that has been submitted to *Intelligent materials systems and structures, 2020:*

H. Vatandoost, M. Hemmatian, R. Sedaghati, S. Rakheja. "Effect of shape factor on compression mode dynamic properties of magnetorheological elastomers"

The effects of shape factor on compression mode dynamic characteristics of isotropic and anisotropic MREs are experimentally investigated. MRE samples with different shape factors (0.375, 0.56, and 0.75) were fabricated in the laboratory and an experimental set up was designed to facilitate measurements of their compression mode stress-strain behavior under different excitation and magnetic flux density. The results revealed strong and coupled dependence of stress-strain properties on the shape factor of the isotropic and anisotropic MREs. The isotropic and anisotropic MREs revealed maximum shape factor-stiffening effect of up to 77% and 111% for the compression elastic modulus, respectively, when shape factor was increased from 0.375 to 0.75. The maximum shape factor effects on the loss factor of both types of MREs were obtained as 120% and 49%, respectively. Results generally suggest nonlinear effects of the SF on both the off- and on-state MRE properties and increasing the SF can enhance the relative MR effect in terms of both the elastic modulus and the loss factor of both MREs. A simple shape factor-, strain-, frequency- and magnetic field-dependent phenomenological model was subsequently presented to estimate the compression mode elastic and loss moduli of both types of MREs. A reasonably good agreement was obtained between the model results and the experiment data for the ranges of shape factor and loading conditions considered. The results suggest that the shape factor constitutes an important consideration for designs of MRE-based devices, particularly when the size and weight are of concern.

Chapter 5 presents the following article that has been under review in *Polymer Testing Journal:*

H. Vatandoost, R. Sedaghati, S. Rakheja, M. Hemmatian. "Effect of pre-strain on compression mode dynamic properties of magnetorheological elastomers: Experiment and modeling",

The effects of pre-strain on compression mode dynamic characteristics of both isotropic and aligned magnetorheological elastomers (MREs) are experimentally investigated considering wide ranges of particle volume fraction (15%, 30%, and 45%), frequency (1 to 30 Hz), and magnetic

flux density (0 to 750 mT) under different levels of pre-strain (6%, 11%, and 21%). Results exhibited strong dependence of MRE behavior on the pre-strain, which was further coupled with the effects of the particle volume fraction and frequency, and the magnetic field. The elastic and loss moduli of isotropic MREs consistently increased in a nonlinear manner, when pre-strain increased from 6% to 21%, suggesting pre-strain stiffening and pre-strain dampening effects, respectively, while anisotropic MRE showed dissimilar trends depending on particle volume fraction. Results revealed higher pre-strain effects for isotropic MREs than anisotropic MREs. The relative MR effect in view of elastic modulus ($MR_{\acute{E}}$) for both types of MREs consistently decreased with increasing pre-strain, while in view of loss factor (MR_{η}) showed the same trend only for anisotropic MRE. MR_{η} of isotropic MRE generally showed maximum around 11% pre-strain. Results further revealed maximum $MR_{\acute{E}}$, up to 286%, 973% and 2258% for the isotropic MRE, respectively, with volume fraction of 15%, 30% and 45%, and obtained as 320%, 293%, and 386% for anisotropic MRE. Simple phenomenological models were subsequently proposed to predict the compressive moduli as well as stress-strain hysteresis characteristics of both types of MREs. A reasonably good agreement was observed between the models' results and the experiment data for the ranges of pre-strain, volume fraction, frequency, and magnetic flux density considered. The developed models can be effectively employed for the development and design of controllable MRE-based adaptive devices operating in compression mode.

Chapter 6 presents the following article that has been under review in *Magnetism and Magnetic Materials Journal*:

H. Vatandoost, S. Rakheja, R. Sedaghati. "Effect of volume fraction on compression mode dynamic properties of magnetorheological elastomers: Experiment and modeling"

The effects of iron particle volume fraction (PVF) on the dynamic compression mode properties of isotropic and anisotropic magnetorheological elastomers (MREs) are experimentally investigated considering wide ranges of excitation frequency (1 Hz to 30 Hz), strain amplitude (2.5% to 20%) and magnetic flux density (0 to 750 mT). MRE samples with three different PVFs (15%, 30% and 45%) were fabricated in the laboratory and a test rig was designed to measure their magneto-mechanical characteristics. The effect of PVF on the loss modulus, denoted as PVF-dampening was substantially higher compared to that on the elastic modulus, denoted as PVF-stiffening. Moreover, PVF effects on compression mode properties of the isotropic MRE were

greater compared to the anisotropic MRE, and showed coupled dependence on the excitation and magnetic field conditions. Results revealed that strain-rate stiffening of isotropic MRE increased with increasing PVF while slightly decreased for anisotropic MRE. Besides, strain-softening of both MREs increased with increasing PVF. Results were also suggesting of strong dependence of MR effect on the loading conditions, apart from the PVF. MR effect in view of elastic and loss moduli for isotropic MRE increased with increasing PVF from 15% to 45% at 1 Hz, but at higher frequency they become maximum around 30% PVF, regardless of strain amplitude. Both MR effects for anisotropic MRE, however, become minimum around 30% PVF, irrespective of frequency and strain amplitude. Owing to the observed coupled effects of the loading factors with the PVF, a simple phenomenological model was formulated considering independent functions in PVF, excitation frequency, strain amplitude and magnetic flux density for predicting compression elastic and loss moduli of both MREs. The proposed model required identifications of only six unknown constants, showed reasonably good agreements with the measured data.

CHAPTER 2

MAGNETIC FORCE COMPENSATION OF AN OPTIMALLY DESIGNED ELECTROMAGNET

2.1 Introduction

Considering numerous potential applications of MREs, substantial efforts have been made for characterizations of MREs in the recent years. The reported studies have generally focused on identifications of storage and loss moduli of MREs as functions of the magnetic field, strain amplitude and excitation frequency or the strain rate [7-9], although these have employed different experimental methods and MREs with different volume fractions of iron particles. Although MREs can be employed in different deformation modes, the majority of the reported studies have focused on their properties in the shear mode, where the MR effect tends to shrink under higher shear deformations due to increasing distance between the magnetic particles [14-16]. Relatively fewer studies have investigated the properties of MREs in the compression mode, even though MREs exhibit considerably higher MR effect during compression partly due to reduced particle distances [17-19].

The limited efforts reported on characterizations of MREs in the compression mode may be partly due to complexities associated with the experimental setup. Since, unlike the shear mode, the compression mode measurements require applications of the mechanical loading and the magnetic field in the same direction, which poses a considerable design complexity for the laboratory fixtures. Firstly, a number of studies have attempted to circumvent this difficulty by employing permanent magnets [20-22], which do not permit controllable magnetic field. Although many electromagnets have been designed, including air core [17, 23], open path magnetic circuit [6, 24-26], closed path magnetic circuit [27, 28], providing a controllable magnetic field using a reasonable size and weight of the electromagnet yet constitutes the primary challenge for compression mode characterization mode, which, indeed, is a fundamental necessity for practical applications of MREs.

Secondly, the compression mode characterization requires compression of the MRE specimen positioned within the gap between two magnetic poles. This causes variations in the magnetic field and thus the magnetic force attributed to pull between the two magnetic poles of the electromagnet. The force measured during the experiments is thus the sum of the magnetic force developed by the

electromagnet and the viscoelastic force attributed to the MRE. The magnetic force may be substantially higher compared to the viscoelastic force, especially under low deformations of the MRE and high magnetic field intensities. The compression mode characterizations thus involve compensation for the magnetic force, which is not of concern in the shear mode since the viscoelastic and magnetic forces occur in the orthogonal directions.

The magnetic force compensation is, indeed, a complex task due to the phase differences between the two force components, variations in the magnetic force with changes in the gap (deformation) and more importantly the effects of the MRE sample. In the reported studies, the contribution of the magnetic force has been either neglected [10, 17] or measured as a function of the air gap in the absence of the MRE specimen. The latter approach, however, can yield considerable errors in the induced magnetic force, since the presence of MRE within the air gap can significantly alter the magnetic flux density and thus the magnetic force due to magnetization of iron particles within the MRE [29, 30]. The magnetic force component thus also depends on the deformation amplitude (which directly affects the air gap), input frequency, and permeability of the MRE, apart from the intensity of the magnetic field. The magnitude and phase of the magnetic force are known to be a nonlinear function of the air gap, which varies with the applied displacement. Development of a systematic methodology for identifying the viscoelastic force by compensating for the magnetic force is thus desirable for accurate characterizations of compression mode properties of MREs.

The present study is aimed to address the above-stated challenges through developments of: (i) an optimal UI-shaped electromagnet for realizing magnetic field up to 1 Tesla in the direction of the mechanical loading while limiting the overall weight and dimensions; and more importantly (ii) a systematic methodology for compensating for the magnitude and phase of the magnetic force. Experiments were performed to characterize static and dynamic magnetic force, and the flux density in the center of the air gap with and without the MRE. A simple phenomenological model was developed in order to predict magnetic force as a function of the magnetic flux density, displacement magnitude and frequency. The measured data and the model were used to develop a systematic methodology for identifying viscoelastic force of the MRE by compensating for the dynamic nonlinear magnetic force. An experiment was subsequently designed to obtain compression mode characteristics of an isotropic MRE subject to 1.68 mm pre-deformation and

broad ranges of displacement amplitude, excitation frequency and magnetic flux density, using the proposed force compensation technique. The resulting force-deflection data are used to assess the significance of the magnetic force compensation by evaluating the MRE properties in terms of equivalent stiffness and damping.

2.2 Design of a UI-shaped electromagnet

A UI-shaped electromagnet is designed with a closed path core to achieve magnetic flux density along the direction of mechanical loading. The electromagnet comprises two coils in the U-section and one coil in the I-section, as shown in Figure 2.1(a) and 2.1(b). The proposed UI-shaped configuration with closed path magnetic core can yield relatively higher magnetic flux density with reasonable size and weight. A lumped-parameter model of the UI electromagnet is formulated considering the fringing and leakage flux by employing the equivalent magnetic circuit (EMC) [51] to identify optimal design parameters in a computationally efficient manner. Figure 2.1(c) and 2.1(d) illustrate the leakage and fringing flux permeance ($\mathcal{P}$) paths and the EMC circuit, respectively. The air gap length l_g and cross-sectional area of the core were set to 8 mm and 32mm×32mm, respectively, in order to characterize compression mode properties of cylindrical MRE samples with different dimensions/shape factors in accordance with standardized compression test methods for rubbers [52, 53].

Owing to the symmetry, one half of the electromagnet, is considered for formulating the EMC, where $\mathcal{R}_{U_1}$, $\mathcal{R}_{U_2}$ and $\mathcal{R}_I$ are the core reluctances between nodes 1-2, 2-3 and 3-1, respectively (Figure 2.1(d)). Furthermore, $\mathcal{R}_{lf}$, $\mathcal{R}_{ff}$, $\mathcal{R}_{bf}$ and $\mathcal{R}_{rf}$ are the left, front, back and right-side fringing flux reluctances, respectively. In Figure 2.1(d), $\mathcal{R}_g$ and $\mathcal{R}_l$ denote the air gap and the leakage flux reluctances, respectively.

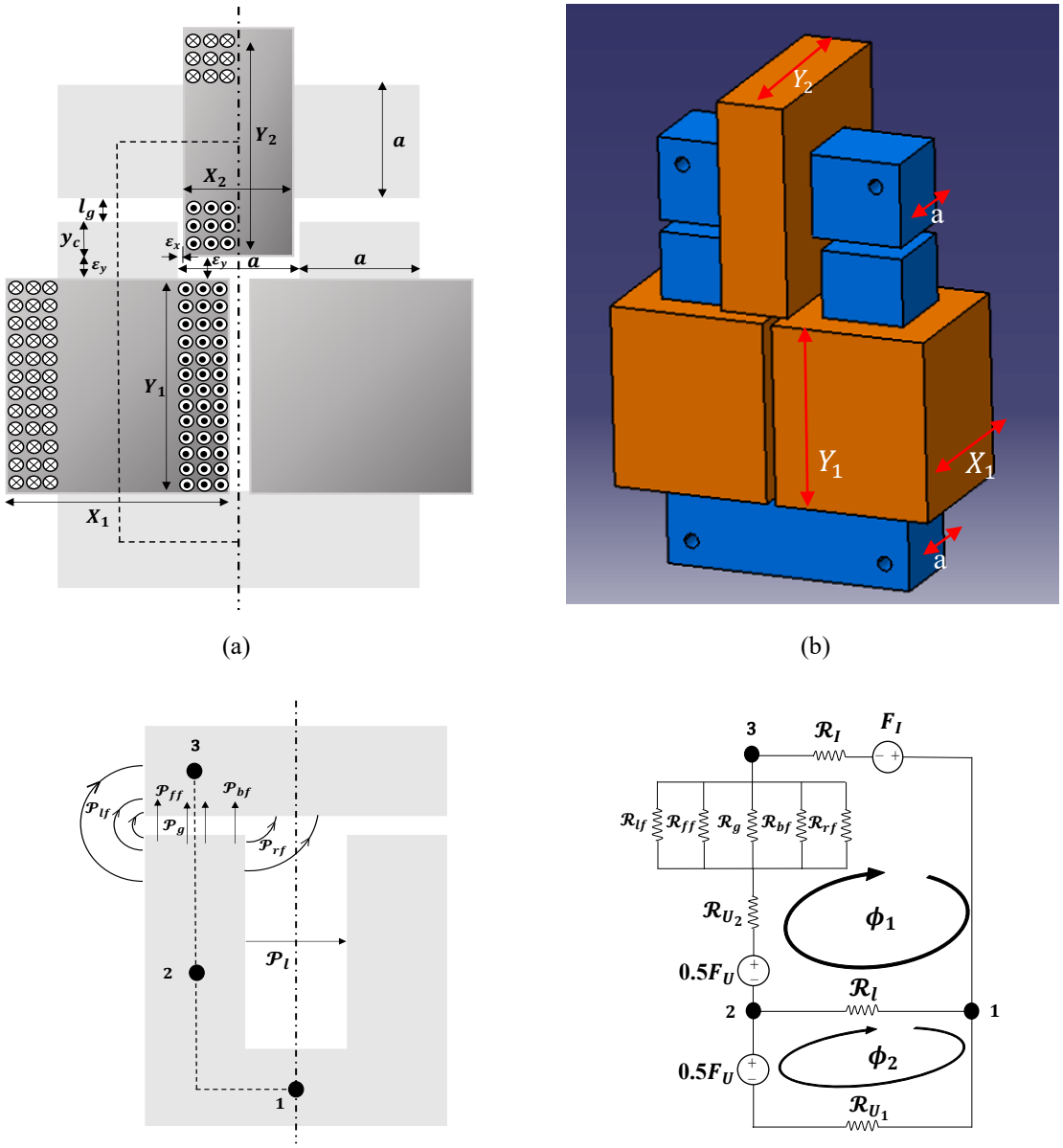

Figure 2.1 UI-shaped electromagnet: (a) schematic, (b) 3D view, (c) leakage and fringing flux permeance paths, and (d) EMC model.

These reluctances can be obtained from the geometric parameters, as shown in Figure 2.1(a) and the magnetic permeability, as [51, 54]:

$$\mathcal{R}_{U_1} = \frac{3a + Y_1}{2\mu_0\mu_r A}; \qquad \mathcal{R}_{U_2} = \frac{0.5Y_1 + y_c + \varepsilon_y}{\mu_0\mu_r A} \tag{2-1}$$

$$\mathcal{R}_I = \frac{a + 0.5X_2 + \varepsilon_x}{\mu_0\mu_r A}; \qquad \mathcal{R}_{lf} = \frac{\pi}{\mu_0 a[ln\,(1 + \frac{\pi a}{l_g})]} \tag{2-2}$$

$$\mathcal{R}_{ff} = \frac{\pi}{\mu_0 a[\ln(1+\frac{\pi a}{l_g})]}; \qquad \mathcal{R}_g = \frac{l_g}{\mu_0 A} \tag{2-3}$$

$$\mathcal{R}_{bf} = \frac{\pi}{\mu_0 a[\ln(1+\frac{\pi a}{l_g})]}; \qquad \mathcal{R}_{rf} = \frac{\pi}{2\mu_0 a[ln(1+\frac{\pi a}{4l_g})]} \tag{2-4}$$

$$\mathcal{R}_l = \frac{2}{\mu_0 a\left[2\left(\frac{Y_1 + y_c + \varepsilon_y + l_g}{a}\right) - \frac{1}{\pi}\right]} \tag{2-5}$$

where μ_0, μ_r, A, ε_y and ε_x are magnetic permeability of vacuum, relative magnetic permeability of the core, cross section area of the core, and vertical and horizontal clearances between the windings and the core legs, respectively, and $y_c = (Y_2 - a)/2$. By implementing the magnetic circuit analysis related to the EMC model, the magnetic flux in the air gap ϕ_g can be obtained as:

$$\phi_g = \left(\frac{\frac{\mathcal{R}_{tf}}{\mathcal{R}_g}}{1+\frac{\mathcal{R}_{tf}}{\mathcal{R}_g}}\right)\left(\frac{(\mathcal{R}_{U_1}+\mathcal{R}_l)F_I + 0.5(\mathcal{R}_{U_1}+2\mathcal{R}_l)F_U}{(\mathcal{R}_{U_1}+\mathcal{R}_l)(\mathcal{R}_I+\mathcal{R}_{tg}+\mathcal{R}_{U_1}+\mathcal{R}_l) - \mathcal{R}_l^2}\right) \tag{2-6}$$

where $\mathcal{R}_{tg}$ is the total gap reluctance, which includes the total fringing reluctance $\mathcal{R}_{tf}$ and $\mathcal{R}_g$. F_I and F_U are magnetomotive forces (MMFs) attributed to the I- and U- cores, respectively, given by [55]:

$$F_I = K_{wu} N_I I = K_{wu}\left(\frac{X_2(Y_2 - a)}{\pi d^2}\right) I \tag{2-7}$$

$$F_U = K_{wu} N_U I = K_{wu}\left(\frac{2Y_1(X_1 - a)}{\pi d^2}\right) I \tag{2-8}$$

where K_{wu}, I and d are the window utilization factor, current and diameter of the bare conductor, respectively. N_U and N_I are the number of turns in coils of the U- and I-cores, respectively. The window utilization factor K_{wu} is obtained from [55]:

$$K_{wu} = K_{ai} K_b K_{ed} \tag{2-9}$$

where K_{ai}, K_b and K_{ed} are the air and conductor insulation, bobbin and edge factors, respectively.

2.2.1 Design specifications and constraints

For the compression mode characterizations of MREs, it is desirable to design the electromagnet to realize high flux density with lower weight and overall dimensions. The reported studies have used very large size electromagnets, which may not be feasible in many applications [56, 57]. Apart from the weight and size, the heat generated by the electromagnet must be limited such that the temperature of the windings does not exceed the maximum allowable temperature of the conductor within a specified operating time, which is denoted as 'working time (WT)' hereafter. The allowable working time WT_a can be estimated from [58]:

$$WT_a = \frac{\rho_c l_w \pi d^2}{4 h_c A_c} \ln\left(\frac{\theta_{ss} - \theta_\infty}{\theta_{ss} - \theta_{max}}\right) \tag{2-10}$$

where θ_{ss}, θ_∞, and θ_{max} are the steady-state temperature of the winding, ambient temperature and maximum allowable temperature of the conductor. In the above Equation l_w, ρ_c, h_c and A_c are the conductor length, mass density of conductor, coefficient of natural convection heat transfer and side area of the windings, respectively. The optimal design of the electromagnet is thus strongly dependent on the working time as well as total electromagnet mass M_T, which can be obtained from:

$$M_T = K_s \rho_{mc} a^2 l_c + \frac{\rho_c l_w \pi d^2}{4} \tag{2-11}$$

where K_s, ρ_{mc} and l_c are the lamination stacking factor, mass density of the magnetic core and core length, respectively. Length of conductor (l_w) can be calculated from the geometry of winding and conductor's diameter using the following relation based on the arithmetic progression:

$$l_w = 4\left(a[N_U + N_I] + d^2\left[\frac{N_U^2}{Y_1} + \frac{2N_I^2}{X_2}\right]\right) \tag{2-12}$$

Furthermore, considering the B-H curve of the core, the saturation magnetic flux density, B_{St}, of the electromagnet was set as 1.1 *T*.

2.2.2 Design Optimization

A constrained minimization problem is formally formulated so as to maximize the magnetic flux, such that:

$$\text{Minimize: } J(V) = -\phi_g \tag{2-13}$$

where $V = [X_1\ Y_1\ X_2\ Y_2\ d\ I]^T$ is the design vector of dimensional parameters ($X_1\ Y_1\ X_2\ Y_2$) shown in Figure 2.1, and conductor diameter and current.

The above minimization function is subject to following side constraints:

$$\begin{cases} X_2 + 2\varepsilon_x \le a \\ a - X_1 \le 0 \\ a - Y_2 \le 0 \\ 1 \le I \le 10\ A \\ 10 \le AWG(d) \le 30 \end{cases} \tag{2-14}$$

The conductor diameter d is limited by varying AWG from 10 to 30, while the current I is limited to a maximum of 10 A. The nonlinear constrained minimization problem stated in Equations (2-13) and (2-14) has been solved using the powerful sequential quadratic programing (SQP) algorithm considering different working times, ranging from 1 to 30 min, and the total mass ranging from 2 to 25 kg. The search process was terminated when the magnetic flux density in the gap (B_g) approached saturation.

Figure 2.2 illustrates the variations in B_g obtained from optimal solutions corresponding to different limiting values of the WT and total mass. It is evident that the optimal solution greatly depends on WT, where each WT corresponds to a specific mass that limit the temperature increase of the windings below the maximum allowable temperature of the conductor. Increasing the working time resulted in considerably higher mass, which corresponds to saturation of the air gap, while the peak magnetic flux density approached slightly above 1 T, irrespective of WT. The optimal design leading to total mass of 5 kg and WT of 5 min was considered adequate for laboratory characterization. The UI-shaped electromagnet was subsequently fabricated using the corresponding optimal design parameters, as: X_1=64.3, Y_1=59.6, X_2=14.0, Y_2=67.6, d=1.52 mm and I=5.86 A. It is noted that the combined electrical resistance of the three coils is 3.98 ohms. Thus, the maximum power consumption of the U-I device to provide magnetic flux density of 1 T is 136.67 watt, which is quite practical for implementation of MREs into practice.

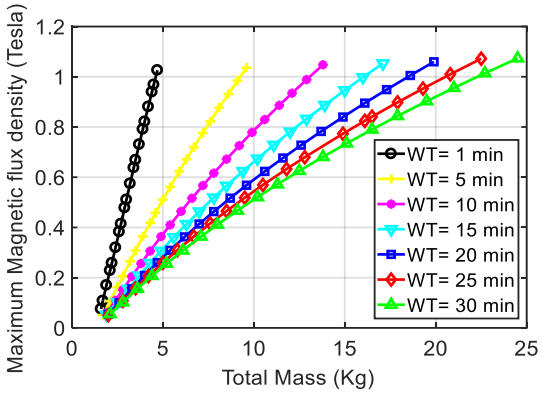

Figure 2.2 Dependency of the magnetic flux density within air gap of an optimal solution on the total mass and working time.

2.3 Experimental methods

The experiment design involved three different series of experiments. The first series of experiments focused on characterizations of magnetic force and magnetic flux in the air gap without the MRE, and measurements of air gap flux in the presence of an isotropic MRE under static variations in the air gap. The second series of experiments characterized the magnetic force under dynamic variations in the air gap length. The data acquired during the first two series were used to build a general systematic methodology for compensating for the magnetic force between two poles of the electromagnet as a function of magnetic flux density, displacement magnitude, and excitation frequency. The third series of experiments was conducted to characterize compression mode properties of an isotropic MRE using the proposed compensation method.

2.3.1 Static magnetic force and flux measurements

The magnetic force and flux density at the center of the air gap were initially measured under different combinations of the air gap length and current. The electromagnet was installed on a servo-hydraulic material test system (MTS) with the lower mount (U-core) fixed to the actuator and upper mount (I-core) attached to a fixed cross-beam via a 9 kN load cell, as shown schematically in Figure 2.3(a). A cylindrical silicon rubber sample (9 mm thick) was positioned in the air gap, and a Gauss meter probe was inserted in the middle of the rubber sample to measure the air gap magnetic flux density (B_g), as shown in Figure 2.3(b). This permitted the measurement of the air gap magnetic flux density as functions of the gap and the coil current, while assuming that the relative magnetic permeability of the rubber sample is similar to that of the air. A thermocouple was installed on one of the coils around the U-core to monitor its surface

temperature, and a large size fan was used, when needed, to ensure that the winding temperature remained below 40℃. A 100 V power supply was used to apply controlled direct current (DC) to the electromagnet, which was varied from 1 A to 6 A in increments of 1 A. It is noted that we have not used alternating current (AC) in this dissertation. For each applied current, the air gap length was varied from 9 mm to 3 mm by displacing the actuator in increments of 1 mm, which was measured using a Linear Variable Differential Transformer integrated within the actuator.

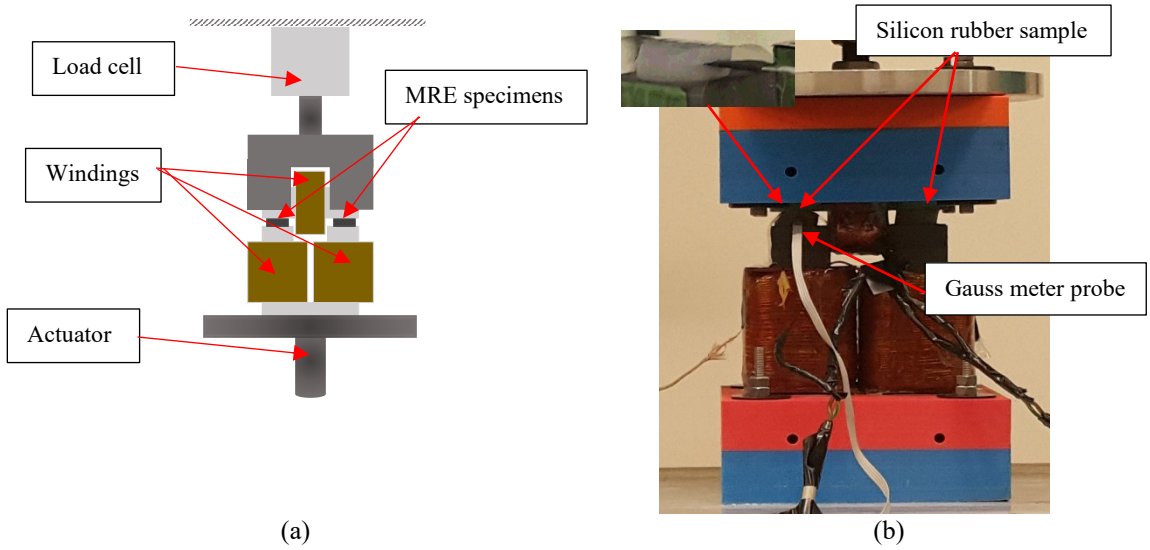

Figure 2.3 Schematic illustration of the experimental set up for measurements of air gap flux density and total force in the compression mode (a); placement of rubber samples (or MRE) in the air gap with the Gauss probe (b).

The magnetic flux corresponding to each combination of the gap length and the current was initially measured with the rubber sample positioned in the air gap. The experiments were repeated without the rubber specimen in order to acquire the magnetic force under same combinations of the gap length and the coil current. Figure 2.4(a) and 2.4(b) illustrate variations in the measured magnetic flux density in the center of the air gap and the magnetic force, respectively, as functions of the gap length and applied current. Both the magnetic flux density and the force increased with increase in the current and decreased with increase in the gap length in a nonlinear manner. The results suggest saturation of the flux density and the force under current exceeding 5 A, especially for the smaller gap lengths. It can be further inferred that the effective magnetic permeability within the air gap changes from nonlinear to a linear regime as the gap length increases, as seen in

Figure 2.4(a). The results in Figure 2.4(c) show that the magnetic force increases with the flux density at the center of the air gap in a nonlinear manner, irrespective of the gap length.

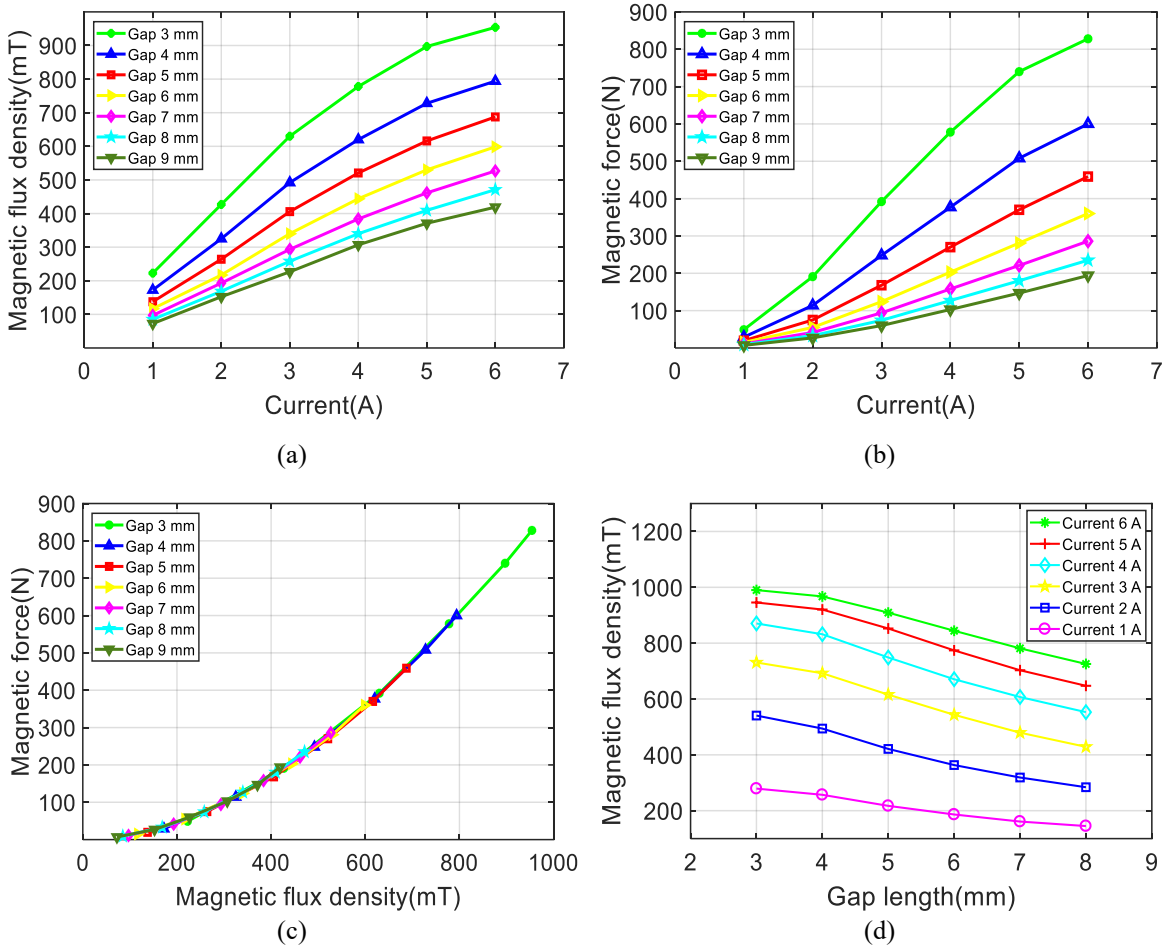

Figure 2.4 Variations in (a) air gap magnetic flux density, and (b) magnetic force as functions of coil current and gap length, (c) correlation between air gap magnetic force and flux density, and (d) variations in the magnetic flux density measured within the isotropic MRE as functions of gap length and applied current.

Considering that the MRE sample in the air gap may alter the magnetic flux density, subsequent experiments were performed to measure the magnetic flux density inside an isotropic cylindrical MRE specimen at different levels of the gap length and the coil current. For this purpose, the Gauss meter was positioned inside the MRE by slightly piercing the specimen around the mid-plane. Figure 2.4(d) illustrates the variations in the measured magnetic flux induced within the isotropic MRE as function of the gap length and coil current. Results suggest that the magnetic

flux density decreases as the gap length increases, while it increases considerably with increase in current. The saturation of the magnetic flux density at higher current levels is also evident in the figure. A comparison of the results presented in Figure 2.4(a) and (d) suggest that presence of MRE in the air gap leads considerably higher magnetic flux density. This is due to relatively higher magnetic permeability of the MRE compared to the air. The relative change in the magnetic flux density can yield an estimate of relative magnetic permeability of the MREs as a function of the gap length.

2.3.2 Dynamic magnetic force measurements

The second series of experiments was designed to measure the magnetic force developed between two poles of the electromagnet in the absence of the MRE in the air gap in order to consider the effect of magnetic hysteresis loss and eddy currents on the force magnitude and the phase. The lower U-core of the electromagnet was subjected to harmonic displacements at different frequencies ranging from 0.1 to 50 Hz, while magnetic flux density was varied from 0 to 750 mT by varying the coil current.

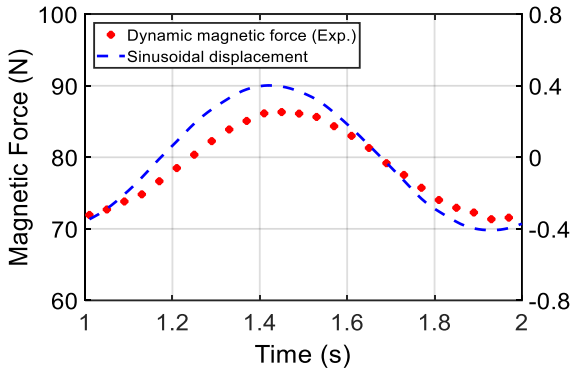

Figure 2.5 Variations in magnetic force under 0.4 mm amplitude harmonic displacement at 1 Hz (flux density= 450 mT).

The experiment involved factorial combinations of four displacement amplitudes ($\overline{l_g}$= 0.2, 0.4, 0.8 and 1.6 mm), six levels of excitation frequency (f= 0.1, 1, 10, 20, 30, and 50 Hz), and six levels of the magnetic flux density (B_g= 0, 150, 300, 450, 600 and 750 mT). The magnetic force was subsequently measured under different excitation conditions and magnetic flux densities. As an example, Figure 2.5 shows time-histories of the measured magnetic force and the displacement excitation (amplitude=0.4 mm, f=1 Hz) under B_g=450 mT. The results illustrate notable magnitude

of the magnetic force suggesting the significance of its compensation for deriving viscoelastic force developed by an MRE in the compression mode. The results also show notable phase difference between the magnetic force and the displacement (air gap length), which is attributed to the generated eddy currents. This phase can also be observed as hysteresis in force-displacement characteristics. The hysteresis as a result of induced eddy currents within a ferromagnetic material subject to a variable magnetic field, has also been observed in a mechanical harmonic oscillator for energy dissipation purposes [59].

2.3.3 Compression mode characterization of MRE

The final series of experiments was designed to characterize compression mode properties of an isotropic MRE in accordance with the standardized methods defined for compression testing of rubbers [52, 53]. For this purpose, a batch of isotropic MRE was fabricated in the laboratory using silicone rubber (Eco-Flex Series, Smooth-on) as the matrix and 30% volume fraction of carbonyl iron particles (diameter ranging from 3.9 to 5μm), as described in [5]. Two identical MRE cylindrical samples (8 mm thick) were bonded between the U- and I-cores of the electromagnet using a thin layer of an industrial adhesive, as shown in Figure 2.3(b). The samples were subject to pre-deformation of 1.68 mm and the force-displacement characteristics of the MRE were acquired under selected ranges of magnetic flux density, and displacement amplitude and frequency. The desired flux density was realized by applying the current in accordance with the relation established from the results shown in Figure 2.4(d). A factorial approach was used considering four different levels of displacement amplitudes (ε = 0.2, 0.4, 0.8 and 1.6 mm) which correspond to displacement amplitude of 0.2, 0.4, 0.8 and 1.6 mm, respectively, six different frequencies (f = 0.1, 1, 10, 20, 30 and 50 Hz) and six levels of flux density (B_g = 0, 150, 300, 450, 600 and 750 mT). It should be noted that characterization of MREs within the selected range of loading frequency and strain amplitude, could be effectively utilized for design and development of semi-active MRE-based engine mounts. Since, engine mounts are generally intended to have high damping and high stiffness at low frequency excitation (1-50 Hz), when amplitude of engine vibration generally exceeds 0.3 mm [60]. These requirements could be achieved by employing MREs.

The force and displacement signals were acquired during each measurement using a National Instruments Data Acquisition board, while the sampling rate was adjusted in the 50 to 3000 Hz so

as to acquire a total of 100 measurements per cycle, irrespective of the excitation frequency. The measured force is the sum of the magnetic force due to pull between the poles of the electromagnet and the viscoelastic force of the MRE. The characterization of the MRE properties thus necessitates compensation for the magnetic force.

2.4 Compensation for the magnetic force

From the experimental data, it is evident that the magnitude of the magnetic force is strongly dependent on the magnetic flux density apart from the loading conditions. Moreover, there exists a phase difference between the magnetic force and the deflection, which is mainly dependent upon the excitation frequency. In this section, the data acquired during first two series of experiments are used to formulate a general systematic methodology for predicting the magnetic force as a function of the magnetic flux density, and displacement magnitude and frequency.

2.4.1 Estimation of static magnetic force

For a given flux density, the magnetic force developed between two poles of a electromagnet can be obtained from [61]:

$$F_g = -\frac{B_g^2 A_g}{2\mu_0} \tag{2-15}$$

where magnetic flux density $B_g = \phi_g / A_g$ with A_g being the cross-section area of the air gap. The magnetic flux ϕ_g can be obtained from Equation (2-6). The observed saturation of the magnetic flux, however, cannot be described by the analytical EMC model. Alternatively, the trends observed in Figure 2.4(a) are used to formulate a phenomenological model for the magnetic flux density as a function of the air gap length and the coil current, such that:

$$B_g = a_1 e^{-a_2 l_g}(1 - e^{-a_3 I}) \tag{2-16}$$

Furthermore, the results in Figure 2.4(c) suggest that the magnetic force can be directly related to the flux density using the following power relation, irrespective of the gap length:

$$F_g = a_4 B_g^{a_5} \tag{2-17}$$

Substituting for B_g from Equation (2-16) in the above relation yields:

$$F_g = b_1 e^{-b_2 l_g}(1 - e^{-a_3 I})^{a_5} \quad (2\text{-}18)$$

where$b_1 = a_4 a_1^{a_5}$ and $b_2 = a_2 a_5$. Considering Figure 2.4(d), another relationship similar to Equation (2-16) can be used for the magnetic flux density within the isotropic MRE as a function of the air gap length and the coil current can be formulated as:

$$B_g = a_{11} e^{-a_{22}\varepsilon}(1 - e^{-a_{33} I}) \quad (2\text{-}19)$$

The coefficients in above relations are identified through least square error minimization between the model-predicted and measured results, which are summarized in Table 2.1. The identified models revealed coefficient of determination, R^2, in the order of 0.99.

Table 2.1 Identified coefficients of the magnetic force and flux models.

b_1	b_2	a_3	a_5	a_{11}	a_{22}	a_{33}
2.24×10^9	288	0.12	1.8	2549	95.72	0.15

It should be noted that the corresponding coil current for a desired magnetic flux density in absence and presence of the MRE specimen in the gap can also be obtained by manipulating Equations (2-16) and (2-19), respectively, as:

$$I = \frac{-1}{a_3}\left[ln\,(1 - \frac{B_g}{a_1 e^{-a_2 l_g}})\right] \quad (2\text{-}20)$$

$$I = \frac{-1}{a_{33}}\left[\ln\,(1 - \frac{B_g}{a_{11} e^{-a_{22}\varepsilon}})\right] \quad (2\text{-}21)$$

A finite element (FE) model of the electromagnet was also formulated using the FEMM software to estimate the magnetic force and flux density as functions of the gap length and the current considering the saturation nonlinearity. The model also permitted the analysis of distribution of the magnetic flux density in the air gap. The 2D-planar magneto-static FE model, shown in Figure 2.6(a), was analyzed for different air gap lengths and coil currents. As an example, Figure 2.6(b) and 2.6(c) illustrate distribution of the magnetic flux density for the current, I= 3 A, and air gap length of l_g=8 mm. As it can be realized, the magnetic flux density in the center of air

gap is nearly uniform, particularly when width of the cross section varying from 5 mm to 25 mm. MRE specimens with diameter of 18 mm were placed within this range.

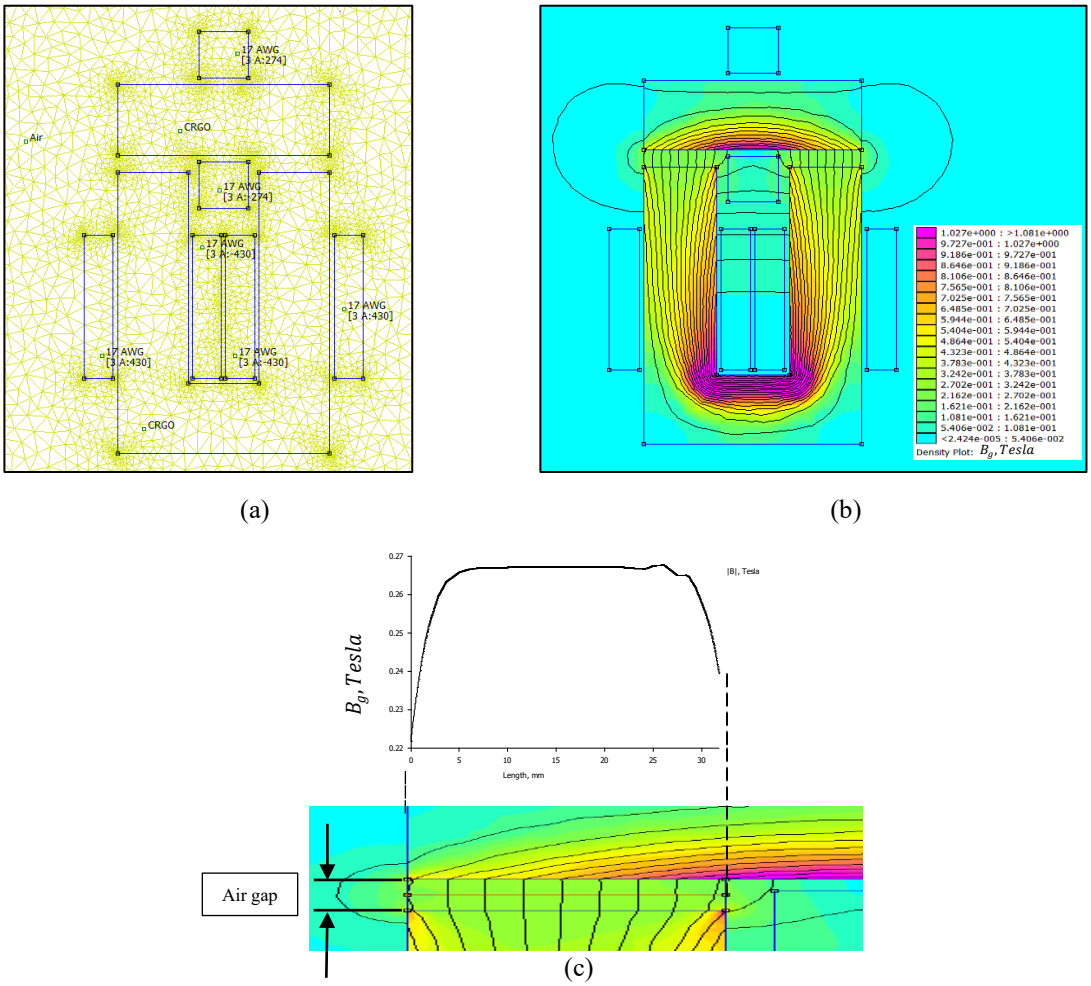

Figure 2.6 FEMM simulation model of the electromagnet (a), magnetic flux density distribution under 3 A current and gap length of 8 mm (b), and distribution of magnetic flux density in the air gap (c).

The effectiveness of the analytical, phenomenological and FE models in predicting the magnetic force and flux density in the air gap is evaluated through comparisons with the measured data, as shown in Figure 2.7(a) to 2.7(d). The results are limited to two different gap lengths (5 mm and 8 mm), as examples, while the coil current is varied from 1 to 6 A. The comparisons suggest that the FE and phenomenological models yield reasonably good estimations of the magnetic flux density and force for the ranges of current and gap length considered. Owing to the linear magnetization curve, the analytical model yields good prediction of magnetic flux density only for coil current up to 3 A. The saturation of the magnetic flux density under higher coil current is more

accurately predicted by the phenomenological and FE models, as seen in Figure 2.7(a) and 2.7(b) for air gap lengths of 5 mm and 8 mm, respectively. The FE model, however, yields relatively higher deviations from the measured data, especially in the magnetic force, under relatively higher currents and lower gap length, as seen in Figure 2.7(d).

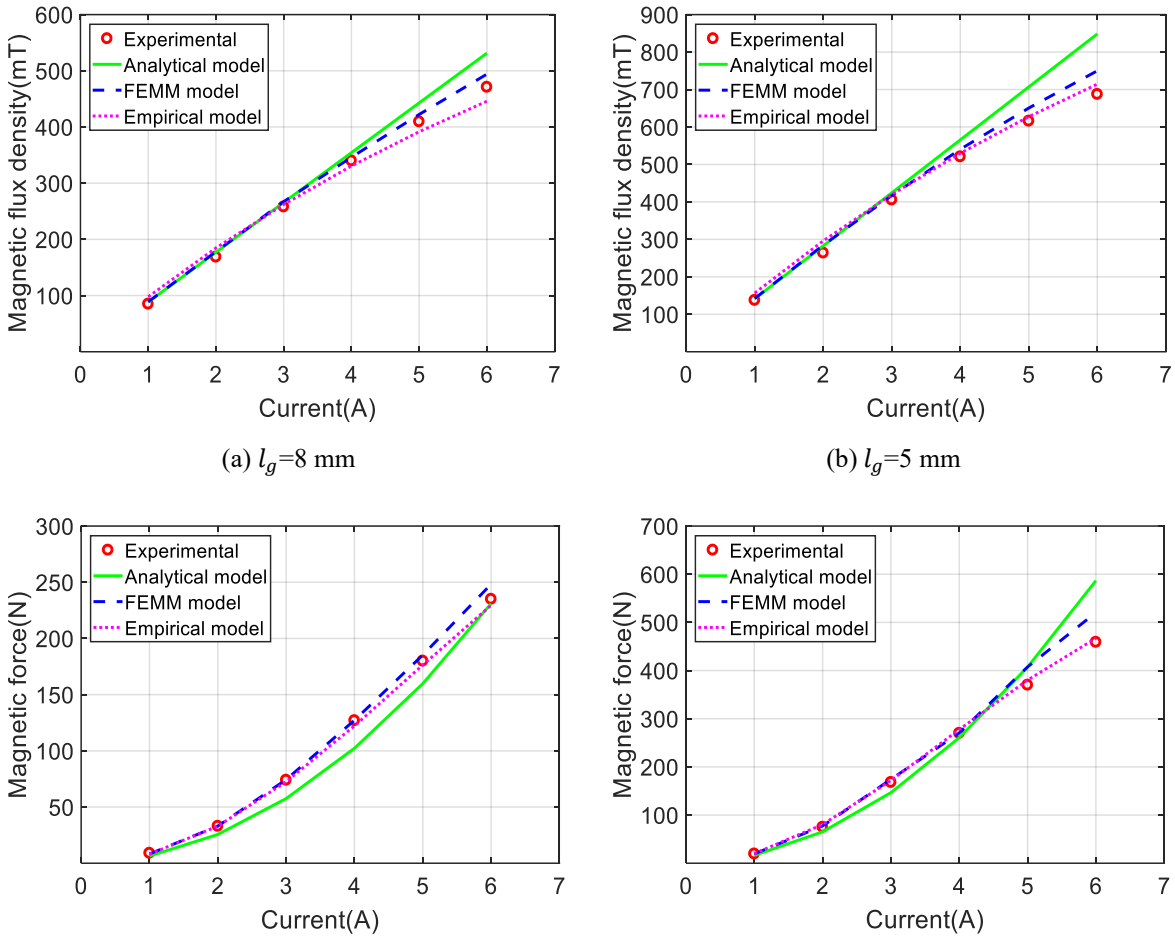

(a) l_g=8 mm (b) l_g=5 mm

(c) l_g=8 mm (d) l_g=5 mm

Figure 2.7 Comparisons of the magnetic flux density (a, b) and the magnetic force (c, d) predicted from the analytical, phenomenological and finite element models with the measured data for two different gap lengths (l_g = 5 and 8 mm).

2.4.2 Estimations of dynamic magnetic force characteristics

The magnetic force developed under dynamic variations in the air gap may be estimated from Equation (2-18) considering harmonic variations in the gap length:

$$l_g = l_0 + \bar{l_g}\cos(2\pi f t) \tag{2-22}$$

where the parameter l_0 is the static gap length, $\overline{l_g}$ is the variation in the gap length or the displacement amplitude and f is the excitation frequency.

Figure 2.8 compares the time-history of the force estimated from Equation (2-18) with the measured data under 0.8 mm amplitude excitation at the frequency of 1 Hz, and two different levels of flux density (B_g= 300 and 600 mT), as examples. The results also show the variation in the air gap length ($\overline{l_g}$). The comparisons show substantial differences between the predicted and measured magnetic forces. The model predicted force is in phase with the displacement excitation, while the measured force exhibits notable phase difference. The observed magnitude and phase differences are attributable to magnetic hysteresis [62-64] together with the eddy current [65-68] during cyclic loading. Similar trends were also observed under other loading conditions. It can be further inferred that the magnitude of magnetic force increases considerably as the magnetic flux density increases from 300 mT to 600 mT. The comparisons thus suggested that the magnetic force predicted from the static magnetic flux density would lead to considerable errors in both the magnitude and the phase.

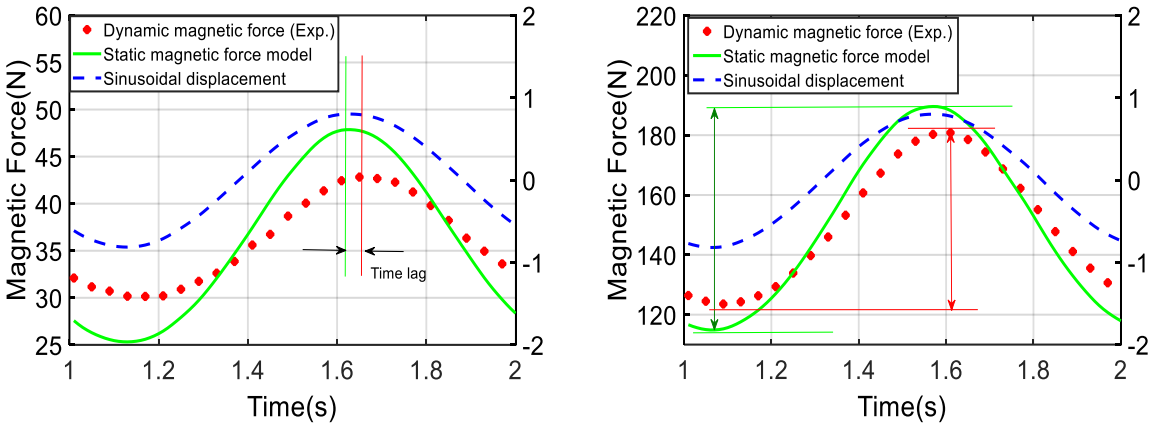

Figure 2.8 Comparison of static and dynamic magnetic force at frequency of 1 Hz and displacement amplitude of 0.8 mm: (a) B=300 mT; and (b) B=600 mT.

Figure 2.9 illustrates the differences between the model-predicted and measured magnetic force responses in terms of magnitude ratio (M), defined as the ratio of peak-to-peak measured force to that obtained from the static model, and the phase lag (ϕ) between the measured force and the displacement. The results in the left column show variations in M and ϕ in the 0.1 to 50 Hz frequency range for two different displacement amplitudes (0.8 and 1.6 mm) and B_g= 600 mT.

The effect of flux density is shown in the right column for excitation frequency at 1 Hz. Results show rapid and nearly linear decrease in M with increase in frequency up to 10 Hz. The magnitude ratio remains nearly constant at frequencies above 20 Hz, irrespective of the displacement amplitude. This decrement in M is likely attributed to induced eddy currents due to the harmonic motion, which similar dependency has also been reported for an oscillating magnet in a coil [69] as well as electrical machines [70]. The magnitude ratio, however, increases with flux density and tends to saturate as flux density exceeds 500 mT for both displacement amplitudes. This is likely attributed to decrease in proportion of magnitude of the induced counter magnetic field due to the Lenz's law to the magnetic field which caused it, as the intensity of magnetic field increases.

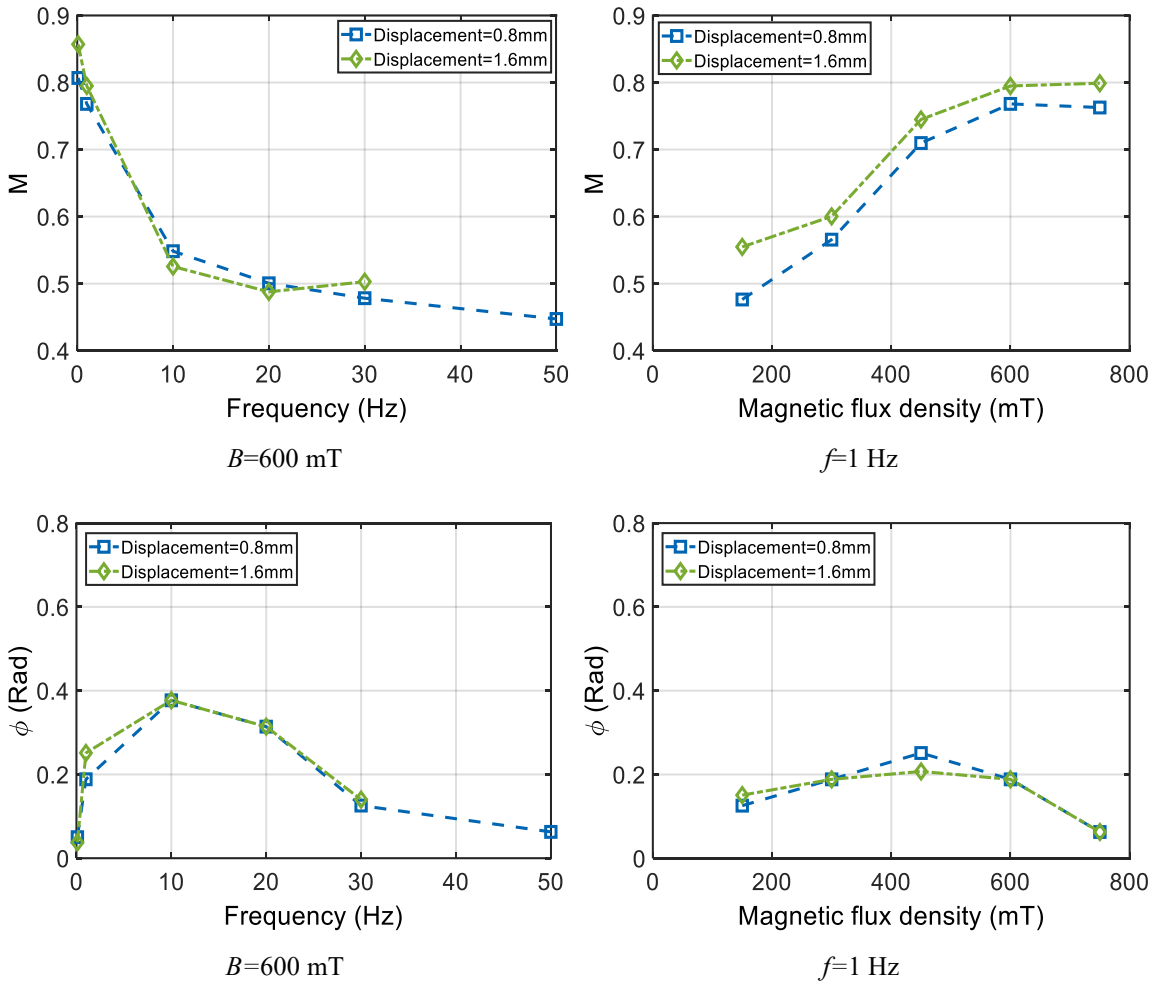

B=600 mT *f*=1 Hz

B=600 mT *f*=1 Hz

Figure 2.9 Effects of frequency (left column) and magnetic flux density (right column) on the magnitude ratio (M) and phase lag (ϕ) under displacement amplitudes of 0.8 mm and 1.6 mm.

The phase lag (ϕ) exhibits notable frequency dependence but relatively small amplitude dependence. It increases considerably with increase in frequency from 0.1 to 10 Hz and decreases notably with further increase in frequency in the 10–30 Hz range. It slightly decreases as the frequency exceeds 30 Hz. A decrease in eddy current induced energy dissipation, which can be related to the phase, with increasing frequency has also been observed for a moving permanent magnet in a conductive tube [71]. The phase lag, however, nearly remains constant with increase in B_g up to about 500 mT, when the force approached saturation. The phase lag decreased with further increase in B_g.

The results in Figure 2.9 suggest that the magnitude ratio and phase between the dynamic and static magnetic force responses are nearly displacement amplitude independent over the ranges of excitation frequency and flux density considered in the study. Moreover, the phase difference is nearly constant up to B_g=600 mT. The phase difference may thus be considered independent of the flux density. The magnitude ratio, however, strongly depend on both the frequency and the flux density. Considering this, the amplitude ratio and phase difference may be expressed using the following relations:

$$M(f, B_g) = a_r f^{b_r}(1 - e^{-c_r B_g}) \qquad \phi(f) = (a_\phi f^{b_\phi} + c_\phi f) \tag{2-23}$$

The coefficients in above relations are identified through minimization of error between the model-predicted and measured results, which are summarized in Table 2.2.

Table 2.2 Identified parameters of proposed relations for predicting the magnitude ratio (M) and phase lag (ϕ).

a_r	b_r	c_r	a_ϕ	b_ϕ	c_ϕ
0.692	-0.094	5.733	0.261	0.661	-0.080

The above relations together with Equations (2-18) and (2-22) yield the dynamic magnetic force as function of the gap length, magnetic flux density, and the excitation frequency, $F_g\left(l_g, B_g, f\right)$. Comparisons of the predicted and measured dynamic magnetic forces over the ranges of flux density and loading conditions revealed notable differences between the two. The deviations between the measured and predicted dynamic magnetic forces ranged from 5% to 10% in the 0.1 to 50 Hz frequency range. The observed differences were attributed to possible

contributions of higher harmonics in the displacement to the induced magnetic field and thus the magnetic force. The dynamic magnetic force was subsequently expressed by an extended Fourier series in order to account for contributions of the higher harmonics, such that:

$$F_g(\overline{l_g}, B_g, f) = [b_1 e^{-b_2 l_0}(1 - e^{-a_3 I})^{a_5}]\Big[I_0(\lambda) + 2M(f, B_g) I_1(\lambda) cos(2\pi f t - \phi(f)) + 2M(f, B_g) I_2(\lambda) cos\Big(2(2\pi f t - \phi(f))\Big)\Big] + \cdots \quad (2\text{-}24)$$

where the I_0, I_1 and I_2 are the modified Bessel functions of order zero, one, and two, respectively, and $\lambda = -b_2 \overline{l_g}$.

Consideration of nine harmonics in the expansion revealed reasonably good agreements between the measured and predicted dynamic magnetic forces in the entire ranges of frequency, flux density and the excitation amplitude. As an example, Figure 2.10, left-column, compares time-histories of the dynamic magnetic force predicted from Equation (2-24) with the measured data, and the static magnetic force obtained from Equations (2-18) and (2-22). The comparisons are illustrated for $\overline{l_g}$= 1.6 mm, B_g= 600 mT and three different excitation frequencies (0.1, 1 and 10 Hz). The right-column further shows comparisons of the predicted and measured dynamic magnetic force-displacement characteristics. The comparisons suggest that the proposed phenomenological-based model based on the Fourier expansion can accurately predict the magnetic force under dynamic loading conditions. Unlike the static force model, the dynamic force model can also accurately describe the hysteresis phenomenon. The model also revealed similar degree of effectiveness over the entire ranges of excitation and flux density considered in the present study.

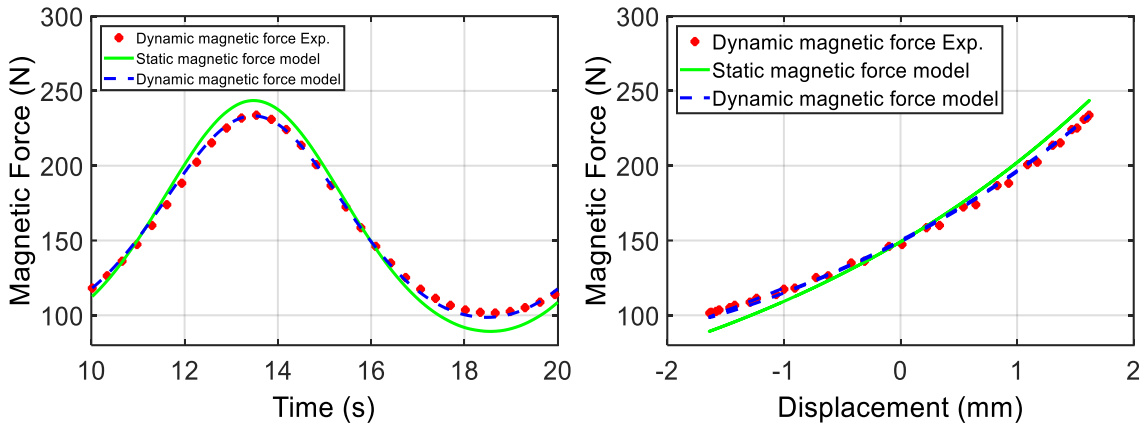

(a)

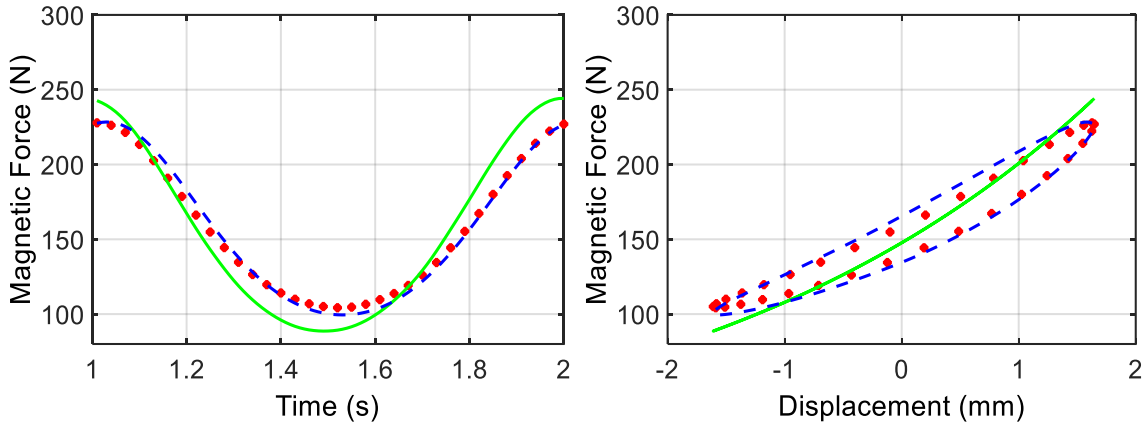

(b)

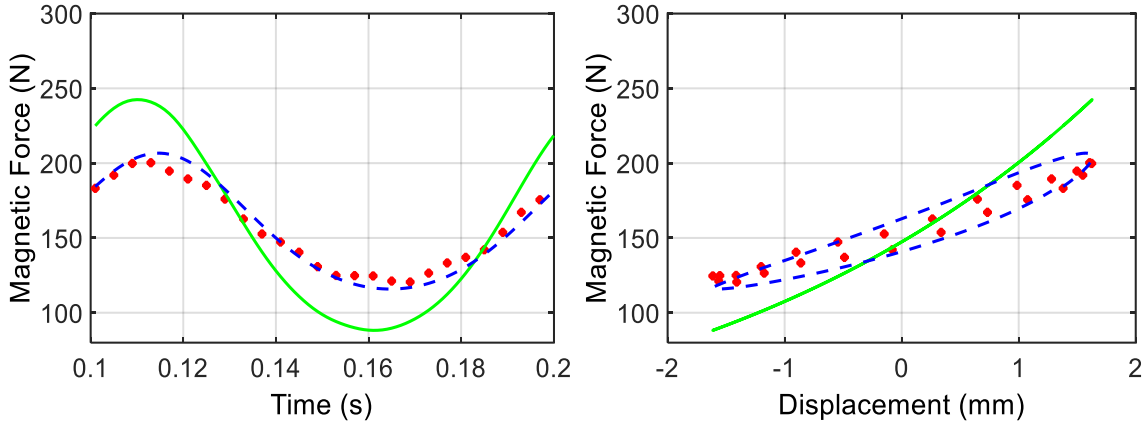

(c)

Figure 2.10 Comparisons of time-histories (left-column) and magnetic force-displacement characteristics (right-column) obtained from the phenomenological models with the measured data for $\overline{l_g}$= 1.6 mm, B_g= 600 mT, and: (a) f= 0.1 Hz; (b) f= 1 Hz; and (c) f= 10 Hz.

It should be noted that the validity of the proposed model is examined using the I vs B_g relation (Equation (2-20)) derived from Figure 2.4(a). The presence of the MRE in the air gap, however, significantly alters the magnetic flux, as evident in Figure 2.4(d). The dynamic magnetic force in the presence of the MRE is thus predicted using the I vs B_{MRE} relation (Equation (2-21)) obtained from Figure 2.4 (d), which is subsequently subtracted from the dynamic force measured during third series of experiments in order to obtain the viscoelastic force developed by the MRE, such that:

$$F_{MRE}(\varepsilon, B_g, f) = F_T(\varepsilon, B_g, f) - F_g^M(\bar{l}_g, B_g, f) \tag{2-25}$$

where F_{MRE} and F_T are the viscoelastic MRE force and total force measured, respectively. F_g^M is the dynamic magnetic force obtained from the proposed model in Equation (2-24) using the current and flux density relation obtained for MRE in the air gap, as described in Equation (2-21).

The significance of the magnetic force compensation is demonstrated through comparisons of F_T, F_g^M and F_{MRE} in Figure 2.11 considering 0.8 mm excitation at 1 Hz and B_g = 450 mT, as an example. It is evident that the post-compensation force-deflection characteristics of the MRE, shown in Figure 2.11(c) differ significantly from the pre-compensation characteristics, shown in Figure 2.11(a). The equivalent stiffness of the MRE specimen with and without magnetic force compensation were obtained as 45.2 and 24.3 N/mm, respectively. The results also show notable effect of force compensation on the energy dissipated by the MRE during each loading/unloading cycle. The equivalent viscous damping coefficient for the MRE with and without dynamic magnetic force compensation were obtained as 3.6 and 8.2 Ns/mm, respectively. These suggest errors in equivalent stiffness and damping in the orders of 46% and 129%, respectively, in the absence of the magnetic force compensation. Results revealed maximum errors up to 90% and 163%, in equivalent stiffness and damping, respectively, which occurred at amplitude, frequency, and flux density of (0.2 mm, 1 Hz, 750 mT), and (1.6 mm, 1 Hz, and 600 mT).

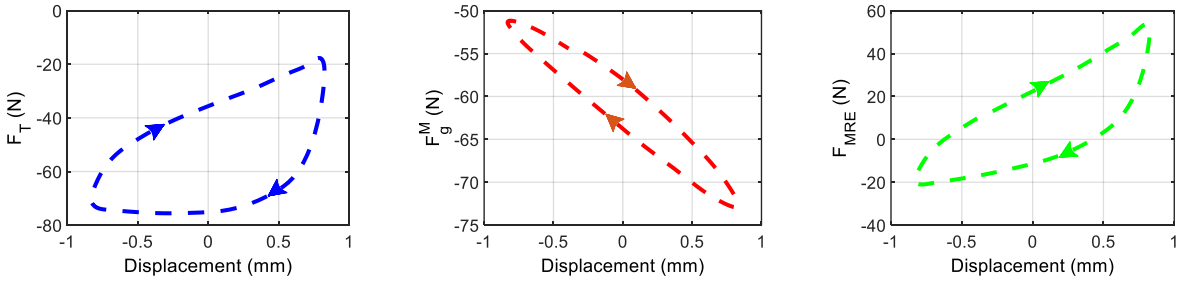

(a) (b) (c)

Figure 2.11 Measured force-displacement characteristics of MRE (a), Dynamic magnetic force-displacement characteristics obtained from the model (b) and Viscoelastic (compensated) force displacement characteristics of MRE (0.8 mm excitation at 1 Hz, and magnetic flux density of 450 mT) (c).

2.5 Conclusions

The accurate prediction of dynamic magnetic force generated during the harmonic tension/compression tests of magnetorheological elastomers (MREs) is of paramount importance for precise characterization of MREs in compression mode of operation. The compensation for the magnetic force was systematically addressed based on measured static and dynamic magnetic forces, and flux density in the center of the air gap with and without the MRE. Results revealed notable phase and magnitude differences between the measured static and dynamic magnetic forces, which are found to be dependent on magnetic flux density and frequency. A simple phenomenological model was proposed to accurately predict the dynamic magnetic force as function of flux density and excitation conditions. A reasonably good agreement was obtained between the model-predicted results and the measured dynamic magnetic force. Results revealed maximum errors in calculating equivalent stiffness and damping of the MRE specimen in the orders of 90% and 163%, respectively, in the absence of the magnetic force compensation.

CHAPTER 3
DYNAMIC COMPRESSION MODE CHARACTERIZATION

3.1 Introduction

MREs can function in shear, squeeze (compression) or combined shear-squeeze modes [56]. The vast majority of the studies have reported dynamic properties of the MREs in the shear mode, where the MR effect tends to diminish under high strain amplitudes due to increasing distance between the magnetic particles [14, 15]. It has been shown that the shear modulus of an isotropic MRE can increase by as much as 60%, when subjected to 1.0 T magnetic flux density [11]. Only a limited number of studies could be found on dynamic behavior of MREs in compression, even though the MREs exhibit enhanced MR effect in the compression mode compared with the shear mode. This is due to decrease in particles' distances during compression [23]. For instance Gordaninejad et al. [17] reported an MR effect of 99% in compression mode compared with 65% in the shear mode. Relatively fewer studies in the compression mode are likely due to complexities associated with the experiment design and constraints. The strain-softening behavior is also less pronounced in the compression mode compared with the shear mode [18]. Furthermore, relatively greater shift in the frequency of an absorber employing MRE in the compression mode has been reported compared to that in the shear mode [72].

Reported studies on compression mode characterizations of MREs have employed diverse approaches and experimental methods, which invariably suggest the difficulty in applying controllable magnetic field to an MRE sample during the characterization process. The vast majority have employed permanent magnets to realize desired magnetic flux density [20, 45, 73], which pose challenges in controlling the flux density. Alternatively, electromagnets realized via air core [17, 74], magnetic core with extra air gap [6, 75] or open magnetic circuit [25, 76] have been used to achieve controllable magnetic field, while permitting mechanical loading simultaneously. A few studies have also employed closed path magnetic core with relatively bulky electromagnets [27, 28]. Reported studies on compression mode characterizations of MREs have been mostly limited to low strain amplitudes [73], low strain rates or excitation frequencies [77, 78], and relatively low magnetic flux density, well below the magnetization saturation limits [46, 47]. Moreover, the large size permanent magnets used in most of the studies generally do not permit magnetic saturation behavior of the MREs, apart from being impractical. Furthermore, the

studies have employed either isotropic or anisotropic MREs. Although MREs normally experience large static pre-strain in semi-active vibration isolators and absorbers applications due to weight of the supported structure or absorber mass, the dynamic compression characterization of MREs superimposed on large static pre-strain has not been reported. Limited knowledge thus exists on relative merits or limitations of the isotropic and anisotropic MREs in the compression mode.

The present study is aimed at compression mode characterizations of both isotropic and anisotropic MREs under broad ranges of strain amplitude (2.5 to 20%), excitation frequency (0.1 Hz to 50 Hz) and magnetic flux density (0 to 750 mT) superimposed on large static pre-strain (21%). The experiment was designed on the basis of standardized test methods for rubber-like materials, described in ASTM D395 [53] and ISO 7743 [52]. The test rig integrated a relatively compact UI-shaped electromagnet to realize magnetic flux density up to1T. Experiments were designed to evaluate magneto-mechanical properties of the isotropic as well as anisotropic MRE samples, fabricated with 30% volume fraction of iron particle. The measured data were analyzed to obtain hysteresis strain-stress curves, and dynamic properties in terms of storage modulus (E') and loss factor (η), and their dependency on the loading conditions together with the applied magnetic flux density. The results are discussed in view of the MR effect and the role of anisotropy of the MRE.

3.2 Experimental Methods

3.2.1 MRE Samples

Isotropic and anisotropic samples of MREs were fabricated in the laboratory with 30% volume concentration of the ferromagnetic particles using the methods described in [5]. Briefly, the spherical carbonyl iron powder (CIP) with diameter ranging from 3.9 to 5 μm were poured into the silicone rubber (Eco-Flex Series, Smooth-on) as the matrix material. The ingredients were blended thoroughly in a glove box for approximately 5 minutes and degassed in a vacuum chamber for 5 minutes under 736 mmHg pressure. The blend was then poured in two sets of plexiglass cylindrical molds (diameter=8 mm; height =100 mm). One set was permitted to cure for nearly 24 hrs at room temperature, while the second set was cured for three hours in the presence of a uniform magnetic flux density of 1.2 T, which was generated by an electromagnet (DXSBV-100; Dexing Magnet Tech. Co., China).

3.2.2 Electromagnet design

Characterization of dynamic behavior of an MRE in the squeeze mode involves of simultaneous applications of the unidirectional magnetic field and the mechanical load. A UI-shaped electromagnet was designed, which could be integrated into an electrohydraulic material test system (MTS) and permit positioning of the MRE specimens within the two air gaps. The design parameters of the electromagnet were identified via parametric optimization so as to realize flux density up to 1 T, with weight constrained to 5 kg. The electromagnet was fabricated with U- and I-shaped cores made of laminated cold-rolled grain-oriented electrical steel (M6-C5; Laminations Specialties, Chicago, USA) and three copper conductor (AWG 17) coils, as schematically shown in Figure 3.1. The coils with 1135 turns permitted airgap flux density in excess of 1 T, when powered by a 100 V and 10 A power supply. The U- and I-shaped cores were fixed to the lower and upper mounts, respectively, which were constructed with a non-magnetic material (ABS plus-P430) to prevent the magnetic flux leakage from the magnetic core circuit. The electromagnet design provided two air gaps for accommodating the MRE samples, as shown in the Figure 3.1.

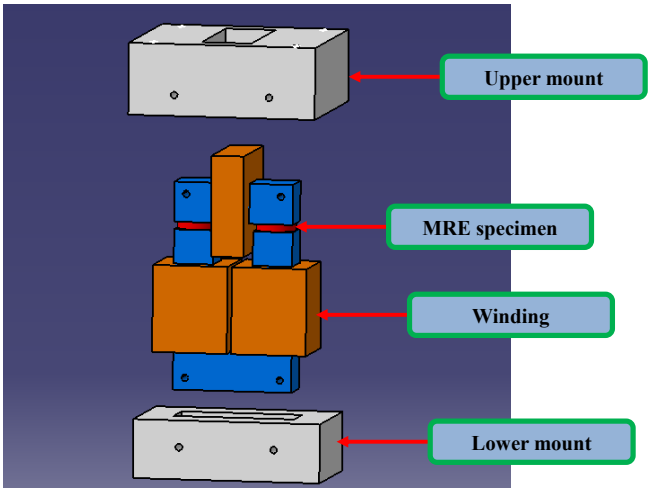

Figure 3.1 Schematic of the UI-shaped electromagnet with upper and lower mounts and MRE specimens.

3.2.3 Experimental setup and methods

The electromagnet with the lower and upper mounts, pictorially shown in Figure 3.2(a), was installed on a servo-hydraulic material test system (MTS) for uniaxial compression of the MRE samples. The lower mount of the electromagnet was fixed to the actuator, while the upper mount

was attached to a fixed beam via a 9 kN load cell. The upper and lower mounts with the I-shaped and U-shaped cores, respectively, were carefully aligned to ensure uniform lengths of both the air gaps.

The MTS was operated in the displacement feedback control mode and the compression displacement (strain) was measured by a Linear Variable Differential Transformer integrated within the actuator. The displacement and force signals were acquired in the LabView platform via a National Instruments Data Acquisition board, as shown in Figure 3.2(b). A thermocouple was installed on the I-core to monitor surface temperature of the coil, and a large size fan was used, when needed, to ensure that the core temperature remains near 35℃±5℃.

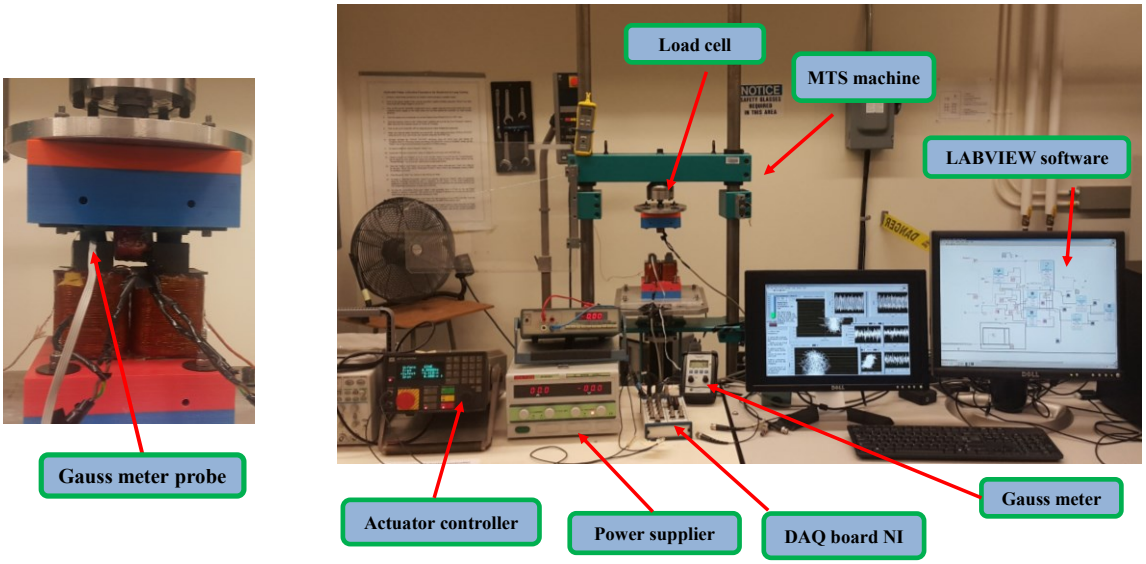

(a) (b)

Figure 3.2 Pictorial views of electromagnet with upper and lower mounts, and MRE specimens in the gaps (a), and uniaxial compression test setup (b).

The experiment design involved three different series of experiments. The first series of experiments was designed for measuring the magnetic flux density both in absence and presence of MRE in the gap. The measurements were conducted at different levels of gap length and current, ranging from 2 to 8 mm and 0 to 6 A, respectively. In the first step, a Gauss meter probe was inserted into a pure rubber sample, which was positioned in one of the air gaps. For each gap length, coil current was gradually varied using a 10 A and 100 V power supply and the magnetic flux density in the air gap was read from the Gauss meter. In the second step, the Gauss meter

probe was placed inside a cylindrical isotropic MRE specimen by slightly piercing the specimen from middle point as shown in Figure 3.2(a). The magnetic flux density induced inside the MRE could thus be measured accurately and directly from the Gauss meter. To the best of the authors' knowledge, the proposed approach to measure directly magnetic flux induction inside a magneto-active material has not been implemented. The same approach was also implemented for the anisotropic MRE specimen. The data were used to determine a relationship among the magnetic flux density, coil current and the gap length, which was subsequently used to derive the related coil current for realizing the desired flux density during the dynamic characterizations of the MRE specimens.

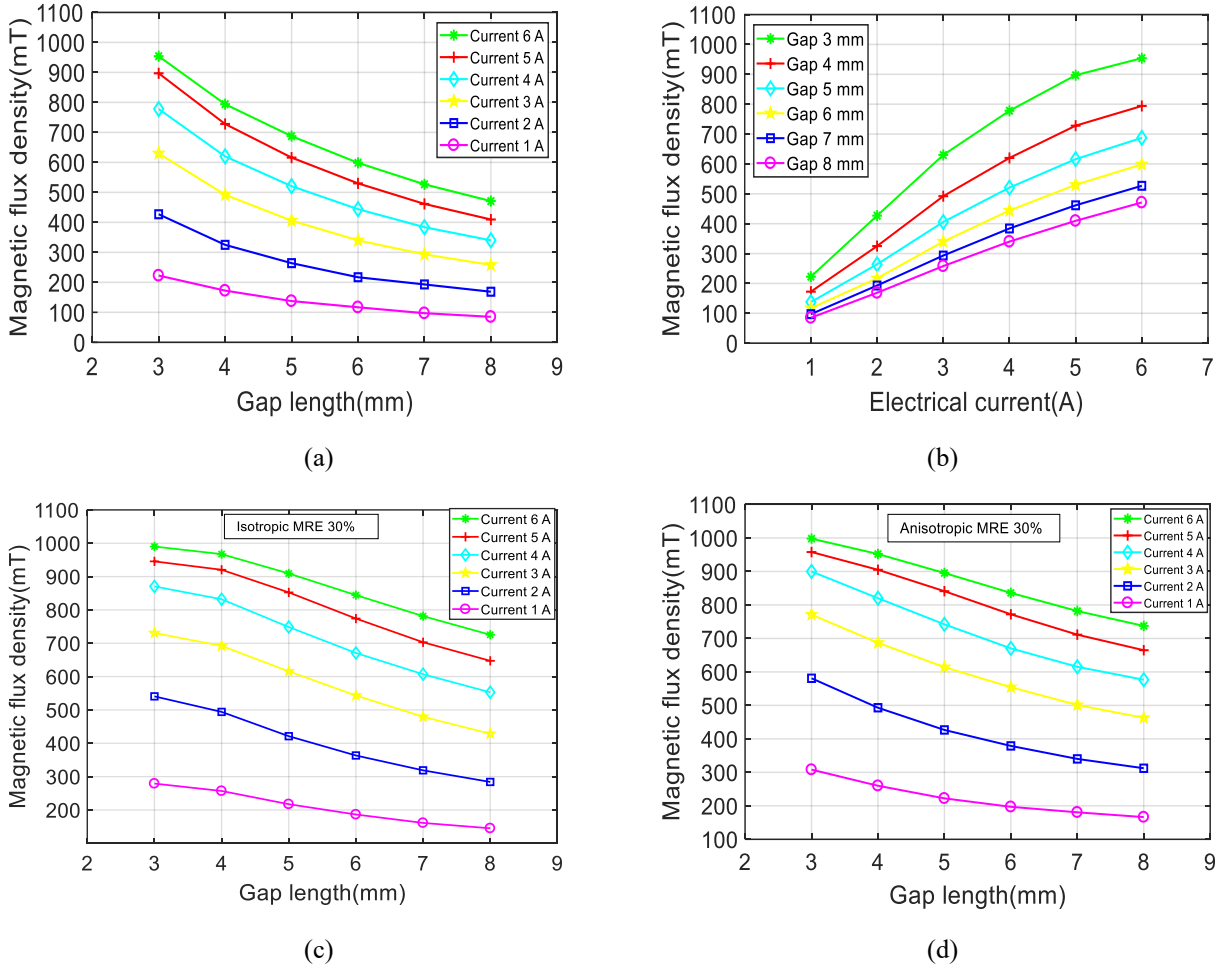

Figure 3.3 Influence of gap length and coil current on the air gap magnetic flux density: (a, b) without MRE specimens; (c) with isotropic MRE specimens; and (d) with anisotropic MRE specimen.

Figure 3.3(a) and 3.3(b) illustrate variations in the magnetic flux density as functions of the gap length and applied current in the absence of the MRE specimen. The results suggest that the

magnetic flux density increases with increase in current and decreases with increase in the gap length in a nonlinear manner. Saturation of the flux density is also evident under current exceeding 5 A, especially with lower gap length. It can be further inferred that the effective magnetic permeability within the air gap changes from nonlinear to a linear regime as the gap length increases, as seen in Figure 3.3(b). Figure 3.3(c) and 3.3(d) show variations in the magnetic flux density, when the isotropic and anisotropic MRE specimens, respectively, are positioned within the air gaps. The results show considerably higher magnetic flux induction due to MRE specimens when compared to that without the specimens. This is due to higher permeability of the MRE compared to the air. Relatively higher magnetic flux density could be observed for the anisotropic specimen compared to the isotropic specimen, particularly under lower currents and larger gap lengths. With increase in the gap length, the iron particles within an anisotropic specimen tend to become more aligned with direction of the magnetic field, especially under low strain amplitude (large gap), which likely contributed to relatively higher magnetic flux density with the anisotropic specimen. An increase in the strain amplitude (lower gap length) tends to disturb alignment of the particles leading to lower the magnetic permeability and thus the flux density of the anisotropic MRE, which has also been observed in a few previous studies [26, 79].

The second series of experiments, involved two steps, was conducted to characterize the magnetic force between two poles of the electromagnet in the absence of MRE specimen in the gap as a function of the air gap length and the applied current ranging from 2 to 8 mm and 0 to 6 A, respectively. For each level of current, the magnetic force developed by the electromagnet was measured by the load cell for varying air gap in both static and dynamic regime. Since the compression mode characterization of MRE involves applications of both the magnetic field and the mechanical loading in the same direction, the measured force comprises the magnetic force developed by the magnetic poles of the electromagnet apart from the viscoelastic force attributed to compression loading of the MRE. The flux and force data acquired in this series of experiments were further scrutinized to establish a systematic methodology that allow predicting the dynamic magnetic force as a function of magnetic flux density, displacement amplitude, and frequency. This method thus permits compensating for the contribution of the correct nonlinear magnetic force to the total measured force during compression mode characterization of MRE.

The third series of experiments was designed for characterization of dynamic properties of the isotropic and anisotropic MRE samples in the compression mode on the basis of standardized methods (Method B) described in ISO 7743 [52]. The method B in this standard recommends bonding the test specimen to the compression plates. It should note that characterization of MREs considering bonding the MREs between the compression plates are better-suited, and can provide more practical and reliable guidance for design and development of many applications based on MREs, such as laminated MRE-based vibration isolators and mounts, when compared with Method A, in which test specimen should be lubricated. For this purpose, cylindrical specimens (diameter=18 mm; thickness=8 mm) of the MREs were firstly cut from the isotropic and anisotropic samples. Then, two MRE specimens were bonded to upper edges of the U-core of the electromagnet using a very thin layer of an industrial adhesive. Each specimen was subjected to 21% pre-strain prior to the dynamic loading. A factorial design of experiments was used considering four different levels of harmonic strain amplitude (2.5, 5, 10 and 20%), five levels of excitation frequency (0.1, 1, 10, 30, and 50 Hz) and six levels of the magnetic flux density (0, 150, 300, 450, 600 and 750 mT). The data acquired during the first series of experiments were used to determine the coil current to realize a desired level of the magnetic flux density. Both the displacement and force signals were acquired in the LabView at a sampling rate ranging from 50 Hz for excitations up to 1 Hz to 5000 Hz for higher excitation frequency of 50 Hz. The data were acquired for four consecutive loading/unloading cycles for each test, and averaged for characterizing the mean stress-strain characteristics of the specimens. The mean measured force was systematically corrected for the magnetic force corresponding to magnetic flux induction inside MRE, frequency and strain amplitude used in each test. Finally, the viscoelastic MRE force was obtained and further analyzed to obtain the stress-strain curves as well as properties of both the isotropic and anisotropic MRE specimens such as relative MR effect, storage modulus (E') and loss factor (η) using the method stipulated in ISO 7743 [52].

3.3 Results and discussion

The measured stress-strain properties of the isotropic and anisotropic MREs, invariably, revealed hysteresis attributed to their viscoelastic nature. The measured data were analyzed to determine the dynamic properties as functions of the strain amplitude, strain rate and the magnetic flux density. These included the damping capacity or energy dissipation per cycle in terms of the area bounded by the hysteresis loop, equivalent stiffness represented by slope of the major axis of the

hysteresis loop that directly relates to the storage modulus, strain stiffening and softening, and peak stress. The results showed strong dependence of the stress-strain behaviors on the strain amplitude, loading frequency and magnetic flux density in addition to the anisotropy feature. These dependencies are illustrated and discussed individually in the following sub-sections.

3.3.1 Strain amplitude effect

Figure 3.4(a) and 3.4(b) illustrate steady-state stress-strain characteristics of the isotropic MRE during a loading/unloading cycle considering different strain amplitudes and zero magnetic field. The results, presented for excitations at 0.1 and 1 Hz, as examples, show nonlinear asymmetric hysteresis behavior during loading and unloading, which becomes more pronounced with increasing strain amplitude. The hysteresis loops are observed to be nearly symmetric and elliptical under the low strain amplitude of 2.5% at the low frequency of 1 Hz, suggesting mostly visco-elastic behavior of the MRE. This was however not evident at the low frequency of 0.1 Hz. Moreover, the loops rapidly become asymmetric with strain amplitude exceeding 5%. Increase and decrease in the spacing between the iron particles during loading and unloading, respectively, contribute to the nonlinearity and asymmetry in the elastic stress. This tendency is evident for both the excitation frequencies in Figure 3.4(a) and 3.4(b).

Moreover, the slope of the major axis of the hysteresis loop, which may be regarded as the equivalent stiffness, decreases with increase in the strain amplitude. This is partly due to the strain amplitude softening phenomenon, also known as the Fletcher-Gent effect [80] or the Payne effect [81]. The degree of softening increases with increase in the strain amplitude. This softening effect is mainly due to weakening of the bond between the filler particles as well as between the rubber matrix and the filler particles, which has been widely reported for natural filled rubbers [81]. Comparable hysteretic stress-strain properties were also obtained for the anisotropic MRE, which exhibit similar dependence on the strain amplitude, as seen in Figure 3.4 (c) and 3.4(d).

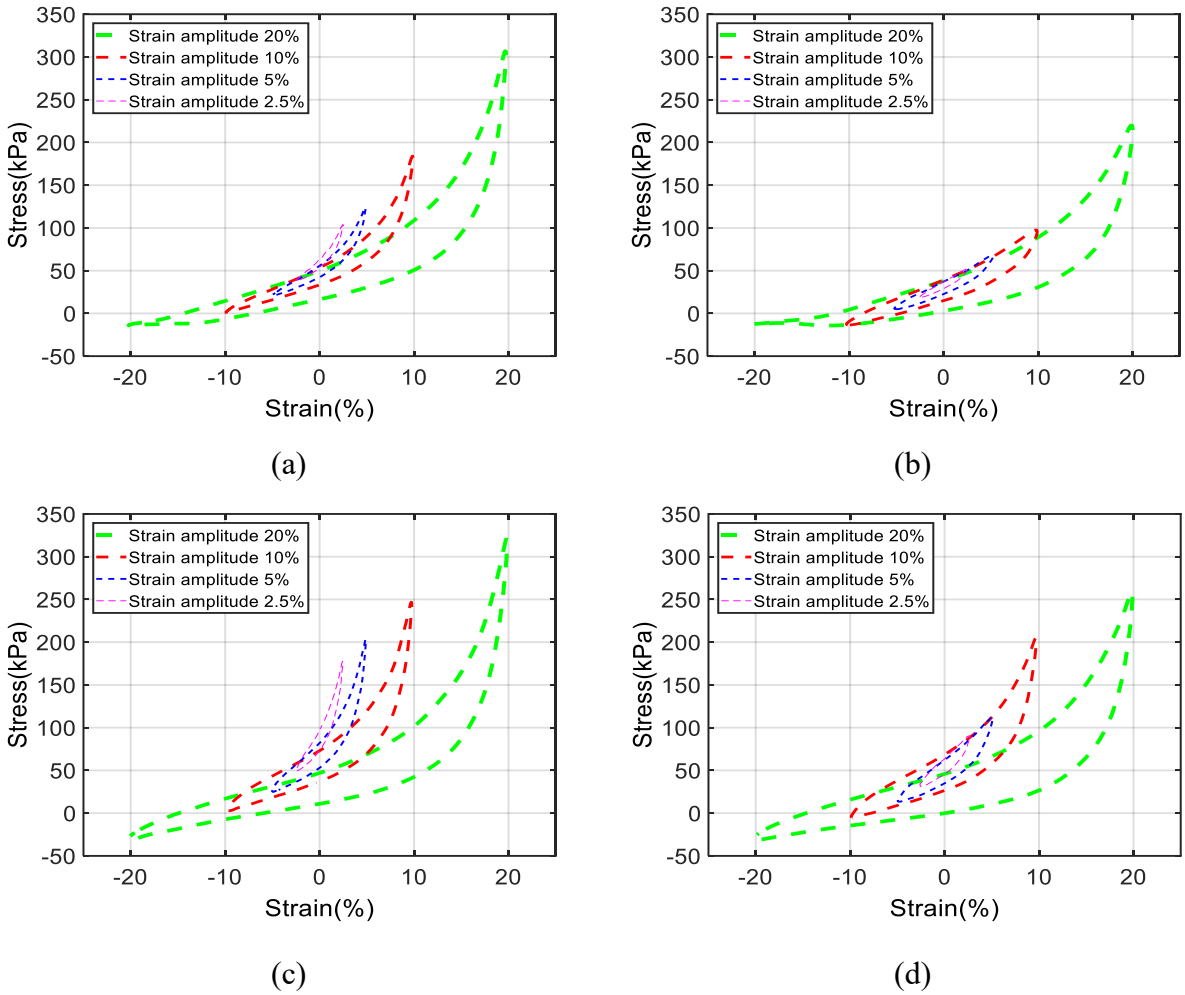

Figure 3.4 Effect of strain amplitude on the stress-strain characteristics of MREs at different excitation frequencies (a) isotropic, 0.1 Hz; (b) isotropic, 1 Hz; (c) anisotropic, 0.1 Hz; (d) anisotropic, 1 Hz (magnetic flux density, B=0).

Apart from the Payne effects, the observed strain-amplitude softening can be in part attributable to Mullins effect, as the experiments were carried out according to the ISO 7743 [52], which does not recommend applying any preconditioning practice to the sample prior to compression testing. Mullins effect defined as stress softening behavior of rubbers which occurs when (i) they experience softening in the first few cycles at a constant amplitude, and (ii) they experience new strains that are higher than those in the past. Unlike the Payne effect which only occurs for filled elastomers, when applied strain amplitude exceeds 0.1-0.15% [82], the Mullins effect occurs for both filled and unfilled elastomers at relatively higher level of strain. Even though preconditioning practice can remove the Mullins effect in scientific experimental characterization

of rubber-like materials, the complex manufactured rubber-like products cannot simply undergo large preconditioning practice before their usage. Since, this leads to in homogeneously distributed softening and thus yielding a location dependent material characteristic [83]. Thus, the results of the presented experimental data in this dissertation can be effectively employed to develop dynamic viscoelastic constitutive models considering both Payne and Mullins effects for design and development of practical and reliable MRE-based devices. Nonetheless, it should note that the transient effect associated with stress-softening due to the Mullins effect at each constant strain amplitude was not recorded. Since, in this dissertation, our experiment design was limited only to the steady-state behavior of MREs.

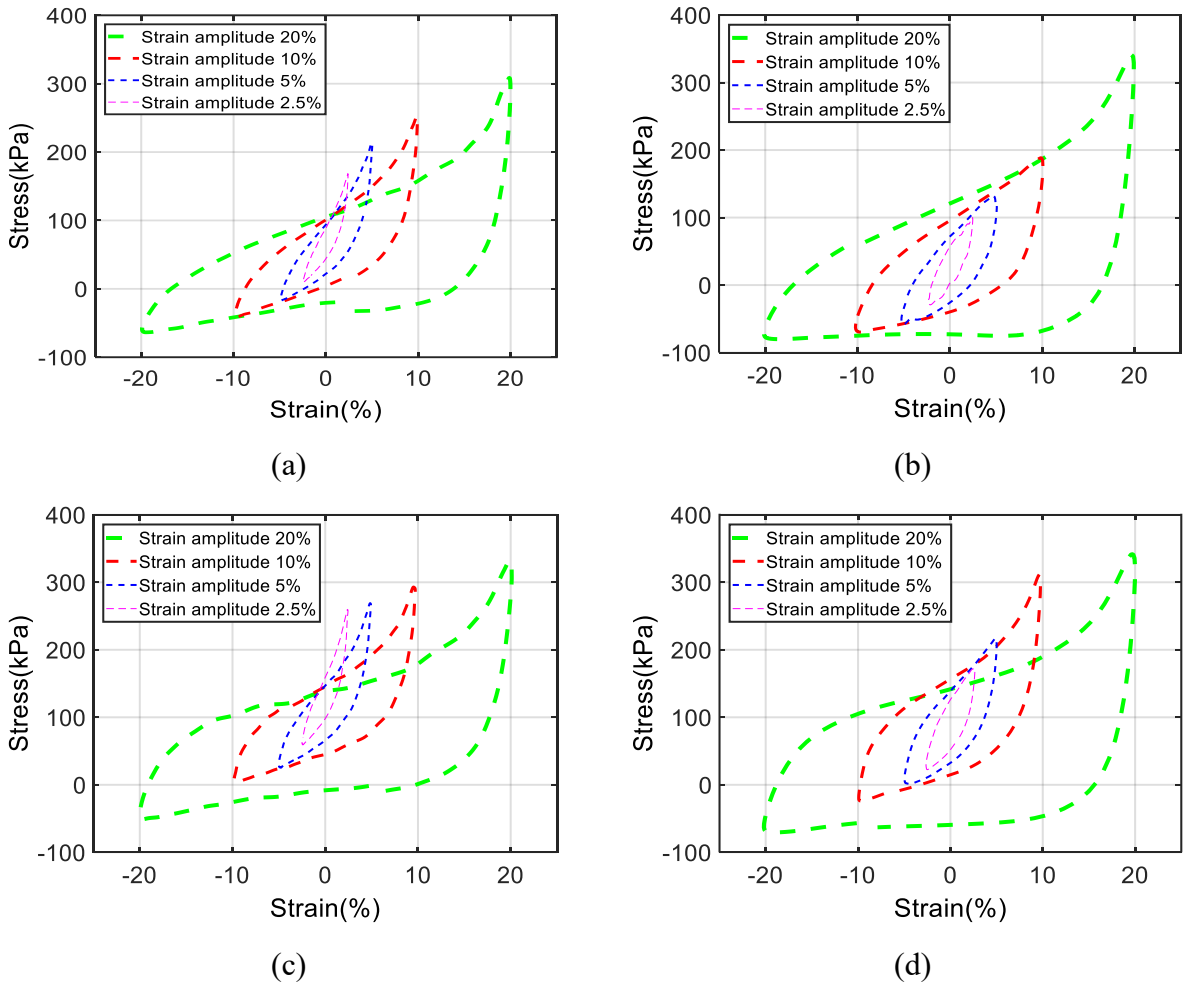

Figure 3.5 Effect of strain amplitude on the stress-strain characteristics of MREs at different excitation frequencies (a) isotropic, 0.1 Hz; (b) isotropic, 1 Hz; (c) anisotropic, 0.1 Hz; (d) anisotropic, 1 Hz (magnetic flux density, B=750 mT).

Figure 3.5 illustrates the effect of strain amplitude on the stress-strain characteristics of the isotropic and anisotropic MREs under the action of a magnetic field (flux density, *B*=750mT). The results reveal more pronounced strain-softening in the presence of magnetic field when compared to the zero-field stress-strain behavior (Figure 3.4). The MREs subject to the magnetic field, yield considerably higher energy dissipation of the MREs, as it is evident from the relatively larger area bounded by the hysteresis loops in Figure 3.5. Moreover, both types of the MREs undergo considerable tension, when strain amplitude exceeds 5%. Higher strain amplitude induces relatively higher peak negative stress (tension). The peak negative stress is considerably higher for the magnetically activated isotropic and anisotropic MREs, when compared to that without the magnetic field. This can be attributed to the magnetic field-stiffening of the MRE that limits recovery or unloading of the specimen. The peak negative stress is relatively greater for the isotropic MRE compared to the anisotropic MRE.

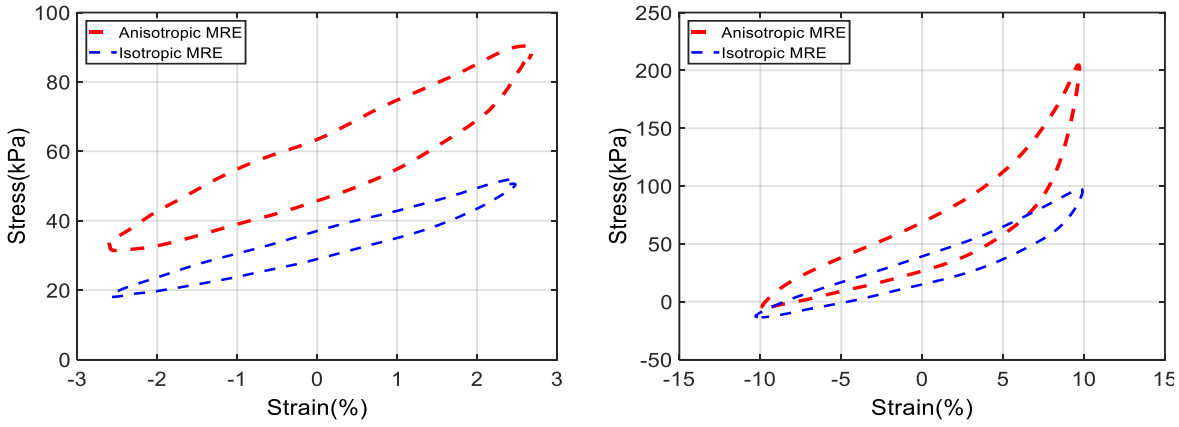

Figure 3.6 Effect of anisotropy on the stress-strain characteristics of the MRE under different strain amplitudes (ε) at a frequency of 1 Hz in the absence of magnetic field: (a) ε=2.5%; (b) ε=10%.

Despite the comparable trends observed for the isotropic and anisotropic MREs, the results suggest significant effect of anisotropy. As an example, Figure 3.6(a) and 3.6(b) compare the stress-strain properties of the isotropic and anisotropic MREs subjected to 2.5% and 10% strain amplitude excitations at a frequency of 1 Hz in the absence of the magnetic field. The results show that the anisotropy yields notably higher equivalent stiffness and greater energy dissipation, when compared to those of the isotropic MRE, irrespective of the strain amplitude and frequency. This is due to higher magnetic interactions among the iron particles oriented in column-like structures

in the anisotropic MRE, which likely contribute to relatively higher stiffening and dampening behaviors. These also cause greater asymmetry in the stress-strain characteristics even under the lower strain amplitude of 2.5%. The observed stiffening and dampening behavior due to anisotropy have also been observed for the MRE in the static compression mode [45]. Furthermore, the degree of anisotropy is known to strongly depend on the particle volume concentration of the MRE. It has been reported that anisotropic MREs with greater iron particle volume fraction yield properties comparable to those of the isotropic MRE with the same particle volume fraction [84].

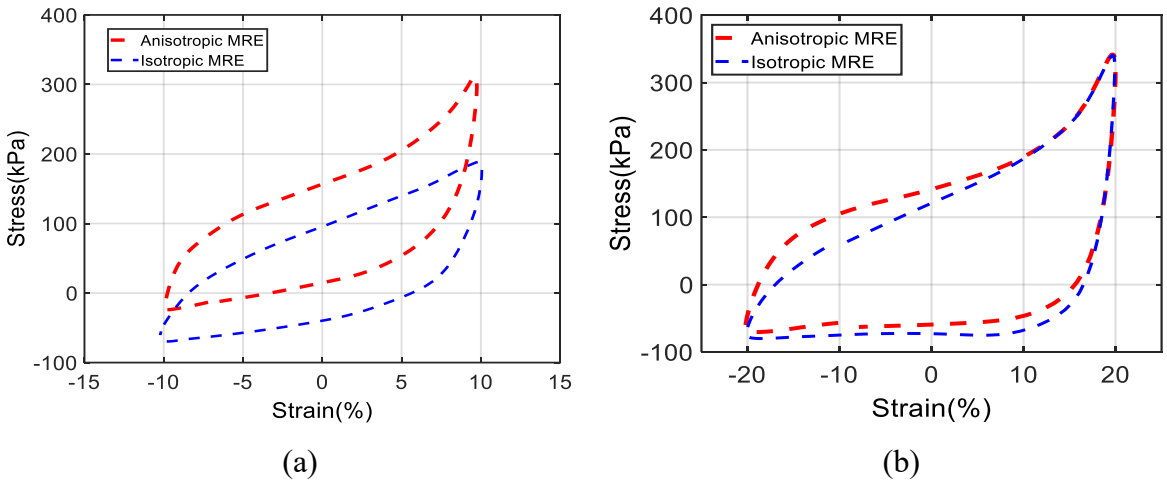

Figure 3.7 Effect of anisotropy on the stress-strain characteristics of the MREs under different strain amplitudes (ε) at a frequency of 1 Hz and magnetic flux density of 750 mT: (a) ε=10%; (b) ε=20%.

Figure 3.7(a) and 3.7(b) further demonstrate the effect of anisotropy on the dynamic behavior of the MREs under the magnetic flux density of 750 mT. The results are presented for two strain amplitudes of 10% and 20%, respectively. The results suggest relatively higher equivalent stiffness of the anisotropic MRE compared to the isotropic MRE under the lower strain amplitude excitation (10%). Both the MREs, however, exhibit comparable peak stress and slope of the stress-strain curves under the 20% strain excitation, while the anisotropy yields only slightly higher energy dissipation.

3.3.2 Magnetic field effect

Figure 3.8 illustrates the effect of magnetic flux density on the stress-strain responses of the isotropic and anisotropic MREs subjected to 5% and 10% strain amplitudes at two different frequencies (f=1 Hz and f=20 Hz). The results are presented for different magnetic flux densities, ranging from B=0 mT to B=750 mT.

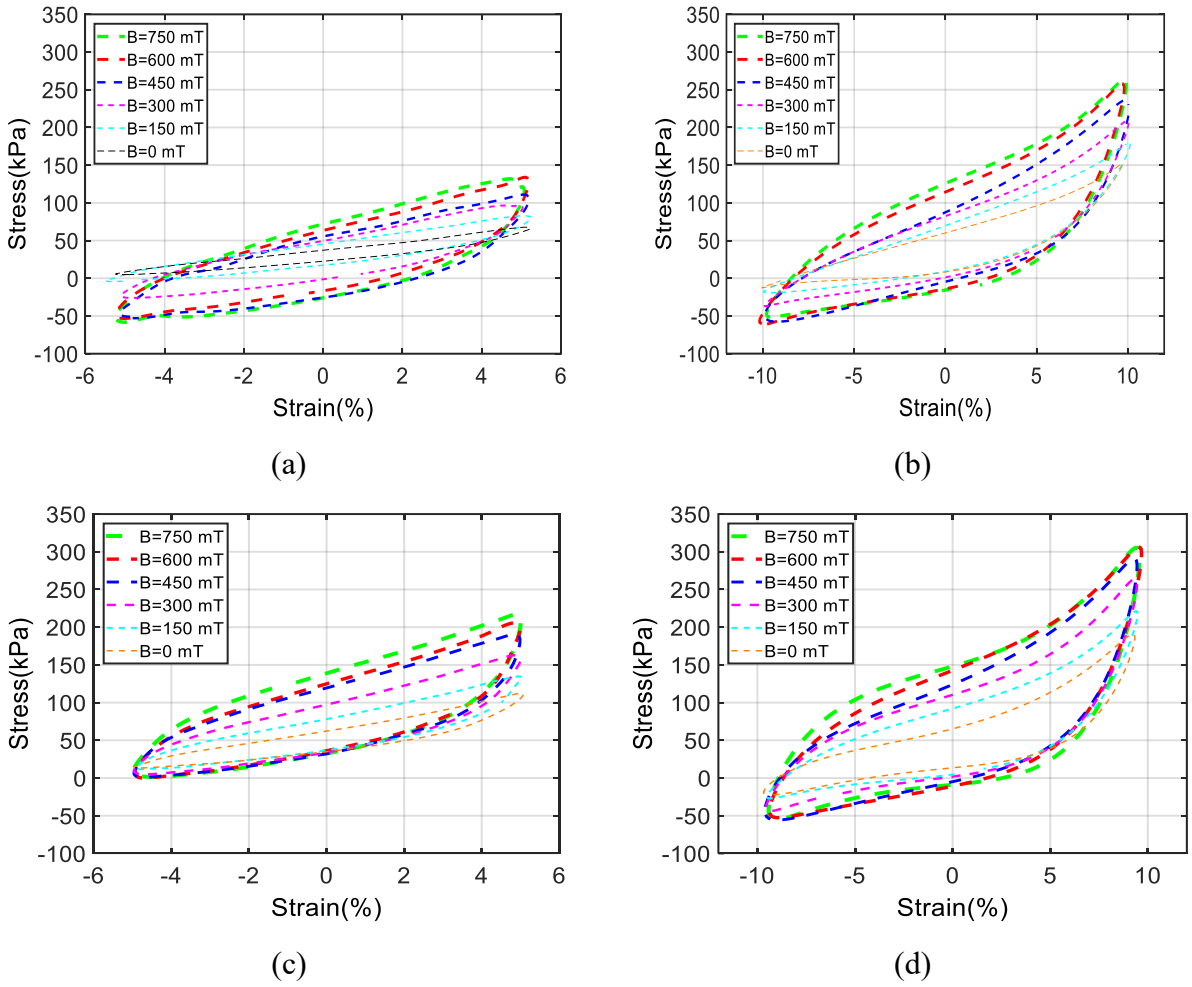

Figure 3.8 Effect of magnetic flux density on the stress-strain characteristics of the MREs under different strain amplitude excitations (a) isotropic, f=1 Hz, ε=5%; (b) isotropic, f=20 Hz, ε=10%; (c) anisotropic, f=1 Hz, ε=5%; (d) anisotropic, f=20 Hz, ε=10%.

The results show that the major axis slope and the area enclosed by the hysteresis loops increase with increase in the magnetic flux density, irrespective of the strain amplitude and the frequency. These suggest magnetic field stiffening of the MRE similar to the strain rate stiffening. The rates of increase in the equivalent stiffness and energy dissipation with the magnetic flux density, however, decrease with increasing magnetic field, which suggest magnetic saturation of the MREs.

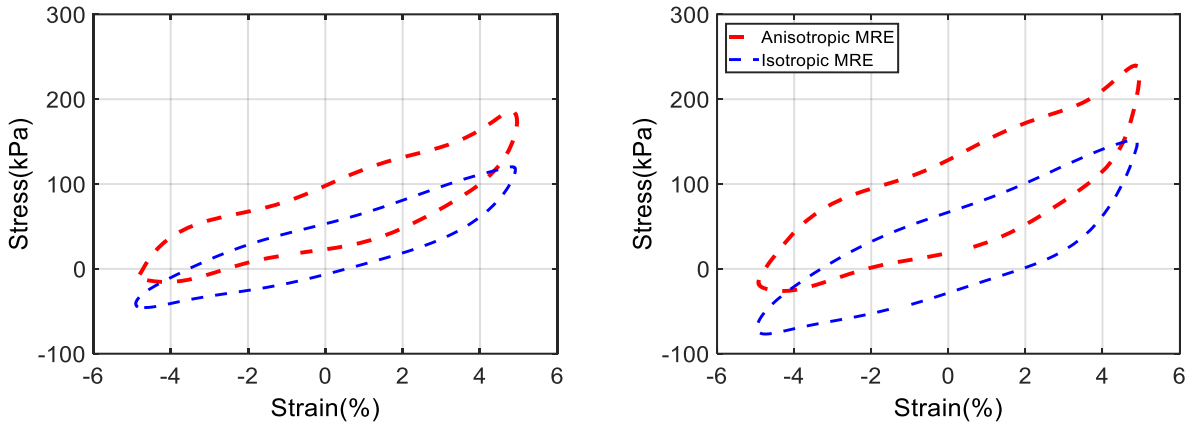

(a) (b)

Figure 3.9 Effect of anisotropy on the stress-strain characteristics of MREs subject to 5% strain and different magnetic flux density: (a) B = 300 mT; and (b) B = 600 mT (f = 10 Hz).

Moreover, the anisotropic MRE yields considerably higher peak stress during loading compared to the isotropic MRE, irrespective of the strain amplitude and frequency. This is likely due to relatively greater confinement of the matrix with arranged chains of magnetic particles during loading, where more closely spaced particles contribute to non-linear increase in the elastic stress. This confinement of the matrix becomes more pronounced with increase in the attraction among the particles under a higher magnetic flux density, which causes greater stiffening during loading and the stress to increase more sharply. Both isotropic and anisotropic MREs exhibit comparable slopes of the major axis under excitation at the higher frequency of 10 Hz, as shown in Figure 3.9, while the anisotropy yields slightly higher energy dissipation.

The controllable magnetic field dependent stiffness and damping properties of isotropic and anisotropic MREs can be used to develop semi-active or active vibration control MRE-based devices in many engineering applications. Some application examples include controllable seat cushions for helicopter pilots and vehicle drivers, adaptive vibration absorber, smart laminated bearing isolator, variable stiffness tires, automotive impact crashworthiness as well as prosthetic devices such as artificial knee and medical shoes, in addition to microscopic applications such as sensors and actuators [56, 57, 85, 86].

3.3.3 Strain-rate effect

Apart from the strain amplitude and magnetic flux density, the data revealed notable effect of the strain rate (excitation frequency). As an example, Figure 3.10(a) and 3.10(b) compare the stress-

strain characteristics of the isotropic MRE obtained under different excitation frequencies, ranging from 1 to 30Hz.

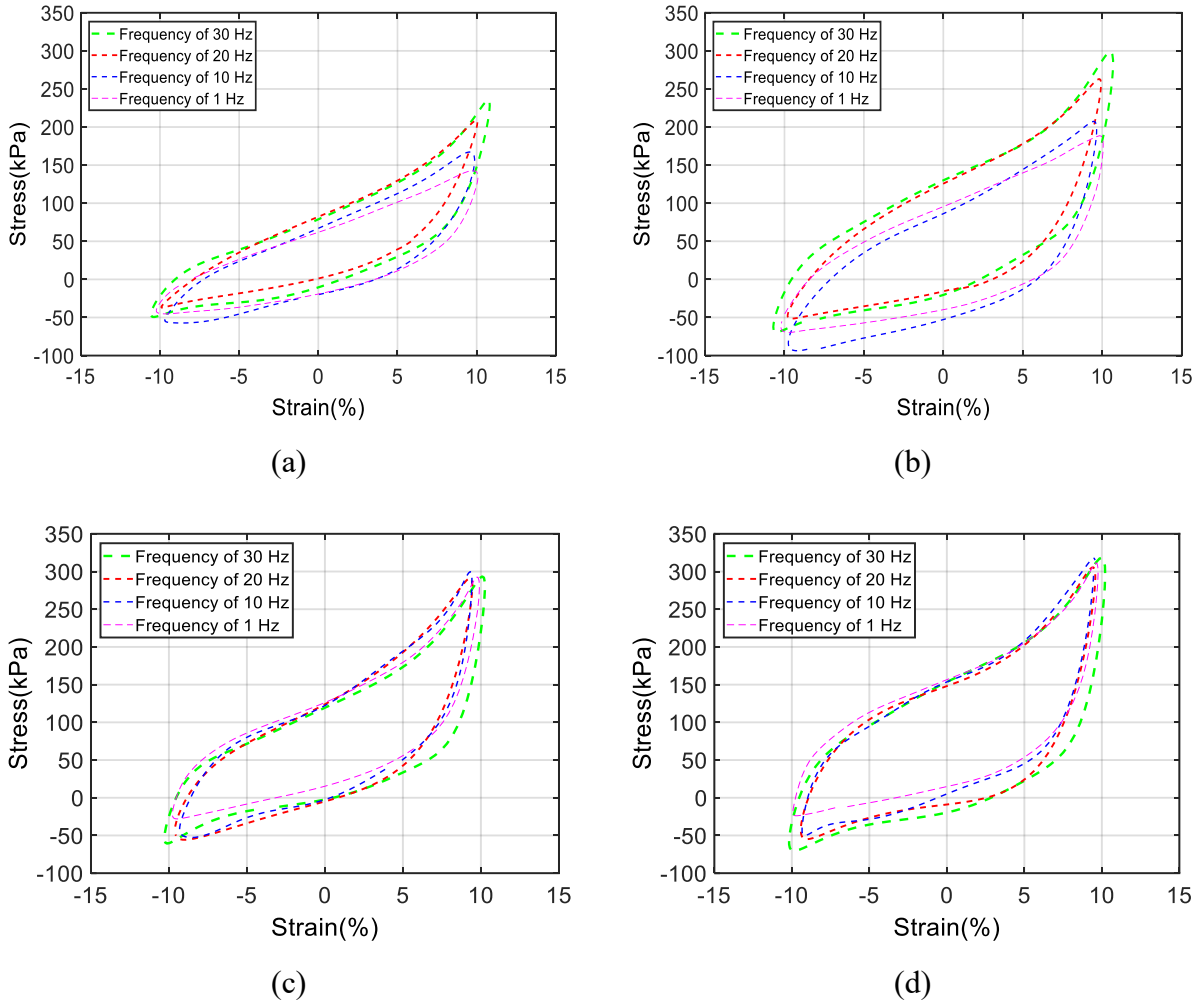

Figure 3.10 Effect of loading frequency on the stress-strain characteristics of MREs under strain amplitude of 10%: (a) isotropic, B = 300 mT; (b) isotropic, B = 750 mT; (c) anisotropic, B = 300 mT; (d) anisotropic, B = 750 mT.

The results, presented for magnetic flux densities of B = 300 mT and B = 750 mT and ε = 10%, show increase in the equivalent stiffness with increasing frequency, suggesting a strain-rate stiffening effect. The peak stress observed during loading also increases with increase in the strain rate. These effects, however, diminish at excitation frequencies above 20 Hz. The strain rate or frequency dependency of the equivalent stiffness, however, is relatively small in case of the anisotropic MRE, when compared to the isotropic MRE, as seen in Figure 3.10(c) and 3.10(d). The effect is particularly insignificant under the higher strain amplitude. The excitations at a higher

frequency also caused the isotropic as well as anisotropic MREs to undergo higher tension during unloading.

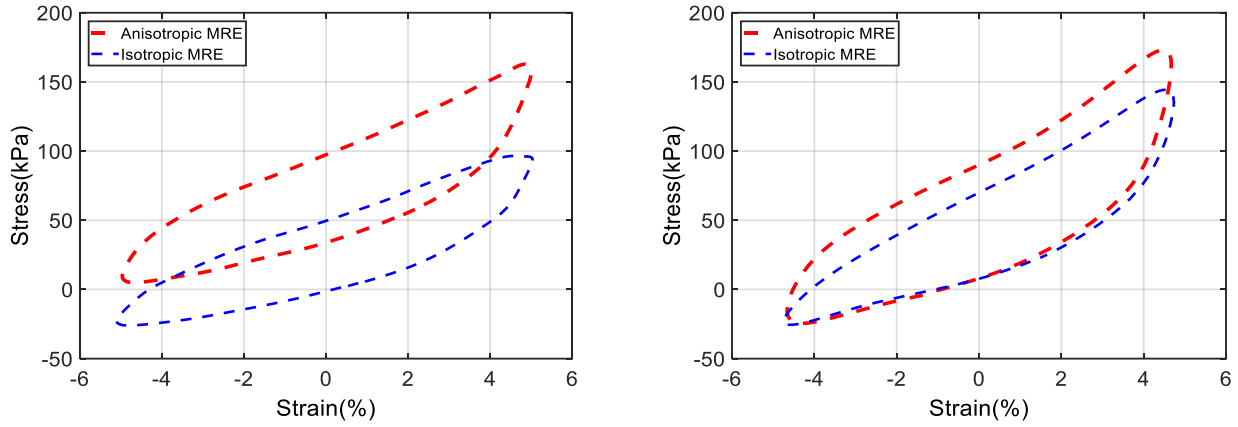

Figure 3.11 Effect of anisotropy on the stress-strain characteristics of MREs subject to 300 mT magnetic flux density and 5% strain at different frequencies: (a) f= 1 Hz; and (b) f= 30 Hz.

Higher strain rate, however, enhances the energy dissipation per cycle by the anisotropic MRE compared to the isotropic MRE, as shown in Figure 3.11. The figure compares the stress-strain characteristics of the isotropic and anisotropic MREs subject to 5% strain excitation at frequencies of 1 and 30 Hz with B = 300 mT. Greater tension of the anisotropic MRE is also evidenced under excitation at 30 Hz compared to that at 1 Hz.

3.3.4 Storage modulus and loss factor

The effects of magnetic field, strain and strain-rate on the dynamic properties of the MREs in the compression mode are further assessed in terms of the storage modulus (E') and the loss factor (η), defined as the ratio of the loss modulus (E'') to the storage modulus. The measured data were analyzed to determine E'' using the standardized method for compression mode properties of rubbers, described in ISO 4664-1[87]. Owing to the considerable nonlinearity in the measured stress-strain data, the storage modulus was estimated as the ratio of peak-to-peak stress to peak-to-peak strain, as suggested for rubbers in [88]. Figure 3.12(a) to 3.12(c) illustrate variations in the storage modulus and loss factor of both the isotropic and anisotropic MREs over the ranges of strain amplitude, excitation frequency and flux density, respectively, considered in the study. The results are presented for selected values of other input factors, as examples.

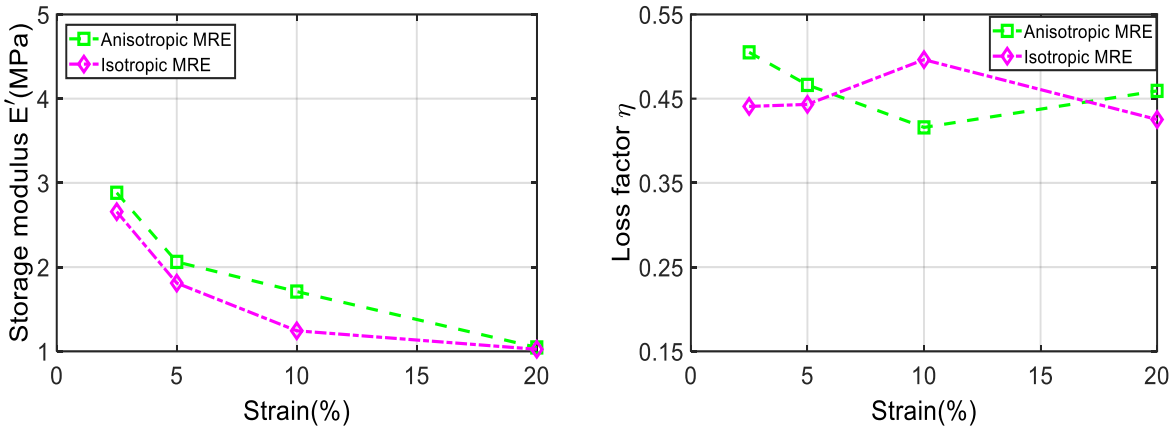

(a)

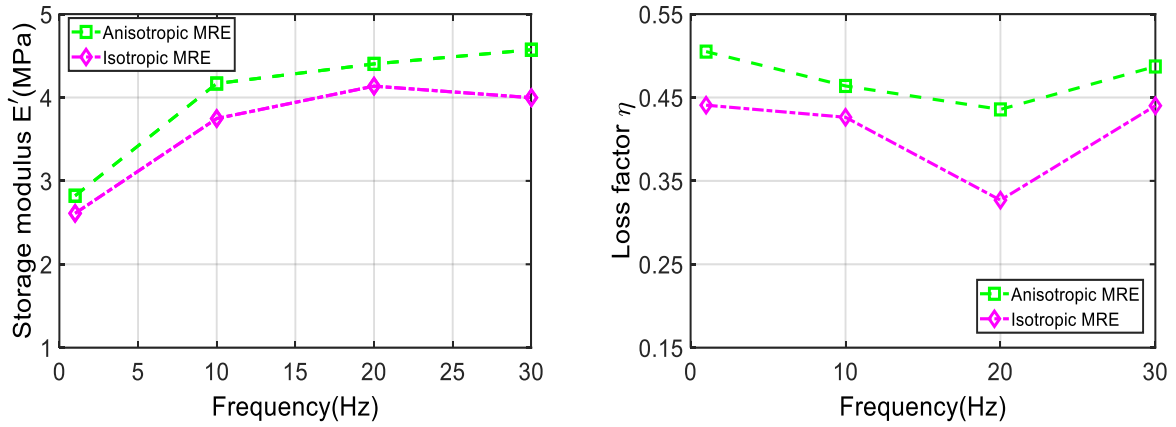

(b)

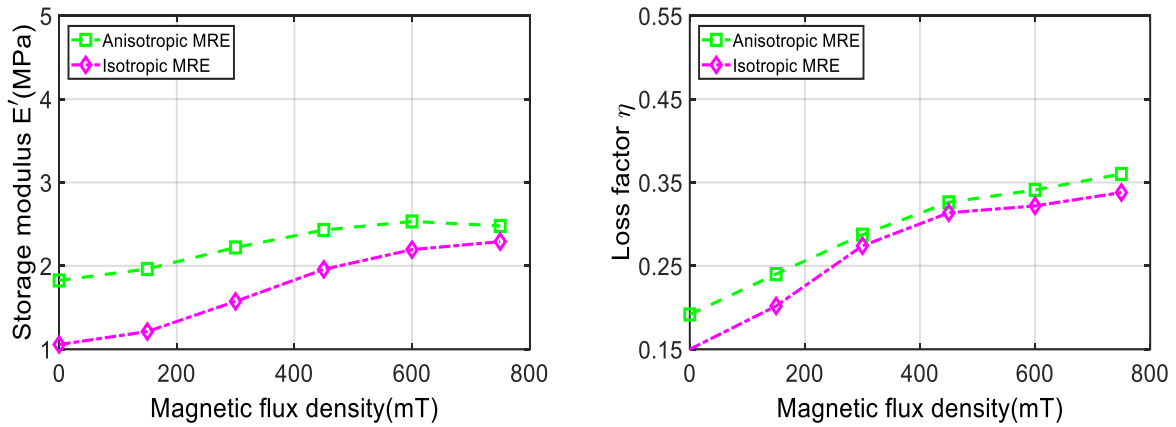

(c)

Figure 3.12 Effects of (a) strain amplitude ε (B = 300 mT; f = 1 Hz); (b) frequency f (B = 750 mT; ε = 2.5%); and (c) magnetic flux density B (f= 0.1 Hz; ε = 5%) on the storage modulus and loss factor of the isotropic and anisotropic MREs.

The results, presented in Figure 3.12(a) for f=1 Hz and B= 600 mT, show that the anisotropy contributes to notably higher storage modulus compared to the isotropic MRE. The storage moduli of both the anisotropic and isotropic MREs decrease considerably with increase in the strain amplitude, and approach comparable values under the high strain input of 20%. This is consistent with decreasing equivalent stiffness under increasing strain amplitude observed in Figure 3.4 and Figure 3.5, which is also denoted as strain amplitude softening or the Payne effect [15]. Higher strain deformation causes greater lateral bulging of the MRE and reduced magnetic permeability of the anisotropic MRE. The effect of anisotropy thus diminishes under the higher strain amplitude excitation.

The loss factor of both the MREs lie in the 0.42 to 0.5 range for B=600mT and the strain amplitudes considered, as seen in Figure 3.12(a). A clear pattern with variations in the strain amplitude is not evident, which is partly due to the definition of the loss factor. The loss factor may be considered nearly strain-independent. The anisotropy, however, yields relatively higher loss factor in the entire ranges of frequency and flux density, as seen in Figure 3.12(b) and 3.12(c), respectively. The storage modulus of the anisotropic MRE is also considerably higher than that of the isotropic MRE in the considered ranges of frequency and flux density, suggesting relatively higher strain-rate and magnetic field-stiffening of the anisotropic MRE, as observed in Figure 3.8 and Figure 3.10. Although the results in Figure 3.12(b) and 3.12(c) are presented for ε = 2.5% and B = 750 mT, and ε = 5% and f = 0.1 Hz, respectively, similar trends were observed under other input conditions. The storage moduli of both types of MREs increase in an exponential manner with increasing frequency and magnetic flux density and approach saturation near f = 20 Hz or B = 600 mT. The anisotropy, however, leads to saturation at relatively lower level of flux density, which may be attributed to its relatively higher magnetic permeability. The storage modulus of the isotropic MRE decreases slightly in the 20 to 30 Hz frequency range, which has also been observed for natural rubbers subject to compression loading [89]. This also causes the loss factor to increase in the 20 to 30 Hz range, as seen in Figure 3.12(b). The loss factor also increases with increasing flux density and tends to saturate near B = 600mT. Furthermore, the strain-rate softening behavior of loss factor due to frequency up to 20 Hz has also been observed in previous studies on compression characterization of both isotropic and anisotropic MRE superimposed on zero pre-strain condition [6, 23].

The effects of magnetic flux density on the storage modulus and loss factor of the MREs are further evaluated in terms of the relative MR effects in view of the storage modulus ($RMRS_B$) and the loss factor ($RMRL_B$). The relative MR effects are defined for a given magnetic flux density, as:

$$\%RMRS_B = \frac{E'_B - E'_{B=0}}{E'_{B=0}} \times 100 \quad (3\text{-}1)$$

$$\%RMRL_B = \frac{\eta_B - \eta_{B=0}}{\eta_{B=0}} \times 100 \quad (3\text{-}2)$$

where E'_B and η_B are storage modulus and loss factor of the MRE for given magnetic flux density B, and $E'_{B=0}$ and $\eta_{B=0}$ are the corresponding values under B = 0. The relative MR effects are generally defined as the relative changes in the storage and loss moduli from zero field to a specified flux density or the maximum available flux density [5, 84]. The reported values show wide variations due to differences in the maximum flux density considered in different studies apart from the lack of consideration of the saturation effects.

Figure 3.13(a) to 3.13(c) illustrate variations in $RMRS_B$ of the isotropic and anisotropic MRE considering magnetic flux density of 300, 450 and 750mT, respectively. The results are presented for three different amplitudes of strain excitation (2.5%, 5% and 10%) in the 0.1 Hz to 30 Hz frequency range. The results show that the relative MR effect in view of the storage modulus generally decreases with increase in the strain amplitude, irrespective of the loading frequency and the flux density, for both the isotropic and anisotropic MREs. Under the 2.5% and 5% strain inputs at 0.1 Hz, the $RMRS_B$ of the isotropic MRE increased from about 50% to nearly 150% and 115%, respectively, when B was increased from 300mT to 750mT. The $RMRS_B$ under 10% strain excitation at 0.1 Hz increased from about 26% to nearly 60% for identical change in B. The $RMRS_B$ of the isotropic MRE exhibits notable frequency dependence, which is relatively small for the anisotropic MRE. For the isotropic MRE, the $RMRS_B$ increased considerably with increase in frequency from 0.1 to 10 Hz but decreased notably with further increase in frequency in the 10 to 20 Hz range. The maximum relative MR effect is evident near 10 Hz, irrespective of the flux density. The maximum values of $RMRS_B$ varied from 170% to 340%, 140% to 235%, and 105% to 180%, respectively, under 2.5%, 5% and 10% strain excitations, when B was increased from 300 mT to 750 mT.

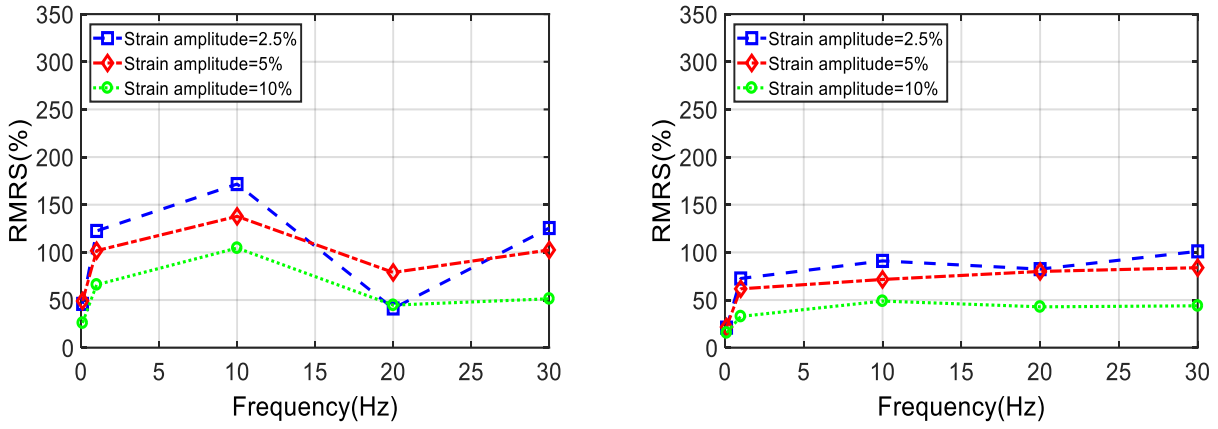

(a)

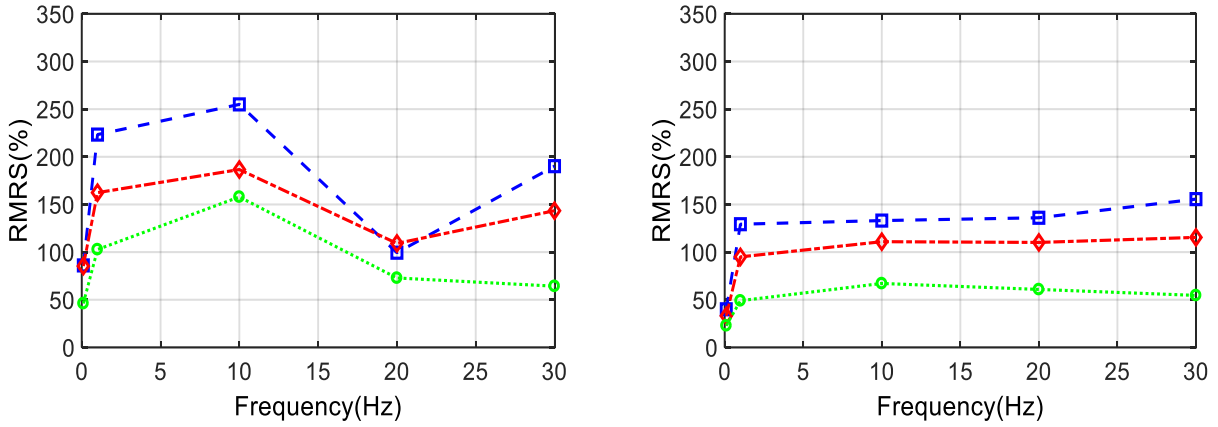

(b)

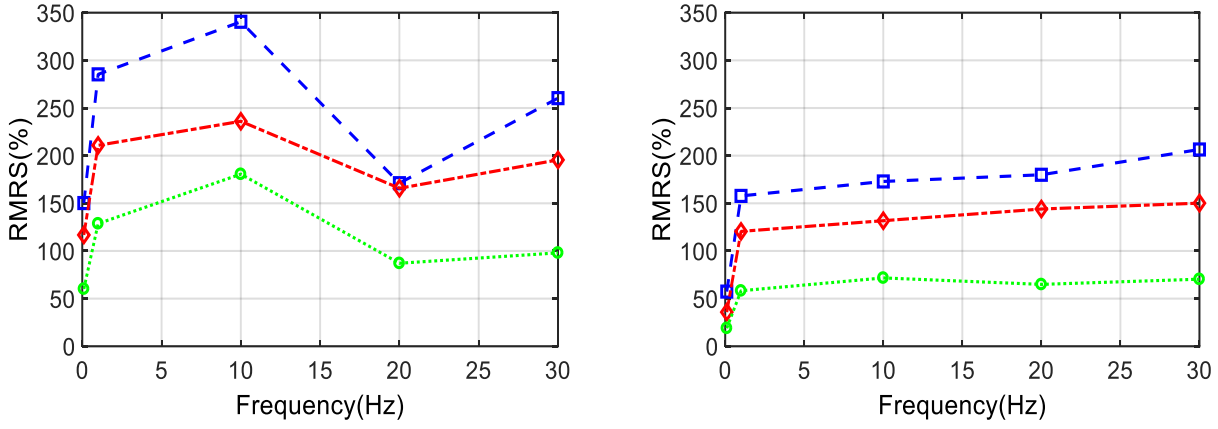

(c)

Figure 3.13 Relative MR effect in view of storage moduli ($RMRS_B$) of the isotropic (left column) and anisotropic (right column) MREs subject to magnetic flux density of: (a) 300 mT; (b) 450 mT; and (c) 750 mT.

The $RMRS_B$ of the anisotropic MRE is substantially lower compared to the isotropic MRE, with considerably lower sensitivity to excitation frequency in the 1 to 30 Hz range. This can be partly attributed to high pre-strain, which may distort the chain-like structure of iron particles in the anisotropic MRE leading to reduced magnetic permeability. This tendency has also been observed in a few studies reporting compression storage modulus under static [26] and dynamic conditions [79]. Furthermore, the pre-strain causes relatively greater strain-softening of the anisotropic MRE compared with the isotropic MRE, as observed in Figure 3.4 and Figure 3.5. For the 0.1 Hz excitation, the $RMRS_B$ exhibits lower sensitivity to variations in the strain amplitude. Reported studies have suggested relatively small increase in the relative MR effect of the anisotropic MRE compared with the isotropic MRE, especially for relatively higher particle volume fractions of about 30% [45, 84]. Under the 2.5% strain inputs at 0.1 Hz, the $RMRS_B$ of the anisotropic MRE increased from about 20% to nearly 57% when B was increased from 300mT to 750mT. The corresponding increase under 10% strain is observed to be nearly negligible (16% to 19%). The $RMRS_B$ increased considerably to 158% and 60% under 2.5% and 10% strain, respectively, with increase in frequency to 1 Hz, when B=750mT. The $RMRS_B$ varied only slightly with further increase in the frequency to 30Hz, irrespective of the strain amplitude and the flux density, as seen in Figure 3.13. Increase in strain amplitude resulted in considerably lower $RMRS_B$ in this frequency range. The results suggest small to negligible strain rate stiffening of the anisotropic MRE, as it was observed in Figure 3.10 and Figure 3.11. The results show maximum storage modulus MR effects up to 340.47% and 206.47% for the isotropic and anisotropic MREs, respectively, that were observed under 2.5% strain and loading frequencies of 10 and 30 Hz, respectively.

Furthermore, Figure 3.13 shows a peak in $RMRS_B$ under loading frequency of 10 Hz only for the isotropic MRE. It is attributable to the superior strain-rate stiffening of the isotropic MRE as compared with the anisotropic MRE, when frequency increased from 0.1 Hz to 10 Hz, which is added to enhanced magnetic field stiffening effect within (0.1 -10 Hz) frequency range. This is attributable to relatively greater amount of rubber trapped within particles in the isotropic MRE compared to the anisotropic MRE. Increasing the loading frequency, thus, leads to relatively higher strain-rate stiffening of the isotropic MRE. The $RMRS_B$, however, decreases with further increase in loading frequency, ranging from 10 Hz to 20 Hz, due to greater strain-rate stiffening effect of zero-field storage modulus.

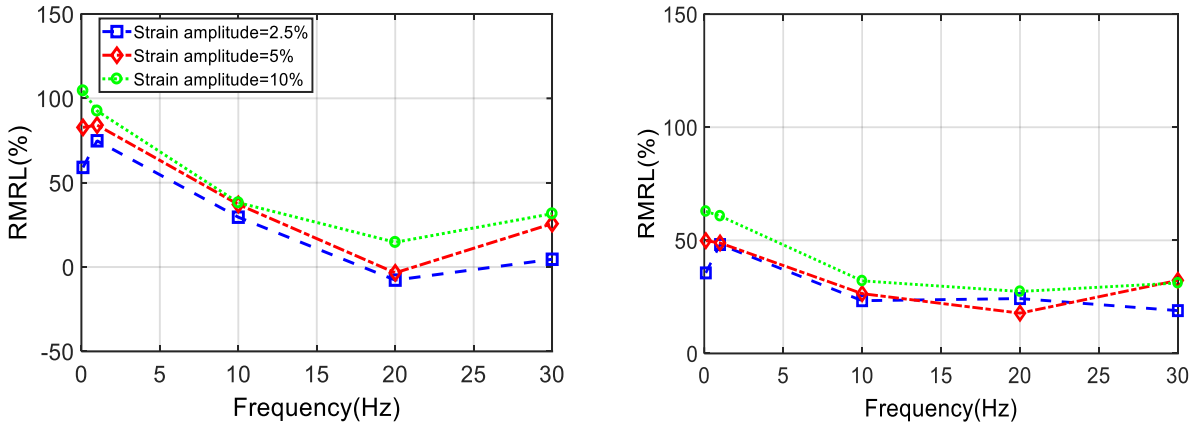

(a)

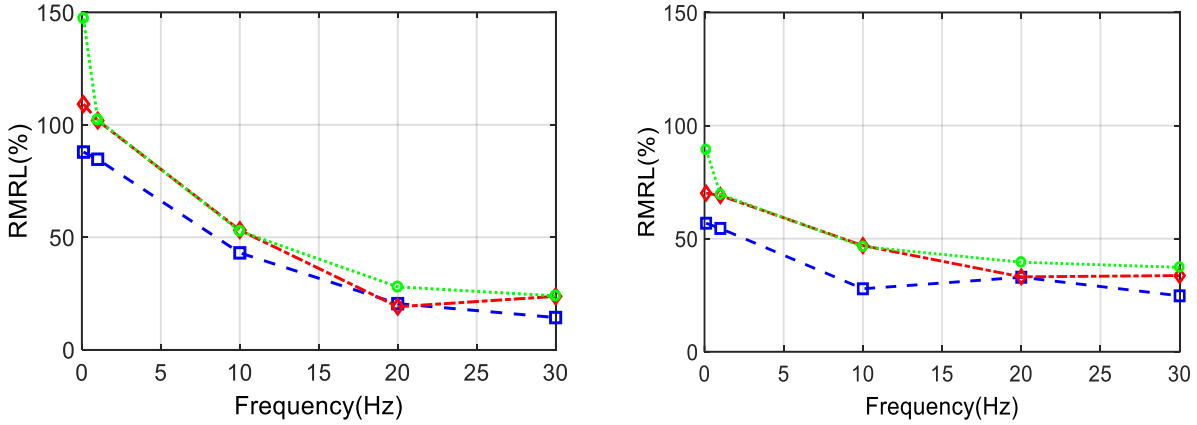

(b)

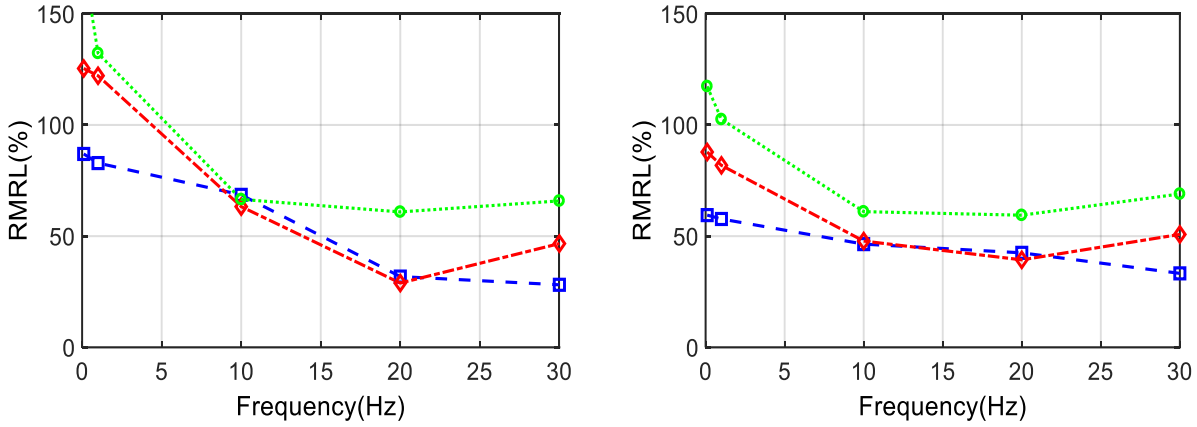

(c)

Figure 3.14 Relative MR effect in view of loss factor ($RMRL_B$) of the isotropic (left column) and anisotropic (right column) MREs subject to magnetic flux density of: (a) 300 mT; (b) 450 mT; and (c) 750 mT.

The observed notched at loading frequency of 20 Hz is attributable to the strain-rate softening of isotropic MRE, which can be seen from Figure 3.12(b), within 20-30 Hz frequency range. The strain-rate softening may be in part due to the slow recovery of MRE samples. Since, we observed considerable delay in the force signal during unloading part of the force-displacement cycle at higher level of frequency, thereby inducing negative stress, and thus rate-softening effect. This slightly reduces the zero-field modulus, and thus increases the $RMRS_B$ of the isotropic MRE due to field-stiffening effect within 20-30 Hz frequency range.

Figure 3.14(a) to 3.14(c) illustrate variations in $RMRL_B$ of the isotropic and anisotropic MREs for B= 300, 450 and 750mT, respectively. The results are presented for 2.5%, 5% and 10% strain amplitudes in the 0.1 Hz to 30 Hz frequency range. Results suggest relatively small effect of strain amplitude on the $RMRL_B$ in the 2.5% to 5% strain range, especially for the isotropic MRE. Higher MR effect, however, is observed under 10% strain excitation in the entire frequency range for both the isotropic and anisotropic MREs. The maximum values of $RMRL_B$ for isotropic MRE varied from 105% to 173%, 93% to 132%, and 38% to 67%, respectively, under 0.1 Hz, 1 Hz, and 10 Hz frequency, when B was increased from 300 mT to 750 mT. The corresponding maximum values for anisotropic MRE varied from 63% to 117%, 61% to 103%, and 32% to 61%, respectively, under 0.1 Hz, 1 Hz, and 10 Hz excitations for identical values of B. Under the 2.5% and 5% strain inputs at 0.1 Hz, the $RMRL_B$ of the isotropic MRE increased from about 60% and 83% to nearly 87% and 125%, respectively, when B was increased from 300mT to 750mT. The $RMRL_B$ under 10% strain excitation at 0.1 Hz increased from about 105% to nearly 173% for identical change in B. The $RMRL_B$ for both isotropic and anisotropic MREs generally diminishes with increase in the loading frequency, particularly in the 0.1 to 20 Hz frequency range. The RMRL for the isotropic MRE decreased considerably from 87% and 173% to 28% and 66% under 2.5% and 10% strain amplitudes, respectively, with increase in frequency from 0.1 Hz to 30 Hz, for B=750 mT. The corresponding $RMRL_B$ values for the anisotropic MRE varied from 59% and 117% to 33% and 69% under 2.5% and 10% strain amplitude. Anisotropy resulted in relatively lower $RMRL_B$ compared to the isotropic MRE under excitations up to 10 Hz, irrespective of the strain amplitude and the flux density. Both types of MREs, however, revealed compared $RMRL_B$ values under excitations at 20 and 30 Hz. This is also evident from the frequency saturation effect of the dissipated energy observed in Figure 3.10.

Near zero values of $RMRL_B$ were obtained for the isotropic MRE subject to 300 mT flux density together with 2.5% strain amplitude at 20 Hz, as seen in Figure 3.14(a). The measured data under this strain excitation also showed a slight decrease in the loss factor of the isotropic from MRE, when the magnetic flux density was increased from 0 mT to 300 mT. This trend in the loss factor with increasing magnetic field has also been observed in the reported for the isotropic and anisotropic MREs in the shear mode [90]. Results also revealed maximum change in $RMRL_B$ of up to 188.32% and 216.24% (B=750 mT) for the isotropic and anisotropic MREs, respectively, under 20% strain amplitude at frequency of 0.1 Hz. The broad changes observed in the loss factor and the storage moduli of the MREs in the compression mode thus offer meritorious potential for applications in adaptive MRE-based vibration isolators, where the pre-strain is expected to be relatively large.

3.4 Conclusion

The stress-strain characteristics of the isotropic and anisotropic MRE specimens under large static pre-strain showed nonlinear and asymmetric hysteresis behavior, which were more pronounced with increasing strain amplitude. An increase in the magnetic flux density further augmented the asymmetry in the stress-strain characteristics, which showed strong dependency on the strain amplitude and the strain rate, apart from the anisotropy. Anisotropic MRE suggested greater nonlinear behavior even under the low strain amplitude of 2.5%. The measured properties suggested notable magnetic field- and strain rate-stiffening and strain amplitude softening tendencies in addition to strain-stiffening near the extremum of loading. The strain amplitude softening was more pronounced for the anisotropic MRE as compared with the isotropic MRE both in absence and present of the applied magnetic field. The results also revealed saturation of the storage modulus and loss factor, and thus the MR effect as the magnetic flux density and excitation frequency approached 600mT and 20Hz, respectively. Both the slope of the major axis and enclosed area of the stress-strain hysteresis loops, which can be related to storage modulus and the loss factor, respectively, revealed strong dependence on the strain amplitude, strain-rate and the applied magnetics flux density, apart from the anisotropy. The storage moduli of both the anisotropic and isotropic MREs decreased considerably with increase in the strain amplitude, and approached comparable values under the high strain amplitude of 20%. The anisotropy of the MRE contributed to relatively higher storage modulus, irrespective of the excitation frequency, strain amplitude and magnetic flux density. The storage moduli of both types of MREs generally

increased in an exponential manner with increasing frequency and magnetic flux density and approached saturation near 20Hz and *B*=600mT. The anisotropy, however, revealed saturation at relatively lower levels of the magnetic flux density. The higher loss factor was observed for the anisotropic MRE compared to the isotropic MRE in the entire ranges of frequency and magnetic flux density considered in the study. The loss factor increased with increasing flux density and approached saturation near *B*=600mT. With the application of the 750 mT magnetic flux density, the isotropic and anisotropic MREs revealed up to 340.47% and 206.47% increase in the storage modulus under the low strain amplitude of 2.5%, respectively. These occurred near 10 Hz and 30 Hz, respectively, for the isotropic and anisotropic MREs. The maximum relative changes in the loss factors of the isotropic and anisotropic MREs were observed as188.32% and 216.24%, respectively, which occurred under 20% strain at 0.1 Hz. The results showed broad changes in the compression mode storage modulus and loss factor, and thus the MR effects, under the application of the magnetic field suggesting that MREs offer attractive potential for applications in controllable structures and vibration isolators.

CHAPTER 4
SHAPE FACTOR EFFECTS

4.1 Introduction

Considering compression mode characterization of MREs, the vast majority of the reported studies have considered specific sizes of MRE specimens, which differ considerably in dimensions. The variations in dimensions of MREs can be related in a more general fashion to the SF, defined as the ratio of the loaded area of the elastomer to the lateral surface area that is free to bulge. Many other studies, however, have shown that the MR effect of MREs is strongly affected by sample dimensions even in the static regime [41-43].

Reported studies suggest relatively limited knowledge on the effects of the SF on dynamic properties of the MREs in the compression mode, although the effects on the properties of elastomers are well known. The performance of the devices employing passive elastomers, particularly the laminated rubber isolators and elastomeric bearings, is strongly affected by shape factor primarily due to increase in their compression modulus with increase in the SF [31]. The dynamic properties of MREs are thus expected to depend on the SF. While the SF effect on zero-field properties of an MRE is similar to that of a passive filled-elastomer, the dynamic properties of the MRE may exhibit significant SF effect in the presence of a magnetic field. Diguet [35] showed that the magnetostriction and demagnetizing field of a cylindrical MRE are strongly dependent on the SF since the dipolar energy density depends on the sample shape. Increasing the SF from 0.35 to 1.2 resulted in nearly 300% increase in the axial force generated by the cylindrical MRE in the static regime, which was attributed to higher dipolar interactions within the cylindrical MRE [35].

It has been reported that the compression modulus of bonded passive elastomers varies with the SF in a quadratic manner [91]. To the best of the authors' knowledge, a similar SF-dependent model has not yet been attempted for estimating the dynamic storage and loss moduli of MREs. Liao et al. [92] proposed a constitutive relation to describe the compression mode properties of MREs under very large strain rates, varying from 3200 s^{-1} to 5600 s^{-1} considering the hyper-elasticity, visco-elasticity, and the magnetization. Koo et al. [20] presented an artificial neural network model to predict the behavior of MRE subject to specific frequency and strain amplitude, with magnetic flux density ranging from 0 mT to 600 mT. Bellelli and Spaggiari [45] developed a

phenomenological model to predict the compression mode stiffness of a MRE in the quasi-static regime. The reported models, however, have been developed for a constant SF of the MRE.

Moreover, studies reporting experimental characterizations and analytical models of MREs generally neglect potential contributions of the MRE dimensions or SF. A better understanding of the shape factor effects is thus desired for optimally designing MRE-based devices. This study is aimed at analyses of the shape factor effects on the compression mode properties of both isotropic and anisotropic MREs. The study involved experimental characterizations of cylindrical isotropic and anisotropic MRE specimens with three different shape factors, which were realized by varying the samples' diameter in the 12 to 24 mm range. The force-deflection properties of each MRE sample, fabricated with 30% volume fraction of iron particles, were acquired under harmonic excitations (strain amplitudes: 2.5 to 20%) at frequencies ranging from 0.1 to 30 Hz, and magnetic flux density up to 750 mT. The measured data were analyzed to evaluate the effect of SF on the compression moduli and loss factor of the isotropic and anisotropic MREs. A simple phenomenological model is subsequently proposed estimating the compression mode elastic moduli of both types of MREs as functions of the shape factor, strain amplitude, strain rate and magnetic flux density.

4.2 Experimental setup and methods

4.2.1 MRE samples

A number of isotropic and anisotropic MRE samples with different sizes were fabricated in the laboratory to achieve three different values of the shape factor (*SF*), defined as [31]:

$$SF = \frac{compression\ loading\ area}{free\ to\ bulge\ area} \tag{4-1}$$

The SF of a cylindrical specimen can also be expressed as the ratio of the sample diameter to four times the sample thickness, such that:

$$SF = \frac{\pi r^2}{2\pi r h} = \frac{D}{4h} \tag{4-2}$$

where r, d and h are the sample's radius, diameter and height or thickness, respectively.

The dimensions of the MRE samples were chosen in accordance with the current standards for compression testing of rubber-like materials. The International and American standards on

characterizations of compression mode properties of elastomers, however, recommend different values of the SF. The ISO 4664-1 [87] recommends SF in the 0.25 to 1.25 range, while ASTM D395 [53] and ISO 7743 [52] suggest SFs in the 0.55 to 0.62 range. In this study, 8 mm thick MRE samples with three different diameters (12, 18 and 24 mm) were fabricated to realize three different values of SF: 0.375, 0.56, and 0.75. The volume concentration of the ferromagnetic particles of both the isotropic and anisotropic MREs was held constant as 30%.

4.2.2 Test setup and methods

An experiment was designed to investigate the effect of shape factor on dynamic compression mode properties of both the isotropic and anisotropic MREs considering the standardized methods described in ASTM D395 [53] and ISO 7743 [52]. For this purpose, a test setup was designed to characterize compression mode properties of MREs of different SF, which comprised a custom-designed U-I core electromagnet. The fixture with the electromagnet was mounted on a servo-hydraulic material testing machine (MTS), as shown in Figure 4.1. The fixture permitted application of unidirectional compression loading together with the magnetic field to two identical MRE specimens positioned within two air gaps of the electromagnet (Figure 4.1).

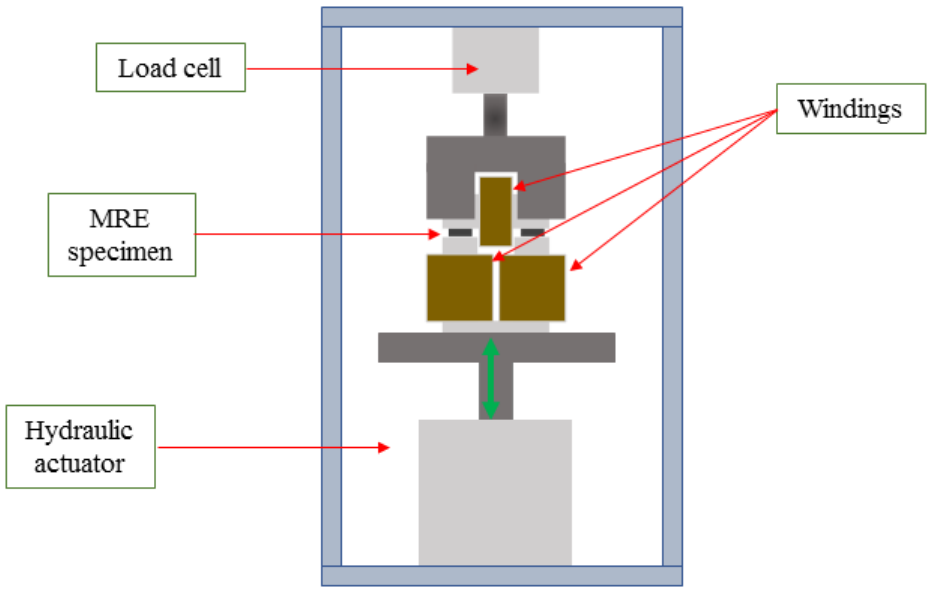

Figure 4.1 Schematic of the test setup for compression mode characterization of the MRE.

The lower part of the electromagnet (U-core) was attached to the actuator of the servo-hydraulic test system, while the upper part (I-core) was connected to a fixed beam via a load cell. Both the lower and upper sections were carefully aligned vertically to ensure uniform magnetic

field in both the air gaps. Two identical cylindrical MRE samples, cut from the MRE batches fabricated in the laboratory, were bonded to the U- and I- magnetic cores using a thin layer of an industrial adhesive in order to apply compression loading via controlled displacement of the servo-hydraulic actuator. A pre-strain of 21% was applied to each MRE sample by displacing the hydraulic actuator.

The experiment design involved broad variations in strain amplitude, strain rate and the magnetic flux density. A factorial design of experiments approach was used considering five different levels of magnetic flux density (B = 0, 150, 300, 450, 600 and 750 mT), four levels of strain amplitude (ε=2.5%, 5%, 10%, 20%) and five levels of excitation frequency (f= 0.1, 1, 10, 20 and 30 Hz) for each MRE with specific SF. The relationships between the flux density and the coil current, established for both the isotropic and anisotropic MREs in the air gap, were used to determine the coil current required to induce a desired flux density. The relationship and the associated method have been described in chapter two of this dissertation. A similar relationship was also formulated for the anisotropic MRE derived using the reported methodology. A 10 A and 100 V power supply was used to generate coil current required for the desired flux density. Each MRE sample set was subject to harmonic deformation corresponding to selected strain amplitude, excitation frequency and the magnetic flux density. The force and displacement signals were acquired during each measurement using a National Instruments (NI) Data Acquisition (DAQ) board, while the sampling rate was set to 50, 100, 1000, 2000, 3000 Hz for excitation frequency of 0.1, 1 , 10, 20, and 30 Hz, respectively.

4.2.3 Data analysis

The steady-state force and displacement data, acquired for three consecutive oscillation cycles, were processed via a low-pass filter and averaged for characterizing the mean force and displacement characteristics of the specimens. Since the compression mode characterization of MRE involves applications of both the magnetic field and the mechanical loading in the same direction, the measured force comprises two components: (i) the magnetic force developed by the magnetic poles of the electromagnet; and (ii) the viscoelastic force attributed to compression loading of the MRE. The magnitude of the magnetic force may be greater than that of the viscoelastic force, especially under low deformations and higher magnetic flux density. It has been shown that the magnetic force due to electromagnet is strongly dependent on the magnetic flux

density, air gap length and the excitation frequency, discussed in chapter two of this dissertation. Moreover, there exists a phase between the magnetic force and displacement input to the MRE, which is also dependent upon the excitation frequency and the flux density. The nonlinear magnetic force of the U-I electromagnet was estimated using the phenomenological model reported in Equation (2-24), which was subsequently subtracted from the measured force to obtain the field dependent viscoelastic force attributed to deformation of the MRE. The resulting force and displacement data were used to obtain stress-strain characteristics of the MREs with different SFs and loading conditions. The stress-strain characteristic of the isotropic and anisotropic MREs were subsequently analyzed to evaluate effects of SF coupled with the variations in the magnetic flux density, strain amplitude and the excitation frequency (strain-rate).

The dynamic properties of the MREs in the compression mode were further assessed in terms of the compression mode elastic modulus (E'), loss modulus (E'') and the loss factor (η). The loss factor, defined as the ratio of the loss modulus to the elastic modulus, was computed using the standardized method for determining dynamic properties of rubbers, as described in ISO 4664-1 [87], such that:

$$\eta = tan\delta = \frac{E''}{E'}; \qquad \delta = \sin^{-1}\left[\frac{Energy\ disspted\ per\ cycle}{\pi F_0 X_0}\right] \tag{4-3}$$

where F_0 and X_0 are peak force and peak displacement, respectively, and δ is the loss angle determined from the energy dissipated by the MRE during a loading/unloading cycle, which is obtained from the area bounded by the hysteretic force-deflection curve obtained for the MRE corresponding to each test condition.

The elastic (E') and loss (E'') moduli of the MRE were obtained using the method described in ISO 4664-1 [87], such that:

$$E' = E^* \cos(\delta); \quad E'' = E^* \sin(\delta) \tag{4-4}$$

where E^*, complex compression modulus, can be obtained as quotient of the ratio of peak to peak stress to the peak to peak strain amplitude. In accordance with ISO 7743 [52], the compression modulus in the static regime is obtained as mean of the moduli obtained for 10% and 20% strain amplitudes:

$$E_c = \frac{1}{2}\left[\frac{\sigma_{10\%}}{\varepsilon_{10}\%} + \frac{\sigma_{20\%}}{\varepsilon_{20}\%}\right] \quad (4\text{-}5)$$

where $\frac{\sigma_{10\%}}{\varepsilon_{10}\%}$ and $\frac{\sigma_{20\%}}{\varepsilon_{20}\%}$ are the slopes of the stress-strain curves during loading corresponding to 10% and 20% strain, respectively.

4.3 Compression mode stress-strain characteristics

4.3.1 Effect of shape factor on stress-strain characteristics

The steady-state stress-strain characteristics of the isotropic and anisotropic MREs with different shape factors, invariably, revealed hysteresis behavior, which is ascribed to viscoelastic nature of the MREs. The stress-strain characteristics are analyzed in view of the major axis slope and the area bounded within the loop, which relate to equivalent stiffness and damping property of the MREs, respectively. The results, in-general, revealed strong dependency of the properties on the SF and anisotropy, apart from the mechanical loading conditions (strain amplitude and frequency) and the magnetic field.

Figure 4.2(a) and 4.2(b) illustrate the effect of SF on the quasi-static stress-strain characteristics of the isotropic and anisotropic MREs, subject to peak strain of 5% and 10%, respectively, at a low frequency of 0.1 Hz in the absence of the magnetic field (B=0). The results exhibit asymmetric and nonlinear stress-strain hysteresis loops for both isotropic and anisotropic MREs, which is more pronounced under the higher strain excitation of 10%. Results show important effects of SF on both the equivalent stiffness and the effective damping property of the MREs. Increasing the SF from 0.375 to 0.75 shows notable increase in the slope of the major axis of the hysteresis curves, suggesting 'SF-stiffening' effect. This tendency has been reported for rubber-cork composite materials under uniaxial compression loading [93]. The friction at the loaded surfaces is known to resist expansion of the bonded rubber specimen during tests, which contributes to relatively higher effective modulus of the rubber. The surface friction is also dependent on the loaded area and thus the SF.

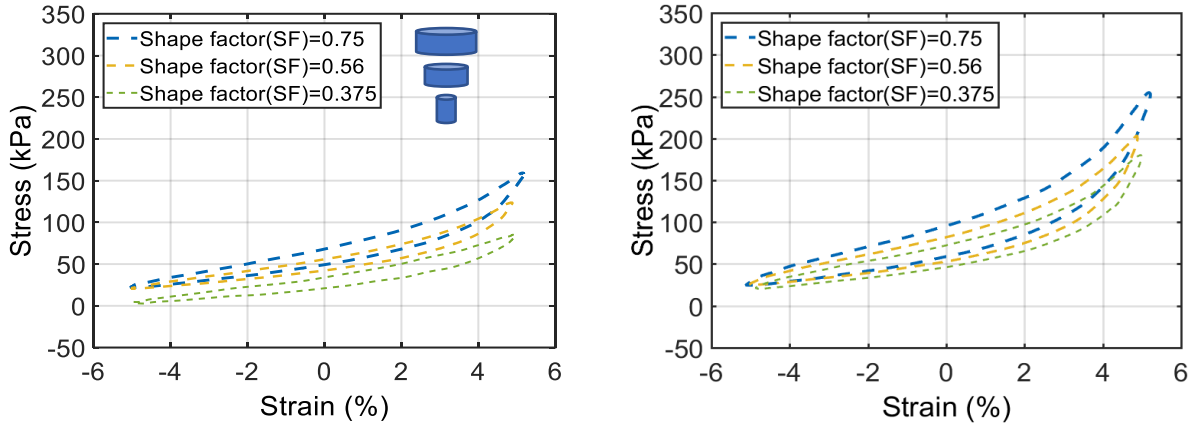

(a)

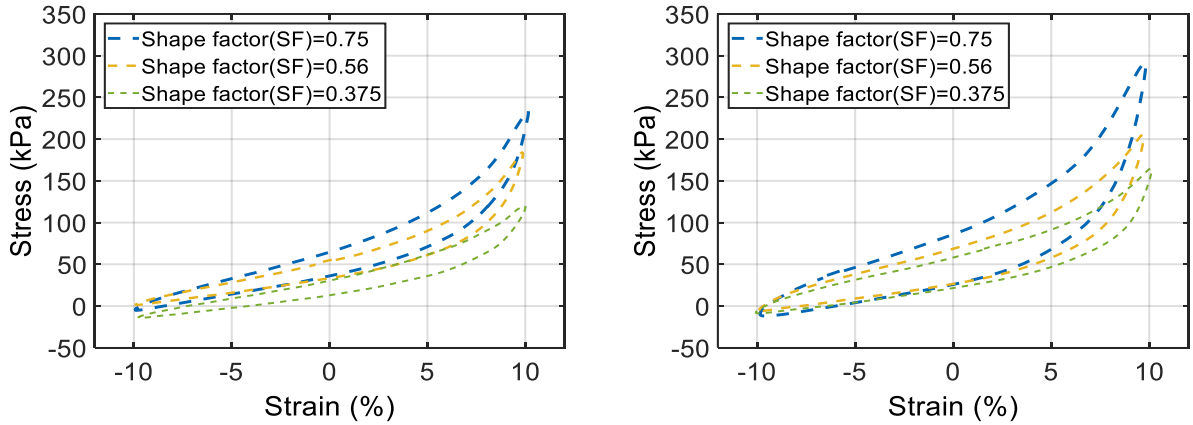

(b)

Figure 4.2 Effect of shape factor on stress-strain characteristics of isotropic (left column) and anisotropic (right column) MREs under two different strain amplitudes: (a) 5%; and (b) 10% (B=0; f=0.1 Hz).

Results further demonstrate that increasing the SF from 0.375 to 0.75 yields notable increase in the area bounded by the hysteresis curves, thereby increasing the effective damping of the MRE, which is denoted as the 'SF-dampening effect' hereafter. This tendency can be partly attributed to increase in the loaded surface area with increase in the SF, which would also cause higher surface friction. The dependency of the equivalent damping on the SF has also been observed for filled rubbers subject to complex loading [94]. From the results, it is also evident that the SF-stiffening effect is generally more pronounced than the SF-dampening effect. For the chosen excitation, increasing the SF from 0.375 to 0.75 revealed SF-stiffening in the orders of 60% and 37% for the isotropic and anisotropic MREs, respectively. The corresponding SF-dampening effects for the

isotropic and anisotropic MREs were about 23% and 36%, respectively. Furthermore, an increase in the SF yields notably higher peak stress during compression loading, which is more pronounced under higher strain excitation. Increasing the SF from 0.375 to 0.75 resulted in nearly 82% and 100% increases in the peak stress of the isotropic MRE subject to 5% and 10% strain amplitude excitation, respectively. The corresponding increases for the anisotropic MRE were obtained as 40% and 94%. Increasing the SF from 0.56 to 0.75 resulted in more pronounced effects on the peak stress, equivalent stiffness and damping, when compared to those obtained with SF increase from 0.375 to 0.56. This suggests nonlinear effects of the SF.

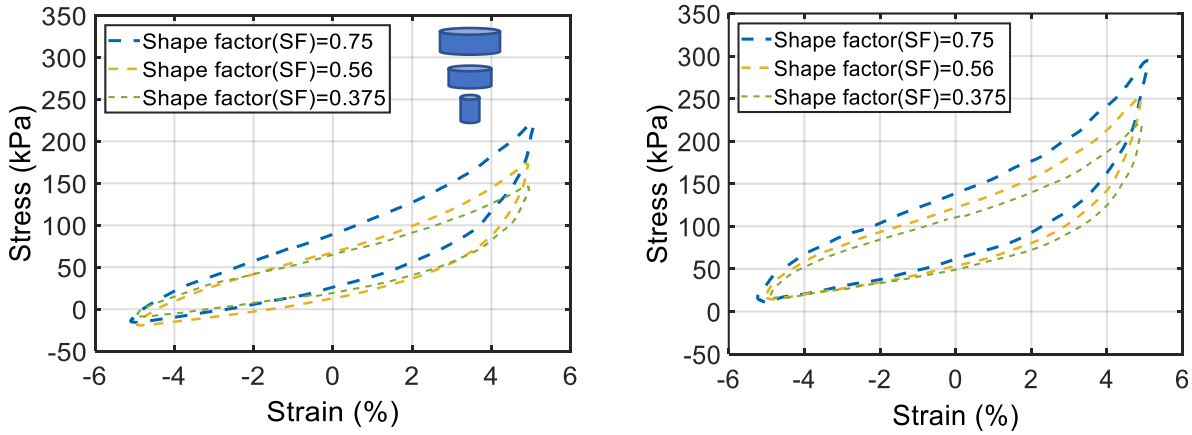

(a)

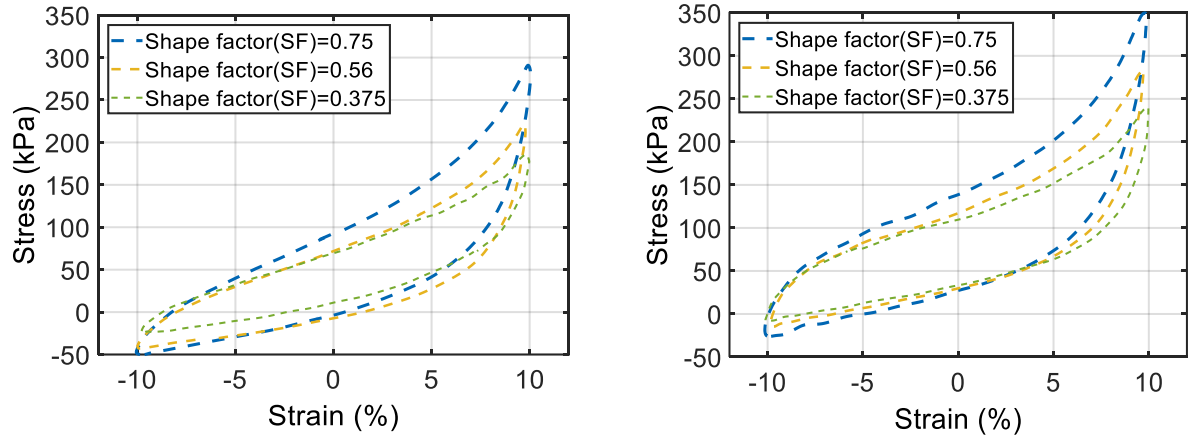

(b)

Figure 4.3 Effect of shape factor on stress-strain characteristics of isotropic (left column) and anisotropic (right column) MREs under different strain amplitudes: (a) 5%; and (b) 10% (B=450 mT; f=0.1 Hz).

Results also show that the anisotropy yields relatively greater SF-stiffening and SF-dampening effects even under the lower strain amplitude of 5%. This can be attributed to the column-like structures of the iron particles chains within the matrix of the anisotropic MRE, which contributes to higher stiffening effect compared to the isotropic MRE.

Figure 4.3 illustrates the effect of SF on the stress-strain characteristics of the isotropic and anisotropic MREs in the presence of a magnetic field (B=450 mT). The results, presented for 5% and 10% peak strains at 0.1 Hz, suggest more significant effects of SF when compared to those observed for the passive MREs (B=0). This can be partly attributed to increase in the demagnetizing energy of MRE composite with an increase in the SF in presence of a magnetic field. Diguet [35] investigated properties of disk- and needle-type MREs under a magnetic field and reported considerably higher demagnetizing energy for the disk-type MRE. Results show that an increase in SF yields relatively higher peak stress, equivalent stiffness, energy dissipation and asymmetry in the stress-strain characteristics of both the isotropic and anisotropic MREs in the presence of the magnetic field, even under the lower strain amplitude of 5%. Besides, the magnetic field-stiffening and -damping of MREs have been widely reported under both shear and compression loadings of MREs [9]. The SF-stiffening effect tends to be more pronounced with increase in magnetic flux density for both isotropic and anisotropic MREs, as shown in Figure 4.4. The figure illustrates the SF effect on the stress-strain characteristic of MREs subject to 10% strain amplitude and B=600 mT, as examples.

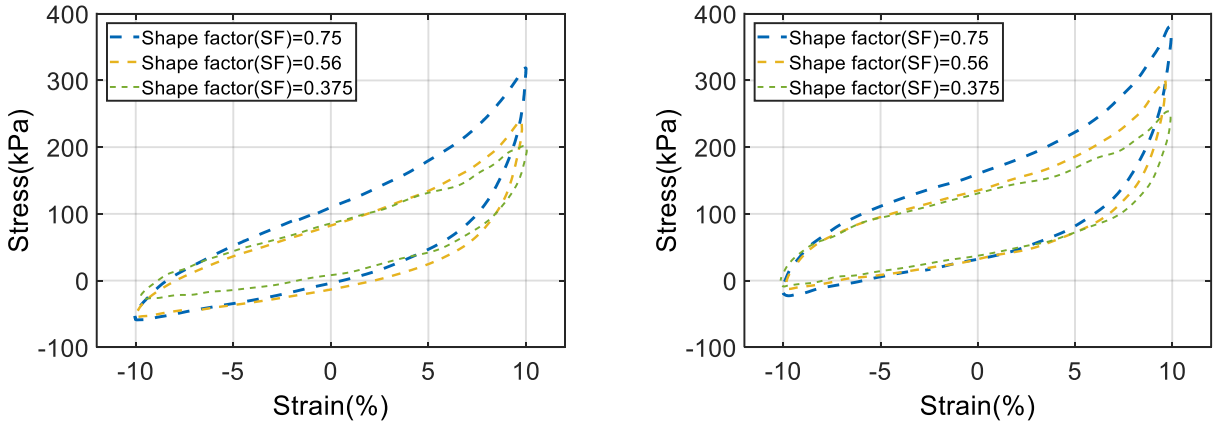

Figure 4.4 Effect of shape factor on stress-strain characteristics of the isotropic (left column) and anisotropic (right column) MREs under higher magnetic flux density (B=750 mT) and 10% strain amplitude at 0.1 Hz.

Figure 4.5(a) and 4.5(b) illustrate the effect of SF on the stress-strain characteristics of the isotropic and anisotropic MREs subject to 5% strain at two different frequencies (1 Hz and 10 Hz). Results, presented for B=300 mT, suggest that increasing SF from 0.375 to 0.56 yields only minimal effect on the stress-strain characteristics. The same variations in SF, however, revealed notable SF-stiffening effect in the quasi-static regime (Figure 4.2 and Figure 4.3). The strain-rate stiffening is thus considered to be more pronounced compared to SF-stiffening effect in this range of SF. The substantially higher SF-stiffening effect is evident in Figure 4.4 and Figure 4.5, when SF is increased from 0.56 to 0.75. The results thus suggest coupled SF- and strain rate-stiffening of the MREs.

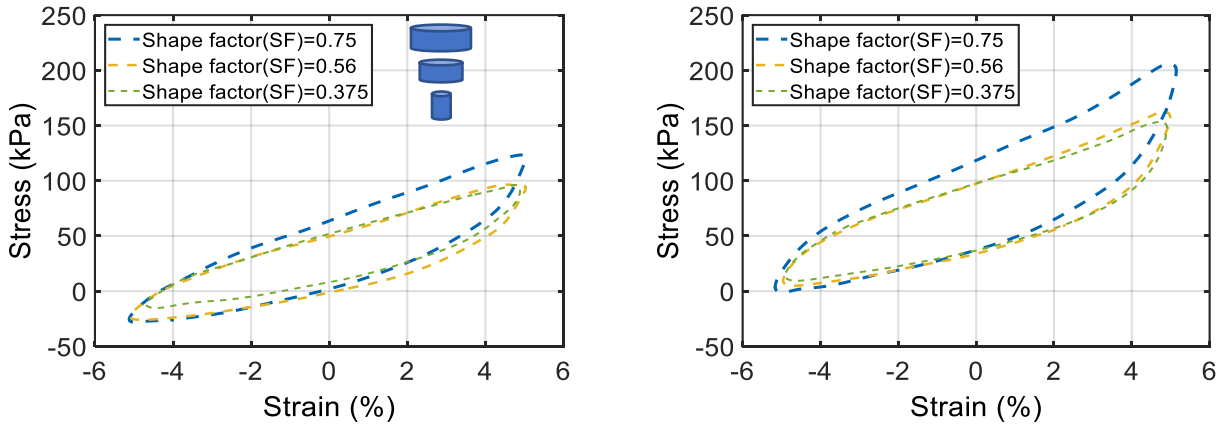

(a)

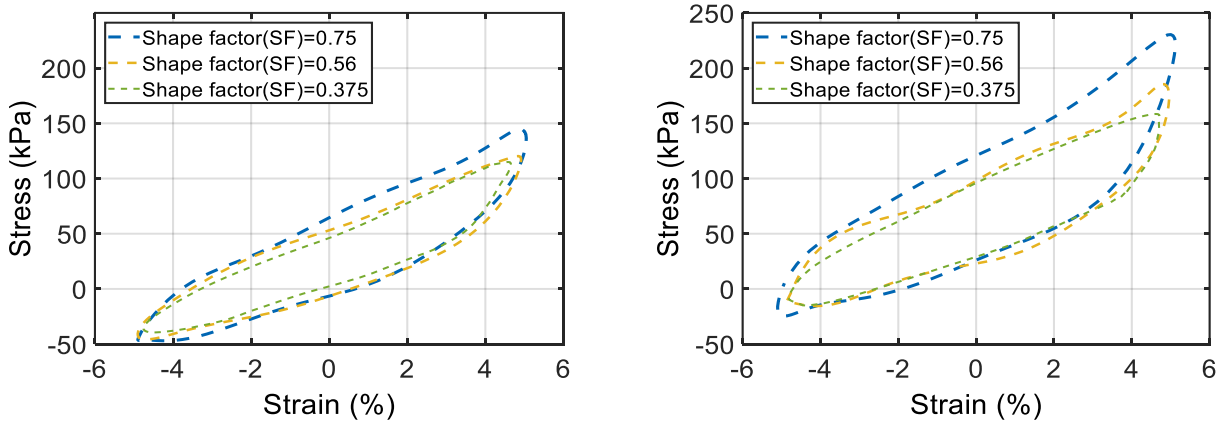

(b)

Figure 4.5 Effect of shape factor on stress-strain characteristics of isotropic (left column) and anisotropic (right column) MREs subject to %5 peak strain at different frequencies: (a) f= 1 Hz, (b) f= 10 Hz. (B=300 mT).

4.3.2 Effect of shape factor on the compression moduli and loss factor

The effect of SF on the dynamic properties of the isotropic and anisotropic MREs in the compression mode are further evaluated in terms of the elastic modulus(E'), loss modulus (E'') and the loss factor (η), defined as the ratio of the loss modulus (E'') to the elastic modulus (E'). Figure 4.6 illustrates variations in the moduli and the loss factor of both the isotropic and anisotropic MREs with respect to SF for the ranges of strain amplitude considered in the study. The results are presented for magnetic flux density of 450 mT and frequency of 1 Hz, as examples. The elastic modulus of both the isotropic and anisotropic MREs increase with increase in the SF, irrespective of strain amplitude. This is consistent with the SF-stiffening effect observed in the stress-strain characteristics (Figure 4.2 and Figure 4.3). Relatively higher SF-stiffening effect is evident for the anisotropic MRE compared to the isotropic MRE, which tends to decrease with increase in strain amplitude for both types of MREs. This is attributed to relatively higher strain-softening effect [9]. The elastic modulus of the isotropic MRE increased from about 1.86 MPa to 2.69 MPa under 2.5% strain, and from about 0.98 MPa to 1.34 MPa under 20% strain, when SF is increased from 0.375 to 0.75. These correspond to approximately 45% and 0.37% increase in the elastic modulus. The corresponding SF-stiffening effects for the anisotropic MRE specimen were relatively higher and in the orders of 50% and 48%, under 2.5% and 20% strain amplitudes, respectively. The results also suggest saturation of the elastic modulus with increasing SF of the anisotropic MRE under 20% strain amplitude, as seen in Figure 4.6(a). This is due to the stiffening effect of the anisotropy coupled with strain-softening, which likely becomes more predominant under extreme SF of 0.75.

The loss modulus of both types of MREs also increase with increase in SF, as seen in Figure 4.6(b). This is consistent with the SF-dampening effect observed in Figure 4.2 and Figure 4.3. For the isotropic MRE, the rate of change of loss modulus with respect to the SF decreases with increase in the SF. The SF-dampening effect tends to saturate under higher SF, especially for lower strain amplitudes. This trend, however, is not evident for the anisotropic MRE, which suggests monotonic increase in loss modulus with increasing SF. The reported studies have shown nearly quadratic increase in loss modulus of bonded rubbers with increasing SF [91]. A clear trend in the loss factor with the SF, however, is not evident (Figure 4.6(c)), especially for different strain amplitudes, which is mostly attributed to its definition.

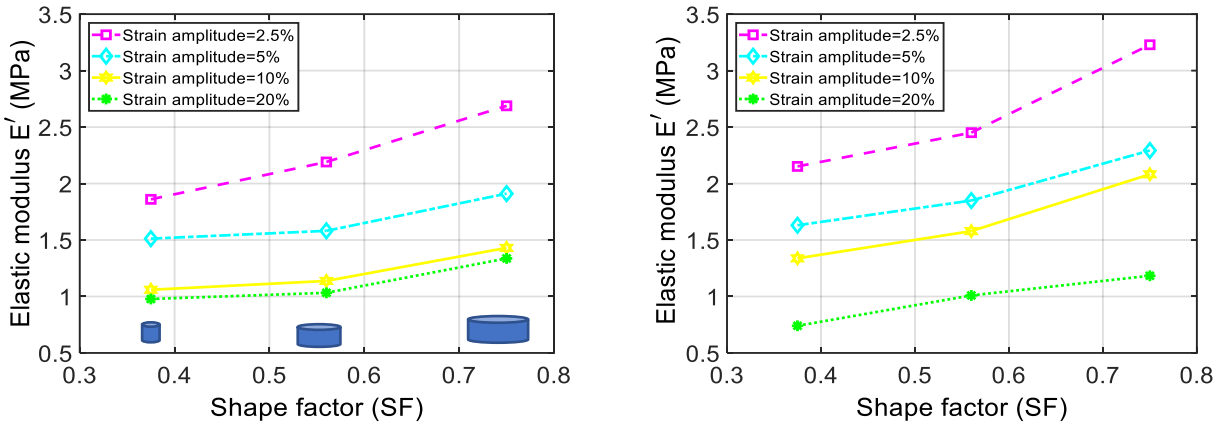

(a)

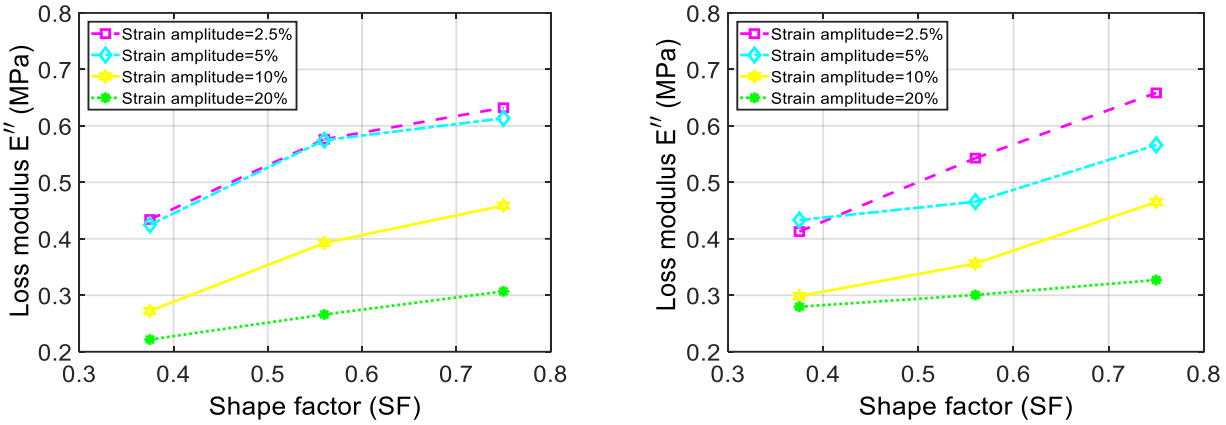

(b)

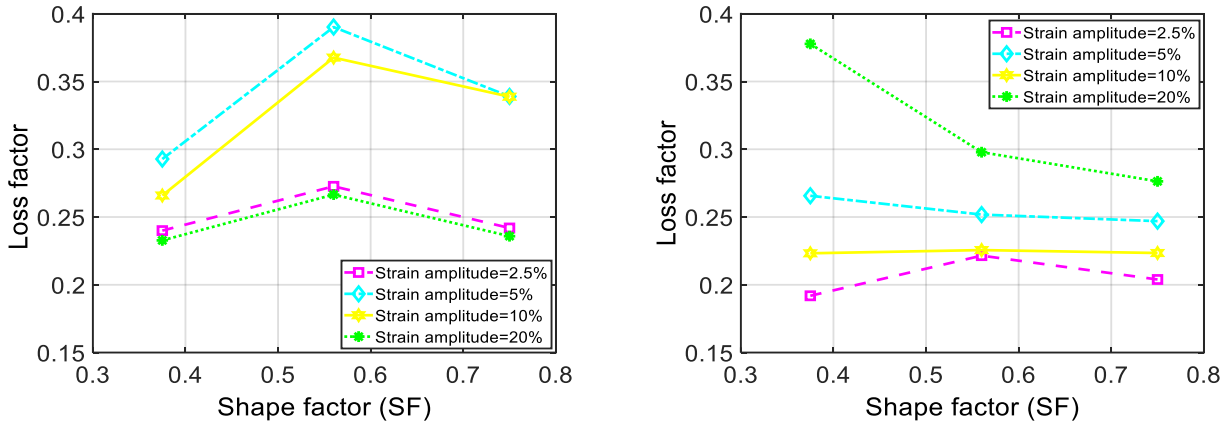

(c)

Figure 4.6 Effect of shape factor on the compression mode elastic modulus (a), loss modulus (b) and loss factor (c) of the isotropic (left column) and anisotropic (right column) MREs for different strain amplitudes (f=1 Hz, and B=450 mT).

Two types of MREs exhibit notably different variations in the loss factor with increasing SF. For the isotropic MRE, the loss factor increases with increase in the SF from 0.375 to 0.56, and decreases with further increase in the SF from 0.56 to 0.75, irrespective of strain amplitude. Loss factor of the anisotropic MRE, however, generally decreased with increase in the SF for the entire range considered. The 2.5% strain amplitude excitation, however, formed an exception, where the variation in the loss factor is similar to that of the isotropic MRE.

Moreover, the loss factor of the anisotropic MRE can be considered to be nearly constant in the range of SF considered for strain amplitudes up to 10%. This is due to similar SF-dependent variations in both the elastic and loss moduli of the anisotropic MRE. Results further demonstrate that the anisotropic MRE yields relatively lower loss factor compared to the isotropic MRE in the entire range of SF and strain amplitude up to 10%. This implies relatively higher SF-stiffening and lower SF-dampening effects of the anisotropic MRE with particles chain structures compared with the isotropic MRE. For the isotropic MRE, the loss factor increased considerably with increase in the strain amplitude from 2.5% to 5% but decreased notably with further increase in strain amplitude in the 10 to 20 % range, irrespective of SF.

Figure 4.7 illustrates the effects of SF on variations in the elastic and loss moduli, and the loss factor of both the isotropic and anisotropic MREs considering different excitation frequencies (1, 10 and 20 Hz). The results are presented for 5% strain amplitude and B= 600 mT, as examples. The results show that the elastic and loss moduli of the isotropic as well as anisotropic MREs generally increase with increase in SF, irrespective of the excitation frequency. Increasing the excitation frequency from 1 to 10 Hz yields considerable increases in both the moduli. The frequency effect, however, diminishes with further increase in the frequency, suggesting saturation of the moduli under higher strain rates, irrespective of the SF. The similar trends were also observed under higher excitation frequency of 30 Hz. The excitation at 1 Hz revealed 22.34% and 42.10% increases in the elastic moduli of the isotropic and anisotropic MREs, respectively, when SF increased from 0.375 to 0.75. The corresponding SF-stiffening under excitations at 10, 20 and 30 Hz were in the orders of 10% and 30% for the isotropic and anisotropic MREs, respectively.

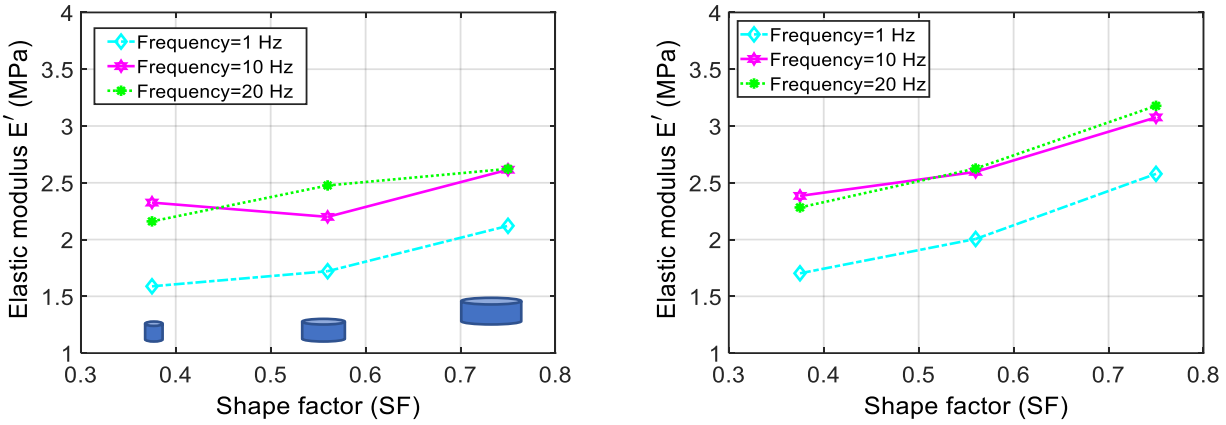

(a)

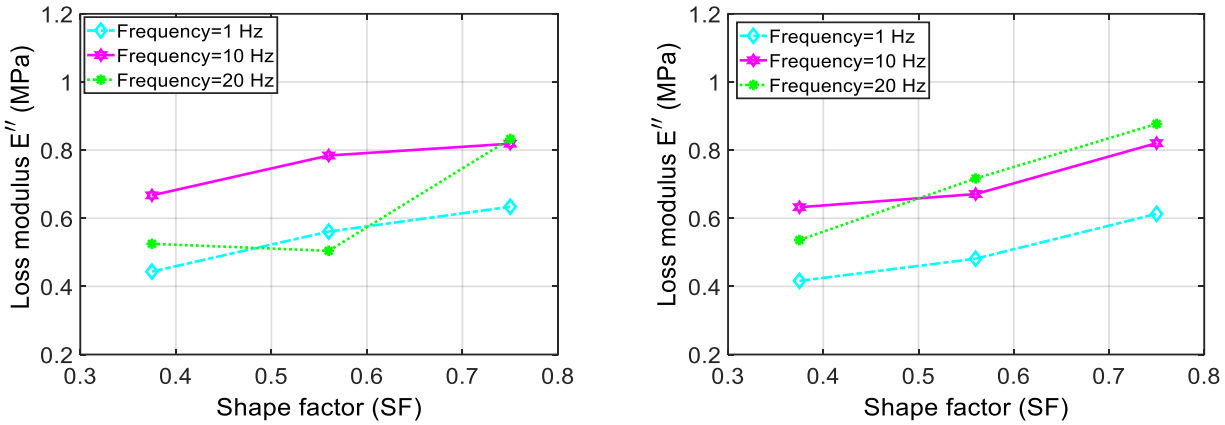

(b)

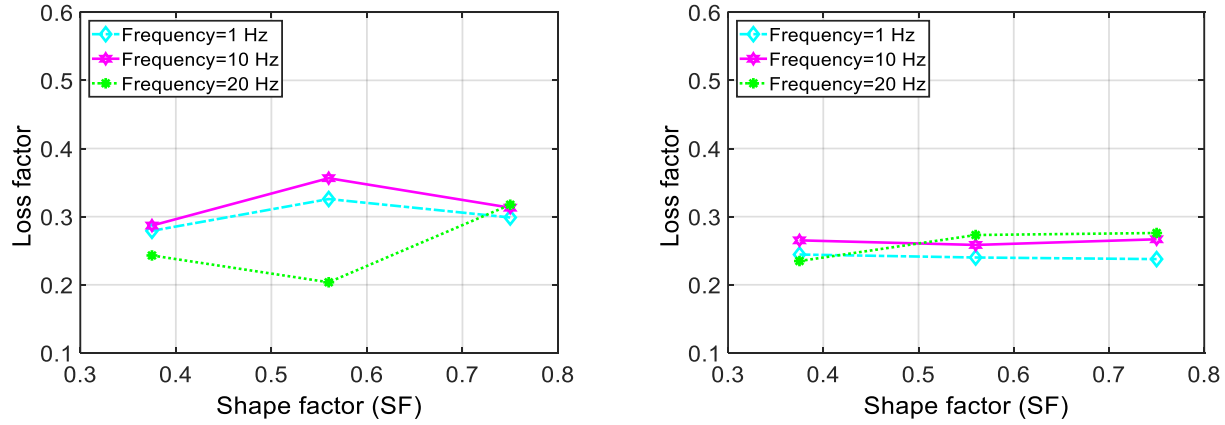

(c)

Figure 4.7 Effect of shape factor on the compression mode elastic modulus (a), loss modulus (b) and loss factor (c) of the isotropic (left column) and anisotropic (right column) MREs under different excitation frequencies (strain amplitude=5%, and B=600 mT).

This implies that the strain-rate stiffening limits the SF-stiffening of MREs. Similar behavior has also been reported for passive elastomers by Payne [95], which showed that the effective storage modulus increases with the SF according to a square law, when the excitation frequency is below 10 Hz. The results also suggest very small to negligible effect of the excitation frequency on the loss factors of both types of MREs in the entire range of SF for the magnetic flux density of 600 mT, as seen in Figure 4.7(c). This is due to comparable variations in the elastic and loss moduli with respect to both the SF and the excitation frequency, and in-part due to saturation under the relatively higher magnetic flux density. The results suggest nearly constant loss factor for the 5% strain excitation, irrespective of the excitation frequency and the SF. This is also consistent with the results presented in Figure 4.6.

Figure 4.8 illustrates variations in the elastic and loss moduli, and the loss factor of both the MREs with respect to SF considering different levels of the magnetic flux density. The results are displayed, as examples, for 2.5% strain amplitude at a frequency of 1 Hz. The elastic modulus of both the isotropic and anisotropic MREs increased with the SF, irrespective of magnetic flux density, as it was observed in Figure 4.6. The increase in the modulus, however, is more pronounced for the anisotropic MRE. By increasing SF from 0.56 to 0.75, for instance, the elastic modulus of the anisotropic MRE increased from about 1.86 MPa to 2.6 MPa and from 2.81 MPa to nearly 3.6 MPa for B=300 mT and B=600 mT, respectively. These correspond to 39.8% and 28.1% increase in the elastic modulus. The corresponding SF-stiffening was observed as 25.2% and 18.1% for the isotropic MRE, for B=300 mT and B=600 mT, respectively. This implies that the magnetic field-stiffening limits the SF-stiffening of MREs, suggesting coupled SF- and field-stiffening of the MREs. The elastic modulus increases significantly with increase in the magnetic flux density up to 600 mT, while the SF-stiffening varies only slightly with increase in B. Saturation in the moduli of both the MREs is observed for B in excess of 450 mT.

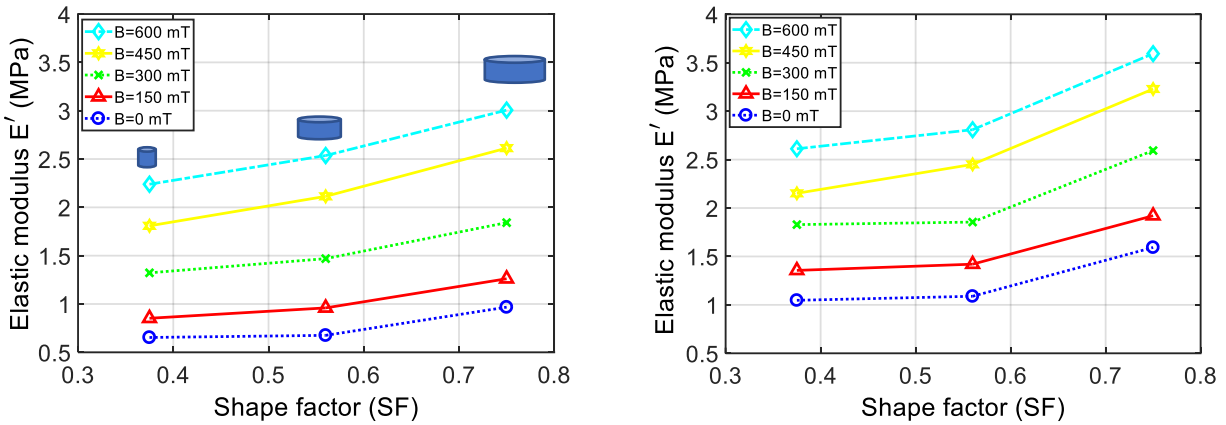

(a)

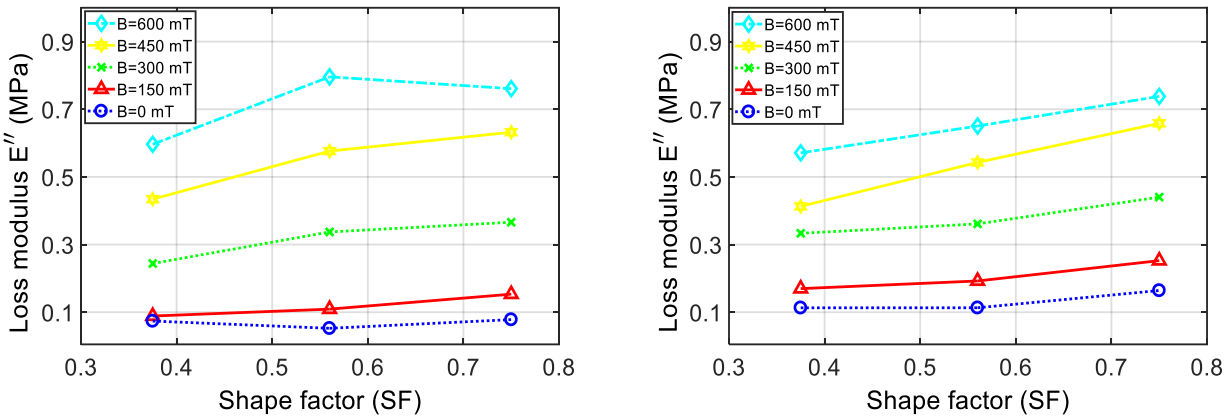

(b)

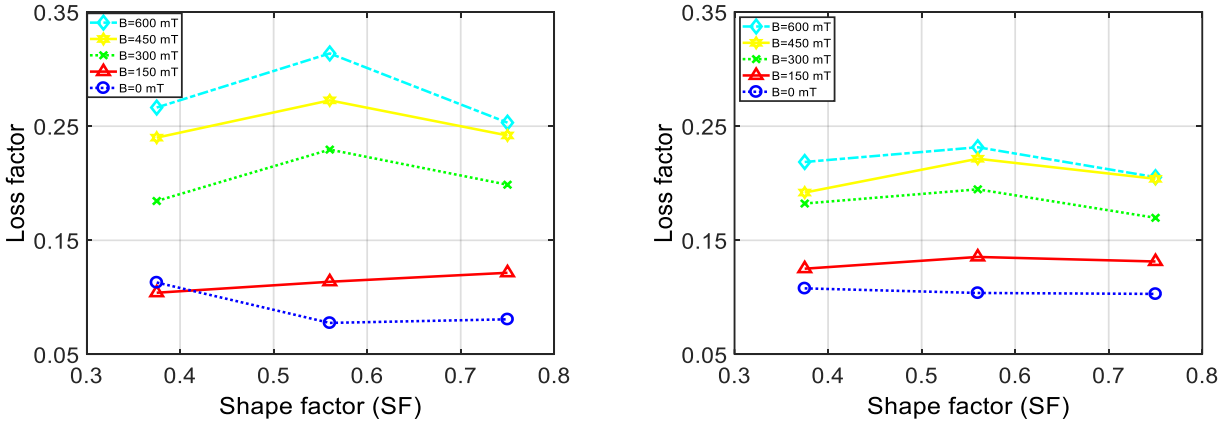

(c)

Figure 4.8 Effect of shape factor on the compression mode elastic modulus (a), loss modulus (b) and loss factor (c) of isotropic and anisotropic MREs under different levels of magnetic flux density (strain amplitude =2.5%, f=1 Hz)

The loss modulus of both the isotropic and anisotropic MREs also generally increased with increase in SF, irrespective of magnetic flux density, as shown in Figure 4.8(b). The results show trends similar to those observed in Figure 4.6, while the increase in the magnetic flux density enhances the loss modulus in the entire range of the SF range considered. The results also showed saturation of the loss modulus as *B* exceeds 450 mT, as it was observed for the elastic modulus in Figure 4.8(a). The results also suggest relatively higher rate of change of loss modulus with respect to the SF in the 0.375 to 0.56 range compared to that in the 0.56–0.75 range. This tendency is opposite to that observed for the elastic modulus. The SF effect on the loss factor is generally small for both types of MREs, as seen in Figure 4.8(c). This tendency is also observed in Figure 4.6 and Figure 4.7. The loss factor, however, generally increases with increase in the magnetic flux density up to about 450 mT.

The effects of SF on the elastic modulus and loss factor of the MREs are further evaluated and quantified in terms of the relative SF effect in view of the elastic modulus ($RSF_{\acute{E}}$) and the loss factor (RSF_{η}). These are defined for a given strain amplitude, frequency and magnetic flux density, as:

$$\%RSF_{\acute{E}} = \frac{E'_{SF_{max}} - E'_{SF_{min}}}{E'_{SF_{min}}} \times 100 \tag{4-6}$$

$$\%RSF_{\eta} = \frac{\eta_{SF_{max}} - \eta_{SF_{min}}}{\eta_{SF_{min}}} \times 100 \tag{4-7}$$

where $E'_{SF_{max}}$ and $\eta_{SF_{max}}$ are the elastic modulus and loss factor, respectively, corresponding to maximum value of SF, and $E'_{SF_{min}}$ and $\eta_{SF_{min}}$ correspond to minimum value of SF. The results obtained for the ranges of SF, strain amplitude, frequency and magnetic flux density, considered in the study, revealed maximum $RSF_{\acute{E}}$ corresponding to the highest SF of 0.75. The maximum $RSF_{\acute{E}}$ of 77% was obtained for the isotropic MRE corresponding to 10% strain amplitude at 0.1 Hz excitation frequency and zero-field condition. It was obtained as 111% for the anisotropic MRE corresponding to 20% strain amplitude, excitation frequency of 0.1 Hz and magnetic flux density of 750 mT. The maximum values of RSF_{η} for the isotropic and anisotropic MREs were obtained as 120% and 49%, respectively. These occurred under identical loading conditions (strain amplitude= 2.5%; *f*= 30 Hz) but *B*=300 mT and *B*=150 mT for the isotropic and anisotropic MREs,

respectively. The maximum values of RSF_η for the isotropic and anisotropic MREs were observed for the SF values of 0.56 and 0.75, respectively, which are also evident in Figure 4.6 to Figure 4.8.

4.3.3 Influence of shape factor on the relative MR effect

The effects of SF on magnetic field-dependent properties of the MREs are further evaluated in terms of the relative MR effect, which describes the relative change in elastic modulus ($MR_{\acute{E}}$) or loss factor (MR_η) from the zero-field condition to a specified or maximum available flux density [5, 84]. The relative MR effects are evaluated considering given excitation conditions (strain amplitude and frequency), while the specified/maximum flux density is taken as 600 mT. Figure 4.9(a) and 4.9(b) illustrate variations in relative MR effects of the isotropic and anisotropic MREs for SF ranging from 0.375 to 0.75, while the strain amplitude is varied from 2.5% to 10% at an excitation frequency of 1 Hz. The results generally suggest gradual increase in $MR_{\acute{E}}$ for both isotropic and anisotropic MREs with SF ranging from 0.375 to 0.56, irrespective of strain amplitude. This is also consistent with the results presented in Figure 4.8. While the $MR_{\acute{E}}$ for the isotropic MRE increases notably with SF, the increase is very small to negligible for the anisotropic MRE. The $MR_{\acute{E}}$, however, decreases with further increase in SF from 0.56 to 0.75 range, when the strain amplitude is lower than 10%, as observed in Figure 4.9(a). The decrease is substantially small for the anisotropic MRE compared to the isotropic MRE. Ivaneyko et al. [43] analytically investigated the relative MR effect of an undeformed isotropic MRE composite with 30% volume fraction subject to a uniform magnetic field, and showed substantial decrease in the MR effect as SF exceeded 0.56. The $MR_{\acute{E}}$ of the isotropic MRE, however, increases with increase in SF from 0.56 to 0.75 for the strain amplitude of 10%. This is also consistent with the results presented in Figure 4.3 and Figure 4.4, which suggest more demagnetizing field in presence of magnetic field for the disk-type MRE and MRE becomes further flat at relatively higher strain due to lateral bulging. For the isotropic MRE, the relative MR effect, $MR_{\acute{E}}$, increased from 243% to 275% and 171% to 188% under 2.5% and 5% strain amplitudes, respectively, when SF was increased from 0.375 to 0.56. The corresponding MR effect for the anisotropic MREs ranged from 149% to 158%, and 96% to 107% under 2.5% and 5% strain amplitudes, respectively.

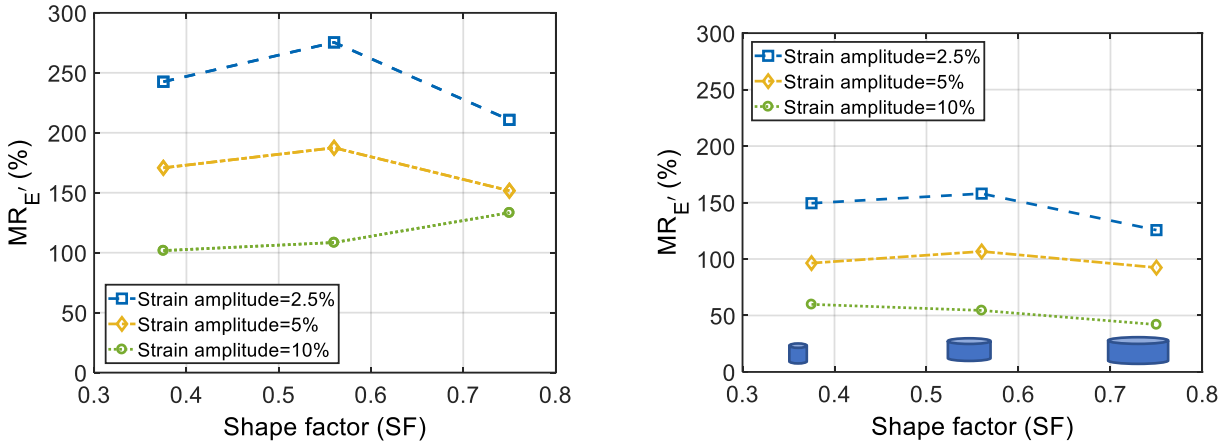

(a)

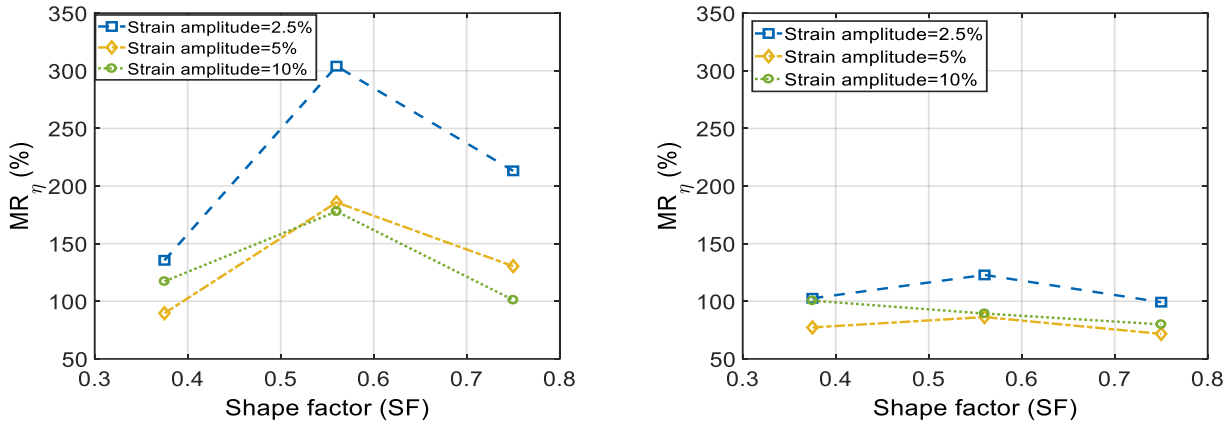

(b)

Figure 4.9 Dependency of relative MR effect in view of elastic modulus (a) and loss factor (b) on the shape factor of the isotropic (left column) and anisotropic (right column) MREs under different strain amplitudes (B= 600 mT; f=1 Hz).

The MR effect in view of loss factor, MR_η, also shows similar trends with respect to variations in SF, as seen in Figure 4.9(b). For the strain amplitude ranging from 2.5% to 10%, the anisotropy of the MRE showed only minimal effect of SF on MR_η. The SF effect, however, is quite significant for the isotropic MRE. The MR_η for the isotropic MRE increased significantly with increase in SF from 0.375 to 0.56 but decreased remarkably with further increase in SF in the 0.56 to 0.75 range, irrespective of strain amplitude. These are also consistent with the results presented in Figure 4.8.

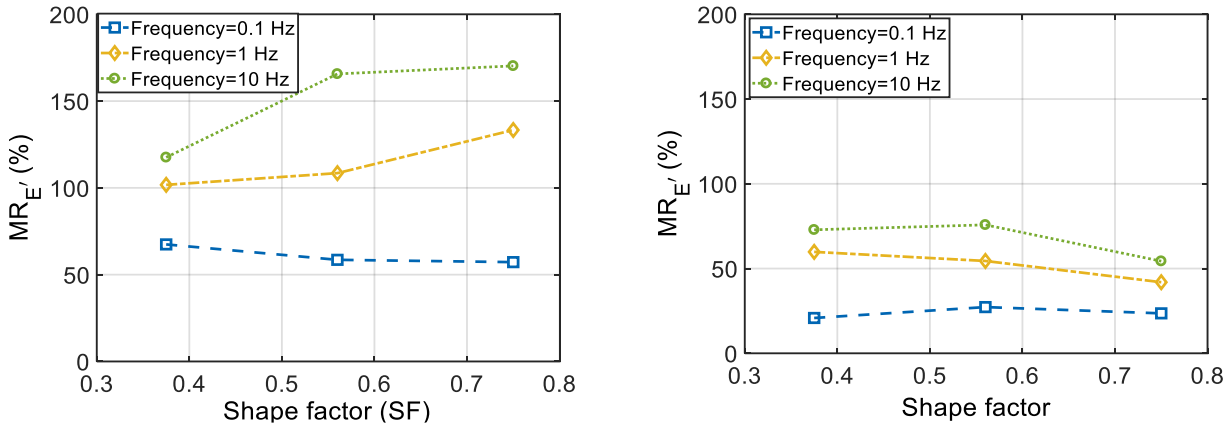

(a)

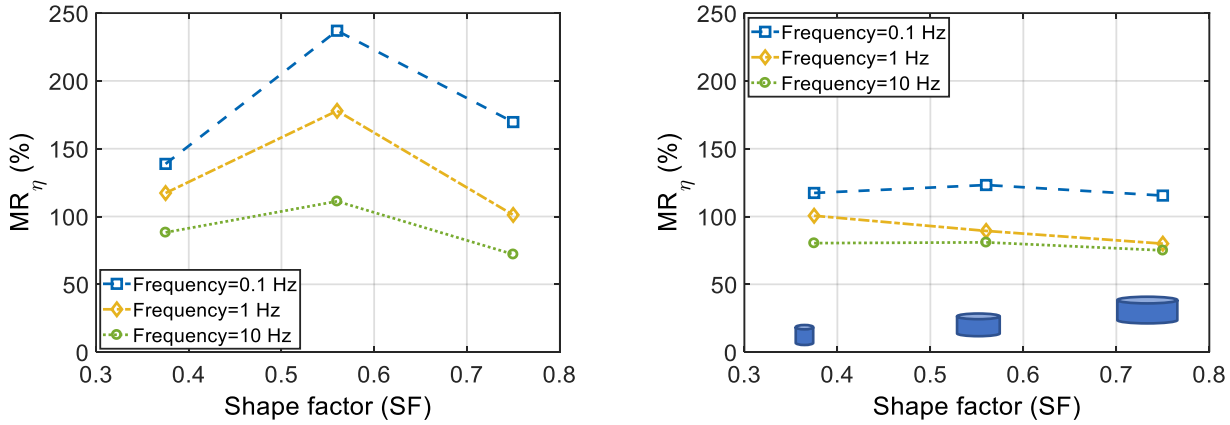

(b)

Figure 4.10 Dependency of relative MR effect on shape factor of the isotropic and anisotropic MREs at magnetic flux density of 600 mT under strain amplitude 10%: compression elastic modulus (a) and loss factor (b).

Figure 4.10(a) and 4.10(b) illustrate variations in $MR_{\acute{E}}$ and MR_{η} of the isotropic and anisotropic MREs, respectively, with respect to SF considering different excitation frequencies (0.1, 1 and 10 Hz) and 10% strain amplitude. In the quasi-static condition (0.1 Hz), the $MR_{\acute{E}}$ decreases and increases only slightly for the isotropic and anisotropic MREs, respectively, with increasing SF. This tendency has also been reported for the compression storage modulus [17] and magnetically induced stress [41] for the isotropic MREs in the static regime. Opposite trends, however, are observed at 1 and 10 Hz. For the isotropic MRE, the $MR_{\acute{E}}$ increases with increase in SF when frequency exceeds 0.1 Hz, while it decreases or increases very slightly for the anisotropic MRE. Under excitations at 1 and 10 Hz, the $MR_{\acute{E}}$ of the isotropic MRE increased from about 102%

to 109% and 118% to 166%, respectively, when SF increased from 0.375 to 0.56. Increasing the SF from 0.56 to 0.75 resulted in substantially higher $MR_{\dot{E}}$ at 1 Hz but considerably smaller at 10 Hz. This is consistent with the coupled SF- and strain rate-stiffening of the MREs observed in Figure 4.5 and Figure 4.7. The $MR_{\dot{E}}$ for the anisotropic MRE, on the other hand, decrease with increase in SF from 0.56 to 0.75, irrespective of the excitation frequency.

The SF dependence of the MR_{η} for different excitation frequencies (Figure 4.10(b)) is similar to that observed in Figure 4.9 for different strain amplitudes. For the isotropic MRE, the MR_{η} increased considerably with increase in SF from 0.375 to 0.56 but decreased remarkably with further increase in SF in the 0.56 to 0.75 range, irrespective of loading frequency. In the 0.375 to 0.56 range of SF, the MR_{η} varied from 139% to 237%, 117% to 178% and 88% to 111%, respectively, under 0.1 Hz, 1 Hz, and 10 Hz excitation frequencies. The MR_{η} of the anisotropic MRE, however, exhibits minimal variations in the entire range of the SF. In the 0.375 to 0.56 range of SF, the variations in MR_{η} of the anisotropic MRE were in the orders of 6%, 10% and 1%, respectively, under excitations at 0.1, 1 and 10 Hz.

Results also revealed maximum relative MR effect, $MR_{\dot{E}}$, under B=750 mT, up to 318% and 210% for the isotropic and anisotropic MREs, respectively, with SF of 0.56 and 0.375, respectively. These were observed under the strain amplitude of 2.5% at frequency of 10 Hz and 30 Hz, respectively, for the isotropic and anisotropic MREs. The maximum MR_{η} for the isotropic and anisotropic MREs, up to 304% and 310%, were observed for 2.5% and 20% strain amplitudes, respectively, at 1 Hz and, SF of 0.56 and 0.375.

4.4 Model development for predicting the compression moduli

The MRE-based vibration isolators and absorbers generally involve bonding of the MREs with different SF between elastic structures, which may further lead to a geometric non-linearity and thus the SF variations. A novel phenomenological model is formulated for predicting the SF-dependence of the compression mode properties of the MREs, which can facilitate the designs of MRE-based devices. In the absence of a magnetic field, the MRE can be considered as passive viscoelastic media. It has been reported that the compression modulus of bonded passive elastomers varies with the SF in a quadratic manner as [91]:

$$E_c = E_0(1 + \beta(SF)^2) \quad (4\text{-}8)$$

where E_c and E_0 are the effective compression modulus and Young's modulus of rubber, respectively [52]. The constant β is called the shape coefficient, which has been reported as 2 for bonded rubbers [96].

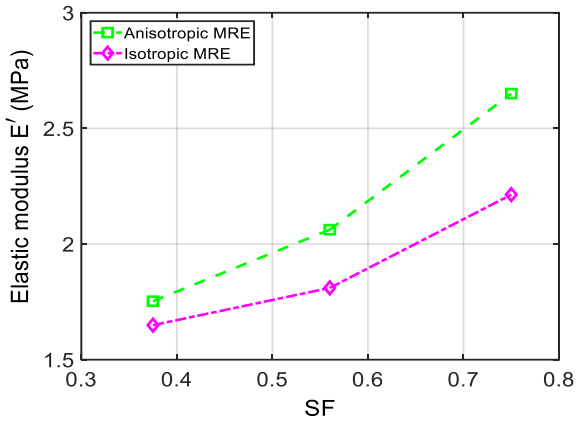

(a) B=600 mT, ε=5%, f=1 Hz

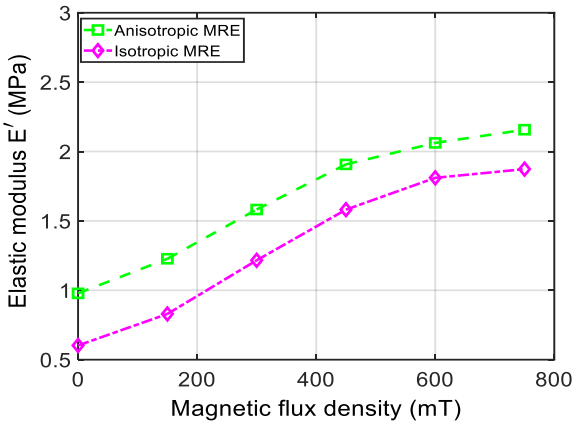

(b) ε=5%, f=1 Hz, SF=0.56

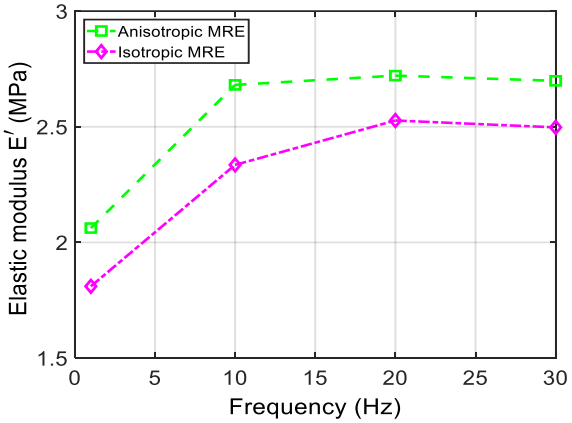

(c) B=600 mT, ε=5%, SF=0.56

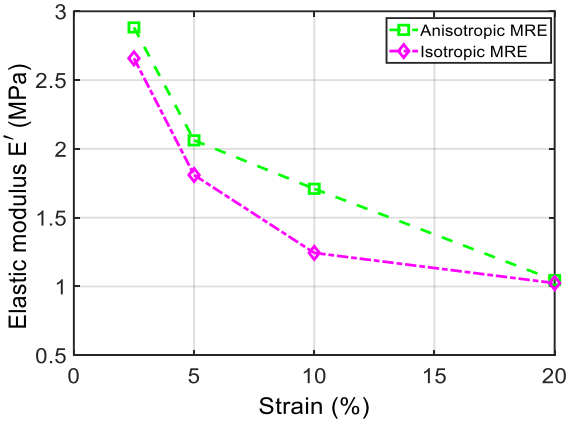

(d) B=600 mT, f=1 Hz, SF=0.56

Figure 4.11 Effects of SF, magnetic flux density, frequency and strain on the compression elastic modulus of the isotropic and anisotropic MREs.

The strong effect of the SF on the compression mode properties is also evident from the results, presented in Figure 4.2 through Figure 4.10, which is further coupled with the loading conditions (strain amplitude, frequency and magnetic flux density), as seen in Figure 4.11(a) to 4.11(d). Although, the results are presented for selected input factors, similar trends were observed

under other loading conditions. Results suggest increase in the elastic modulus of both the isotropic and anisotropic MREs with SF increasing from 0.375 to 0.75. The elastic moduli increased with increase in the magnetic flux density and frequency but decreased with increase in strain amplitude in a nonlinear manner, as shown in Figure 4.11(b) to 4.11(d). The moduli tend to saturate under higher flux density, excitation frequency and strain amplitude.

Owing to the observed coupled dependence of the elastic and loss moduli on the SF, strain amplitude, frequency and magnetic flux density, the effective compression moduli may be expressed by a phenomenological relation for both isotropic and anisotropic MREs, as:

$$E(SF, f, \varepsilon, B) = (a_1 + a_2(SF)^{a_3})(1 - e^{-a_4 f})\,(e^{-a_5 \varepsilon})\left(\frac{2}{1 + e^{-a_6 B}}\right) \tag{4-9}$$

where E represents the elastic (E') or loss (E'') moduli. The proposed model involves six unknown parameters, a_1 to a_6, which are identified through minimization of the error function, J, between the model-predicted and measured responses as:

$$J(a_1, .., a_6) = \sum_{i=1}^{M}\sum_{j=1}^{N}\sum_{k=1}^{O}\sum_{l=1}^{P}\left(E(SF, f, \varepsilon, B) - E_m(SF, f, \varepsilon, B)\right)^2 \tag{4-10}$$

where E_m is elastic or loss modulus obtained from the measured data, and indices i, j, k and l represent the measured or simulation outcomes corresponding to specific values of the SF, frequency, strain amplitude, and magnetic flux density, respectively. M, N, O and P represent the number of outcomes corresponding to the respective input factors considered in the error function, which were taken as 3, 5, 4, and 6, respectively. All the coefficients were constrained to be positive ($a_i > 0$; i=1,2,..6). The error minimization problem was solved using the Genetic algorithm (GA) followed by the nonlinear Sequential Quadratic Programming (SQP) technique in order to obtain accurate convergence to global minima, as suggested in [61]. Repeated solutions were obtained considering different initial values of the coefficients, which converged to nearly identical solutions, summarized in Table 4.1 for the elastic and loss modulus models for both the isotropic and anisotropic MREs.

Table 4.1 Identified coefficients of the proposed phenomenological model for predicting the elastic and loss moduli of the isotropic and anisotropic MREs.

Parameter	a_1	a_2	a_3	a_4	a_5	a_6
Isotropic						
E'	2.80	9.90	10.50	1.30	0.60	4.20
E''	0.54	1.75	8.01	1.34	0.38	4.18
Anisotropic						
E'	2.70	3.80	5.00	1.50	0.50	4.20
E''	0.50	0.60	3.60	1.20	0.40	4.30

The effectiveness of the proposed models is examined by comparing the model-predicted moduli with the measured data under different levels of the input factors. For instance, Figure 4.12 and Figure 4.13 compare the model-predicted elastic and loss moduli, respectively, of the isotropic and anisotropic MREs with the measured data for three different values of the SF. It should be noted that the elastic moduli are presented for ε=5%, f=1 Hz, and two different levels of the flux density (B= 0 and 450 mT), while the loss moduli are illustrated for ε=2.5%, f=10 Hz, and two levels of the flux density (B= 0 and 150 mT). The figures also show the estimation of the measured data by a data-driven model proposed by Sapouna [40], which suggests linear dependence of both dynamic and static modulus with shape factor as:

$$E = E_{ref}(1 + 3(SF - SF_{ref})) \tag{4-11}$$

where E, SF_{ref}, and E_{ref}, are the dynamic modulus, original or lowest possible shape factor (reference SF) considered, and the dynamic modulus corresponds to the referenced shape factor. The figures also present the variations in the effective moduli of the bonded rubber, obtained from the model proposed by Payne [96]. The comparisons suggest that the proposed phenomenological-based model can predict the elastic and loss moduli of both types of MREs reasonably well for the range of the SF considered in the study. A similar degree of agreements between the model and measured data were also observed over the entire ranges of SF, excitation and flux density considered in the study. In the passive mode (absence of the applied magnetic field), it is evident that the Payne's model [96] underestimates the moduli for both the isotropic and anisotropic MREs.

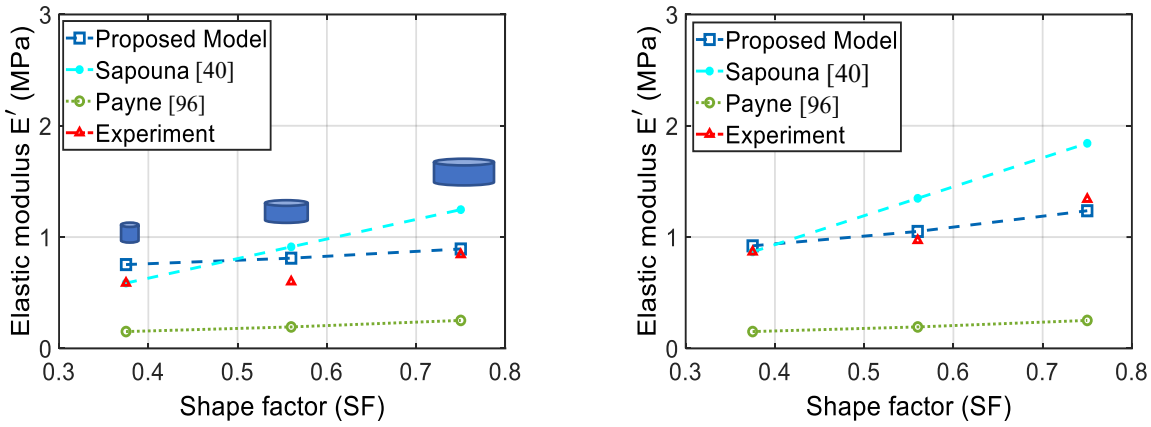

(a)

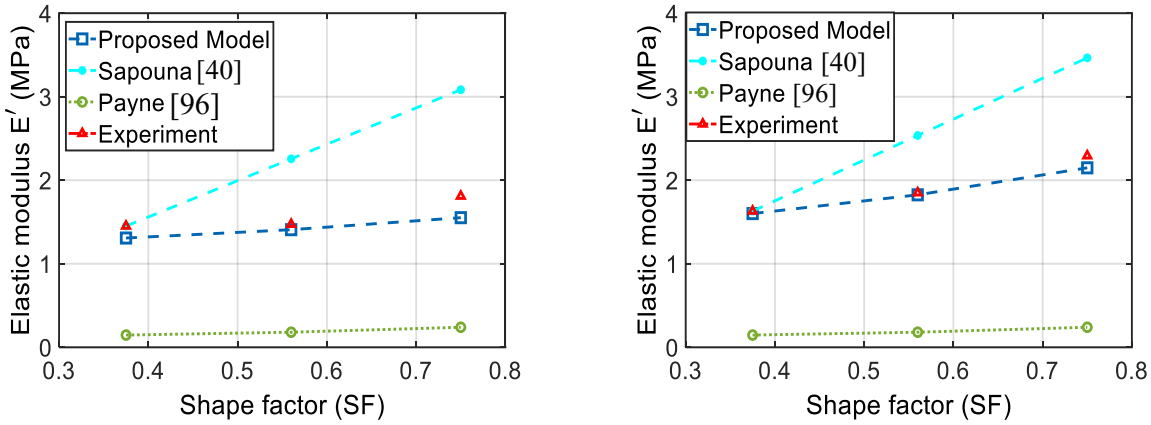

(b)

Figure 4.12 Comparisons of the SF-dependent compression elastic modulus predicted from the proposed phenomenological model with those derived from the Sapouna's model [40], Payne's model [96] and the measured data for the isotropic (left column) and anisotropic (right column) MREs subject to 5% strain at 1 Hz: (a) $B = 0\ mT$ and (b) $B = 450\ mT$.

Comparison further revealed the outperformance of the proposed phenomenological model compared with the linear model in predicting the elastic modulus of both types of MREs and loss modulus of anisotropic MRE at all loading conditions, while slightly overestimating the loss modulus of the isotropic MRE at the selected loading conditions. It is evident that the Payne's model [96] underestimates the moduli for both kinds of MREs over the range of SF considered. This would be expected considering nature of the Payne's model, which has been developed for passive elastomers.

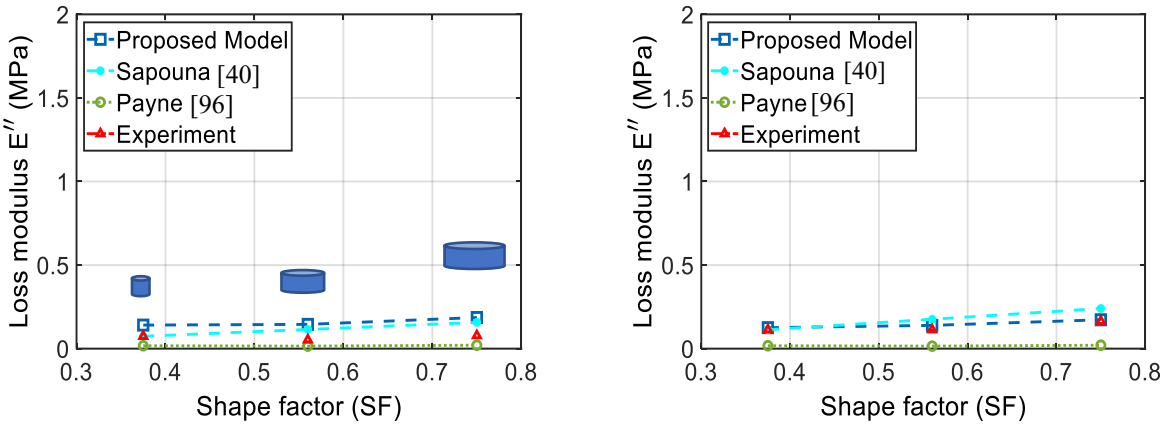

(a)

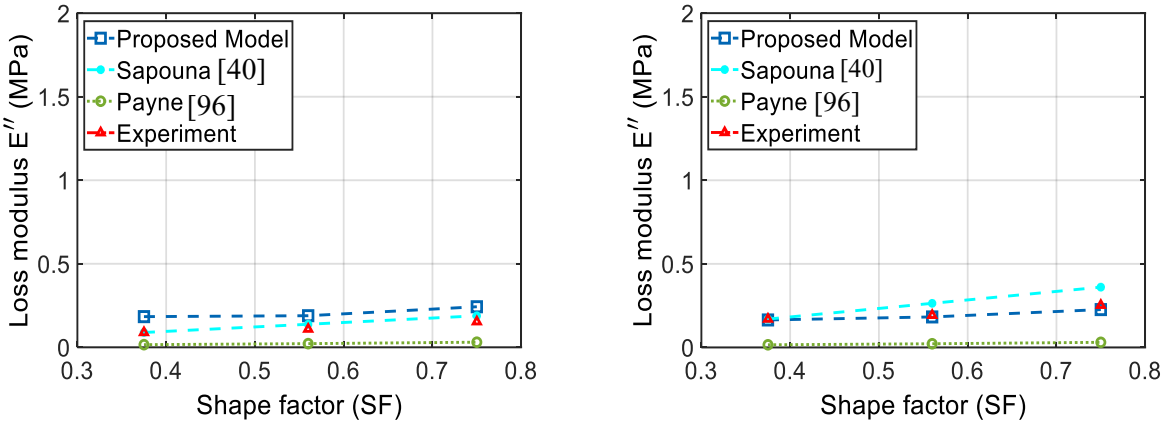

(b)

Figure 4.13 Comparisons of the SF-dependent loss modulus predicted from the proposed phenomenological model with those derived from the Sapouna's model [40], Payne's model [96] and the measured data for the isotropic (left column) and anisotropic (right column) MREs subject to 2.5% strain at 10 Hz: (a) $B = 0\ mT$ and (b) $B = 150\ mT$.

4.5 Conclusion

The effects of shape factor (SF) on the compression behaviors of the isotropic and anisotropic MREs in the dynamic mode were systematically investigated experimentally under broader ranges of excitation frequency, strain amplitude and magnetic flux density. The results showed strong dependence of the elastic and loss moduli of the isotropic and anisotropic MREs on the SF, which was further coupled with the effects of the strain amplitude and frequency, and the magnetic field. The elastic and loss moduli of both MREs generally increase in a nonlinear manner with increase in SF, regardless of loading condition and the magnetic flux density. The SF-stiffening effect,

however, was somewhat limited in the presence of anisotropy, strain-softening, and strain-rate-stiffening of the MREs. The isotropic and anisotropic MREs revealed maximum shape factor-stiffening effect of up to 77% and 111% for the compression elastic modulus, respectively, when shape factor was increased from 0.375 to 0.75. The peak shape factor effects on the loss factor of the isotropic and anisotropic MREs were obtained as 120% and 49%, respectively. Results generally suggest nonlinear effects of the SF on both off- and on-state MRE properties and increasing SF can enhance the relative MR effect in view of both the elastic and loss factor of the isotropic and anisotropic MREs. The simple phenomenological model proposed for predicting SF-dependent moduli of the MREs has provided good agreements with the measured data for the ranges of magnetic and mechanical loadings considered. The proposed model could thus serve as a guidance for designing MR-based devices involving different sizes and shapes of MREs.

CHAPTER 5
PRE-STRAIN EFFECTS

5.1 Introduction

Many studies have investigated the behavior of MREs in compression mode, as summarized in Table A1 and Table A2. These tables reveal that vast majority of the studies have neither reported nor assessed the effect of pre-strain (or pre-stress) on dynamic behavior of MREs in compression mode. However, in many applications involving compression of the MRE such as vibration isolators and absorbers, the MRE will likely undergo comprehensive static strain due to weight of the supported structures. The static pre-strain can considerably alter the MR effect due to decrease in the distance between the magnetizable particles. Despite its important significance, very limited studies have been conducted on the effect of pre-strain on the viscoelastic and hysteresis behavior of MREs. Koo et al. [20], Martins et al. [44], and Vatandoost et al. [21] have characterized properties of MREs under specified constant pre-strain of 5%, 6.5%, 0%, respectively. Lee et al. [26] characterized compressive properties of anisotropic MREs in static regime and showed that lower level of pre-strain in the specimen resulted in higher stress changes upon applying the magnetic field of 300 mT. Sapouna [40] experimentally assessed the effect of pre-strain on dynamic behavior of MREs at a constant frequency of 5 Hz and obtained 50% and 30% increases in the storage and loss modulus of anisotropic MRE, respectively, and correspondingly 25% and 5% for isotropic MRE, when pre-strain was increased from 2% to 10%; however, the effect of pre-strain, particularly in a wide range, at different frequencies and higher levels of magnetic flux density has not been investigated.

As it can be realized, reported studies suggest relatively limited knowledge on the effects of the pre-strain on dynamic properties of the MREs in the compression mode. It should be noted that the pre-strain effects on the properties of filled elastomers are well known. In filled elastomers, an increase in storage and loss moduli is observed with increasing pre-strain [32]. The dynamic properties of MREs are thus expected to depend on the pre-strain. While the pre-strain effect on off-state properties of an MRE is comparable to that of a passive filled-elastomer, the dynamic properties of MREs may show significant pre-strain effect in the presence of the magnetic field. Kalina et al. [36] numerically investigated the effect of mechanical pre-load on deformation dependent properties of structured (anisotropic) and unstructured (isotropic) MREs by means of a

microscale continuum approach. They showed that by varying the pre-load, different effects can occur depending on the microstructure of MREs, predominately, the interaction of particles in wavy chains, which is responsible for their macroscopic behavior such as magnetostriction strain. Besides, the MR effect, which is highly dependent on the local spatial distribution of magnetizable particles [43], apart from particle volume fraction, is highly dependent on the pre-strain as it can considerably alter the distance between the magnetizable particles.

Considering above, the effect of pre-strain is of paramount importance as it significantly affects the viscoelastic properties of MREs and thus should be considered in the design of MRE based devices under compression mode. The present study aims at thorough experimental examination of the effect of pre-strain on the dynamic compression mode properties of both isotropic and anisotropic MREs comprising different particle volume fraction under varied frequency and magnetic flux density. The force-deflection properties of isotropic and anisotropic MRE samples, fabricated with 15%, 30%, and 45% volume fraction of iron particles, were acquired under harmonic excitation with strain amplitude of 2.5% superimposed on three different pre-strains, including 6%, 11%, and 21% at frequencies ranging from 0.1 to 30 Hz, and magnetic flux density up to 750 mT. The measured data were subsequently analyzed to assess the effect of pre-strain on the compression moduli and loss factor of the isotropic and anisotropic MREs, apart from MR effect. A novel phenomenological-based model is afterward proposed to predict the compression mode elastic moduli as well as stress-strain hysteresis loops of both types of MREs as functions of the pre-strain, volume fraction, frequency and magnetic flux density. The study should provide guidance for potential applications of MREs in vibration isolators and absorbers, where the pre-strain plays an important role.

5.2 Experimental Methods

5.2.1 MRE samples

Several isotropic and anisotropic MRE batches with 15%, 30%, and 45% volume concentrations of carbonyl iron particles (CIPs), corresponding to 56.5%, 76%, and 86% mass faction of CIPs, respectively, were fabricated in the laboratory. The spherical magnetically soft CIPs (SQ, BASF Inc., Germany), with diameter varying from 3.9 to 5 μm were embedded inside a very stretchable platinum-based silicone elastomer (Eco-Flex 00-20, Smooth-On Inc., USA) as the medium. The complete fabrication procedure is presented in [9].

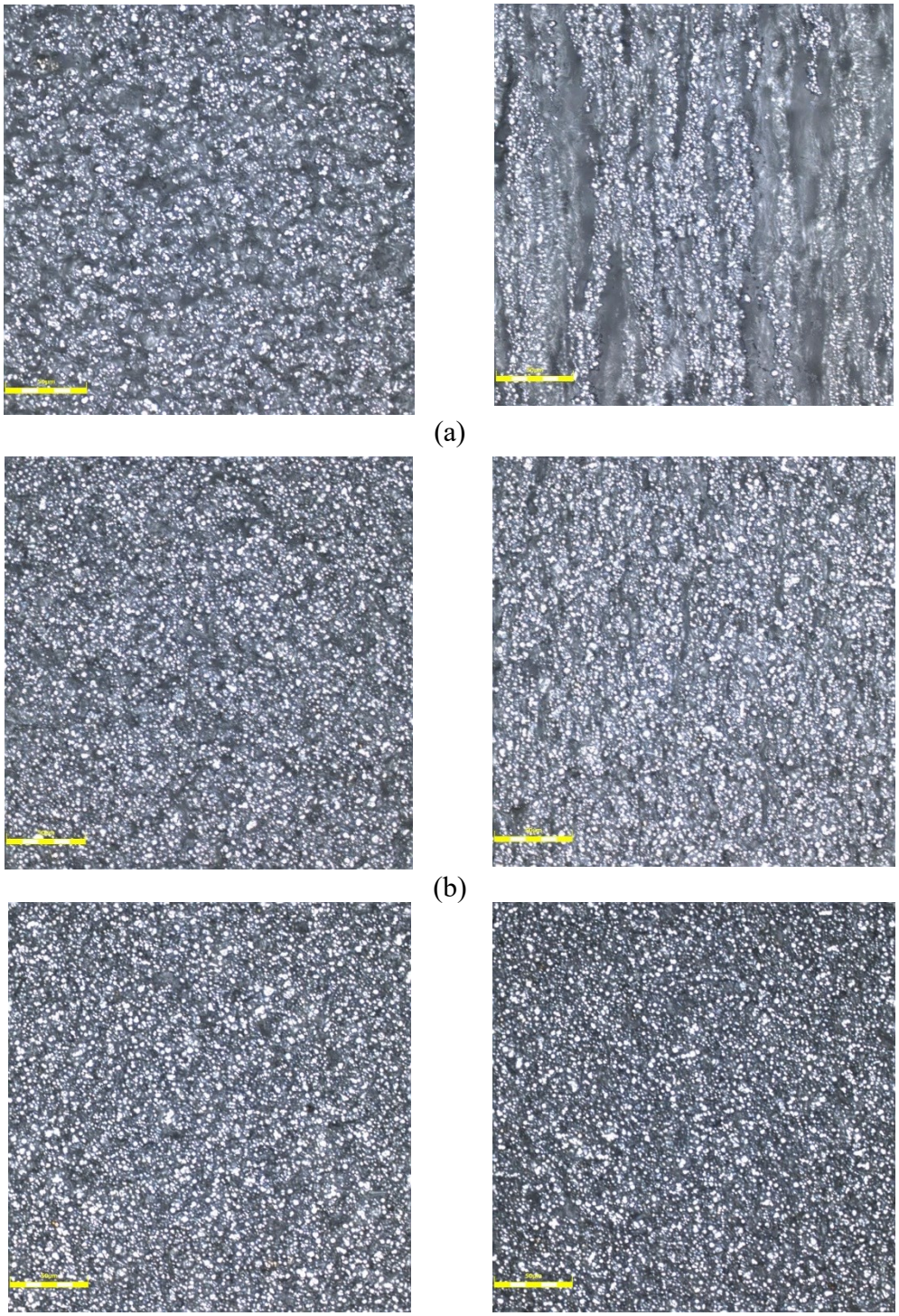

Figure 5.1 Microstructure images of fabricated isotropic (left column) and aligned (right column) MREs samples taken by Confocal microscopy with 50X magnifications: (a) 15% volume fraction, (b) 30% volume fraction, and (c) 45% volume fraction.

In a nutshell, the CIP were initially added to the medium and then thoroughly blended using a mixer for around 5 minutes. The blended mixture was then degasified in a vacuum apparatus for almost 5 minutes under negative pressure of 736 mmHg, and then slowly placed into two molds, made of cylindrical plexiglass (radius=50 mm; thickness =8 mm). One of two batches was allowed to cure for almost 24 hrs at room temperature, whilst the other batch was cured for three hours within a homogenous magnetic flux density of 1200 mT, provided by an adjustable air gap electromagnet. Subsequently, several cylindrical MRE specimens with diameter and thickness of 18 mm and 8 mm, respectively, were cut from both batches. The dimension of MRE specimens were chosen in accordance with the current standards for compression testing of rubber-like materials (ISO 7743 [52]). It is noted that the anisotropic MRE samples were vertically cut parallel to the chain orientation of magnetic particles.

The distribution of magnetic particles inside MREs was evaluated utilizing an engineering laser confocal microscope (OLYMPUS LEXT OLS4000). In this regard, the MRE specimens were vertically sliced parallel to chain orientation employing a scalpel, and then placed under the microscope. Figure 5.1 demonstrates the microstructure of both MREs with various particle volume fractions. The white spots in the pictures are the iron particles and the grey backdrop demonstrates the medium of the isotropic (left column) and aligned (right column) MRE specimens. For the isotropic and anisotropic MREs, correspondingly, homogeneous distribution of particles and the chains of particles in the medium can be clearly observed. Figure 5.1 further reveals that the aligned chains, however, are more noticeable for relatively lower level of particle volume fraction.

5.2.2 Test rig

A test apparatus was custom-built to identify pre-strain dependent characteristics of MREs with different particle volume fraction (15%, 30%, and 45%). The experimental test setup has been extensively elaborated in [9]. In summary, the setup contained a U-I design of a compact electromagnet, which allowed application of magnetic flux density of up to 1 T in the compression direction of the MRE. Two identical MRE specimens, either two isotropic or two anisotropic MRE specimens, were bonded to the U- and I-form cores of the electromagnet as displayed in Figure 5.2, which were fixed on the actuator of a material testing system. The U-shaped core of the electromagnet was connected to the actuator shaft and the I-section was linked to an immovable

beam via a 9kN load cell. The experiments were performed employing the regulated techniques outlines in ISO 7743 [52] for characterizing force-displacement (stress-strain) characteristics of each type of MRE specimen subject to harmonic excitations with strain amplitude (ε_0) of 2.5% superimposed on different static pre-strains. Hence, the pre-strain applied prior to the harmonic compression excitations. While, there is no specific level of static pre-strain have been suggested for dynamic testing of rubbers [87, 88], the levels of static pre-strains should be selected such a way that the samples stay undamaged during the tests. Staying in compression region ($\varepsilon_p > \varepsilon_0$) was another key factor in selecting the levels of the pre-strains in the present study. Considering this, the static pre-strains were selected as ε_p=6%, 11%, and 21%.

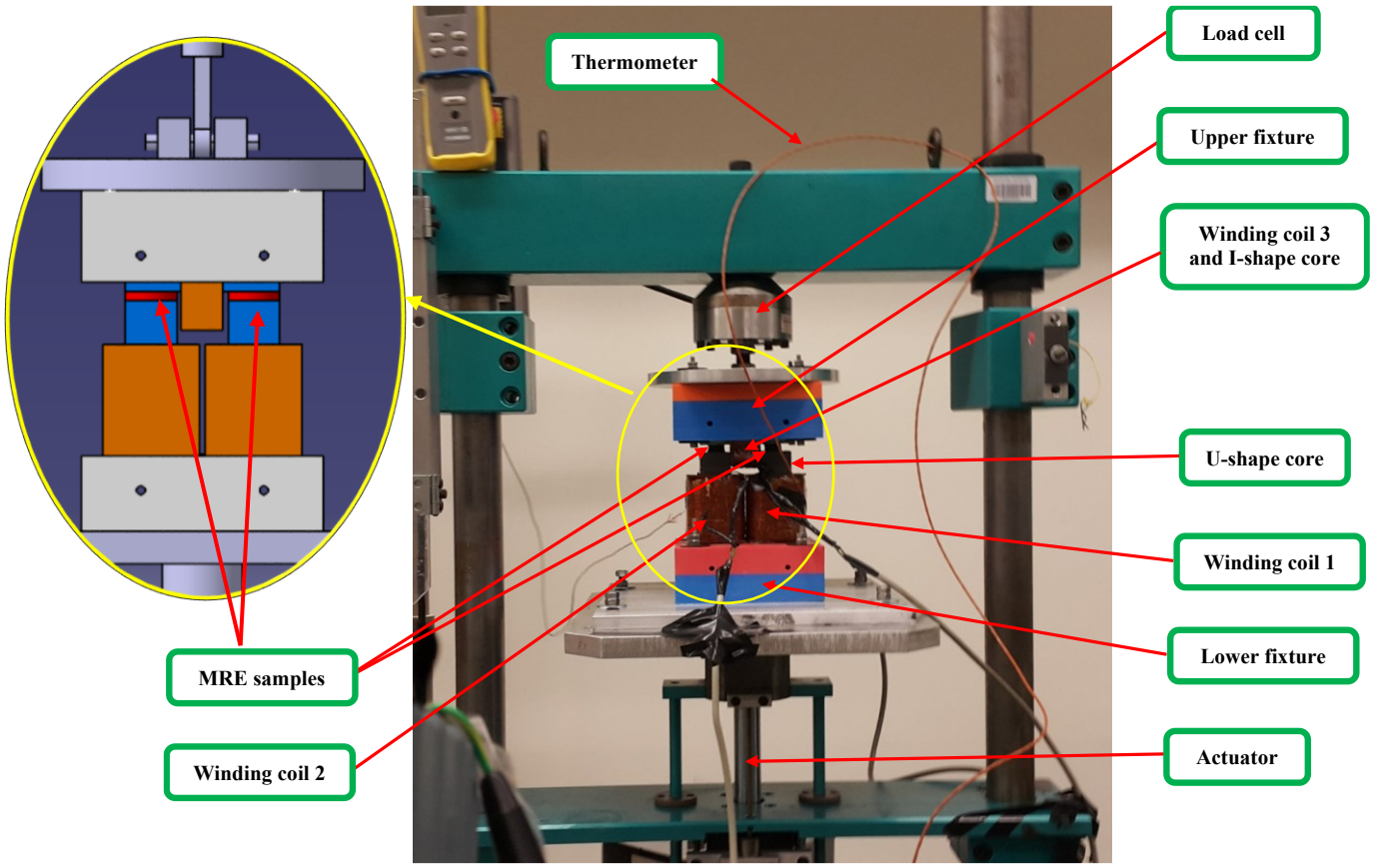

Figure 5.2 Pictorial illustration of the test setup for compression mode characterization of the MRE: The red cylinders in the left picture illustrate the position of two MRE samples.

It should be noted that the considered wide range of static pre-strain superimposed by small sinusoidal excitation can be found in numerous applications such as vibration isolators and absorbers, engine mounts and automotive tires, in which such large level of pre-strains are

expected and inevitable due to weight of the supported structures by MREs. It is also noted that even though such large static pre-strains may temporarily destroy the filler network, application of magnetic field can easily reconstruct the broken filler network. It is due to the fact that a very soft silicone rubber was chosen as the matrix, thereby not only maximizing the relative MR effect but also allowing magnetic particles to easily structure themselves in presence of magnetic field. Thus, multiple uniaxial experimental tests have been conducted in which the static pre-strain was initially applied and then the harmonic tests were performed on the specimen at different values of magnetic flux density as well as excitation frequencies. Hence, the experiment design involved factorial combinations of three pre-strains (ε_p=6%, 11%, and 21%), applied at four different frequencies (f= 1, 10, 20 and 30 Hz) together with six different amounts of magnetic flux density (B = 0, 150, 300, 450, 600 and 750 mT) on each particle volume fraction of the MRE specimen, thereby leading to a total of 216 tests.

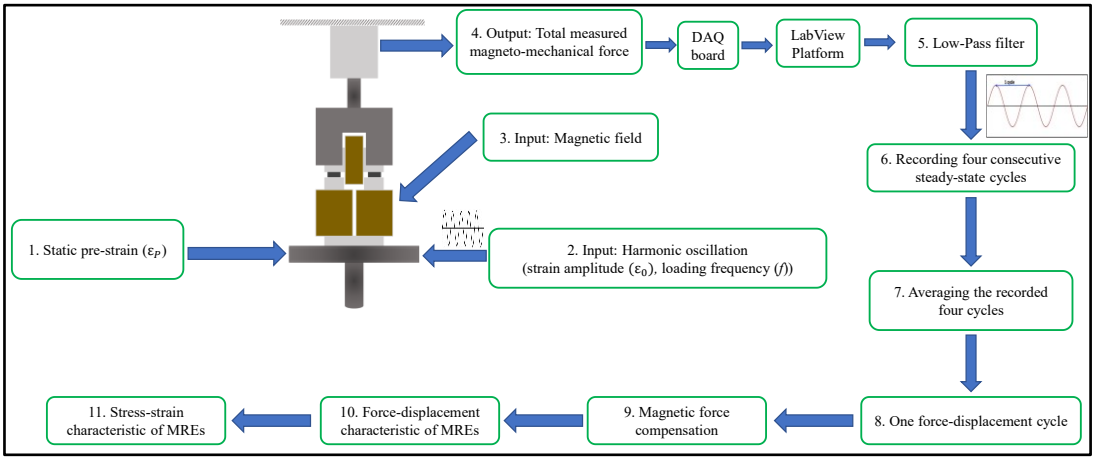

Figure 5.3 Schematic diagram of the test process and data analysis.

Controlled magnetic flux was realized employing a 1000-Watt power supply. It is noted that the magnetic flux induction within air gap of the electromagnet in absence and presence of MREs were calculated and summarized in [9]. It should be noted that the force measured during compression mode characterization of an MRE consists of two components: (i) the magnetic pull force generated between I-form and U-form cores of the electromagnet; and (ii) the compression viscoelastic force of the MRE. The force and displacement measurements considering wide range of magnetic flux density were also performed without presence of the MRE specimens within air gap. These measurements were, hence, employed to establish a systematic methodology to precisely predict the magnetic pull force developed by the electromagnet in presence of MRE in

the gap [9]. The experimental and magnetic force compensation procedures have been described in detail in Chapter 2 of this dissertation. The calculated pull force was deducted from the overall force, recorded by the load cell, in order to extract the field-dependent viscoelastic force of the MRE. The corresponding schematic diagram of the test process and subsequent data analysis are depicted in Figure 5.3.

5.2.3 Data analysis

The force-displacement data were collected in LabView during each trial employing a sampling frequency incrementing from 50 Hz to 5000 Hz, depending on the loading frequency. The steady-state force and displacement data, acquired during four successive oscillation cycles, were low-pass filtered and averaged for subsequent analyses of corresponding stress-strain characteristics, as depicted in Figure 5.3. The cut-off frequency of the low-pass filter ranged from 2 Hz to 200 Hz, depending on the loading frequency. By compensating for the magnetic force employing the phenomenological model reported in Equation (2-24), the resulting force and displacement data related to compression of MRE subsequently obtained from total force, measured by load cell. These data are, afterward, employed to acquire stress-strain behavior of the MREs, the compression mode elastic (E') and loss (E'') moduli, which represent energy storage and dissipation characteristics of MREs, respectively. The compression moduli are commonly approximated by the slope of the main axis and the closed area of the stress-strain curves, correspondingly, employing peak-to-peak measurement [87] as:

$$E^* = \left|\frac{\sigma_0}{\varepsilon_0}\right| = \sqrt{(E')^2 + (E'')^2} \tag{5-1}$$

$$E'' = \frac{E_d}{\pi \varepsilon_0^2} \tag{5-2}$$

where E^*, σ_0, and ε_0, are the complex modulus, maximum stress, maximum strain amplitude. Besides, $E_d = \oint \sigma d\varepsilon$ represents the dissipated energy per cycle which can be obtained from the confined area within the stress-strain curves. Significant inaccuracies may be anticipated for MREs with relatively higher particle volume fraction, which can reveal nonlinearities such as strain-stiffening effect, particularly at the end of loading path in stress-strain characteristics even under relatively lower deformations. Hence, in this study the compression elastic and loss moduli are calculated on the basis of the first harmonic approach using Fourier series of the experimental

records, which the ASTM D5992-96 [97] suggests this method for approximating moduli of the rubber-like materials demonstrating nonlinear hysteretic features, as

$$\sigma(t) = \sigma_m + \sum_n \varepsilon_0\left(E_n' sin(n\omega t) + E_n'' cos(n\omega t)\right) \tag{5-3}$$

where σ denotes the steady-state output stress and σ_m represents mean stress, corresponding to an applied pre-strain. $n, \omega,$ and t represent an integer for indexing number of harmonics, angular frequency and physical time, respectively. The first harmonic compression elastic and loss moduli, $n = 1$, namely, E_1', and E_1'' can be regarded as linear estimation to a nonlinear viscoelastic reaction, which can be visualized as a perfect ellipse (equivalent linear stress-strain characteristic) [98]. To further assess the influences of pre-strain on stress-strain features of both MREs in terms of the energy storage (or equivalent stiffness) and energy dissipation (equivalent damping) characteristics, the 'pre-strain stiffening' and 'pre-strain-dampening' effects are defined here on the basis of the estimated first harmonic compression elastic and loss moduli, respectively, from the experimental results as:

$$\%\text{Pre-strain-stiffening} = \frac{E'_{\varepsilon_{p_{max}}} - E'_{\varepsilon_{p_{min}}}}{E'_{\varepsilon_{p_{min}}}} \times 100 \tag{5-4}$$

$$\%\text{Pre-strain-dampening} = \frac{E''_{\varepsilon_{p_{max}}} - E''_{\varepsilon_{p_{min}}}}{E''_{\varepsilon_{p_{min}}}} \times 100 \tag{5-5}$$

where $E'_{\varepsilon_{p_{max}}}$ and $E''_{\varepsilon_{p_{max}}}$ are the compression mode elastic and loss moduli, respectively, corresponding to the maximum pre-strain of 21%.$E'_{\varepsilon_{p_{min}}}$ and $E''_{\varepsilon_{p_{min}}}$ are the reference compression moduli corresponding to the lowest pre-strain of 6%. To provide a direct and precise description for the test results, all the quantitative results of the linear slope of the main axis and the region bounded by the stress-strain curves, compression mode elastic and loss moduli, loss factor together with the pre-strain stiffening and pre-strain dampening effects for both types of MREs are summarized in Table B1 through Table B11, and Figure B1 through Figure B16 in the Appendix B. It is also noted that the data related to the loading frequency of 20 Hz and 30 Hz for all the pre-strains, particularly, at higher level of flux density could not be obtained considering the high applied current to the electromagnet and safety issue. Therefore, for the sake of consistency, the results related to the loading frequency of 20 Hz and 30 Hz, together with maximum flux density of 750 mT, are just presented in the Appendix B.

5.3 Experimental Results

In the following sections experimental data are analyzed to systematically investigate the effect of pre-strain on stress-strain behavior, viscoelastic properties (compression elastic and loss moduli) as well as relative MR effect of isotropic and anisotropic MREs.

5.3.1 Effect of pre-strain on stress-strain characteristics

The experimental stress-strain features of the isotropic and anisotropic MREs with different volume fractions, consistently, showed hysteresis phenomenon mostly attributed to viscosity of medium of MREs. Results indicated great dependence of the stress-strain behaviours on the pre-strain, anisotropy, volume fraction, frequency and the magnetic flux density. As an example, Figure 5.4 exemplifies the impact of pre-strain on the stress-strain traits of the isotropic and anisotropic MRE samples with three different volume fractions (15%, 30%, and 45%) subject to harmonic excitation of 1 Hz without presence of the magnetic field. The results exhibit relatively linear viscoelastic behaviour in which hysteresis loops are nearly elliptical for both types of MREs, which is more pronounced under the lower levels of pre-strain and volume fraction. Results also revealed that both the main axis slope and the region bounded by the stress-strain hysteresis curve, which can be considered as the equivalent stiffness and damping, respectively, enhance with increasing the pre-strain from 6% to 21%. This behavior is consistent with those previously reported for passive filled-elastomers under uniaxial loading [32]. The particle-matrix and particle-particle interactions are the two main reinforcement mechanisms, that can explain the increase in modulus of filled-elastomers compared to that of unfilled-elastomers [99]. The reinforcement mechanisms can be enhanced in a linear and quadratic manner, respectively, for low and high filler volume fraction, taking into account interactions between neighborhood particles [100]. By increasing the static pre-strain, the effective volume faction of filled-elastomer increases due to immobilized occluded [100] and surface-bound [101] elastomeric matrix, thereby, increasing the equivalent stiffness of filled-elastomers.

Moreover, the increase in the equivalent damping of filled-elastomers due to increasing pre-strain may be attributed to the enhanced friction between magnetic particles as results of their relative motions to the surrounding elastomeric medium as well as particle-medium interaction [102]. Even though the results presented for the loading frequency of 1 Hz, similar tendency was also observed at the other loading frequencies considered in this study, as can be realized in

Tables B1-B3. Results shown in Figure 5.4 also suggest that the impact of pre-strain on the equivalent stiffness and damping becomes more pronounced by incrementing the volume fraction of iron particles, irrespective of loading frequency. Besides, the stress-strain hysteresis loops move upward with increasing pre-strain which is probably due to the strain amplification effect which enhances the filler-matrix interaction [101]. This tendency has also been reported for passive filled rubber-like materials [103]. Increasing pre-strain from 6% to 21%, yields notably higher peak stress during compression loading as shown in Figure 5.4.

Results also show that at the zero magnetic flux density, the isotropic MREs revealed higher pre-strain stiffening and pre-strain dampening effects compared to the anisotropic MREs, irrespective of loading frequency and particle volume fraction, which can also be realized from Table B4 and B5. This can be ascribed to the lower number of particle-matrix interactivities in anisotropic MREs in which many particles are close to each other or even aggregated within particle chains, causing lower pre-strain stiffening effect, compared to isotropic MREs. As an example, increasing the pre-strain from 6% to 21% yielded pre-strain stiffening effects of up to 52%, 182%, and 743% for the isotropic MREs with 15%, 30%, and 45% particle volume concentrations, respectively. The corresponding pre-strain stiffening effects for the anisotropic MRE were found to be 15%, 35%, and 70%. Besides, the corresponding pre-strain dampening effects for the isotropic MREs were obtained as 135%, 137%, and 1115% compared with 27%, 74%, and 152% for the anisotropic MREs, corresponding to 15%, 30%, and 45% particle volume concentrations, respectively.

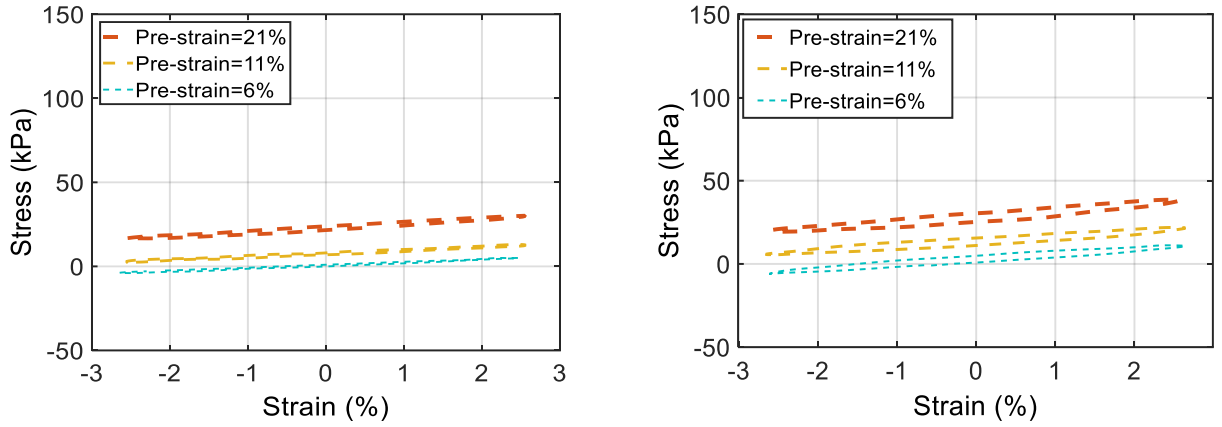

(a)

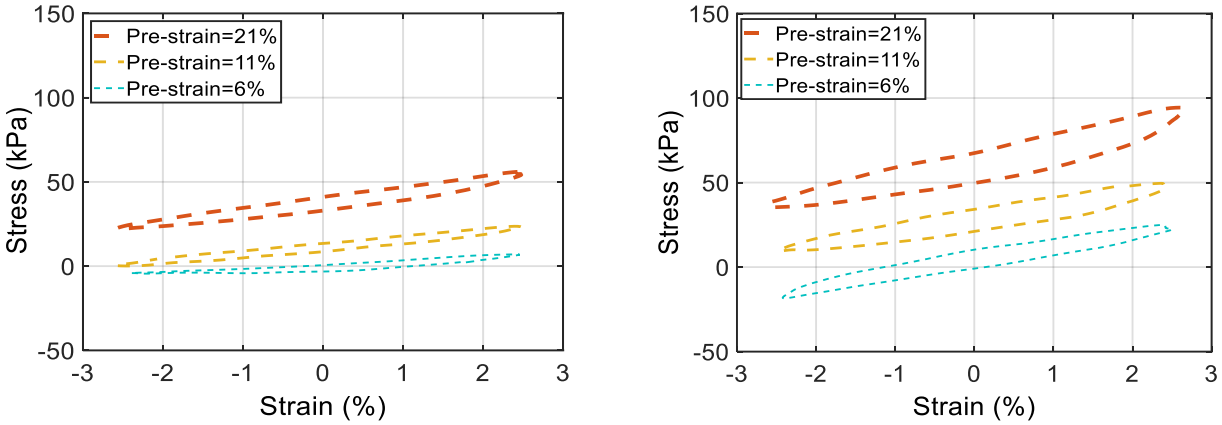

(b)

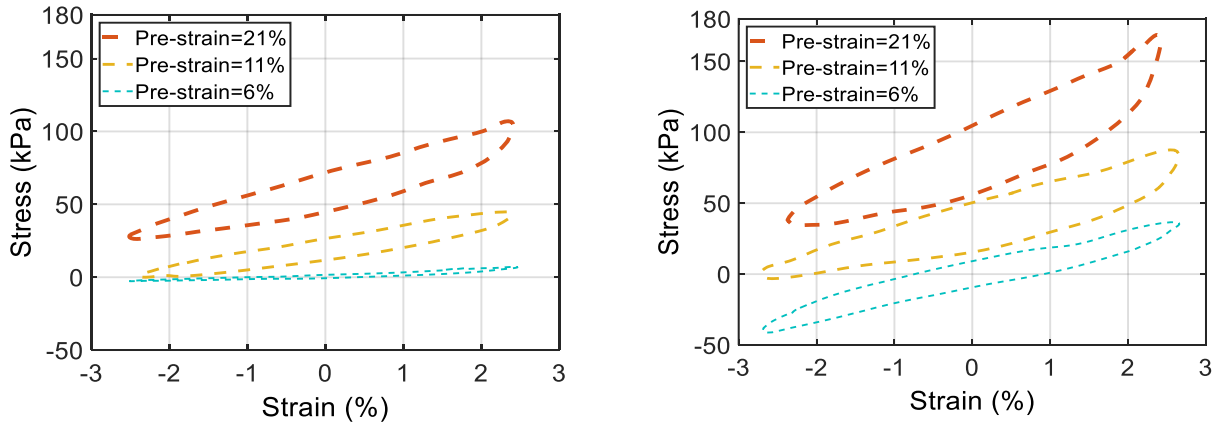

(c)

Figure 5.4 The effect of pre-strain on the strain-stress characteristics of the isotropic (left column) and anisotropic (right column) MREs with different particle volume fractions: (a) 15%, (b) 30%, and (c) 45% (ε= 2.5%, f= 1 Hz, and B= 0 mT).

Figure 5.5 demonstrates the impact of pre-strain on the stress-strain properties of both sorts of MREs with three different volume fractions (15%, 30%, and 45%). The results are presented for driving frequency of 1 Hz in the presence of magnetic field (B=450 mT), as example. Figure 5.5 shows that pre-strain stiffening effects of both MREs enhances when particle volume fraction increases, which is also observed in absence of field according to the Figure 5.4. Relatively similar tendency was also observed at the other loading frequencies, as can be realized by Table B4. The results, nonetheless, show that increasing pre-strain from 6% to 21%, generally yielded lower pre-strain stiffening effect for both MREs, when compared with those observed in the absence of the magnetic field (Figure 5.4), irrespective of particle volume fraction. This is in part attributed to the fact that the relatively higher pre-strain of 21% causes particles get too close to each other, which becomes more pronounced in presence of magnetic field owing to magnetic attraction, thereby relatively lowering number of dipole-dipole interactions among magnetic particles. The observed decrement in pre-strain stiffening effect, however, is more pronounced for the isotropic MRE due to greater distance between magnetic particles as compared with anisotropic MRE, thus appearing further susceptible to variation in pre-strain. As an example, for the chosen conditions (f=1 Hz, B=450 mT) and particle volume fraction of 30%, increasing pre-strain from 6% to 21%, yielded relatively lower pre-strain stiffening effects of 26% and -0.3% for the isotropic and anisotropic MREs, correspondingly, in comparison with those attained without presence of magnetic field, 182% and 35%, respectively.

It is also noted that the observed reduced pre-strain stiffening of both types of MREs, when pre-strain increased from 6% to 21% is not caused by the matrix failure. It is because that the zero-field elastic modulus of both types of MREs consistently increased with increasing pre-strain from 6% to 21%, regardless of loading frequency and particle volume fraction, which can also be realized from Figures B1, B4, and B7, and also from Figures B10 to B14. However, these when pre-strain increased from 6% to 11%, only elastic modulus of the anisotropic MRE generally decreased, which is due to breaking of filler network. Instead, the magnetic interactions between particles is rather more dominant than polymer elasticity in altering the stiffness of MRE at higher level of pre-strain.

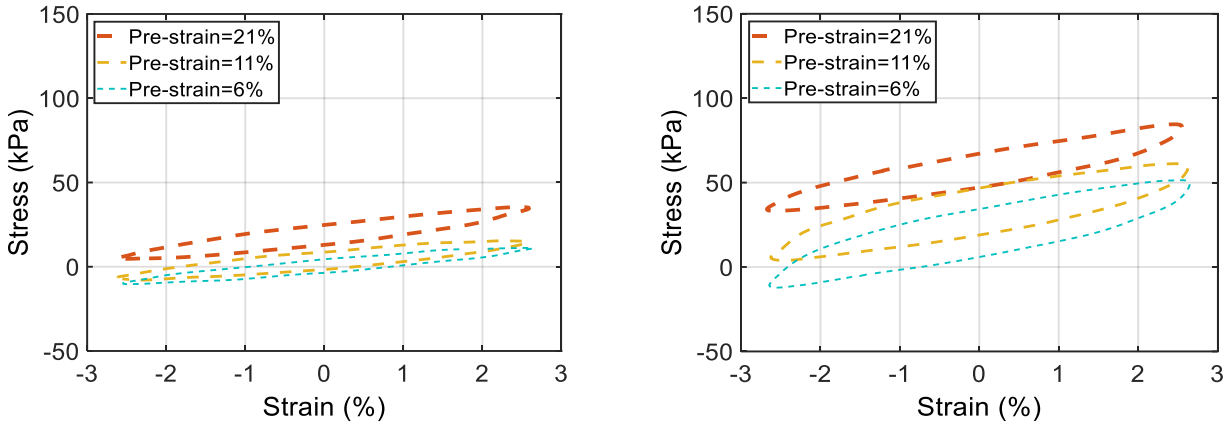

(a)

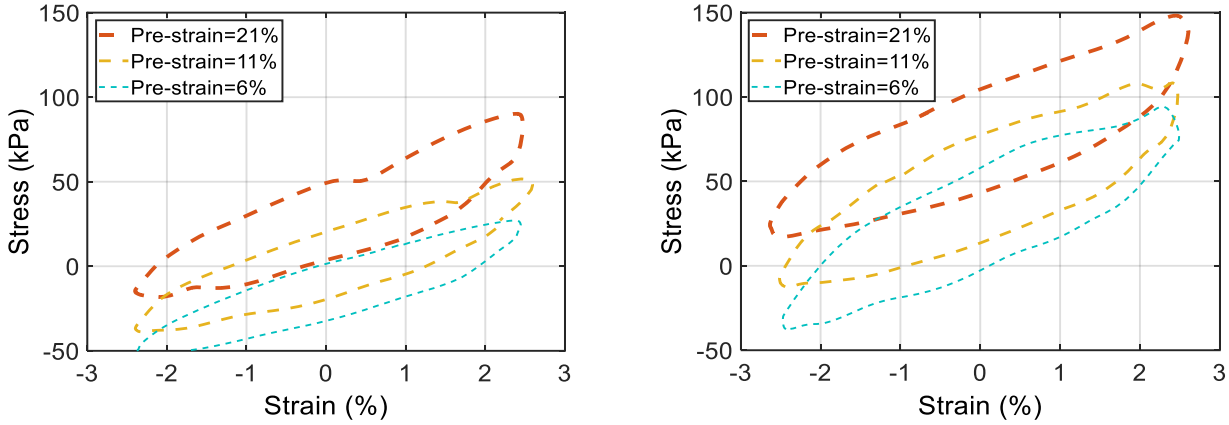

(b)

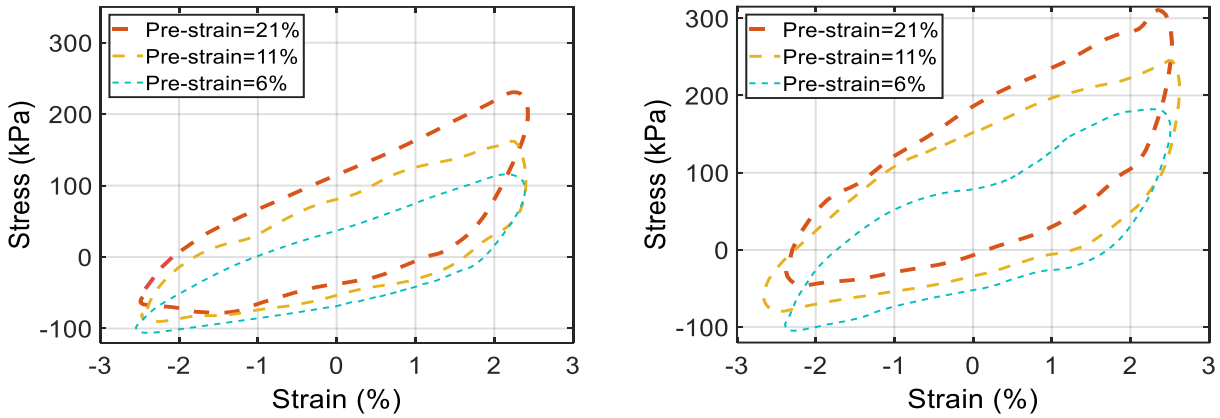

(c)

Figure 5.5 The effect of pre-strain on the strain-stress characteristics of the isotropic (left column) and anisotropic (right column) MREs with different particle volume fractions: (a) 15%, (b) 30%, and (c) 45% (ε=2.5%, f= 1 Hz, and B= 450 mT).

More particularly, the very low or negative pre-strain stiffening effect for the anisotropic MRE in the presence of magnetic field, can mostly credited to this fact that the magnetic particles are already close to each other within chains of anisotropy at relatively lower level of pre-strain (6%), then become too close to each other at higher level of pre-strain (21%). At the same time applying magnetic field causes magnetic particles touch each other, thereby relatively reducing the number of particle-particle interactions or may even disturb the alignment of the particles, and thereby leading to slight softening effect. Figure 5.5 further implies that the negative pre-strain stiffening for the anisotropic MRE is more observed at lower level of 15% as compared 30% particle volume fraction. It is attributed to comparatively greater distance of iron particle within chains of anisotropy at relatively lower level of particle volume fraction of 15% as compared to 30% according to Figure 5.1, thereby becoming more sensitive to alteration in pre-strain. The negative pre-strain stiffening effect has also been observed for an isotropic MRE [104] and anisotropic MRE [105] in shear mode.

Considering energy dissipation properties, Figure 5.5 shows that the pre-strain dampening effect is generally less pronounced in presence of magnetic field in comparison with that in nonattendance of magnetic field, irrespective of particle volume fraction. This is also observed at the other loading frequency, as can be perceived from Table B5. Furthermore, in presence of magnetic field, pre-strain-dampening effect for the isotropic MRE is also more pronounced than the anisotropic MRE, irrespective of particle volume fraction, loading frequency. For instance, for the chosen excitation in Figure 5.5, increasing pre-strain from 6% to 21%, yielded 36% and 1% pre-strain dampening effects for the isotropic and anisotropic MREs with 30% particle volume fraction, respectively, while resulted in 137% and 74% in the zero field. Further examination of results at other loading conditions revealed that pre-strain dampening of the anisotropic MRE consistently increased with increasing particle volume fraction, irrespective of loading frequency and magnetic flux density, as can also be viewed from Table B5. However, a comparable tendency was not detected for the isotropic MRE, when magnetic field exists.

Figure 5.6(a) and 5.6(b) illustrate the influence of pre-strain on the stress-strain features of the isotropic and anisotropic MREs with particle volume fraction of 30% subjected to two different frequencies (1 Hz and 10 Hz), as examples. Results, presented for B=600 mT, suggest that increasing pre-strain from 6% to 21% yields relatively minimal effect on the stress-strain

properties of both MREs in terms of linear slope (equivalent stiffness), when frequency increases from 1 Hz to 10 Hz. More particularly, the pre-strain stiffening effect of the isotropic MREs slightly increases as frequency increases, while the anisotropic MRE showed very small decrement. In general, relatively similar trends were found at the other level of magnetic flux density, as can be noted from Table B4. Figure 5.6 further revealed that pre-strain impact on energy dissipation characteristics of both MRE is comparatively less pronounced, when frequency increased from 1 Hz to 10 Hz. Similar tendency was also seen at other flux density only for the anisotropic MRE.

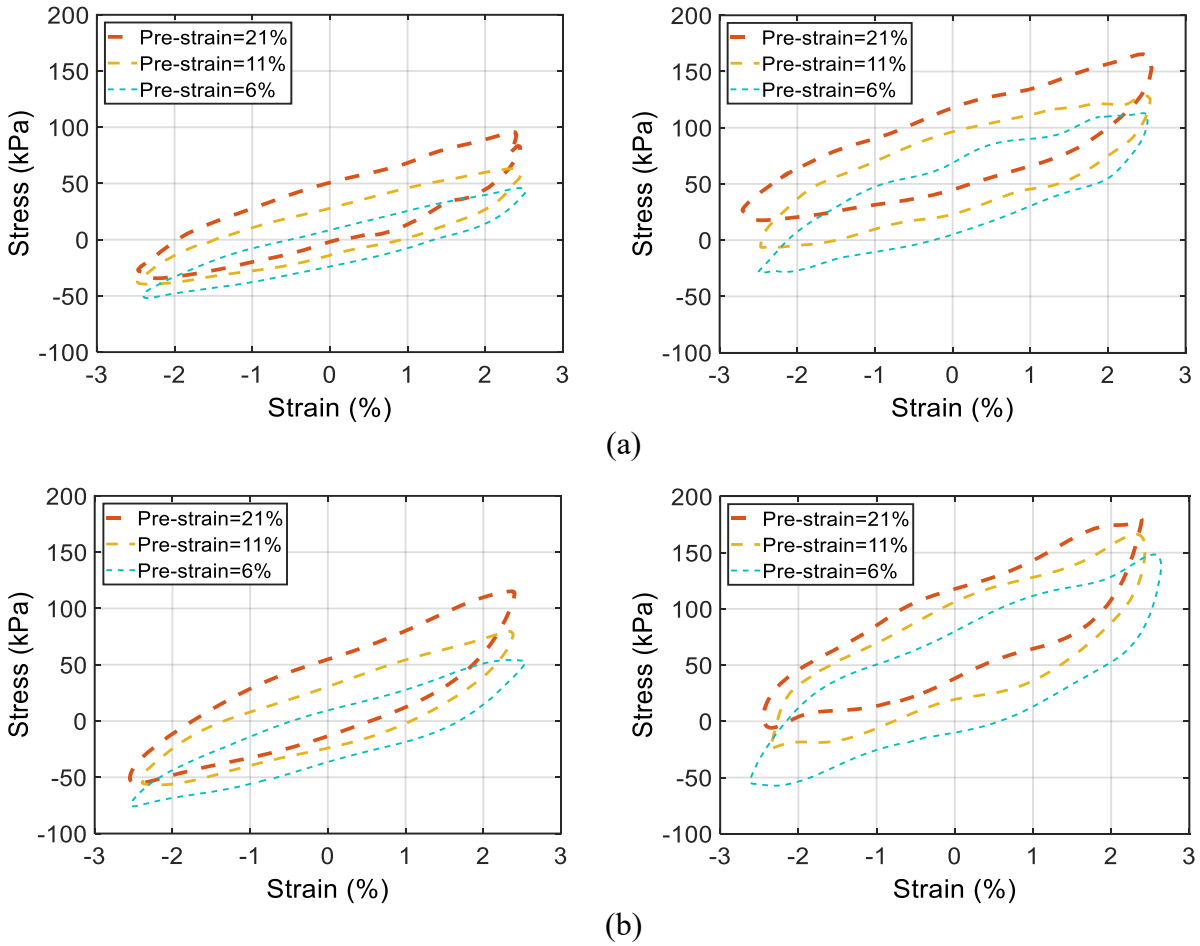

Figure 5.6 Effect of pre-strain on stress-strain characteristics of the isotropic (left column) and anisotropic (right column) MREs with 30% volume fraction under magnetic flux density of 600 mT subject to %2.5 peak strain at different frequencies: (a) f= 1 Hz, (b) f= 10 Hz.

Further examination of the results at the other particle volume fraction in, magnetic field exists, revealed that pre-strain-stiffening of the isotropic MRE with 15% particle volume fraction

tends to decrease with increasing loading frequency, while the 45% isotropic MRE increases with loading frequency in a general manner, irrespective of level of magnetic flux density, according to the Table B4. On the other hand, pre-strain-stiffening for anisotropic MRE is slightly increased with increasing loading frequency in a general manner, irrespective of particle volume fraction and magnetic flux density. Furthermore, results showed that pre-strain dampening of the isotropic MRE with particle volume fraction of 15% consistently decreased with increasing driving frequency, while generally increased when particle volume fraction exceeds 15%. Pre-strain dampening for anisotropic MRE with 15% and 30% generally showed decrement with increasing driving frequency only when flux density exceeds 150 mT, whereas 45% anisotropic MRE revealed increment with incrementing loading frequency, as can be noticed from Table B5.

5.3.2 Effect of pre-strain on the compression moduli and loss factor

The impact of pre-strain on the dynamic viscoelastic characteristics of the isotropic and anisotropic MREs in the compressive loading are further evaluated in the form of the elastic modulus (E'), loss modulus (E''), and the loss factor (η), which the latter is described as a fraction of the loss modulus over the elastic modulus, by presenting Figure 5.7 and Figure 5.8 and related to the particle volume fraction of 30%. It is noted that the specific data associated with the compression moduli at all the loading conditions and particle volume fractions are summarized in Tables B6 to B8 in the Appendix B. Figure 5.7 illustrates the effects of pre-strain on behavior of the compression moduli and loss factor of the two isotropic and anisotropic MREs, as examples, at distinct driving frequencies (1, and 10 Hz) under magnetic flux density of 150 mT. Results display that the elastic modulus of the isotropic MRE rises in a nonlinear way with increasing pre-strain, ranging from 6% to 21%, independent of excitation frequency, which is consistent with the pre-strain stiffening effect observed in the stress-strain characteristics (Figure 5.4 and Figure 5.5). For the anisotropic MRE, however, the elastic modulus slightly decreases with rising in the pre-strain from 6% to 11%, and then rises with further increment in the pre-strain from 11% to 21%, notwithstanding the driving frequency. Quite comparable trend has also been detected but for an isotropic MRE with 33% particle volume fraction in shear mode in which the MRE at first softens before it become stiff [104]. The initial decrease in the elastic modulus of anisotropic MRE can be in part credited to the breaking of particle network, thereby reducing the binding of the medium to the particle network. While the increment in the elastic modulus of anisotropic MRE at higher pre-strain is likely due to greater compression of the trapped medium within the anisotropic chains, apart from

slight increasing in the effective volume fraction of filled rubbers, like MREs, under increasing pre-strain [101].

Figure 5.7(b) shows that the loss modulus of the isotropic MREs rises with incrementing pre-strain, without regard to loading frequency. This tendency has also been observed for an isotropic MRE foam subjected to frequency of 10 Hz, when compressive pre-strain increased from 35% to 50% [106]. The loss modulus of the anisotropic MRE, nevertheless, shows comparable results under increasing pre-strain at lower frequency of 1 Hz, while decreases with increase in the pre-strain when loading frequency exceeds 1 Hz. It should be mentioned that a decrement in the loss modulus of chloroprene rubbers by increasing the pre-strain superimposed by a small uniaxial compression oscillation has also been noticed [107]. Chloroprene rubbers are synthetic rubbers like the employed silicone elastomer for fabrication of the examined MRE specimens in this study.

Figure 5.7(c) demonstrates that rising pre-strain from 6% to 21% yields pretty comparable loss factor for the isotropic MRE, while loss factor of the anisotropic MRE increases within (6% to 11%) pre-strain range and then decreases with further increment of pre-strain from 11% to 21%. Examination of the results at the other flux densities showed that the loss factor of the isotropic MRE also showed trends similar to that of the anisotropic MRE, when magnetic flux density exceeds 150 mT. Even though the results in Figure 5.7 were presented for specific loading conditions, comparatively same patterns were also noted at the other level of magnetic flux density and driving frequency, as can be noted from Figures B4 to B6 and Table B7, respectively, in the Appendix B.

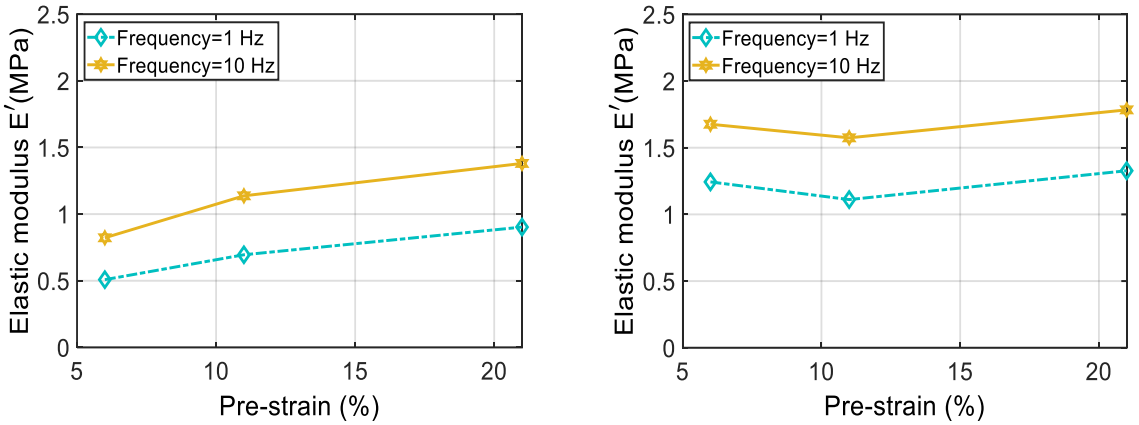

(a)

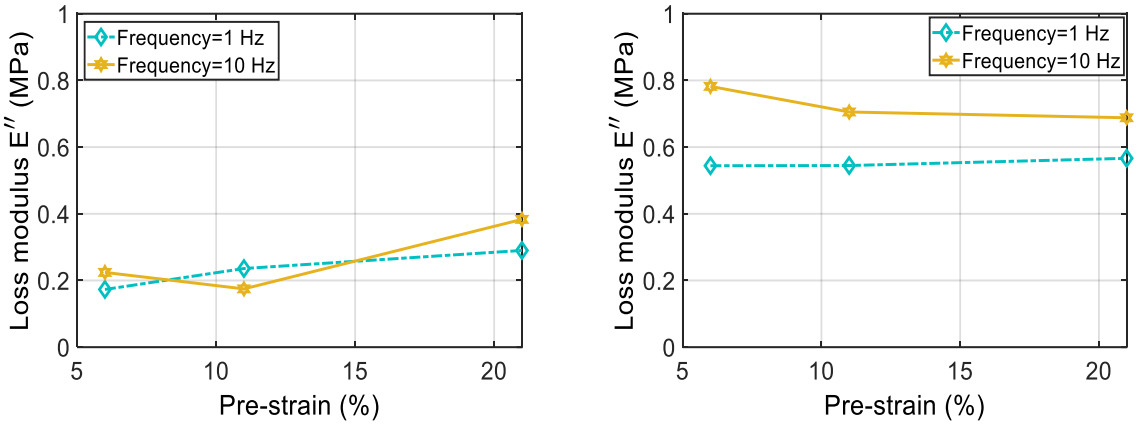

(b)

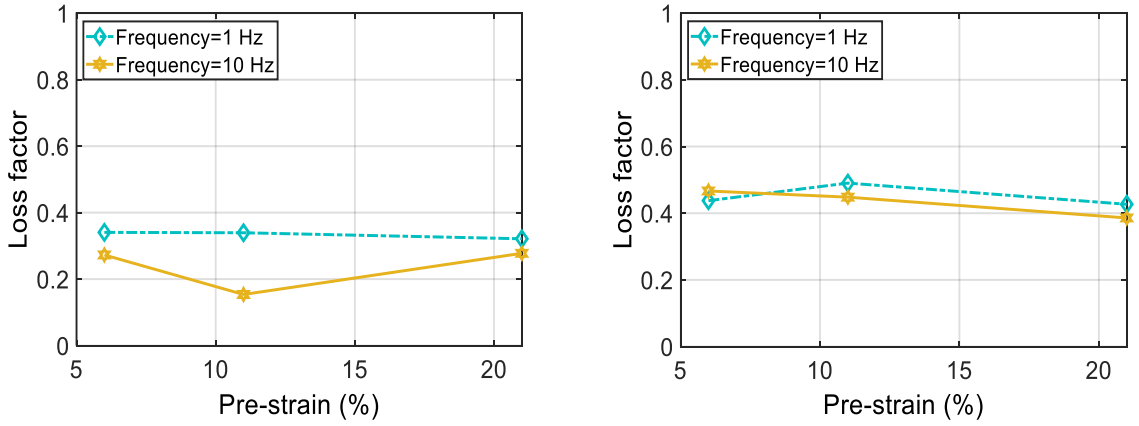

(c)

Figure 5.7 Effect of pre-strain on the compression mod e elastic modulus (a), loss modulus (b), and loss factor (c) of the isotropic (left column) and anisotropic (right column) MREs with volume fraction of 30% under different excitation frequencies (ε=2.5%, and B=150 mT).

Figure 5.8 illustrates changes in the elastic and loss moduli of both types of MREs with particle volume fraction of 30% under increasing pre-strain considering various degrees of the magnetic flux density. The outcomes are displayed, as example, at a frequency of 1 Hz. As it shows, the elastic modulus of the isotropic MRE continuously increases with the pre-strain, irrespective of magnetic flux density. The elastic modulus of anisotropic MRE, however, firstly decreases with increasing pre-strain from 6% to 11% and subsequently enhances with increment of pre-strain from 11% to 21%, which is consistent with the observed trends in Figure 5.7. Results also show that the loss modulus of the isotropic MRE increases with rising pre-strain, while the anisotropic MRE generally reveals comparable loss modulus under increasing pre-strain, irrespective of magnetic flux density, as can be viewed in Figure 5.8(b). However, zero flux density formed an exception, where only the anisotropic MRE shows slight increment within 6%- 21% pre-strain range. Further examination of the results revealed that the effect of pre-strain on the elastic and loss moduli of both MREs generally decreases with rising in magnetic flux density, thereby suggesting coupled pre-strain and magnetic field effect on the performance of MREs. This trend is also consistent with the stress-strain hysteresis findings presented in Figure 5.4 and Figure 5.5. By increasing pre-strain from 6% to 21%, for instance, the elastic modulus of the isotropic MRE increases from about 0.22 MPa to 0.62 MPa in the absence of magnetic field, corresponding to 182% increase. In the presence of magnetic field (B=450 mT), the elastic modulus of the isotropic MRE increases from about 1.44 MPa to nearly 1.81 MPa, corresponding to 26% increment.

Figure 5.8(c) indicates that the loss factor of both MREs generally increases when pre-strain increased from 6% to 11% and tends to decrease with further increment in pre-strain from 11% to 21%, regardless of magnetic flux density. Loss factor for the isotropic MRE, however, shows relatively comparable trends within the range of pre-strain at comparatively lower level of magnetic flux density compared to the anisotropic MRE, which is consistent with the observed outcomes illustrated in Figure 5.7(c). Furthermore, the elastic modulus of the two kinds of MREs increases significantly with rising in the magnetic flux density up to 600 mT. The rate of enhancement in the modulus, however, relatively reduces when the magnetic flux density exceeds 450 mT, which is ascribed to the magnetic saturation of the MREs with incrementing magnetic flux density.

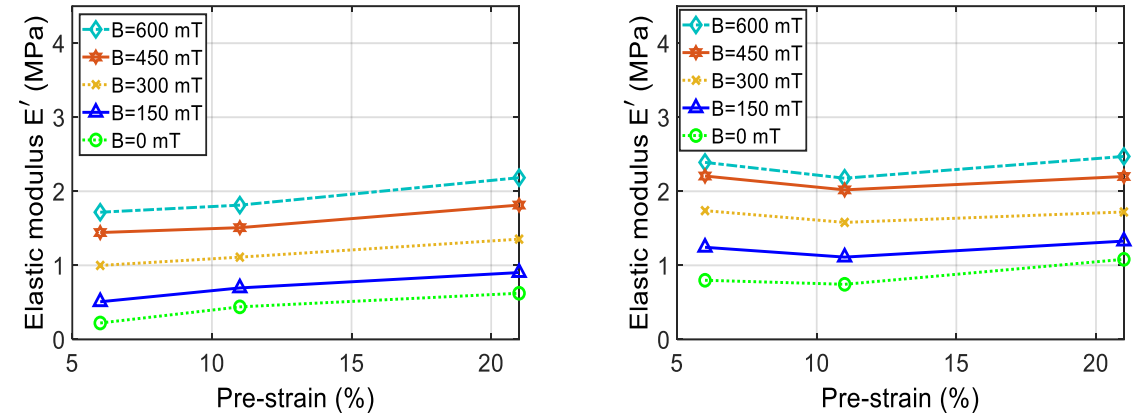

(a)

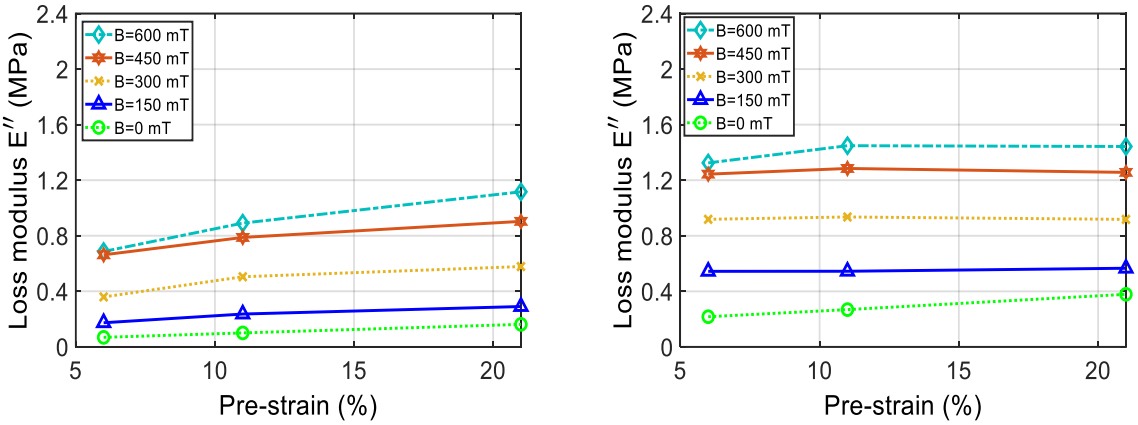

(b)

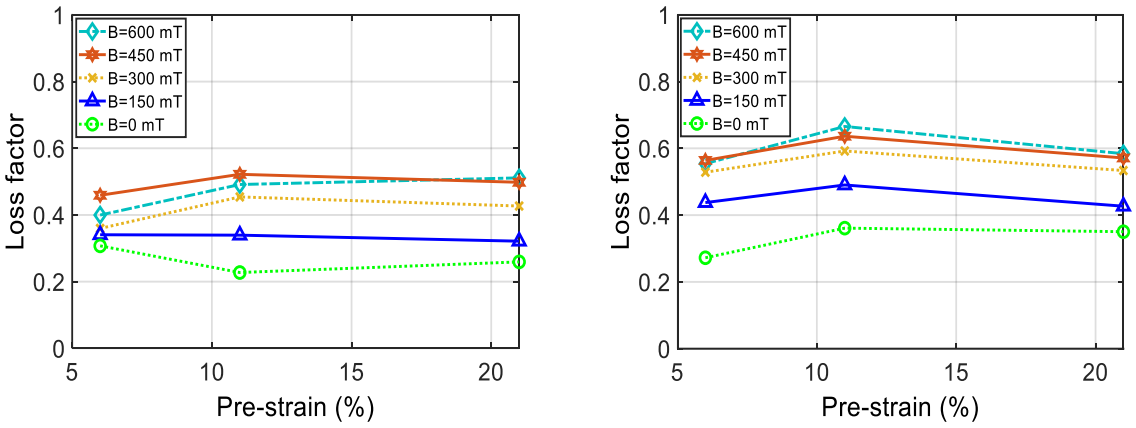

(c)

Figure 5.8 Effect of pre-strain on the compression mode elastic modulus (a), loss modulus (b), and loss factor (c) of isotropic (left column) and anisotropic (right column) MREs with volume fraction of 30% under different levels of magnetic flux density (ε=2.5%, f=1 Hz).

The results shown in Figure 5.8(c) also reveal that the loss modulus of the anisotropic MRE is fairly getting close to each other for fields above 450 mT. This implies that the loss modulus of

the anisotropic MRE starts to show tendency to saturate, irrespective of pre-strain. The tendency for magnetic saturation is, however, more pronounced for the loss factor of both kinds of MREs, when magnetic flux density exceeds 450 mT, as compared with the elastic and loss moduli, as can be realized from Figure 5.8(c). Although Figure 5.7 and Figure 5.8 present the results for the particle volume fraction of 30%, similar tendencies were also found for compression moduli and loss factor of both types of MREs with particle volume fractions of 15% and 45%, regardless of magnetic flux density and loading frequency as shown in Figures B1 to B3, Figures B7 to B14, as well as Table B6 and Table B8 in the Appendix B. However, only the elastic and loss moduli of the anisotropic MRE with 15% particle volume fraction tend to decrease with increase in pre-strain ranging from 6% to 21%, while these moduli unceasingly increased in a consistent manner for 45% anisotropic MRE with the same increment in pre-strain, regardless of loading frequency and magnetic flux density. Furthermore, the pre-strain effects for the isotropic MRE are more pronounced in comparison with the anisotropic MRE, irrespective of particle volume fraction, loading frequency, magnetic flux density. Moreover, without presence of magnetic field, both elastic and loss modulus of both types of MREs, consistently increase with increasing pre-strain, regardless of particle volume fraction and loading frequency.

Examination of entire results revealed maximum pre-strain stiffening effects of 53%, 248%, and 743% for the isotropic MREs with volume fraction of 15%, 30%, and 45%, respectively, when pre-strain increased from 6% to 21%, which can be noted from Table B4 in the Appendix B. These were occurred at zero flux density as expected, according to Figure 5.5 through Figure 5.8, whilst under excitation of 30 Hz, 10 Hz, and 1 Hz, respectively, for the volume fraction of 15%, 30%, and 45%. The corresponding effects for the anisotropic MREs were obtained as 30%, 44%, and 70%. These were also happened at zero magnetic field as anticipated, whereas at excitation frequency 30 Hz, 20 Hz, and 1 Hz, correspondingly, for the volume fraction of 15%, 30%, and 45%.

5.3.3 Influence of pre-strain on the relative MR effect

Further assessments are made to study the influences of pre-strain on magnetic field-dependent properties of the isotropic and anisotropic MREs in form of relative MR effect, which designates the relative alteration in elastic modulus ($MR_{\acute{E}}$) or loss factor (MR_{η}) from the off-state condition to a given or maximum possible flux density [84]. The relative MR effects are calculated

considering given excitation conditions (pre-strain and frequency), and different maximum flux densities. It is noted that the specific data related to relative MR effects at all the loading conditions and particle volume fractions are summarized in Table B9 through Table B11 together with Figures B15 and B16 in the Appendix B. However, as examples, Figure 5.9(a) and 5.9(b) exemplify variations in $MR_{\dot{E}}$ and MR_{η} of both types of MREs with particle volume fraction of 30% with respect to pre-strain under magnetic flux density of 600 mT considering two levels of driving frequency 1 Hz and 10 Hz. The results suggest nonlinear decrease in $MR_{\dot{E}}$ for the isotropic MRE with increasing pre-strain, irrespective of the excitation frequency. This is also consistent with the results presented in Figure 5.5 and Figure 5.8, suggesting coupled pre-strain and field-stiffening of the MREs. The $MR_{\dot{E}}$ for the anisotropic MRE also decreases almost linearly with pre-strain ranging from 6% to 21%, although the decrease is very small to negligible under increasing pre-strain from 6% to 11%, irrespective of loading frequency.

The results presented in Figure 5.9(a) is also consistent with the results presented in Figure 5.4 and Figure 5.5, suggesting less magnetic field dependent properties, when particles getting too close or even touch each other at relatively higher level of pre-strain, which is more pronounced for anisotropic MREs compared to isotropic MREs. Another possible reason is in part attributed to distortion of the column-like structures of particles in the anisotropic MRE under relatively higher pre-strain, yielding to lowered relative magnetic permeability, thus reducing relative MR effect. This inclination has also been reflected in a small number of researches evaluating compressive elastic modulus subject to static [26] and dynamic loadings [79], which is become more pronounced for comparatively greater level of particle volume fraction of 30% [45, 84]. The rate of decrement in $MR_{\dot{E}}$ with increase in pre-strain for anisotropic MREs is less pronounced compared to that for the isotropic MREs. This is mainly due to the existing columnar particle chains in anisotropic MREs including particles which are already close to each other even under relatively lower level of pre-strain, thereby becoming less sensitive to further increment of pre-strain as compared with the isotropic MRE. This behavior, similarly, can happen for the isotropic MRE under relatively higher level of pre-strain. Figure 5.9(a), for instance, proves comparable $MR_{\dot{E}}$ for the isotropic MRE under increasing pre-strain from 11% to 21%.

Results further suggest that the $MR_{\dot{E}}$ for the isotropic MRE is relatively less sensitive to increase in excitation frequency, when pre-strain ranging from 11% to 21% as compared with

(6%-11%) pre-strain range. This is due to the observed nonlinear pre-strain stiffening effect as can be comprehended in Figure 5.7 and Figure 5.8, which limits the strain-rate stiffening effect, defined as stiffening of MREs due to increase in loading frequency, and hence restricts the $MR_{\dot{E}}$. Besides, within the 6%-11% pre-strain range, MREs are relatively softer and thus more sensitive to strain-rate stiffening effect, thereby showing stronger dependence of the $MR_{\dot{E}}$ on the excitation frequency. This is, however, was not observed for the anisotropic MRE.

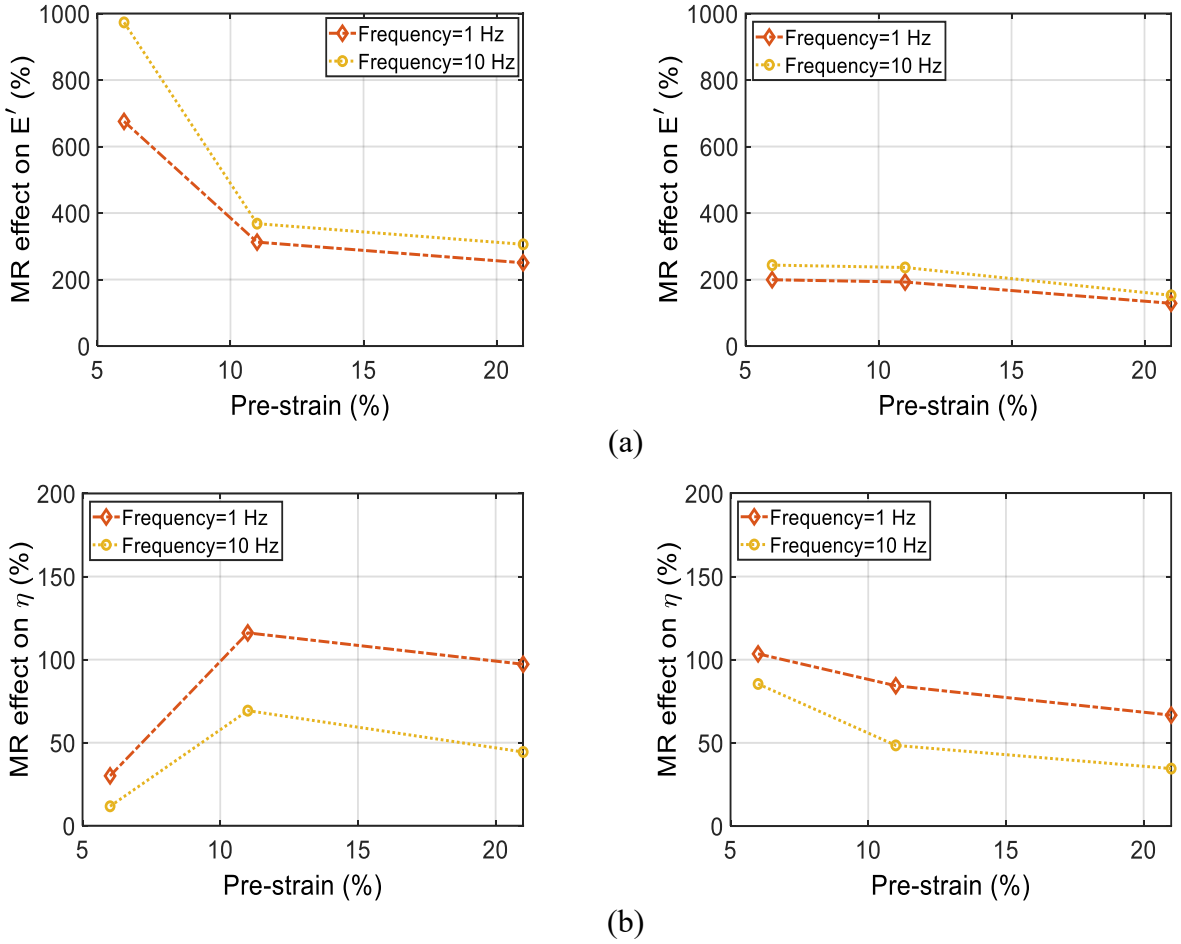

Figure 5.9 The effects of the pre-strain on the relative MR effect in view of elastic (a) and loss factor (b) of the isotropic (left column) and anisotropic (right column) MREs with 30% volume fraction under different excitation frequencies (ε=2.5%, and B= 600 mT).

Figure 5.9(b) demonstrates that the MR effect in view of loss factor, MR_{η}, for the isotropic MRE shows opposite trends with respect to variations in pre-strain from 6% to 11% as compared with $MR_{\dot{E}}$, while decreases with progressive increment of pre-strain from 11% to 21%, irrespective

of loading frequency. The MR_{η} of the anisotropic MRE, however, uninterruptedly reduces with increase in pre-strain rising from 6% to 21%, without being affected by excitation frequency. Further assessment of the attained MR effects at the other loading frequency (20 Hz, and 30 Hz), flux densities varying from 150 mT to 750 mT, and also particle volume fraction (15% and 45%) revealed that both $MR_{\dot{E}}$ and MR_{η} for both types of MREs showed similar trends with respect to increase in pre-strain, ranging from 6% to 21%, as shown in Figure 5.9, according to provided Tables B9 to B11 as well as Figures B15 and B16 in the Appendix B. However, loading frequency of 1 Hz when particle volume fraction is 45%, formed an exception where MR_{η} of the isotropic MRE steadily decreases when pre-strain increases from 6% to 21%.

Further examination of the entire obtained MR effects summarized in Tables B9 to B11 as well as Figures B15 and B16 in the Appendix B, revealed that the anisotropic MRE with particle volume fraction of 15% revealed higher $MR_{\dot{E}}$ in comparison with the isotropic MRE, without regard to pre-strain and loading frequency. Besides, the anisotropic MRE with particle volume fraction of 45% also revealed higher relative MR effect as against the isotropic MRE, at relatively greater level of pre-strain (11-21%), when loading frequency exceeds 1 Hz, according to Figure B16 and Table B11 in the Appendix B. Besides, $MR_{\dot{E}}$ of the anisotropic MRE generally increases with increasing loading frequency, despite of pre-strain and particle volume fraction. Additionally, $MR_{\dot{E}}$ of the isotropic MRE with particle volume fraction of 15% also showed increment with increasing loading frequency. However, at particle volume fraction of the 30%, $MR_{\dot{E}}$ of the isotropic MRE initially increases with loading frequency from 1 Hz to 10 Hz and then slightly reduces with additional increment in strain-rate from 10 Hz to 30 Hz, in spite of pre-strain, and magnetic flux density. While $MR_{\dot{E}}$ of the 45% isotropic MRE generally decreased, when driving frequency rises from 1 Hz to 30 Hz. Moreover, MR_{η} of the isotropic MRE generally drops with growing driving frequency, no matter of pre-strain and particle volume fraction. MR_{η} of anisotropic MRE with 15% particle volume fraction also decreases with increasing loading frequency, while reveals comparable trends under increasing loading frequency when particle volume fraction exceeds 15%, irrespective of pre-strain.

Additional investigation of the calculated MR effects provided in Tables B9 to B11 in the Appendix B, disclosed maximum $MR_{\dot{E}}$ up to 286%, 973% and 2258% for the isotropic MRE with volume fraction of 15%, 30% and 45%, correspondingly. These were obtained at driving strain

rates of 10 Hz, 10 Hz, and 1 Hz, in that order, at minimum pre-strain of 6% as expected. The corresponding $MR_{\dot{E}}$ for the anisotropic MREs are found to be 320%, 293%, and 386%, occurred at minimum pre-strain of 6%, and loading strain-rates of 20 Hz, 20 Hz, and 30 Hz, in the same order, for the volume fraction of 15%, 30% and 45%. Results also revealed maximum MR_{η} up to 676%, 1099% and 6645% for the isotropic MREs with volume fraction of 15%, 30% and 45%, respectively. These were observed at excitation frequency of 1 Hz, 10 Hz, 1 Hz, correspondingly, under relatively lower level of pre-strain of 6%, as expected. The corresponding maximum MR_{η} for anisotropic MREs are also found to be 619%, 537%, and 950%, at excitation strain-rate of 1 Hz, 10 Hz, and 1 Hz, correspondingly, at lower level of pre-strain of 6%.

Further examination of the entire results also suggested that isotropic MREs with 45% and 30% particle volume fraction may be regarded more adapted for designing adjustable MRE-based vibration isolators expose to low (≈1 Hz) and high (≈10 Hz) frequency excitations, in turn, where comparatively greater $MR_{\dot{E}}$ is required and at the same time lower level of static pre-strain (≈6%) is unavoidable. Results, likewise, indicated that the anisotropic MREs are superior compared to the isotropic MRE for designing adaptive MRE-based vibration absorbers, requiring higher payloads with an attempt to track single resonant frequency, where quite lower MR_{η} is desirable, as the lower damping causes higher vibration attenuation for adaptive tuned vibration absorbers [108, 109].

5.4 Model Development

In this section, based on the observed experimental data, pre-strain dependent phenomenological based models have been developed to predict dynamic viscoelastic and nonlinear hysteresis behaviour of both isotropic and anisotropic MREs in compression mode. Apart from the pre-strain effect, the developed models also take into account the variation in the excitation frequency, applied magnetic field as well as volume fraction.

5.4.1 The compression elastic and loss moduli

In many applications involving MREs under compression mode, such as MRE-based vibration isolators and absorbers, MREs will undergo quite large static pre-strain due to weight of the supported structures, before superimposed by any vibration excitation. As discussed in Section 3, the static strain can considerably alter the MR effect in view of elastic and loss factor due to decrease in the distance between the magnetizable particles as well as changing the shape of

specimen. When no magnetic field exists, MREs can be treated like passive filled rubber-like materials. A finite viscoelastic constitutive model has been developed by Hao et. al [110] for estimating the storage and loss moduli of passive filled rubber-like materials in tension mode considering static pre-strain, frequency, and amplitude of excitation. A microscale continuum model has been developed by Kalina et. al [36] which can qualitatively explicate the impact of mechanical preloads on the deformation dependent performance of MREs with orderly and random spatial distribution of the particles. A nonlinear viscoelastic model was developed by Lejon [104] to predict pre-strain dependent properties of isotropic MRE in shear mode under small amplitude of 0.15%. Even though pre-strain is an important design factor in compression mode and has substantial effect on properties of MREs, there is no pre-strain dependent models which can accurately predict the compression elastic and loss moduli together with hysteresis behavior of both isotropic and anisotropic MREs with different volume fractions considering variation in driving strain-rate and magnetic flux density. Such a model can facilitate the analysis and estimation of the performance of tunable MRE-based vibration suppression mechanisms at early stages of their design.

In the present study, therefore, simple phenomenological models are developed for predicting the pre-strain dependence of the viscoelastic features of the MREs under compression mode. It is noteworthy that the strong effects of the pre-strain on the compression mode properties are also evident from the experimental results, presented in Figure 5.4 through Figure 5.9 in Section 3, which are further coupled with the physical and loading conditions (volume fraction, frequency and magnetic flux density). Apart from volume fraction dependent properties, results further implies that the elastic and loss moduli rise with increase in the magnetic flux density and tend to saturate under higher flux density. Besides, the elastic and loss moduli of the two isotropic and anisotropic MREs increase with increment in the excitation frequency in a general trend, and mostly show tendency to saturate at relatively higher level of excitation frequency, ranging from 20 Hz to 30 Hz, relatively regardless of particle volume fraction, pre-strain, and magnetic flux density, as can be perceived from Tables B6 to B8 in the Appendix B. Owing to the observed coupled dependence of the elastic and loss moduli on the pre-strain, volume fraction, frequency and magnetic flux density, the effective compression elastic and loss moduli of both isotropic and anisotropic MREs may be expressed by simple phenomenological-based models as:

$$\begin{cases} E'(\varepsilon_p,\phi,f,B) = E_0\beta_0'(1+\beta_1'(\varepsilon_p)^{\beta_2'})(1+\beta_3'\phi+\beta_4'\phi^2)(1-e^{-\beta_5' f})(\dfrac{2}{1+e^{-\beta_6' B}}) \\ E''(\varepsilon_p,\phi,f,B) = E_0\beta_0''(1+\beta_1''(\varepsilon_p)^{\beta_2''})(1+\beta_3''\phi+\beta_4''\phi^2)(1-e^{-\beta_5'' f})(\dfrac{2}{1+e^{-\beta_6'' B}}) \end{cases} \quad (5\text{-}6)$$

where E' and E''represents the elastic and loss moduli, sequentially. E_0 is the Young's modulus of the silicone elastomer based medium, taken as 0.0606 MPa [8]. ε_p, ϕ, f, and B are the static pre-strain, particle volume fraction, loading frequency, and magnetic flux density. The proposed phenomenological model is based on the multiplicative split of the moduli into a pre-strain dependent, volume fraction dependent, frequency dependent, and -magnetic field dependent parts, with only seven parameters. To effectively predict pre-strain, frequency and magnetic field dependent properties, a power function, exponential, and fractional models were proposed, respectively. For volume fraction dependent properties, however, the Einstein-Guth model [33], which can estimate complex modulus of filled rubbers, was employed considering general coefficients. The proposed model involves seven unknown parameters, β_0' to β_6' and β_0'' to β_6'', for each elastic and loss moduli, correspondingly, which were determined with minimization of the fault functions J' and J'' between the model-predicted moduli and respective experimentally measured responses as:

$$\begin{cases} J'(a_1,..,a_6) = \sum_{i=1}^{M}\sum_{j=1}^{N}\sum_{k=1}^{O}\sum_{l=1}^{P}\left(E'(\varepsilon_p,\phi,f,B) - E_m'(\varepsilon_p,\phi,f,B)\right)^2 \\ J''(a_1,..,a_6) = \sum_{i=1}^{M}\sum_{j=1}^{N}\sum_{k=1}^{O}\sum_{l=1}^{P}\left(E''(\varepsilon_p,\phi,f,B) - E_m''(\varepsilon_p,\phi,f,B)\right)^2 \end{cases} \quad (5\text{-}7)$$

where E_m' and E_m'' are elastic and loss moduli obtained from the measured data, respectively, and indices *i*, *j*, *k* and *l* denote the experimental data corresponding to specific values of the pre-strain, volume fraction, frequency, and magnetic flux density, respectively. *M*, *N*, *O* and *P* stand for the number of outcomes corresponding to the respective input factors considered in the error function, which were taken as 3, 3, 4, and 5, respectively. The error minimization problem was solved employing the Genetic algorithm (GA) followed by the nonlinear Sequential Quadratic Programming (SQP) technique for the purpose of acquiring precise convergence to global minima, as suggested in [111]. Repeated solutions were obtained considering different initial values of the coefficients, which all converged to nearly identical solutions, summarized in Table 5.1 and Table

5.2 for the elastic and loss moduli models, respectively, for both the isotropic and anisotropic MREs.

Table 5.1 Identified coefficients of the proposed model for estimating the elastic modulus of both kinds of MREs.

Constant	β_0'	β_1'	β_2'	β_3'	β_4'	β_5'	β_6'
Isotropic MRE							
E'	9.0739	8.2388	0.8689	-8.2219	25.8811	0.8379	4.7096
Anisotropic MRE							
E'	11.3866	72.6082	3.8618	-3.6533	22.5994	1.7655	5.0534

Table 5.2 Identified coefficients of the proposed model for estimating the loss modulus of both kinds of MREs.

Constant	β_0''	β_1''	β_2''	β_3''	β_4''	β_5''	β_6''
Isotropic MRE							
E''	-227.6527	-1.1122	0.0238	-10.0130	28.2890	1.5030	4.9695
Anisotropic MRE							
E''	-105.6616	-1.0987	0.0109	-8.4531	35.2759	2.1375	5.2561

Figure 5.10 and Figure 5.11 compare the model-predicted elastic and loss moduli of the isotropic and anisotropic MREs, respectively, with the experimental records for three distinct values of the pre-strain as well as volume fraction. Figure 5.10 and Figure 5.11 present the comparison under driving frequency and magnetic flux density of 1 Hz and 300 mT and also 10 Hz and 450 mT, respectively, as examples. The comparisons demonstrate that the proposed simple phenomenological models can reasonably well estimate the elastic and loss moduli of both types of MREs with different particle volume fraction for the range of the pre-strain considered in the study. A quite similar degree of correspondences between the model and measured data were also observed across the full ranges of pre-strain, volume fraction, driving frequency and magnetic flux density examined in this research. The performance of the proposed models was also evaluated quantitatively using the coefficient of determination , R^2, is a statistical measure to inspect the goodness of fit between the measured and model responses. The R^2 for the models, predicting the

isotropic and aligned elastic moduli, were obtained as 93.49% and 87.84%, respectively while were found as 87.40% and 83.99%, for models predicting loss moduli of isotropic and anisotropic MREs, correspondingly. The root-mean-square error (RMSE) was also calculated as 0.496 and 0.607 for the models predicting the isotropic and aligned elastic moduli, respectively. The corresponding RMSE for the models estimating the isotropic and aligned loss moduli were also found to be 0.411 and 0.571, respectively. These indicate that the proposed pre-strain dependent, volume fraction dependent, frequency dependent, and magnetic field dependent model can fairly well capture the elastic and loss modulus of both types of MREs.

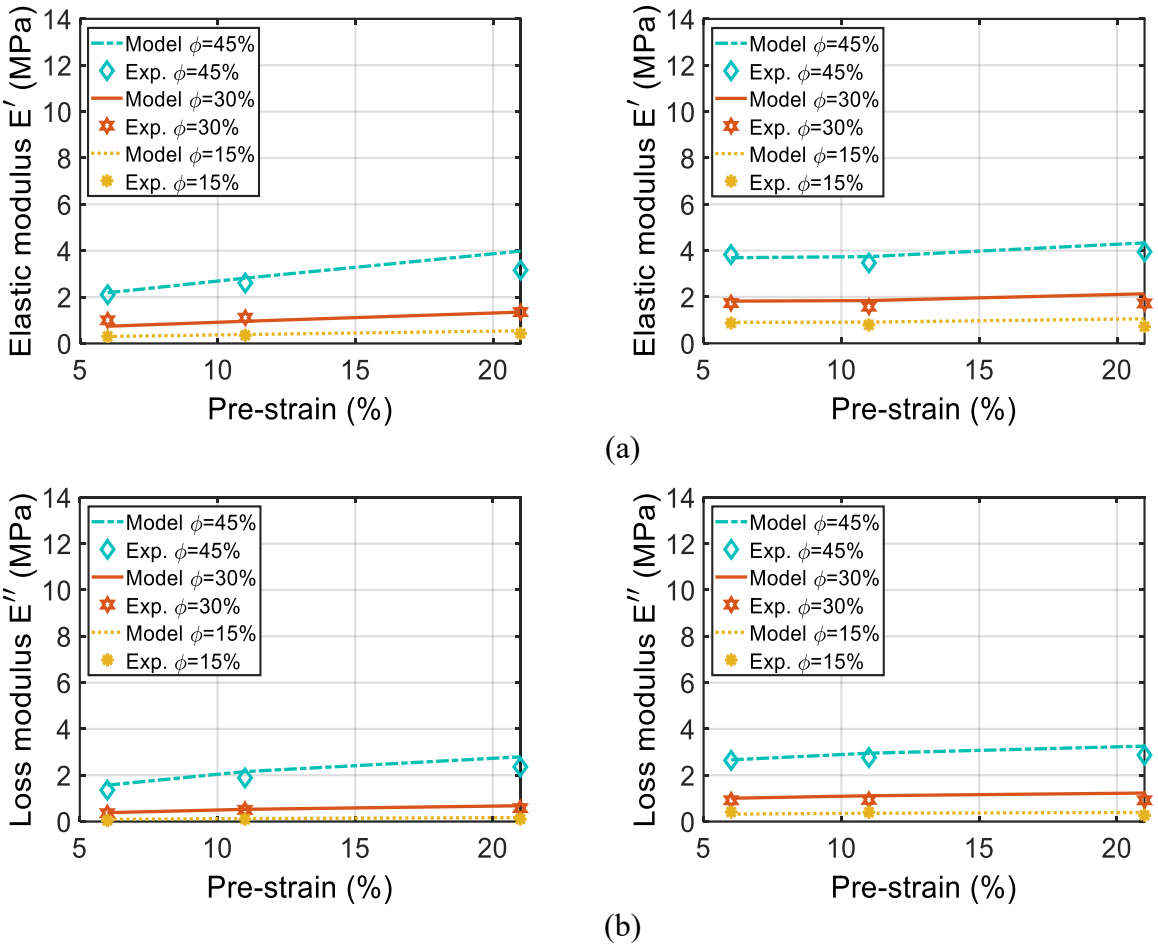

Figure 5.10 Comparisons of the pre-strain dependent compression elastic (a) and loss moduli (b) predicted from the proposed model with the measured data for the isotropic (left column) and anisotropic (right column) MREs with different volume fractions (ε=2.5%, f=1 Hz, B=300 mT).

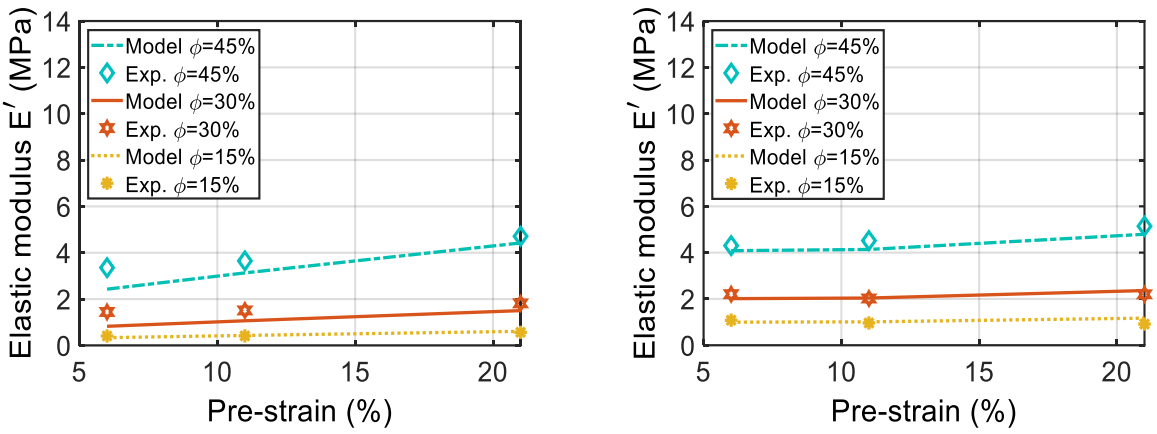

(a)

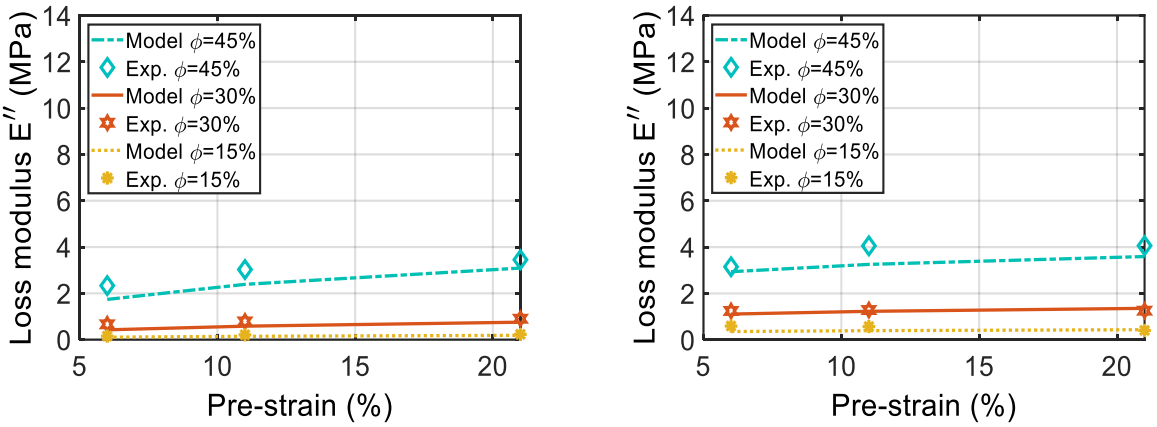

(b)

Figure 5.11 Comparisons of the pre-strain dependent compression elastic (a) and loss moduli (b) predicted from the proposed model with the measured data for the isotropic (left column) and anisotropic (right column) MREs with different volume fractions (ε=2.5%, f=10 Hz, B=450 mT).

5.4.2 Stress-strain hysteresis characteristics

In order to predict stress-strain hysteresis traits of the isotropic and anisotropic MREs subject to harmonic compression deformation, a nonlinear Kelvin-Voigt viscoelastic model was developed in which the stored and dissipated energy elements are lumped and linked in parallel configuration, as shown in Figure 5.12. The proposed model represents the steady-state stress output of the MRE in response to a harmonic excitation input as:

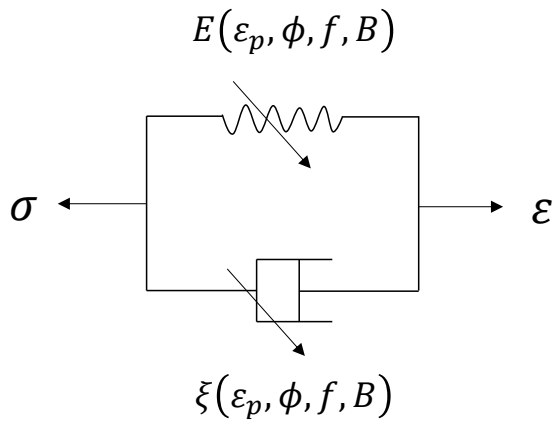

Figure 5.12: Nonlinear viscoelastic model for MREs.

$$\sigma_{MRE}(t) = E(\varepsilon_p, \phi, f, B)\varepsilon(t) + \xi(\varepsilon_p, \phi, f, B)\dot{\varepsilon}(t) \tag{5-8}$$

where $\sigma(t)$, $\varepsilon(t)$, and $\dot{\varepsilon}(t)$ are the stress, strain, and strain-rate, respectively in which *t* represents physical time related to harmonic input oscillation. $E(\varepsilon_p, \varphi, f, B)$ and $\xi(\varepsilon_p, \phi, f, B)$ represent the dynamic elastic modulus and viscosity of the viscoelastic materials. Furthermore, ε_p, φ, f, and B are the pre-strain, particle volume fraction, excitation frequency, and magnetic flux density, respectively. Let us consider a harmonic excitation under complex strain input $\varepsilon^*(t)$ as:

$$\varepsilon^* = \varepsilon_0 e^{i2\pi ft} \tag{5-9}$$

where ε_0 is strain amplitude. In the proposed viscoelastic Kelvin–Voigt model, the elastic modulus $E(\varepsilon_p, \varphi, f, B)$ and viscosity and $\xi(\varepsilon_p, \phi, f, B)$ can be related to the elastic and loss moduli of the MRE. The complex dynamic modulus, E^* can be used to relate complex stress and strain as:

$$\sigma^* = E^*\varepsilon^* = (E' + iE'')\varepsilon^* \tag{5-10}$$

where E' and E'' are the compressive elastic and loss moduli, respectively. Now considering Equations (5-8) and (5-10), the $E(\varepsilon_p, \varphi, f, B)$ and $\xi(\varepsilon_p, \phi, f, B)$ can be expressed with respect to elastic and loss moduli of MREs as:

$$E(\varepsilon_p, \varphi, f, B) = E' \tag{5-11}$$

$$\xi\left(\varepsilon_p, \phi, f, B\right)=\frac{E''}{2\pi f} \tag{5-12}$$

Thus, in the proposed nonlinear viscoelastic model presented in Equation (5-8), the elastic modulus and viscosity components can be identified using storage and loss moduli of the MREs formulated in Equation (5-6).

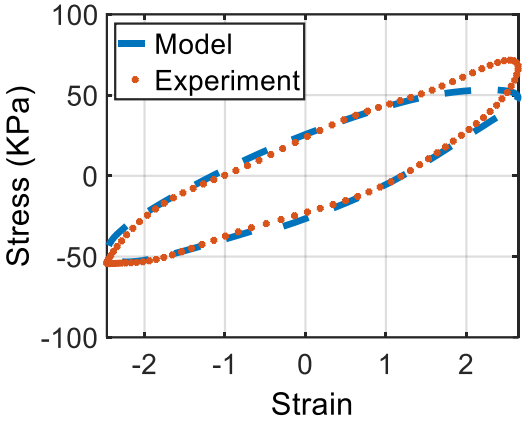

(a) ε_p=11%, φ=30%, f=10 Hz, B=450 mT

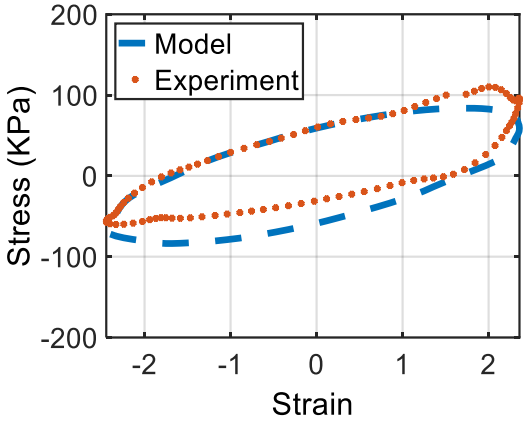

(b) ε_p =6%, φ=30%, f=30 Hz, B=300 mT

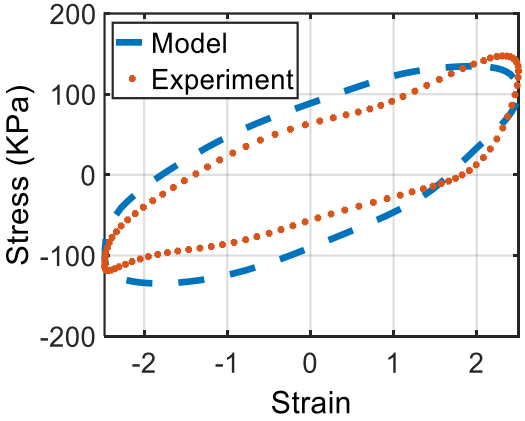

(c) ε_p=11%, φ=45%, f=10 Hz, B=300 mT

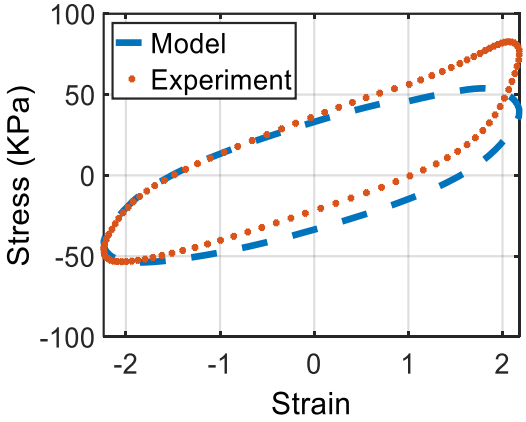

(d) ε_p=21%, φ=45%, f=1 Hz, B=300 mT

Figure 5.13 Comparisons of the stress-strain hysteresis characteristics predicted from the proposed model with the measured data for the isotropic (a, c, and d), anisotropic (b) MREs subject to different level of pre-strain and excitation conditions.

The stress-strain characteristics predicted using the presented nonlinear viscoelastic model are compared with the measured data over the entire ranges of pre-strain, volume fraction, excitation frequency and magnetic flux densities considered in the study. The results revealed a reasonable agreement between the stress-strain hysteresis loops obtained from the presented model and the measured data of the isotropic and anisotropic MRE for varying pre-strain, volume fraction,

excitation frequencies and magnetic flux densities. Figure 5.13, for instance, compares the results obtained from the proposed nonlinear viscoelastic model with the measured data over the range of pre-strain (6%, 11% and 21%) under different excitation frequency (1 Hz, 10 Hz, and 30 Hz) and two magnetic flux density of 300 mT and 450 mT. The results suggest that the presented nonlinear viscoelastic model can reasonably predict the stress-strain hysteresis over wide range of the pre-strain, volume fraction, excitation frequencies and magnetic flux densities.

5.5 Conclusion

The results showed strong dependence of the elastic and loss moduli of isotropic and anisotropic MREs on the pre-strain, which was further coupled with the effects of the volume fraction and frequency, and the magnetic field. The elastic and loss moduli of isotropic MREs consistently increase in a nonlinear manner, when pre-strain increased from 6% to 21%, while anisotropic MRE showed dissimilar trends depending on particle volume fraction. The pre-strain stiffening effect, however, was generally limited in the presence of anisotropy, and magnetic field-stiffening of the MREs, while dramatically enhances with increase in volume fraction, particularly for isotropic MRE. Pre-strain-stiffening and pre-strain dampening effects for isotropic MRE are always more noticeable than anisotropic MRE. Pre-strain dampening of anisotropic MRE always increased with increasing particle volume fraction, while isotropic MRE only showed this trend in absence of magnetic field. Both pre-strain effects of isotropic MRE consistently decreased with increasing frequency in absence of magnetic field, while anisotropic MRE showed similar behavior, when particle volume fraction exceeds 15%, whereas at 15% showed increment with increasing frequency. The relative MR effect considering elastic modulus ($MR_{\acute{E}}$) for both types of MRE consistently decreased with increase in pre-strain, which is more evident for the isotropic MRE as opposed to anisotropic MRE. The relative MR effect pertaining to loss factor (MR_{η}) showed the same trend only for anisotropic MRE. MR_{η} of isotropic MRE generally showed maximum around 11% pre-strain. Results further revealed maximum $MR_{\acute{E}}$, up to 286%, 973% and 2258% for the isotropic MRE, respectively, with volume fraction of 15%, 30% and 45%. The corresponding $MR_{\acute{E}}$ for anisotropic MREs obtained as 320%, 293%, and 386%. Results also revealed maximum MR_{η}, up to 676%, 1099% and 6645% for the isotropic MRE, respectively, with volume fraction of 15%, 30% and 45%. The corresponding MR_{η} for anisotropic MREs obtained as 619%, 537%, and 950%. Results also recommended that isotropic MREs with 45% and 30% particle volume fractions may

be better suited for designing MRE-based vibration isolators under low (≈1 Hz) and high (≈10 Hz) frequency excitations, correspondingly, when lower level of static pre-strain (≈6%) is inevitable. Results, likewise, indicated that the anisotropic MREs are relatively superior compared to the isotropic MRE for designing MRE-based vibration absorbers, when relatively higher level of payload is unavoidable. Simple phenomenological models were proposed for predicting pre-strain dependent compression moduli and stress-strain hysteresis characteristics of both kinds of MREs, which showed a reasonably good agreement with the experimental data across the full spectrum of pre-strain, volume fraction, loading frequency, magnetic flux density investigated. The proposed models could thus serve as a guidance for designing MRE-based devices considering different level of pre-strain and volume fraction.

CHAPTER 6
VOLUME FRACTION EFFECTS

6.1 Introduction

In order to gain better understanding of performance potentials of magnetorheological elastomers (MREs) and to seek guidance on their fabrication and design for diverse applications, mechanical properties of MREs in different operational modes, such as shear, compression, and tension, have been widely characterized in recent years. Many studies, however, have shown that MR effect in compression mode is more pronounced than shear mode. Gordaninejad et al. [17] reported significantly higher compression mode MR effect (99%) compared to 68% observed in the shear mode. Lerner and Cunefare [4] developed MRE-based vibration absorbers, which showed natural frequency shifts up to 507% and 470%, in the compression and shear modes, respectively. Kallio [6] also investigated dynamic properties of unaligned and anisotropic MREs and obtained 39% and 60% MR effects in the shear and compression modes, respectively.

The important design factors affecting the MR effect or properties of MREs include the size, geometry and spatial distribution of the particles, and magnetic particles volume fraction (PVF). The MREs with soft magnetic particles of nearly spherical geometry and sizes ranging from 3 μm to 100 μm have shown enhanced MR effect under an external magnetic field, while large size particles lead to relatively lower off-state modulus [112]. The MREs integrating non-spherical particles have shown relatively higher variations in damping under an external magnetic field when compared to those with spherical particles [113]. Among all the design factors, the particle volume fraction (PVF) has the most significant influence on the MR effect. Both, the spatial distribution and anisotropy of particles are highly dependent on the PVF. Studies have shown that anisotropy can yield higher or lower MR effect depending on the PVF and the pre-strain [9, 10].

It has been suggested that the maximum MR effect of an MRE occurs when the particles are nearly in contact with each other and the voids between adjacent particles are fully filled with the elastomer, which is referred to as the critical particle volume concentration (CPVC). The structural anisotropy may not be beneficial when PVF exceeds the critical value (approximately 30% for iron particles). A few other studies, however, have shown that higher PVF can considerably enhance both the relative and absolute MR effects of MREs in the shear and mixed shear-compression modes [5, 49]. Furthermore, Lerner [50] reported that designing MRE-based

absorbers require MREs with relatively higher PVF, and the MREs in such applications may fail when PVF is below 30%.

Studies reporting experimental compression mode properties of MREs are summarized in Table A1 and Table A2 in chronological order by the author(s). These suggest broad variation in the MR effect, which is likely due to wide differences in PVFs of MREs used in the studies, apart from the mechanical and magnetic loading conditions. The studies employed MREs with particle concentrations in terms of volume and weight, ranging from 1.5% to 33% and 10% to 80%, respectively. The MREs exhibit coupled effects of all the mechanical and magnetic loading conditions together with the PVF. The properties of MREs should thus be investigated considering variations in both the design and the loading factors. The effect of variations in PVF on mechanical properties of MREs, in-particular, have been mostly explored under either static or slowly varying deformations [17, 26, 45] or at a constant frequency [46], or a constant strain amplitude [47], and/or at relatively low magnetic flux density [23]. From Tables A1 and A2, it is evident that only Fuchs et al. [48] characterized MRE samples with different PVFs considering relatively wide ranges of excitation frequency (0.5-45 Hz), strain amplitude (0.1-8%) and magnetic flux density (up to 0.4T). The study used MREs with maximum of 70% iron particles fraction by weight, which roughly corresponded to 24% PVF. The PVF in most of the studies was limited to 30%, although a higher PVF could further enhance relative as well as absolute MR effects in the shear and mixed shear-compression modes [5, 49].

Reported studies suggest relatively limited knowledge on the effects of the PVF on compression mode properties of the MREs under ranges of mechanical and magnetic loading conditions, although the PVF effects on the properties of passive filled elastomers are relatively well known. In accordance with the Einstein-Guth model, the elastic modulus of filled-rubbers increases with increase in PVF [33]. While the effect of PVF on zero-field properties of an MRE is similar to that of a passive filled-elastomer, the dynamic properties of MRE may exhibit more significant PVF effect in the presence of a magnetic field. Kim et al. [37] showed that saturation magnetization of an isotropic MRE composites increases linearly from 229 to 915 mT, when PVF is increased from 11% to 53%. Davis et al. [114] theoretically found an optimal PVF of around 27% which would yield maximum magneto-induced shear modulus of anisotropic MREs. The

experimental study by Woods et al. [115] observed highest relative MR effect in view of compression stiffness of an anisotropic MRE with 25% PVF.

While some of the experimental studies have described the important PVF effects on compression mode properties of MREs under limited variations in loading factors, the reported constitutive models of MREs generally do not permit analyses of the effects of PVF [20, 40]. Moreover, to the best of the authors' knowledge, a volume fraction dependent model has not yet been developed for estimating dynamic compression mode storage and loss moduli of isotropic and anisotropic MREs. A thorough understanding of the volume fraction effects is, consequently, a fundamental necessity for developing reliable constitutive models and designing MRE-based devices.

The primary aim of this study is to investigate the effects of iron PVF on dynamic compressive properties of isotropic and anisotropic MREs under wide ranges of mechanical as well as magnetic loading conditions. For this purpose, an experiment was designed for compression mode characterizations of cylindrical isotropic and anisotropic MREs with three different PVFs (15%, 30%, 45%) under broad ranges of harmonic displacements (strain amplitude: 2.5 to 20%) at frequencies ranging from 0.1 to 30 Hz and magnetic flux density up to 750 mT. The measured data were compensated for the magnetic pull of the electromagnet and analyzed to assess PVF effect on stress-strain characteristics, and compression moduli and loss factor of the isotropic and anisotropic MREs, considering possible coupled effects of PVF and mechanical and magnetic loading conditions. A simple phenomenological model is subsequently formulated for predicting the PVF effect on the elastic and loss moduli as functions of strain amplitude, frequency and magnetic flux density. The PVF effect described by the model and the measured data can provide important guidance for designing compression mode MRE-based devices to be used in different engineering applications.

6.2 Experimental setup and methods

6.2.1 MRE samples

Six cylindrical MRE batches with radius and thickness of 50 mm, and 8 mm, respectively, with three different PVFs (ϕ=15%, 30%, 45%) were fabricated in the laboratory using the methods presented in [9]. Briefly, 3.9 to 5 μm spherical magnetically soft carbonyl iron particles (CIP; BASF-SQ, Germany) were thoroughly mixed into a platinum-based silicone elastomer (Eco-Flex

00-20, Smooth-On Inc., USA). A vacuum chamber was employed to remove entrapped air from the mixture. The mixture for three of the batches were permitted to cure under ambient conditions to realize isotropic dispersion of the iron particles within the matrix. The mixture for the remaining three batches with different PVF were permitted to cure under a relatively strong magnetic field (magnetic flux density = 1200 mT) so as to achieve anisotropic columns of iron particles within the silicone-based medium. The 18 mm diameter and 8 mm thick isotropic and anisotropic MRE specimens were subsequently cut form the respective batches in accordance with the standardized guidelines for compression testing of elastomers [52]. The dispersions of CIP in the MRE samples were examined using an industrial laser confocal microscope (LEXT OLS4000, Olympus Inc.). For this purpose, isotropic and anisotropic samples with different PVF were cut along the thickness direction to view the cross-sections under the microscope. Figure 6.1 depicts, as an example, the microstructures of both types of MREs with 15% PVF, under a magnification of 50. The images clearly show the random and chain like dispersions of CIP in the matrix of the isotropic and anisotropic MREs, respectively.

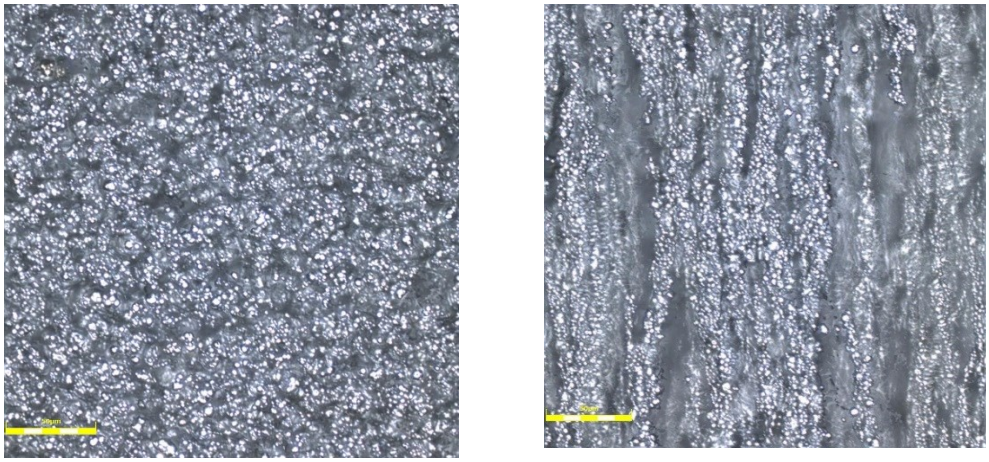

Figure 6.1 Microstructures of the isotropic (left column) and anisotropic (right column) MRE samples with 15% iron particles volume fractions (50X magnification)

6.2.2 Experimental test setup

A test apparatus was custom-designed for magneto-mechanical characterization of compression mode properties of MREs with different particle volume compositions, which has been described in details in [9]. Briefly, the apparatus comprised a U-I design of a compact electromagnet, which permitted application of magnetic flux density of up to 1 T in the compression direction of the MRE. Two MRE specimens were bonded to the U- and I-sections of the electromagnet, which

were fixed on a servo-hydraulic test system, as shown in Figure 6.2. While the U-section of the electromagnet was fixed to the actuator shaft, the I-section was attached to a fixed beam via a 9 kN force transducer. Each specimen was subjected to a relatively large pre-strain of 21% prior to the dynamic loading. The experiments were performed using the standardized methods described in ISO 7743 [52] for characterizing force-deflection (stress-strain) properties of MREs with selected PVFs. The experiment design involved factorial combinations of four different amplitudes of harmonic displacement (strain amplitude, ε=2.5%, 5%, 10% and 20%) applied at five different frequencies (f= 0.1, 1, 10, 20 and 30 Hz) together with five different levels of magnetic flux density (B = 0, 150, 300, 450, 600 and 750 mT). Controlled magnetic flux was achieved using a variable dc-current power supply. The maximum flux density was limited to 750 mT, since the samples showed saturation of the elastic modulus under flux density in excess of 600 mT. Moreover, the force signal revealed considerable delay during unloading. A total of 120 tests were thus performed for each MRE specimen. Controlled magnetic flux was achieved using a variable dc-current power supply.

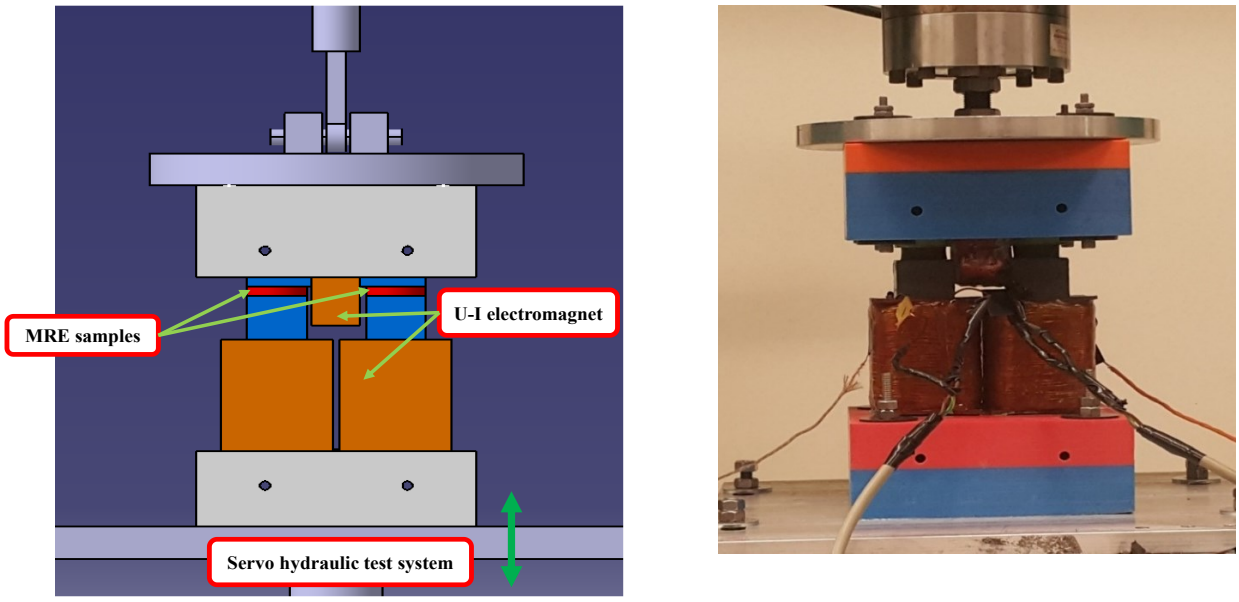

(a) (b)

Figure 6.2 Schematic (a) and pictorial (b) illustrations of test setup for characterization of compression mode properties of MREs [9].

6.2.3 Data analysis

The steady-state force and displacement data were acquired in the LabView for each combination of test variables using the sampling rate ranging from 50 Hz to 5000 Hz depending on the loading frequency. The data were low-pass filtered and stored for four successive oscillation cycles, and averaged to obtain the force-displacement and stress-strain properties corresponding to each test condition. It should be noted that the force measured during compression mode characterization of an MRE comprises two components: (i) the magnetic pull force developed by magnetic poles of the electromagnet; and (ii) the viscoelastic force attributed to compression loading of the MRE. The magnetic force, estimated using the phenomenological model reported in Equation (2-24), was subtracted from the measured force to obtain strain amplitude-, strain rate- and field-dependent viscoelastic force attributed to deformation of the MRE.

The resulting force and displacement data were evaluated to obtain compression mode properties of the MREs such as the compression mode elastic (E') and loss (E'') moduli. The compression mode energy storage and dissipation properties of viscoelastic materials are widely estimated from the slope of the major axis in the vicinity of static equilibrium (pre-strain condition) and the area bounded by the force-deflection (stress-strain) hysteresis loop, respectively [87, 88]. This approach, however, is considered adequate only for linear or nearly linear stress-strain characteristics. Considerable errors may be expected for MREs with relatively higher PVF, which can yield nonlinear stress-strain properties with large asymmetry in compression and tension, especially under higher deformations. Alternate methods have been employed for characterizing the shear modulus of viscoelastic materials in the large amplitude oscillatory (LAO) regimes, such as minimum-strain modulus, large strain modulus, differential modulus and the first harmonic modulus [116]. Owing to symmetric stress-strain curves in the shear mode such methods can provide accurate estimates of the moduli. The standardized method, ASTM D5992-96 [97], also recommends the first harmonic approach using either Fourier series or Fourier transform of the measured data for estimating moduli of the rubber-like materials exhibiting nonlinear stress-strain behaviour. In this study, the first-harmonic modulus approach [97, 116] is used to obtain estimates of compression mode equivalent elastic and loss moduli of the MREs. Although, the identified moduli may not be accurate considering the asymmetric stress-strain properties, especially under higher PVF and strain amplitude, the estimated moduli are considered appropriate for evaluating relative effects of PVF on the compression mode properties of the MREs. The measured stress-

stress data were analyzed to obtain fundamental Fourier series coefficients, which were subsequently applied to obtain equivalent hysteresis loops symmetric about the mean stress, and thereby the equivalent elastic ($E_{eq}{}'$) and loss ($E_{eq}{}''$) moduli.

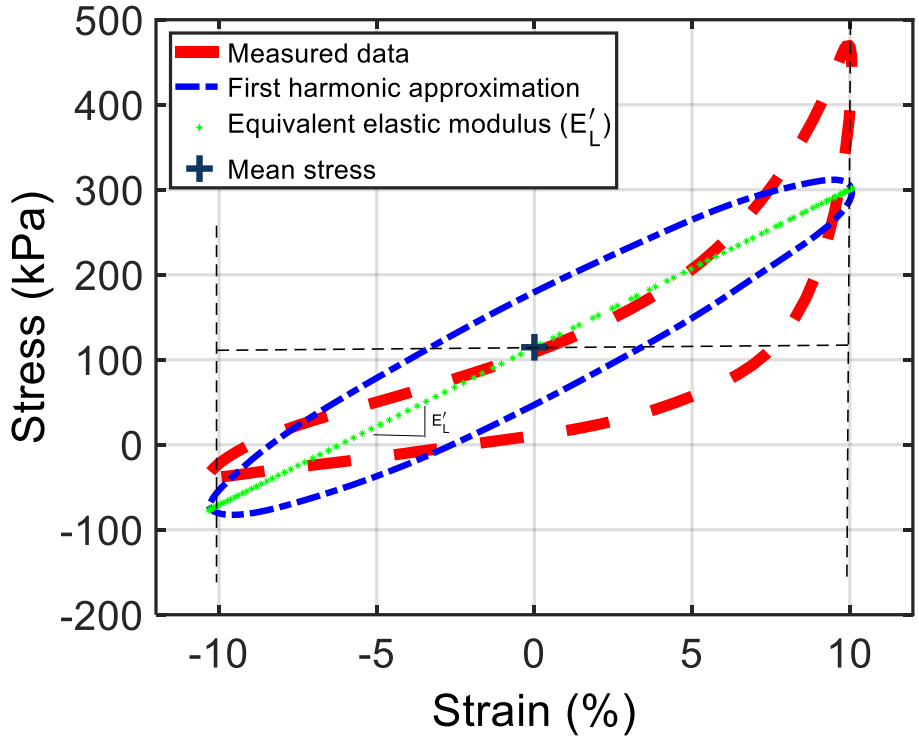

Figure 6.3 A linear approximation to the nonlinear characteristics of the anisotropic MRE with 45% PVF under 10% strain amplitude and loading excitation of 1 Hz at zero field, using the equivalent elastic and loss moduli obtained from the Fourier series representation of the stress response.

As an example, Figure 6.3 compares the equivalent stress-strain properties of an anisotropic MRE with 45% PVF, estimated from the first-harmonic, with the measured data acquired under 10% peak strain at a frequency of 1 Hz in the absence of the magnetic field. The estimated equivalent moduli are used to evaluate relative effects of PVF on the elastic and loss moduli, which are denoted as PVF-stiffening and PVF-dampening effects, respectively. A PVF effect is defined as the relative change in the modulus of the MRE for the maximum change in the PVF considered, such that:

$$\%\text{PVF-stiffening} = \frac{E'_{eq}(\phi_3) - E'_{eq}(\phi_1)}{E'_{eq}(\phi_1)} \times 100 \qquad (6\text{-}1)$$

$$\%\text{PVF-dampening} = \frac{E''_{eq}(\phi_3) - E''_{eq}(\phi_1)}{E''_{eq}(\phi_1)} \times 100 \quad (6\text{-}2)$$

where $E'_{eq}(\phi_3)$ and $E''_{eq}(\phi_3)$ represent the equivalent linear elastic and loss moduli, respectively, corresponding to the maximum PVF, ϕ_3=45%, and $E'_{eq}(\phi_1)$ and $E''_{eq}(\phi_1)$ are the reference moduli for ϕ_1 =15%.

6.3 Results and discussions

6.3.1 Effects of particles volume fraction on stress-strain properties

The steady-state stress-strain properties of the anisotropic and isotropic MREs consistently showed notable hysteresis, and significant effects of PVF apart from those of the magnetic flux density, and strain amplitude and rate. As an example, Figure 6.4(a) and 6.4(b) illustrate the effects of PVF on the off-state (B=0) stress-strain properties of anisotropic and isotropic MREs under peak strains of 2.5% and 10%, at excitation frequency of 1 Hz. The results depict considerable asymmetry and nonlinearity in compression and extension, which is more pronounced for higher PVF, especially under the higher strain input. An increase in PVF also yields notably higher peak stress during compression loading, which is more pronounced at higher strain excitation. This is likely due to greater clustering of particles within the matrix with relatively higher PVF, which contributes to relatively higher stiffness of the MRE together with higher stress. Increasing PVF from 15% to 45% resulted in nearly 235% and 277% increases in the peak stress of the isotropic MRE subject to 2.5% and 10% strain amplitude excitations, respectively. The corresponding increases for the anisotropic MRE were about 320% and 585%, respectively. Results in Figure 6.4 showed substantial increase in the major axis slope of the equivalent linear hysteresis loop as the PVF increased from 15% to 45%, signifying PVF-stiffening feature. This is mainly due to greater filler-matrix and filler-filler interactions with increasing PVF, which has also been theoretically shown by the Einstein-Guth model for filled-rubbers [33]. For the selected loading conditions, the PVF-stiffening effect, is more pronounced for the anisotropic MRE compared to that of the isotropic MRE. This is likely due to additional interactions among particles oriented in a chain-like manner, which may be considered as fibers in a composite material. Results in Figure 6.4 also suggest relatively lower PVF-stiffening effect under the higher strain amplitude, especially for the isotropic MRE, which is attributable to the strain-softening tendency of the MREs. The anisotropic MRE, however, revealed relatively lower variations in the PVF-stiffening with increase in the

strain amplitude. This is likely a result of strain-softening coupled with the stiffening effect due to anisotropy, which is evident at a relatively lower strain amplitude compared to the isotropic MRE.

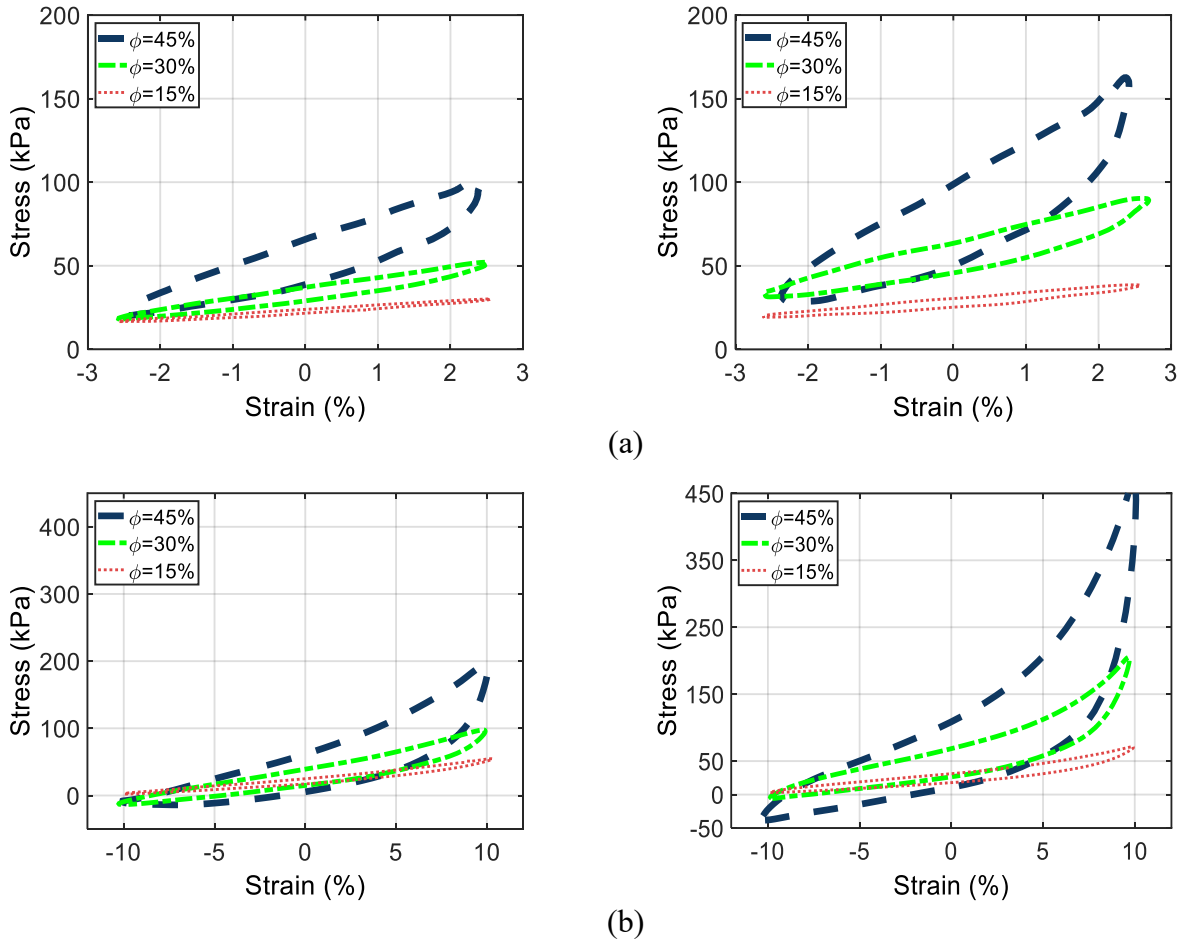

Figure 6.4 Effect of particle volume fraction on stress-strain characteristics of isotropic (left column) and anisotropic (right column) MREs under two different strain amplitudes: (a) ε= 2.5%; and (b) ε = 10% (B=0; f=1 Hz).

An increase in the PVF also yields significant increase in the area bounded by the hysteresis loop and thus the energy dissipation during each cycle, signifying PVF-dampening feature of the MREs. This tendency is also attributable to greater filler-filler and filler-matrix interactions with increased PVF, apart from the viscoelastic properties of the matrix. The results show relatively greater PVF-dampening effect for both types of the MRE compared to the PVF-stiffening effect. This tendency has also been observed for filled-rubbers under dynamic compression loading [117]. Similar to the PVF-stiffening, the PVF-dampening effect becomes less pronounced with increase in the strain amplitude, which is relatively less for the anisotropic MRE. For instance, under the

2.5% strain excitation, the isotropic and anisotropic MREs revealed PVF-dampening effects in the order of 1047% and 852%, respectively. Increasing the strain to 10% resulted in PVF-dampening effects for the isotropic and anisotropic MREs of about 731% and 785%, respectively. The corresponding PVF-stiffening effects for the isotropic and anisotropic MREs were about 427% and 505%, respectively, under 2.5% strain, and 253% and 515% for the 10% strain amplitude excitation. These further imply that the PVF-stiffening and the PVF-dampening of both types of MREs are generally limited by the strain-softening effect of the MREs, when strain amplitude is increased from 2.5% to 10%, suggesting coupled effects of PVF and strain amplitude on the compression mode properties. This trend was also evident under other magnetic flux and loading conditions.

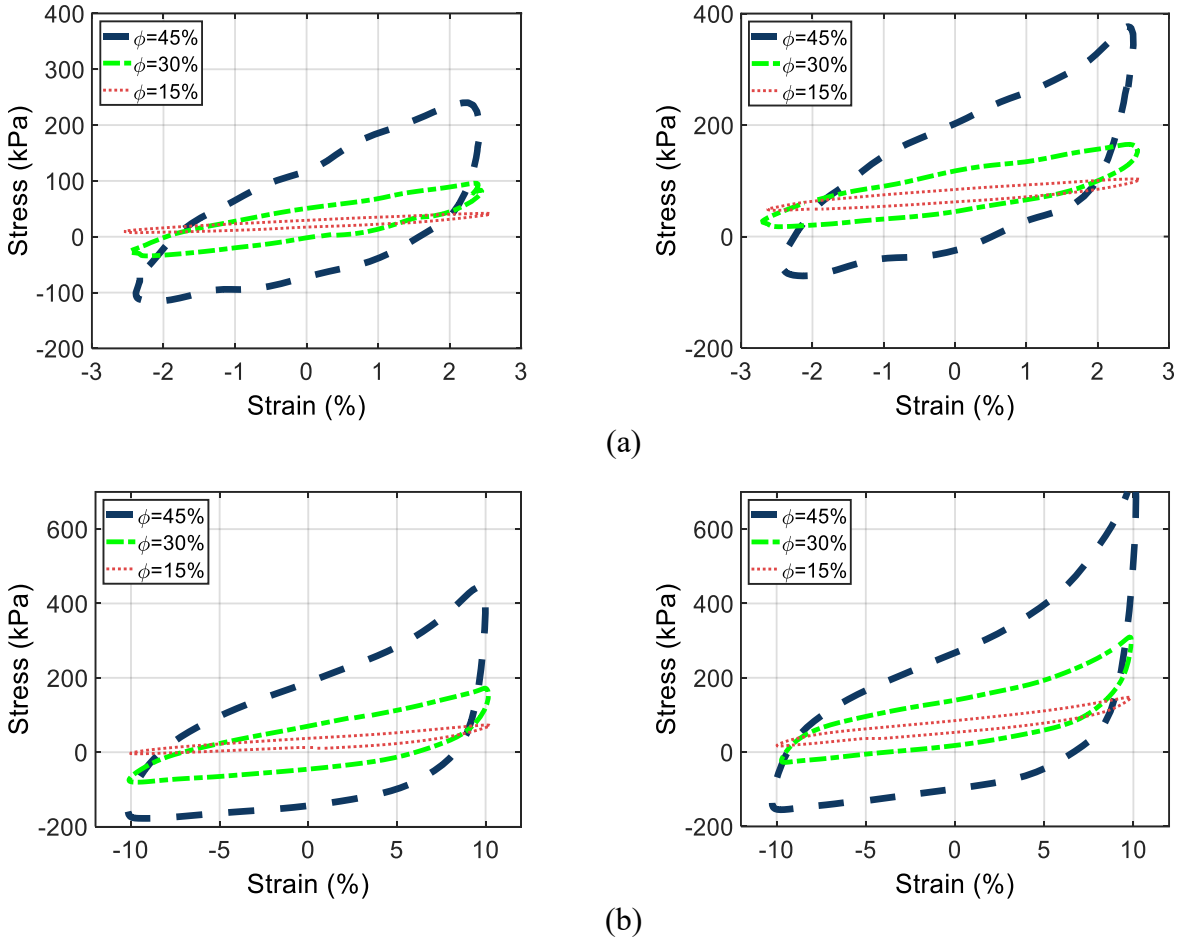

Figure 6.5 Effect of particle volume fraction on stress-strain characteristics of isotropic (left column) and anisotropic (right column) MREs under two different strain amplitudes: (a) ε= 2.5%; and (b) ε= 10% (B=600 mT; f=1 Hz).

Figure 6.5(a) and 6.5(b) illustrate the effects of PVF on stress-strain properties of the anisotropic and isotropic MREs in the presence of a magnetic field (B=600 mT). The results, presented for 2.5% and 10% strain excitations at 1 Hz, show substantially stronger PVF-stiffening for the isotropic MRE when compared to those observed in the off-state. The PVF-stiffening effects observed for the anisotropic MRE, however, are comparable with the off-state values, particularly under the lower strain amplitude of 2.5%. This is likely due to relatively lower spacing between the magnetizable particles within the anisotropic MRE, especially for ϕ=45%, compared to the isotropic MRE. Relatively greater number of dipole-dipole interactions among the particles of the isotropic MRE is thus expected, which contribute to higher stiffening effect in the presence of the magnetic field.

The results obtained for the selected loading conditions, presented in Figure 6.5, revealed PVF-stiffening effects in the order of 713% and 508% for the isotropic and anisotropic MREs, respectively, under the 2.5% strain excitation. Increasing the strain to 10% resulted in PVF-stiffening effects for the isotropic and anisotropic MREs of about 497% and 411%, respectively. The corresponding PVF-dampening effects for the isotropic and anisotropic MREs were about 1553% and 985%, respectively, under 2.5% strain, and 1347% and 1150% for the 10% strain amplitude excitation. The PVF-dampening effect is substantially higher than the PVF-stiffening effect since many design factors of the MRE contribute to the damping property such as viscous flow of the matrix, interactions between the magnetic particles and the matrix, friction and magneto-mechanical effects [118]. The stiffness property of the MRE, on the other hand, is mostly attributed to elastic behavior of the matrix, particle-particle, and particle-matrix interactions.

The stress-strain properties of the MREs, obtained under different levels the of magnetic flux density, revealed that the PVF-stiffening effect for both the anisotropic and isotropic MREs generally increased with increase in the magnetic flux density, irrespective of the strain amplitude and loading frequency. The PVF-dampening of isotropic MRE also increased considerably with the magnetic flux, which was not evident for the anisotropic MRE. The PVF-stiffening with increasing flux density was also less pronounced for the anisotropic MRE compared to the isotropic MRE. This is partly due to the large pre-strain of 21%, which limits the anisotropy effect as the PVF increases.

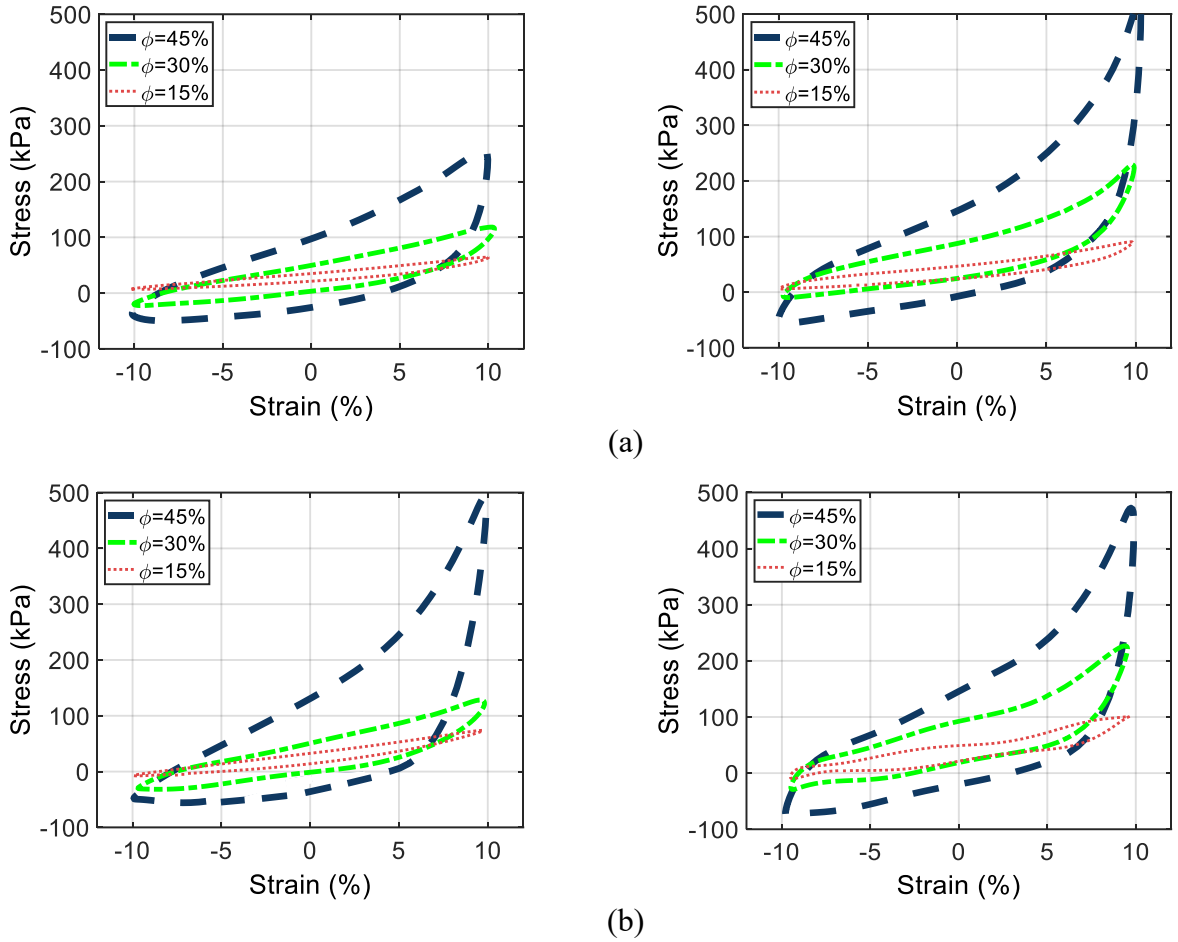

Figure 6.6 Effect of volume fraction on stress-strain characteristics of isotropic (left column) and anisotropic (right column) MREs subject to 10% peak strain at different frequencies: (a) f= 1 Hz, (b) f= 10 Hz (B=150 mT).

Figure 6.6(a) and 6.6(b) show the effects of PVF on the stress-strain hysteretic properties of MREs subjected to excitations at two different rates (1 Hz and 10 Hz). Results are presented for both the anisotropic and isotropic MREs subject to ε=10% and B=150 mT. Results show greater PVF-stiffening effect and peak stress for the isotropic MRE subject to excitation at 10 Hz, when compared to that at 1 Hz, suggesting additional strain-rate stiffening of the isotropic MRE. The stress-strain properties of the anisotropic MRE, however, show negligible or even opposing strain rate effect. Increasing the excitation frequency from 1 Hz to 10 Hz resulted in relatively lower PVF-stiffening but comparable peak stress of the anisotropic MRE, which is partly due to anisotropy-stiffening effect which limits the PVF-stiffening effect of the anisotropic MRE. Besides, this decrement is likely attributed to relatively uneven distribution and confinement of

rubber between particles, which are getting too close or even touch each other in anisotropic chains at PVF of 45%. This causes lower portion of rubber confinement experiences local large deformation compared to the isotropic MRE, thereby lowering rate-stiffening effect. A relatively similar tendency has also been observed by Fuchs et al. [48] for a polybutadiene–PU–based anisotropic MRE under 400 mT.

Figure 6.6(a) and 6.6(b) also show similar but considerably smaller effect of the strain-rate on the PVF-dampening properties of MREs. Increasing the frequency from 1 Hz to 10 Hz yielded only a small increase in the PVF-dampening effect for the isotropic MRE, while the PVF-dampening of the anisotropic MRE decreased slightly. For the selected strain and flux density conditions (B=150 mT and ε=10%), presented in Figure 6.6, increasing the PVF from 15% to 45% at the excitation frequency of 1 Hz revealed PVF-stiffening effects of nearly 332% and 438% for the isotropic and anisotropic MREs, respectively, with the corresponding PVF-dampening effects of 904% and 690%. Increasing the frequency to 10 Hz resulted in PVF stiffening effects of 435% and 325%, respectively, for the isotropic and anisotropic MREs, and the corresponding PVF-dampening effects of 949% and 559%. Results also consistently revealed more noticeable PVF-dampening effects than the PVF-stiffening effects for both type of MREs, irrespective of the magnetic flux density, strain amplitude, and frequency, as shown in Figure 6.4 through Figure 6.6.

6.3.2 Effects of particle volume fraction on the compression moduli

The effect of PVF on the compression mode properties are further investigated in a quantitative manner in terms of the equivalent linear elastic modulus (E_l') and the loss modulus (E_l''), using the method described in section 2.3. Figure 6.7 shows the variations in the elastic and loss moduli of the anisotropic and isotropic MREs with the PVF. As examples, the results are shown for three different strain amplitudes (2.5%, 5% and 10%) at a frequency of 1 Hz, and magnetic flux density of 300 mT. Both the elastic and loss moduli increase in a nonlinear manner with increase in the PVF, irrespective of the strain amplitude and the anisotropy. These are consistent with the PVF-stiffening and PVF-damping effects observed in the stress-strain properties (Figure 6.4 through Figure 6.6). The results also show the strain-softening (Payne effect) of both the MREs, which tends to be substantially higher for the MREs with greater PVF. This is attributable to relatively greater weakening of the bonds among the filler particles and between the rubber matrix and the filler under higher deformations, especially when the compound comprises higher PVF. The rates

of increase in the elastic and loss moduli of both types of MRE with respect to PVF tend to decrease with increase in the strain amplitude. The rates, however, are slightly lower for the anisotropic MRE. This is consistent with the coupled effects of the strain amplitude and the PVF that were observed in the stress-strain properties shown in Figure 6.4 and Figure 6.5.

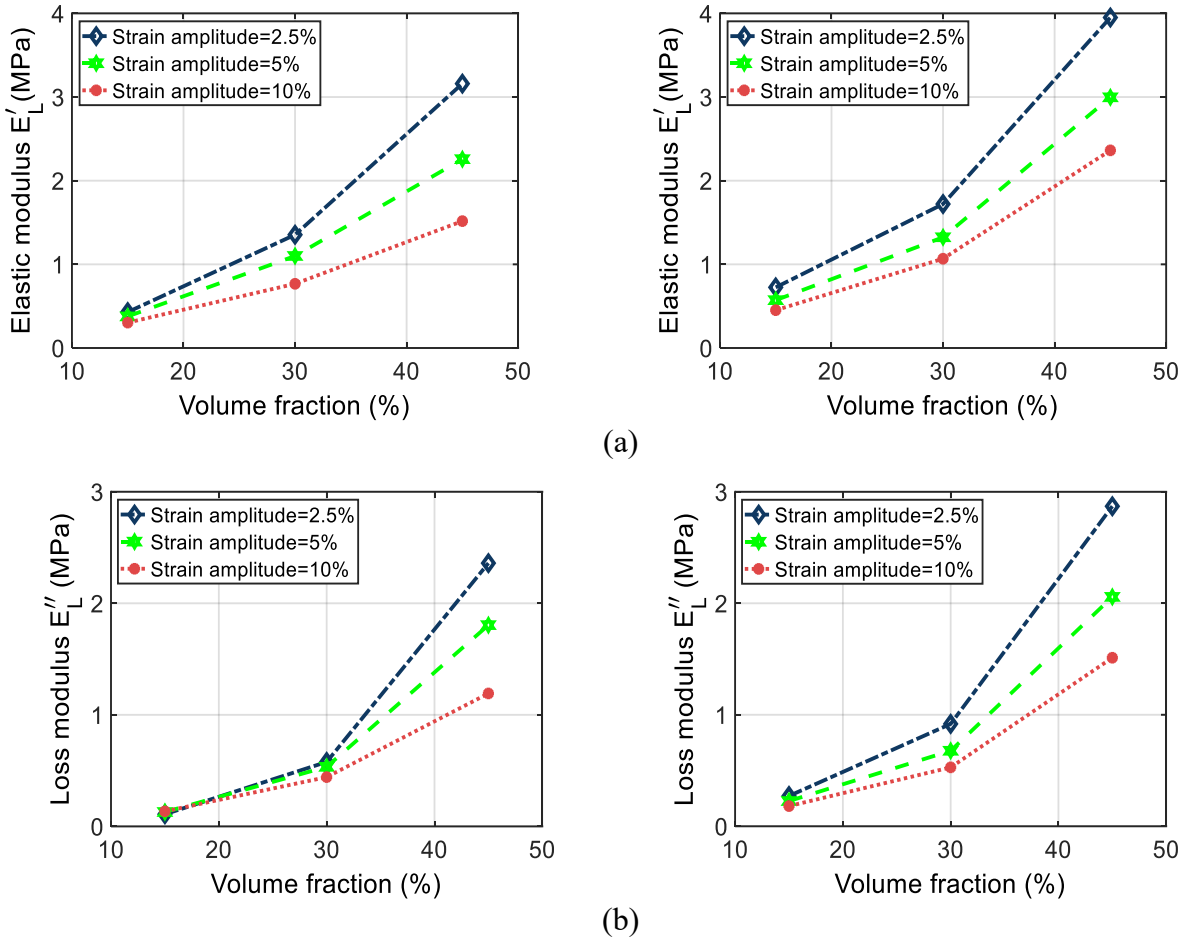

Figure 6.7 Effect of volume fraction on the compression mode elastic modulus (a), and loss modulus (b) of the isotropic (left column) and anisotropic (right column) MREs for different strain amplitudes (f=1 Hz, and B=300 mT).

For the conditions considered in Figure 6.7, increasing the PVF from 15% to 45% resulted in increase in the elastic modulus of the isotropic MRE from about 0.43 MPa to 3.16 MPa under the 2.5% strain excitation. The increase was from about 0.38 MPa to only 2.26 MPa under 5% strain, and from about 0.30 MPa to 1.52 MPa under the 10% strain amplitude. These correspond to approximately 636%, 498%, and 400% increases in the elastic modulus. The corresponding PVF-stiffening effects for the anisotropic MRE were obtained as 445%, 424% and 423%, respectively,

for the 2.5%, 5% and 10% strain excitations, which are generally lower than those obtained for the isotropic MRE, except for the strain amplitude of 10 %. Increasing the PVF from 15% to 45%, revealed relatively greater increase in the loss moduli of both types of MREs. By increasing the PVF from 15% to 45%, the loss modulus of the isotropic MRE increased from nearly 0.11 MPa to 2.36 MPa under 2.5% strain, from about 0.13 MPa to 1.80 MPa under 5% strain, and from around 0.14 MPa to 1.19 MPa under 10% strain. These correspond to approximately 2062%, 1299%, and 782% increases in the loss modulus under 2.5%, 5% and 10% strain excitations. The loss modulus of the anisotropic MRE increased by 956%, 809%, and 735% under the 2.5%, 5%, and 10% strain excitations, respectively. Although the results in Figure 6.7 are presented for f=1 Hz and B=300 mT, similar tendencies were evident under other loading conditions.

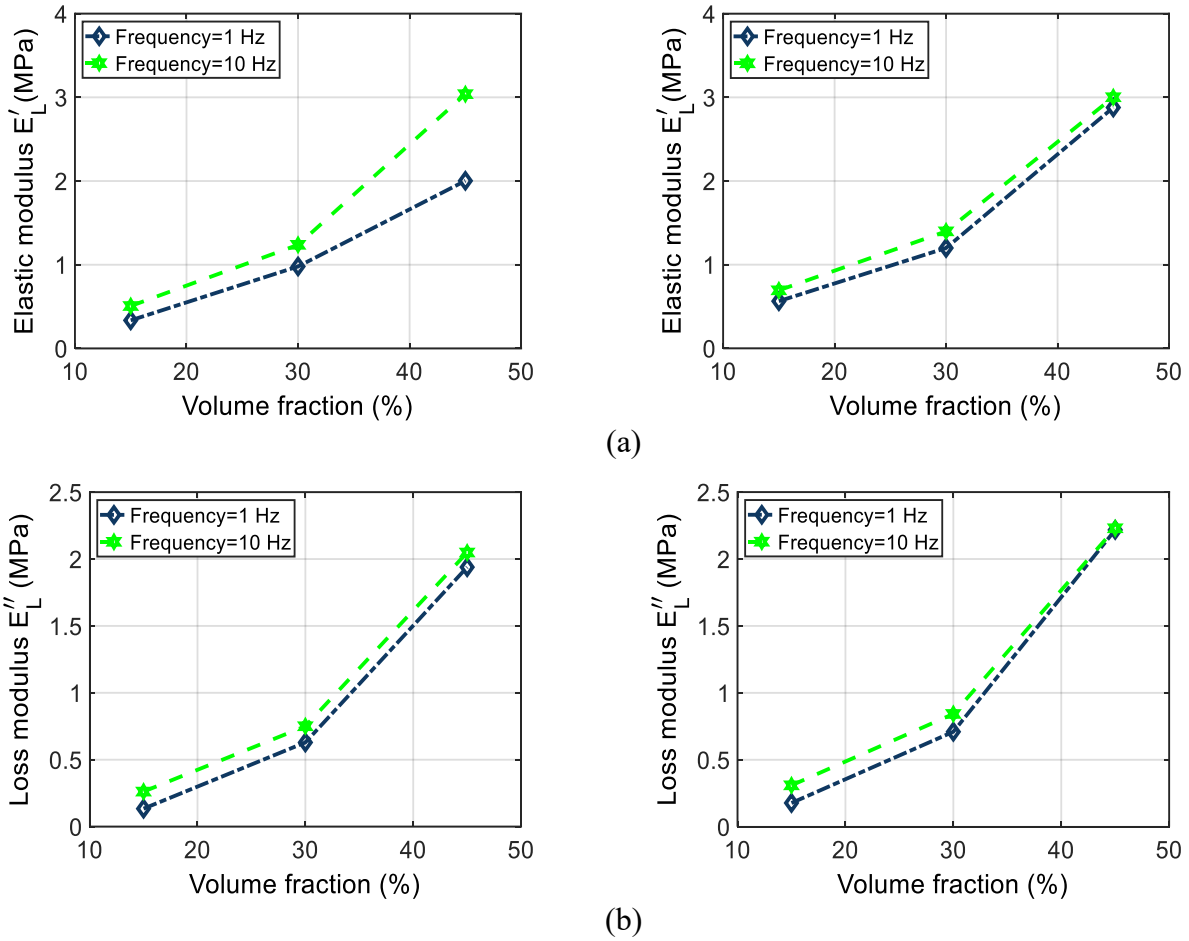

Figure 6.8 Effect of volume fraction on the compression mode elastic modulus (a), and loss modulus (b) of the isotropic (left column) and anisotropic (right column) MREs under different excitation frequencies (ε=10%, and B=600 mT).

Figure 6.8 illustrates the effects of PVF on variations in the elastic and loss moduli considering B= 600 mT and 10% strain excitation at two different frequencies, namely, 1 Hz and 10 Hz. Both the elastic and loss moduli of the MREs increased with increase in PVF in a nonlinear manner, irrespective of the excitation frequency, as it was also observed in Figure 6.7. The results suggest that increasing the excitation frequency yields only slight increase in the loss moduli of both the MREs. The elastic modulus of the isotropic MRE, however, increased considerably with increase in the frequency, especially when the PVF is in excess of 30%. Increasing the excitation frequency resulted in only slight increase in the elastic modulus of the anisotropic MRE, irrespective of the PVF.

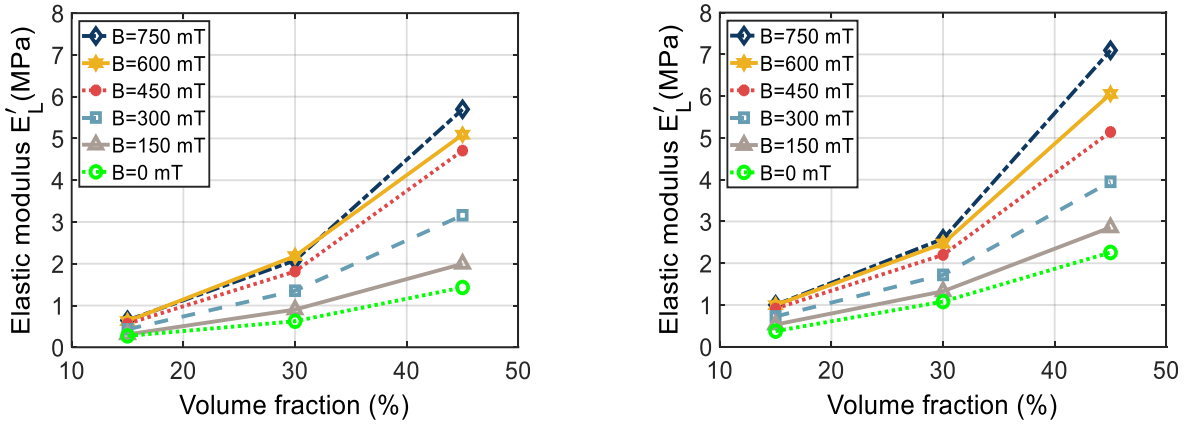

(a)

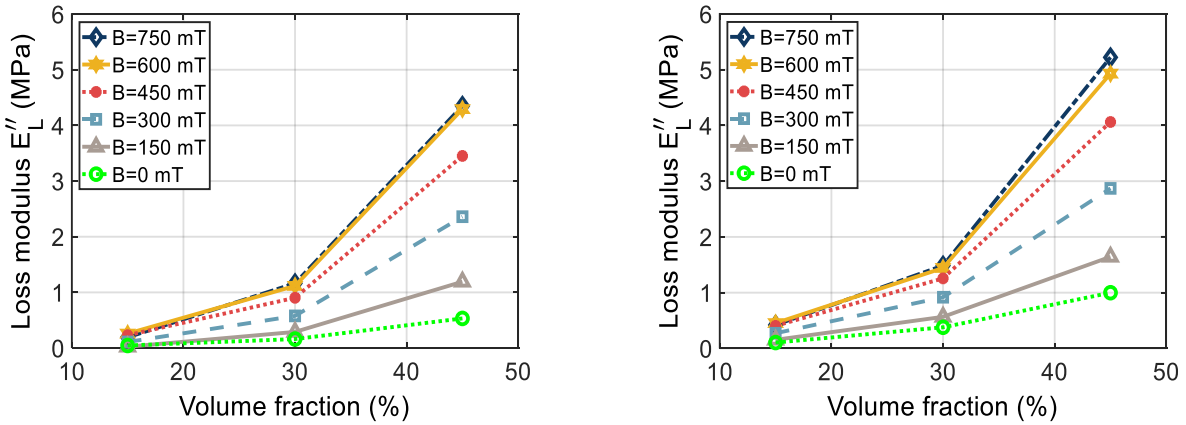

(b)

Figure 6.9 Effect of volume fraction on the compression mode elastic modulus (a), and loss modulus (b) of isotropic and anisotropic MREs under different levels of magnetic flux density (strain amplitude =2.5%, f=1 Hz).

Figure 6.9 illustrates the effects of the PVF on the elastic and loss moduli of the MREs considering different levels of magnetic flux density, ranging from 0 to 750 mT. The results are presented for 2.5% strain excitation at a frequency of 1 Hz, as examples. While the elastic and loss moduli of both types of MREs increase with increase in PVF, as observed in Figure 6.7 and Figure 6.8, increasing the flux density contributes to relatively higher moduli. Results also suggest saturation of the elastic and loss moduli under relatively higher levels of the magnetic flux density. For the selected excitation, the elastic modulus of the isotropic MRE increased from about 0.31 MPa to 2 MPa, from nearly 0.56 MPa to 4.71 MPa, and from 0.65 MPa to nearly 5.7 MPa for B=150 mT, B=450 mT and B=750 mT, respectively, when the PVF was increased from 15% to 45%. These correspond to 548%, 735% and 782% increases in the elastic modulus. The corresponding increases in the equivalent elastic moduli of the anisotropic MRE were obtained as 438%, 462%, and 608% for B=150 mT, B=450 mT and B=750 mT, respectively. The results suggest that increase in the magnetic flux density generally enhances the PVF-stiffening effects for both types of MREs. The increase in the PVF-stiffening with the flux density, however, is more pronounced for the isotropic MRE compared to the anisotropic MRE. This is partly due to the large pre-strain of 21%, which limits anisotropy effect, especially with the higher PVF [9]. The loss moduli of both the MREs also increased with the magnetic field in a similar manner. Results also showed generally higher PVF-dampening of both types of MREs with increasing magnetic flux density from 0 mT to 750 mT.

6.3.3 Influence of particle volume fraction on the relative MR effect

The effects of PVF on magnetic field-dependent properties of the MREs are further investigated in terms of the relative MR effects in view of the elastic modulus ($MR_{\acute{E}}$) and the loss modulus ($MR_{E_L''}$). The relative MR effect is defined as the percent difference between the zero-field and maximum field (750 mT) elastic or loss modulus normalized with respect to the zero-field modulus for a given PVF [5, 84]. Figure 6.10 shows variations in the relative MR effects of the anisotropic and isotropic MREs with the PVF ranging from 15% to 45%. The results are presented for three different strain amplitudes (2.5%, 5% and 10%) applied at two different frequencies (1 Hz and 10 Hz). The results are suggestive of strong dependence of the MR effects on the strain amplitude and excitation frequency, apart from the PVF. Under the excitation at 1 Hz, the $MR_{\acute{E}_L}$ of the isotropic MRE increases with the PVF in a nearly linear manner, irrespective of

strain amplitude. This tendency, however, is not evident under the higher frequency excitation. Under the 10 Hz excitation, the $MR_{E_L'}$ increases with increase in PVF from 15% to 30%, and it decreases with further increase in the PVF, as seen in Figure 6.10 (b). This is partly attributed to the significantly higher strain-rate stiffening of the isotropic MRE with increasing PVF, particularly when the PVF is increased from 30% to 45%, as seen in Figure 6.8(a).

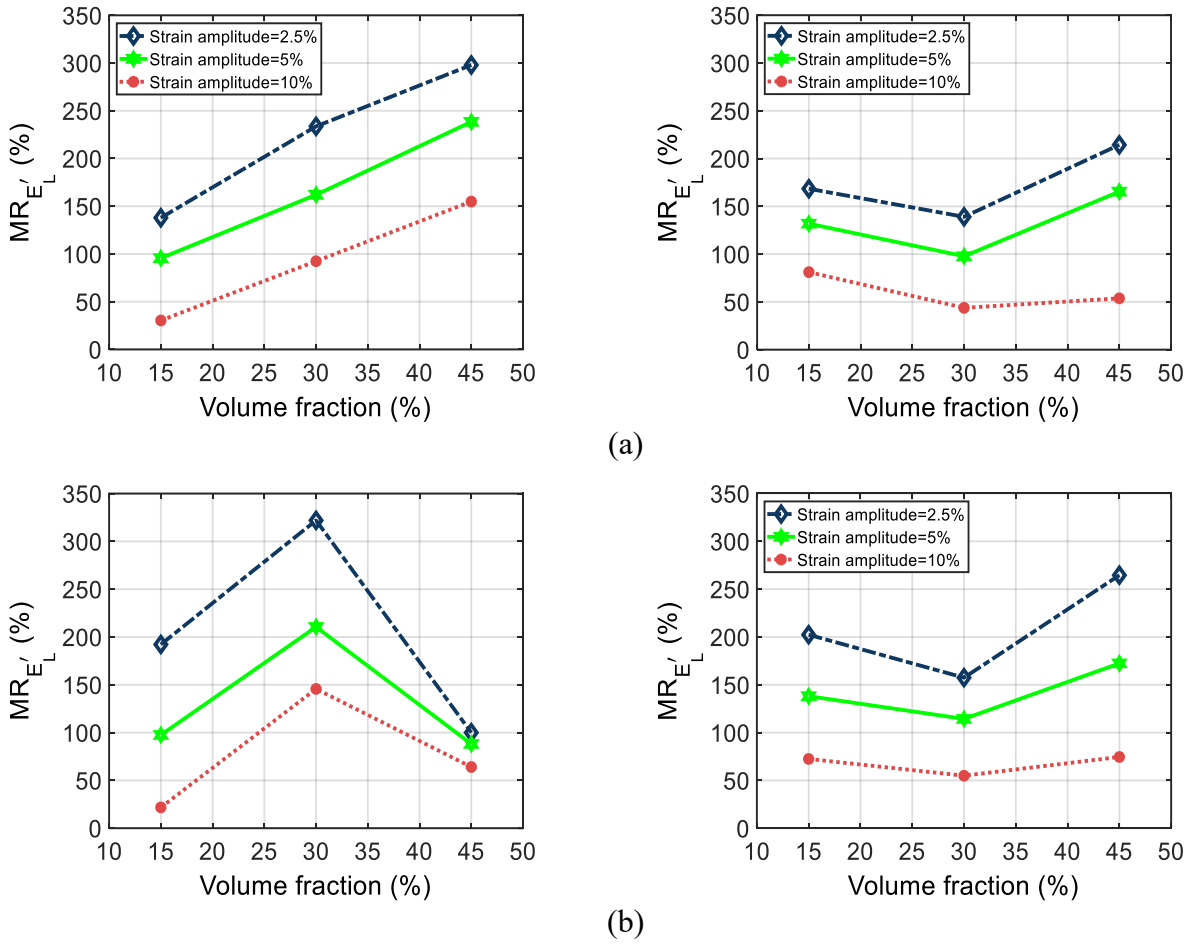

Figure 6.10 Dependency of relative MR effect in view of elastic modulus on the volume fraction of the isotropic (left column) and anisotropic (right column) MREs under different strain amplitudes when B was increased from 0 to 750 mT: (a) f=1 Hz, (b) f=10 Hz.

Furthermore, Suphadon [94] reported that the deformation of the matrix material trapped between adjacent particles is approximately ten times greater than that of the un-trapped matrix in filled elastomers, which was denoted as the strain amplification effect. This effect becomes more pronounced for the isotropic MRE with PVF of 45% when compared to the compared to the

isotropic MRE with 30% PVF. An increase in the loading frequency, causes higher strain amplification and, thereby, relatively higher strain-rate stiffening of the 45% isotropic MRE as compared to the 30% isotropic MRE. The enhanced strain-rate stiffening effect tends to diminish relative increase in compression modulus of the isotropic MRE with 45% PVF with increase in the magnetic flux density.

The relative MR effect of the anisotropic MRE, however, exhibits somewhat opposing trend, although consistent for both the excitation frequencies. The anisotropic MRE exhibits relatively smaller effect of the loading frequency on the elastic and loss moduli, as noticed in Figure 6.8, which is likely due to relatively smaller strain-rate stiffening of the matrix with chain like arrangements of the iron particles. Moreover, the anisotropic MRE exhibits more pronounced magnetic field stiffening (Figure 6.10) compared to the loading frequency effect. For lower PVF of 15%, the anisotropy is strong due to dipole-dipole interactions within the chains of iron particles, which tends to diminish with higher PVF due to substantially lower gap between the particles. This results in relatively lower $MR_{\acute{E}_L}$ as the PVF increases from 15% to 30%. A further increase in the PVF from 30% to 45%, however, causes the $MR_{\acute{E}_L}$ to increase, irrespective of the loading frequency and strain excitation. This has been primarily associated with the wavy chains stiffening mechanism, attributed to the restructuring of the particles [119, 120] that is more pronounced under relatively higher pre-strain, apart from the enhanced chain–chain interactions for the higher PVF MRE. The anisotropic MREs thus exhibit lowest $MR_{\acute{E}_L}$ around 30% PVF, irrespective of the strain excitation and loading frequency. The isotropic MREs, however, yield the highest $MR_{\acute{E}_L}$ under excitations at 10 Hz at 30% PVF. Similar trends were also observed under higher frequency excitations.

Figure 6.10 also shows that the anisotropic MRE yields greater ($MR_{\acute{E}_L}$) compared to the isotropic MRE only for the lower PVF of 15%, irrespective of the strain amplitude and the excitation frequency. The results further suggest that the isotropic MREs with 30% PVF may be better suited for applications involving higher frequency excitations, while those with 45% PVF would be desirable for lower frequency excitations (≈1Hz). The anisotropic MREs with 45% PVF, on the other hand, may be considered better suited for applications involving relatively higher payloads and low deformations.

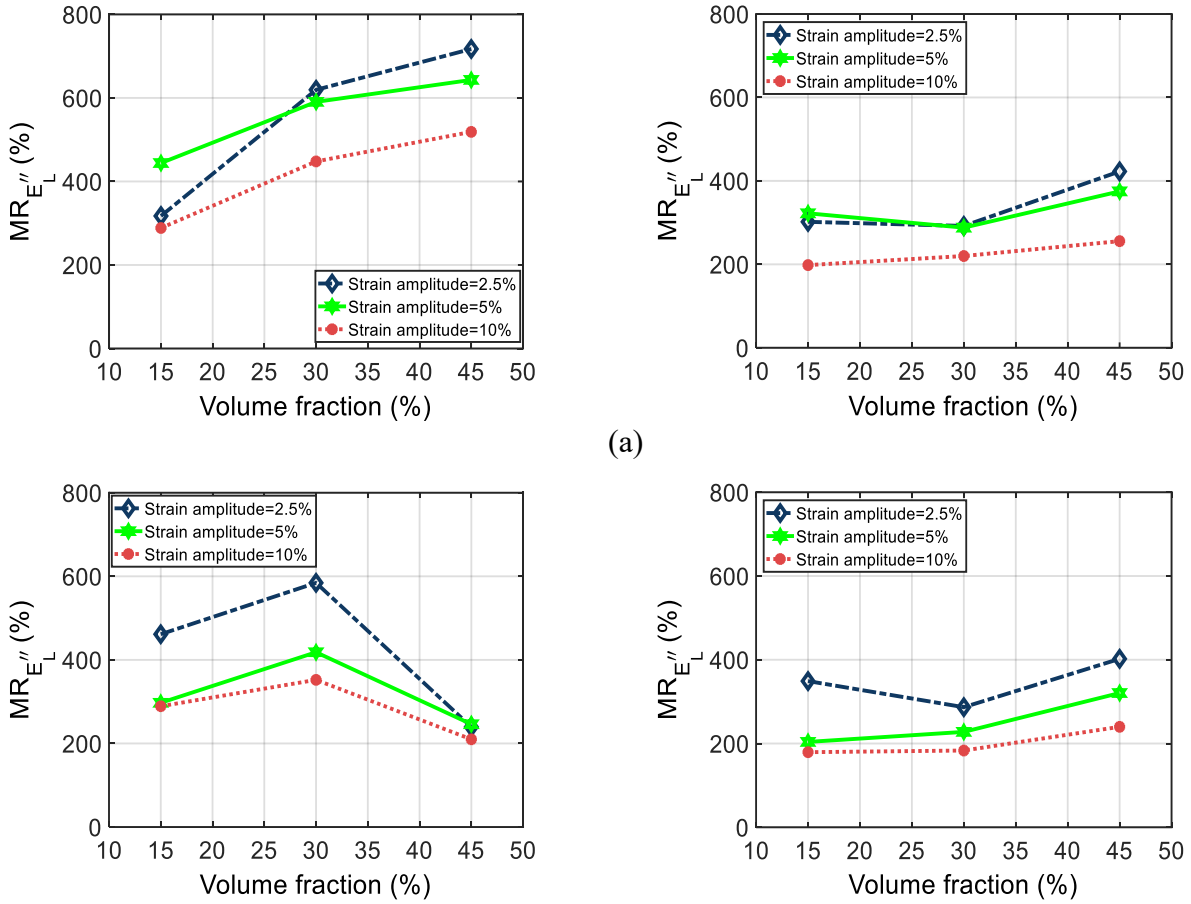

Figure 6.11 Dependency of relative MR effect in view of loss modulus on the volume fraction of the isotropic (left column) and anisotropic (right column) MREs under different strain amplitudes when B was increased from 0 to 750 mT: (a) f=1 Hz, (b) f=10 Hz.

It is noted that Davis [114] and Woods et al. [115] have suggested 27% and 25% as optimum PVFs for anisotropic MREs subjected to small shear and compression strains, respectively, in the static regime. Results also revealed maximum $MR_{E_L'}$ of 233%, 322% and 298%, respectively, for the isotropic MRE with 15%, 30% and 45% PVF under the lowest strain amplitude, as expected. The corresponding maximum $MR_{E_L'}$ for the anisotropic MRE with PVF of 15%, 30% and 45% were obtained as 222%, 158% and 265%, respectively, under the lowest strain amplitude at a frequency of 10 Hz. Similar trends are also evident from the variations in the relative MR effect in view of the loss modulus ($MR_{E_L''}$) for both types of MRE with respect to PVF as shown in Figure 6.11. The $MR_{E_L''}$ of the isotropic MRE, however, is generally far more significant compared with

that of the anisotropic MRE, when PVF is increased from 15% to 45%, irrespective of the excitation frequency and the strain amplitude. The $MR_{E_L''}$ of the anisotropic MRE with PVF of 45%, however, formed an exception under the higher frequency excitation, where the MR effect is relatively greater than that of the isotropic MRE, irrespective of strain amplitude. Results also revealed maximum $MR_{E_L''}$ of 470%, 619% and 717%, respectively, for the isotropic MRE with PVF of 15%, 30% and 45%, respectively. These were generally observed under the lower strain amplitude and excitation frequency (1 Hz). The corresponding maximum $MR_{E_L''}$ for the anisotropic MRE with PVF of 15%, 30% and 45% were obtained as 349%, 292%, and 423%, respectively. These were also mostly observed under the low strain (2.5%) and low excitation frequency.

6.4 Model development for predicting the compression moduli

The compression mode properties of MREs are strongly related to many design factors such as PVF, shape factor, pre-strain, particle size and shape, and matrix properties. Among these, the PVF is the most significant factor that influences the off- as well as on-state compression mode characteristics. The performance of the MRE-based vibration isolators/absorbers is thus expected to strongly depend on the PVF of the MRE. The formulation of a model that can predict the PVF-dependent compression mode properties of MREs is thus desirable to provide essential guidance for designing devices employing MREs in the compression mode. To the best of the authors' knowledge, a PVF-dependent model has not yet been reported for estimating the dynamic compression storage and loss moduli considering a wide range of PVF, apart from the anisotropy and loading conditions. Chen and Jerram [121] reported a rheological model for predicting dynamic shear properties of MREs as a function of the PVF considering small strain amplitude and relatively low magnetic flux density. Liao et al [92] proposed a constitutive model for estimating compression properties of the anisotropic MREs under small strain and low magnetic field. The significant coupled effects of the loading conditions and the PVF, which are evident from the measured properties, however, could not be considered in these models. Koo et al. [20], and Bellelli and Spaggiari [45] developed phenomenological models to predict compression mode behavior of MREs in the static and dynamic regimes, respectively, while the PVF was taken as constant.

In this study, a simple phenomenological model is attempted for predicting the PVF-dependence of the compression mode properties of the isotropic as well as anisotropic MREs. In the absence of a magnetic field, an MRE can be considered as a passive viscoelastic medium. It has been reported that the compression modulus of filled elastomers increases with the PVF in a quadratic manner, such that:

$$E_c = E_0(1 + 2.5\varphi + 14.1\varphi^2) \tag{6-3}$$

where φ is the PVF. E_c and E_0 are the effective compression modulus and Young's modulus of filled and unfilled-rubbers, respectively [33]. The compression mode properties of the MREs, presented in Figure 6.7 through Figure 6.9, suggest that the PVF effects are strongly coupled with the mechanical loading conditions such as the strain amplitude and excitation frequency, apart from the magnetic flux density. While the compression mode properties showed strong dependence on the PVF, the elastic and loss moduli increased with increase in the magnetic flux density and the frequency. The moduli also approached saturation under higher flux density and excitation frequency. Moreover, the elastic and loss moduli decreased with increase in the strain amplitude and showed a tendency to saturate at a higher level of the strain amplitude. Owing to the observed coupled dependence of the elastic and loss moduli on the PVF, magnetic flux density, strain amplitude, and excitation frequency, the effective compression moduli of both types of the MREs may be described by independent functions in PVF, magnetic flux density and the mechanical loading (f, ε), such that:

$$E(\phi, f, \varepsilon, B) = E_0 a_0(1 + a_1\phi + a_2\phi^2)(1 - e^{-a_3 f})\,(e^{-a_4\varepsilon})\left(\frac{2}{1 + e^{-a_5 B}}\right) \tag{6-4}$$

where E represents the elastic (E') or loss (E'') modulus of the MREs, and E_0 is the Young's modulus of the matrix, taken as 0.0606 MPa [8]. The magnetic field dependence of the modulus is modeled by a fractional model in order to describe the magnetic field saturation of the MREs. The exponential functions in the mechanical loading parameters are considered such that the strain softening, rate hardening and saturation tendencies can be represented by the model. A quadratic function is considered to predict PVF dependence of the modulus on the basis of the Einstein-Guth model [33]. The proposed model, presented in Equation (6-4), is considered to be more general since it is based on the observed nonlinear phenomena for somewhat more representative constituents and shape of the MREs. The model structure is primarily motivated by the observed

physical behaviors, namely, the magnetic saturation, strain-rate stiffening and its saturation, and the strain softening. These phenomena are observed for the more representative MREs with widely used primary constituents, namely, the magnetically soft CIP and a highly compliant platinum-based silicone elastomer (Eco-Flex 00-20), which are known to yield relatively higher MR effect. Besides, the proposed model would provide great general guidance for designing the engineering application based on cylindrical MRE at their early design stages. Moreover, the cylindrical samples used in the study are better-suited for the compression mode applications due to their compact design, superior stiffness, and potential for omni-directional vibration isolation. The proposed model is considered to be simple since it involves identifications of only six unknown constants, a_0 to a_5, for each type of MRE. The model structure involves individual functions to describe the dependence of the moduli on the PVF, loading frequency, strain amplitude and the flux density. The model could thus be easily reduced when the effects of one or more of these factors is of lesser significance for a given application. These constants are identified through minimization of the error function, *J*, between the model-predicted and measured moduli over the ranges of the PVF, and mechanical and magnetic loading conditions, as:

$$J(a_1,..,a_6) = \sum_{i=1}^{M}\sum_{j=1}^{N}\sum_{k=1}^{O}\sum_{l=1}^{P}\Big(E(\varphi,f,\varepsilon,B) - E_{exp}(\varphi,f,\varepsilon,B)\Big)^2 \tag{6-5}$$

where E_{exp} is elastic or loss modulus obtained from the measured data, and indices *i*, *j*, *k* and *l* represent the measured or simulation outcomes corresponding to specific values of the PVF, magnetic flux density, strain amplitude and loading frequency, respectively.

Table 6.1 Identified coefficients of the presented simple phenomenological model for estimating the elastic and loss moduli of the isotropic and anisotropic MREs.

Constant	a_0	a_1	a_2	a_3	a_4	a_5
Isotropic MRE						
E'	41.09	-8.61	27.67	0.79	14.03	3.70
E''	16.67	-10.14	31.98	1.65	10.87	4.25
Anisotropic MRE						
E'	23.60	-6.31	25.86	1.71	11.12	4.00
E''	17.00	-9.14	30.49	2.37	11.11	4.32

Constants M, N, O and P represent the number of discrete input factors considered in the error function, namely, PVF, magnetic flux density, strain amplitude and frequency, which were taken as 3, 4, 4, and 6, respectively. The error minimization problem was solved by successive employment of the Genetic algorithm (GA) and the nonlinear Sequential Quadratic Programming (SQP) technique in order to obtain accurate convergence to global minima. Repeated solutions were also obtained for different initial values of the coefficients, which converged to nearly identical solutions. The identified coefficients for the elastic and loss modulus models for both the anisotropic and isotropic MREs are presented in Table 6.1.

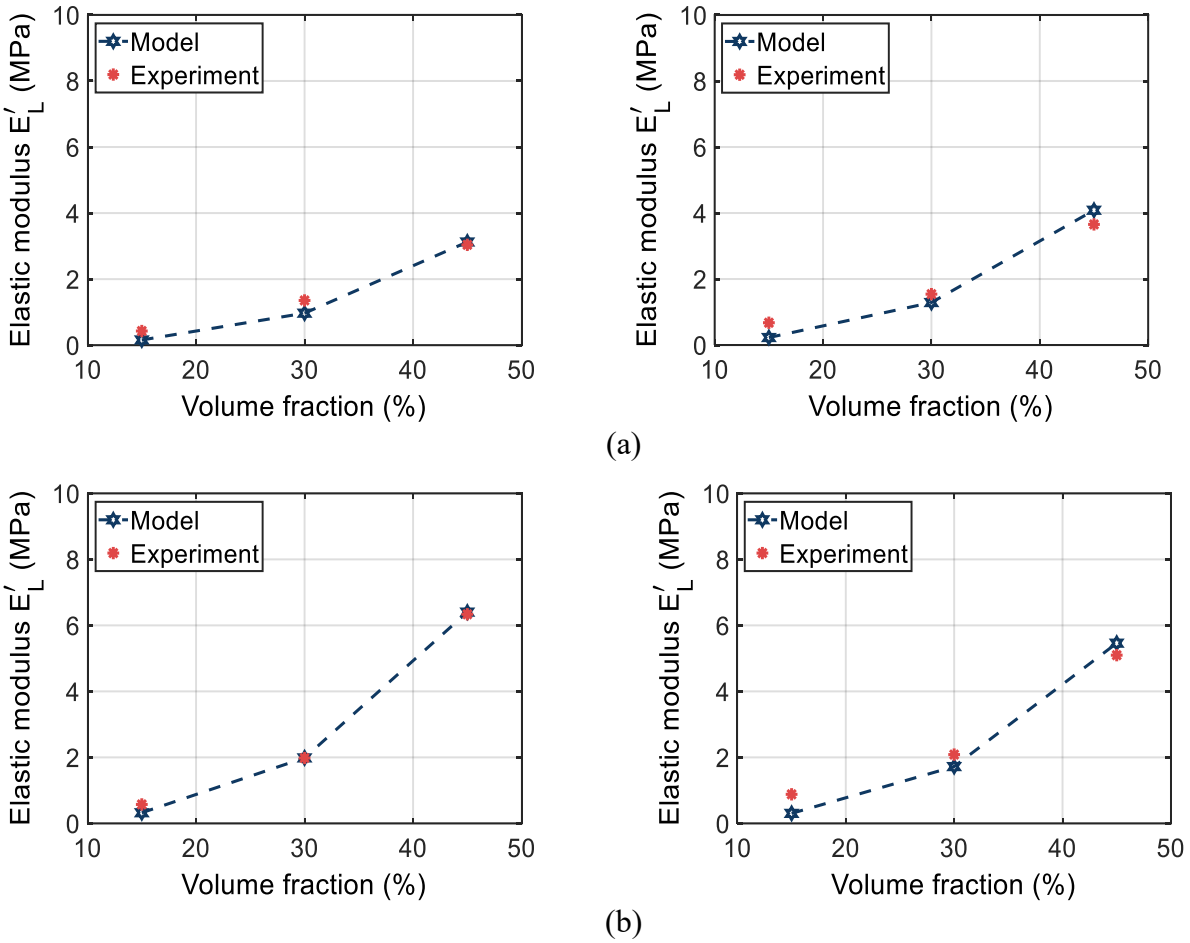

Figure 6.12 Comparisons of the volume fraction dependent compression elastic moduli of the isotropic (left column) and anisotropic (right column) MREs predicted from the proposed model with the measured data under (a) B=450 mT, f=1 Hz, ε=5%, and (b) B=750 mT, f=10 Hz, ε=5%.

The effectiveness of the proposed models is scrutinized by comparing the model-predicted moduli with the experimental data under different mechanical loading and magnetic flux inputs. As an example, Figure

6.12 presents comparisons of the model-predicted and measured elastic moduli, of the anisotropic and isotropic MREs as functions of the PVF, and two different loading conditions (B=450 mT, f=1 Hz, ε=5%; and B=750 mT, f=10 Hz, ε=5%). The model-predicted loss moduli of both types of MRE are also compared with the measured values in Figure 6.13 for the same loading conditions. The comparisons suggest that the proposed simple phenomenological model can provide effective estimates of the elastic and loss moduli of both types of MREs for the entire range of the PVF considered in the study. Moreover, the model can also describe the coupled effects of PVF and the mechanical and magnetic loading conditions with only six constants. Similar degree of agreements between the model-predicted and measured data were also observed under other input conditions, considered in the study.

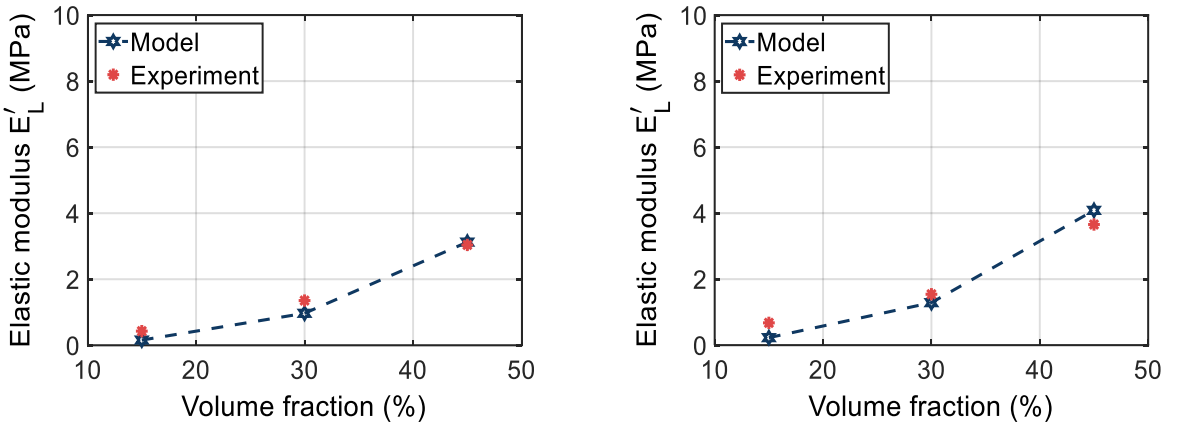

(a)

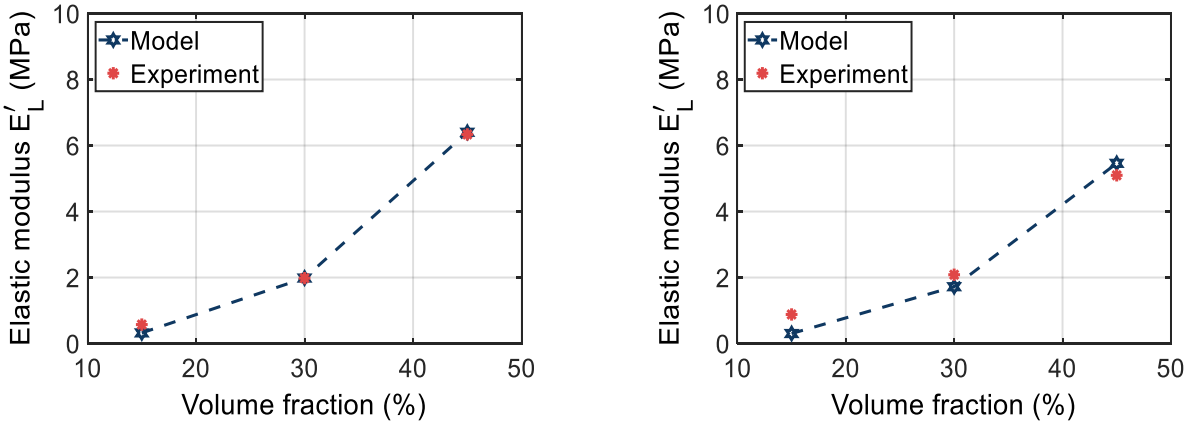

(b)

Figure 6.13 Comparisons of the volume fraction dependent compression elastic moduli of the isotropic (left column) and anisotropic (right column) MREs predicted from the proposed model with the measured data under (a) B=450 mT, f=1 Hz, ε=5%, and (b) B=750 mT, f=10 Hz, ε=5%.

6.5 Conclusion

The present study experimentally investigated the particle volume fraction (PVF) dependence of the compression mode properties of the anisotropic and isotropic MREs under wide ranges of magnetic flux density, strain amplitude and loading frequency. Results showed that the elastic and loss moduli of both types of MREs generally increase with increase in PVF in a nonlinear manner. The effect of PVF on the loss modulus of both types of MREs was more pronounced than on the elastic modulus. Results were generally suggestive of greater PVF-stiffening and PVF-dampening of the isotropic MRE compared to the anisotropic MRE. The PVF-dependent stiffening and dampening effects were also observed to be strongly coupled with those caused by variations in the strain amplitude, loading frequency and the magnetic flux density. The PVF-stiffening and PVF-dampening of both types of MREs consistently decreased with increase in the strain amplitude, which was more noticeable for the isotropic MRE in comparison with the anisotropic MRE. Both PVF effects of the anisotropic MRE consistently decreased with increase in excitation frequency, while the PVF-stiffening of the isotropic MRE increased with the frequency. Results also revealed that strain-rate stiffening of isotropic MRE increased with increasing PVF while slightly decreased for anisotropic MRE, whereas strain-softening of both MREs increased with increasing PVF. Results were also suggesting of strong dependence of MR effect on the loading conditions, apart from the PVF. MR effect in view of elastic ($MR_{E_L'}$) and loss ($MR_{E_L''}$) moduli for the isotropic MRE increased with increasing PVF from 15% to 45% at 1 Hz, but at higher frequency they become maximum around 30% PVF, regardless of strain amplitude. Both MR effects for the anisotropic MRE, however, become minimum around 30% PVF, irrespective of loading conditions. Results also suggested that isotropic MREs with 45% and 30% PVF may be considered better suited for designing MRE-based devices subject to low (≈1 Hz) and high (≈10 Hz) frequency excitations, respectively. The anisotropic MREs with 45% PVF are better suited for applications involving relatively higher payloads, and low amplitude deformation at a higher frequency (≈10 Hz), where relatively higher MR effect in terms of the elastic modulus is desirable. A simple phenomenological model with only six constants was subsequently proposed for predicting compression elastic and loss moduli, which showed a reasonably good agreements with the moduli obtained from the measured data for the entire ranges of PVF, magnetic flux density, strain amplitude and excitation frequency considered in the study. The proposed model could serve

as an efficient tool for designing MRE-based devices, particularly when the large natural frequency shift and/or energy dissipation properties are of concern.

CHAPTER 7
CONCLUSIONS AND RECOMMENDATIONS

7.1 Major contributions

This dissertation presents a systematic study of compression mode characteristics of MREs and the role of essential design factors on the properties of the MRE composites. These included the pre-strain, shape factor, anisotropy and volume fraction of magnetic particles. The roles of selected design factors are analyzed and thoroughly discussed, which would provide essential design guidance for MRE-based vibration control devices. Phenomenological models are further proposed to obtain estimates of elastic and loss moduli of the MRE as functions of the selected design parameters. The major contributions of the dissertation research are summarized below:

- An optimal design of a UI-shaped electromagnet is proposed for compression mode magneto-mechanical measurements of MREs with minimal mass and maximal flux density capacity of 1T.

- A methodology is formulated for compensation for the dynamic magnetic force developed during harmonic tension/compression loading of the MRE. The force compensation strategy included the analytical and phenomenological models of the electromagnet for estimating the dynamic magnetic force as functions of the flux density and the excitation conditions.

- An experimental methodology is formulated for dynamic characterization of isotropic and anisotropic MREs in compression mode under relatively large pre-load (pre-strain) and broad ranges of excitations. The experiment design integrating the electromagnet was employed for investigating the effects of shape factor (SF), pre-strain and particle volume fraction (PVF) on the stress-strain characteristics of both types of MREs.

- Simple phenomenological models are proposed for predicting the compression elastic and loss moduli of both types of MREs as functions of the design and operating factors. The effectiveness of the proposed models is demonstrated by comparing the model-predicted responses with the measured data.

7.2 Major Conclusions

The major conclusions drawn from the study are summarized below:

- The magnetic force developed by the electromagnet revealed notable phase and magnitude differences with respect to the input displacement, which varied with the magnetic flux density and the excitation frequency. Magnitude of the magnetic force is significantly larger than the viscoelastic force due to MREs, especially under higher magnetic flux. It is shown that the magnetic force contribution to the total measured force could yield peak errors in equivalent stiffness and damping of the MRE material in the orders of 90% and 163%, respectively.

- The stress-strain characteristics of the isotropic and anisotropic MREs with nominal SF of 0.56, volume fraction of 30% and pre-strain of 21% showed nonlinear and asymmetric hysteresis behavior, which was more pronounced under higher strain amplitude and higher magnetic flux density. The stress-strain characteristics revealed strongly nonlinear dependency on the strain amplitude and the strain rate, apart from the anisotropy and the magnetic flux density.

- Compression mode properties, invariably, revealed strain amplitude softening of the MREs, which was more pronounced for the anisotropic MRE. The compression elastic moduli of both types of MREs generally increased in an exponential manner with increasing frequency and magnetic flux density while decreased exponentially with increase in the strain amplitude.

- The results also revealed saturation of the compression elastic modulus, loss factor and the relative MR effect as the magnetic flux density and excitation frequency approached 600 mT and 20 Hz, respectively. The anisotropy, however, revealed saturation at relatively lower levels of the magnetic flux density. The anisotropy resulted in relatively higher loss factor and elastic modulus when compared to those for the isotropic MRE, irrespective of the excitation frequency and magnetic flux density.

- The compression elastic and loss moduli of both types of the MREs together with relative MR effect in view of both elastic ($MR_{\acute{E}}$) and loss modulus ($MR_{E''}$) or loss factor (MR_{η}), were observed to be strongly dependent on the SF, pre-strain and the particle volume fraction

(PVF), which were further coupled with the effects of the strain amplitude and frequency, and the magnetic field. The elastic and loss moduli of both MREs generally increased in a nonlinear manner with increase in SF, pre-strain and PVF, irrespective of the loading conditions and the magnetic flux density. The variation in compression elastic and loss moduli of anisotropic MRE with respect to pre-strain, however, showed dissimilar trends depending on particle volume fraction.

- The SF (shape factor)-stiffening effect was limited in the presence of anisotropy, strain-softening, and strain-rate-stiffening of the MREs. The maximum SF-stiffening effect was greater for the anisotropic MRE compared to the isotropic MRE, while the peak SF effect on the loss factor was greater for the isotropic MRE, when SF was increased from 0.375 to 0.75. Increasing SF from 0.375 to 0.56 consistently resulted in substantially higher $MR_{\dot{E}}$ for the isotropic MRE.

- The pre-strain-stiffening effect was also limited with anisotropy, and strain-rate-stiffening of the MREs. Results revealed higher pre-strain effects for isotropic MREs than anisotropic MREs. The relative MR effect in view of elastic modulus ($MR_{\dot{E}}$) for both types of MREs consistently decreased with increasing pre-strain, regardless of PVF, while in view of loss factor (MR_{η}) showed the same trend only for anisotropic MRE. MR_{η} of isotropic MRE generally showed maximum around 11% pre-strain

- Relatively lower effects of particle volume fraction (PVF) were evident under higher strain amplitude for both types of MREs. An increase in PVF showed more pronounced effect on the loss modulus of both types of MREs compared to than on the elastic modulus. Results were generally suggestive of greater PVF effects for the isotropic MRE compared to the anisotropic MRE. Results also showed consistent reductions in the PVF effects for the anisotropic MRE with increase in excitation frequency from 1 Hz to 10 Hz, while the PVF-stiffening of the isotropic MRE increased with increasing excitation frequency.

- Results revealed that strain-rate stiffening of isotropic MRE increased with increasing PVF while slightly decreased for anisotropic MRE. Besides, strain-softening of both MREs increased with increasing PVF.

- Increasing the SF showed comparable increases in the stiffening and dampening behaviours of the MREs, while increasing both pre-strain and PVF resulted in relatively greater dampening effects than stiffening effects. The effects of PVF on compression moduli of both types of MREs were greater than that of SF, and pre-strain effects.

- MR effects of both MREs strongly depend on frequency, strain amplitude and pre-strain. Under large pre-strain of 21%, both the $MR_{\acute{E}}$ and MR_{η} for isotropic MRE continuously increased with increasing PVF from 15% to 45% at 1 Hz, while at 10 Hz they become maximum around 30% PVF, regardless of strain amplitude. These effects for anisotropic, however, become minimum around 30% PVF, irrespective of frequency, and amplitude.

- The 15% anisotropic MRE revealed higher $MR_{\acute{E}}$ and MR_{η} compared to isotropic MRE, regardless of pre-strain, amplitude and loading frequency. The anisotropic MRE with PVF of 45% also showed higher $MR_{\acute{E}}$ compared to isotropic MRE when pre-strain and frequency exceed 6%, 1 Hz, respectively. The 30% isotropic MRE, however, showed higher $MR_{\acute{E}}$ compared to anisotropic MRE, irrespective of pre-strain, SF amplitude, and frequency.

- Results suggested that isotropic MREs with 30% and 45% PVF may be considered better suited for applications involving high (≈10 Hz) and low (≈1 Hz) frequency excitations, respectively. The anisotropic MREs with 45% PVF are better suited for applications involving relatively higher payloads, low amplitude deformation at a higher frequency (≈10 Hz), where relatively higher MR effect in terms of the elastic modulus is desirable.

- Results revealed that the anisotropic MREs are relatively superior compared to the isotropic MRE for designing MRE-based vibration absorbers, requiring higher payloads with an attempt to track single resonant frequency, where quite lower MR_{η} is desirable.

- The proposed models are very practical and beneficial for design and development of highly adjustable MRE-based devices, operating in compression mode.

7.3 Recommendations for future works

This dissertation established a comprehensive framework for compression mode characterizations of isotropic and anisotropic MREs together with the effects of key design and operating factors. Furthermore, simple phenomenological models are proposed for predicting complex properties of MREs as functions of the design and operating factors, which may serve as important design tools for developing MRE-based smart adaptive structures, vibration isolators and vibration absorbers. More efforts, however, are desirable for assessing the effects of properties of magnetic particles and developing generally applicable models of the MREs. Some of the desirable further studies are listed below:

- The compression as well as shear properties of MREs are dependent upon the properties of the magnetic particles. Further efforts are recommended for assessing the effects of particles' size and their magnetic property (soft and hard) on shear and compression characteristics of MREs, which may provide essential knowledge for designing alternate more effective MREs.

- The efforts on MREs are currently limited to DC magnetic field stimulus. It would be desirable to study the magneto-mechanical properties of MREs under exposure to an AC magnetic field, which is expected to enhance the particle-particle and particle-matrix interactions.

- Despite the importance effect of the operating temperature on the viscoelastic properties of the MREs, the temperature effects on compression mode properties of MREs have been addressed in only a few studies. It would be desirable to study the effects of operating temperature on the compression mode properties. This would provide knowledge for designing MRE-based devices operating in adverse temperature conditions.

- Realization of the controllable magnetic field via small size electromagnets continues to be the primary challenge for developing effective MR-based devices. Further efforts are strongly recommended to explore alternate designs of compact electromagnets or an aggregate of micro-sized electromagnets.

- Further efforts in developing effective and generally applicable models of the MREs are most desirable. Strain amplitude-, strain rate- and magnetic flux density-dependent

hysteresis models such as Prandtl-Ishlinskii model may be attempted, which could be conveniently applied for controller synthesis and design.

- MREs offer attractive potentials for developing semi-active/active noise and vibration control systems. Considering that the MR effect of MREs is substantially greater in the compression mode compared to the shear mode, the efforts in developing such devices involving compression/tension of the MREs are strongly recommended.

- Investigating the important and practical design requirements for a MREs-based automotive engine mount in order to quantitatively assess its dynamic behavior, thereby improving the state of the MRE technology.

- Identifying phenomenological models' parameters considering the uncertainty due to complex dependence of MRE behavior on many aspects such as loading factors (amplitude, and frequency) and design factors, including pre-strain, as well as type, size and distribution of iron particles, and also PVF, and SF of the MRE samples.

REFERENCES

[1] Rigbi Z, Jilkén L. The response of an elastomer filled with soft ferrite to mechanical and magnetic influences. *Journal of Magnetism and Magnetic Materials*. 1983;37(**3**):267-76.

[2] Ginder JM, Nichols ME, Elie LD, Clark SM. Controllable-stiffness components based on magnetorheological elastomers. *Proc. SPIE*. 2000;3985:418-25.

[3] Cesmeci S, Gordaninejad F, Ryan KL, Eltahawy W. Design of a fail-safe magnetorheological-based system for three-dimensional earthquake isolation of structures. *Mechatronics*. 2019;64:102296.

[4] Lerner AA, Cunefare KA. Performance of MRE-based Vibration Absorbers. *Journal of Intelligent Material Systems and Structures*. 2007;19(**5**):551-63.

[5] Dargahi A, Sedaghati R, Rakheja S. On the properties of magnetorheological elastomers in shear mode: Design, fabrication and characterization. *Composites Part B: Engineering*. 2019;159:269-83.

[6] Kallio M, Lindroos T, Aalto S, Järvinen E, Kärnä T, Meinander T. Dynamic compression testing of a tunable spring element consisting of a magnetorheological elastomer. *Smart Materials and Structures*. 2007;16(**2**):506-14.

[7] Norouzi M, Sajjadi Alehashem SM, Vatandoost H, Ni YQ, Shahmardan MM. A new approach for modeling of magnetorheological elastomers. *Journal of Intelligent Material Systems and Structures*. 2016;27(**8**):1121-35.

[8] Asadi Khanouki M, Sedaghati R, Hemmatian M. Experimental characterization and microscale modeling of isotropic and anisotropic magnetorheological elastomers. *Composites Part B: Engineering*. 2019;176:107311.

[9] Vatandoost H, Hemmatian M, Sedaghati R, Rakheja S. Dynamic characterization of isotropic and anisotropic magnetorheological elastomers in the oscillatory squeeze mode superimposed on large static pre-strain. *Composites Part B: Engineering*. 2020;182:107648.

[10] Kallio M. The elastic and damping properties of magnetorheological elastomers Ph.D. thesis Finland: Tampere University of Technology; 2005.

[11] Gong XL, Zhang XZ, Zhang PQ. Fabrication and characterization of isotropic magnetorheological elastomers. *Polymer Testing*. 2005;24(**5**):669-76.

[12] Chen L, Gong XL, Li WH. Effect of carbon black on the mechanical performances of magnetorheological elastomers. *Polymer Testing*. 2008;27(**3**):340-5.

[13] Padalka O, Song HJ, Wereley NM, Filer Ii JA, Bell RC. Stiffness and Damping in Fe, Co, and Ni Nanowire-Based Magnetorheological Elastomeric Composites. *IEEE Transactions on Magnetics*. 2010;46(**6**):2275-7.

[14] Xin F-L, Bai X-X, Qian L-J. Modeling and experimental verification of frequency-, amplitude-, and magneto-dependent viscoelasticity of magnetorheological elastomers. *Smart Materials and Structures*. 2016;25(**10**):105002.

[15] Lokander M, Stenberg B. Improving the magnetorheological effect in isotropic magnetorheological rubber materials. *Polymer Testing*. 2003;22(**6**):677-80.

[16] Eem S-H, Jung H-J, Koo J-H. Modeling of magneto-rheological elastomers for harmonic shear deformation. *IEEE Transactions on Magnetics*. 2012;48(**11**):3080-3.

[17] Gordaninejad F, Wang X, Mysore P. Behavior of thick magnetorheological elastomers. *Journal of Intelligent Material Systems and Structures*. 2012;23(**9**):1033-9.

[18] Schubert G, Harrison P. Large-strain behaviour of Magneto-Rheological Elastomers tested under uniaxial compression and tension, and pure shear deformations. *Polymer Testing*. 2015.

[19] Norouzi M, Gilani M, Alehashem SMS, Vatandoost H. Dynamic Characterization and Modeling of Isotropic Magnetorheological Elastomers Under Tensile-Compressive Loadings. *IEEE Transactions on Magnetics*. 2017;53(**9**):1-12.
[20] Koo J-H, Khan F, Jang D-D, Jung H-J. Dynamic characterization and modeling of magneto-rheological elastomers under compressive loadings. *Smart Materials and Structures*. 2010;19(**11**):117002.
[21] Vatandoost H, Norouzi M, Alehashem SMS, Smoukov SK. A novel phenomenological model for dynamic behavior of magnetorheological elastomers in tension–compression mode. *Smart Materials and Structures*. 2017;26(**6**):065011.
[22] Vatandoost H, Alehashem SMS, Norouzi M, Taghavifar H, Ni Y. A Supervised Artificial Neural Network-Assisted Modeling of Magnetorheological Elastomers in Tension–Compression Mode. *IEEE Transactions on Magnetics*. 2019;55(**12**):1-8.
[23] Li R, Sun LZ. Viscoelastic Responses of Silicone-Rubber-Based Magnetorheological Elastomers Under Compressive and Shear Loadings. *Journal of Engineering Materials and Technology*. 2013;135(**2**):021008.
[24] Zhou GY, Li JR. Dynamic behavior of a magnetorheological elastomer under uniaxial deformation: I. Experiment. *Smart Materials and Structures*. 2003;12(**6**):859.
[25] Farshad M, Le Roux M. Compression properties of magnetostrictive polymer composite gels. *Polymer Testing*. 2005;24(**2**):163-8.
[26] Lee JY, Kumar V, Lee DJ. Compressive properties of magnetorheological elastomer with different magnetic fields and types of filler. *Polymers for Advanced Technologies*. 2019;30(**4**):1106-15.
[27] Agirre-Olabide I, Elejabarrieta MJ. A new magneto-dynamic compression technique for magnetorheological elastomers at high frequencies. *Polymer Testing*. 2018;66:114-21.
[28] Bastola AK, Li L, Paudel M. A hybrid magnetorheological elastomer developed by encapsulation of magnetorheological fluid. *Journal of Materials Science*. 2018;53(**9**):7004-16.
[29] Pössinger T. Experimental Characterization, Modeling and Simulation of Magneto-Rheological Elastomers Ph.D. thesis: Ecole Polytechnique; 2015.
[30] Shi X, Liu S, Zhao D, Zhao Z, Cui J, Wang F. Effect of Electromagnetic Force on Dynamic Mechanical Properties of the Magnetorheological Elastomer Under Compression Mode. *Journal of Engineering Materials and Technology*. 2019;142(**2**).
[31] Al-Anany YM, Tait MJ. Experimental assessment of utilizing fiber reinforced elastomeric isolators as bearings for bridge applications. *Composites Part B: Engineering*. 2017;114:373-85.
[32] Thorin A, Azoug A, Constantinescu A. Influence of prestrain on mechanical properties of highly-filled elastomers: Measurements and modeling. *Polymer Testing*. 2012;31(**8**):978-86.
[33] Guth E. Theory of filler reinforcement. *Journal of Applied Physics*. 1945;16(**1**):20-5.
[34] Smallwood HM. Limiting law of the reinforcement of rubber. *Journal of Applied Physics*. 1944;15(**11**):758-66.
[35] Diguet G. Huge Magnetostriction of magneto-rheological composite Ph.D. thesis: University of Grenoble; 2010.
[36] Kalina KA, Metsch P, Kästner M. Microscale modeling and simulation of magnetorheological elastomers at finite strains: a study on the influence of mechanical preloads. *International Journal of Solids and Structures*. 2016;102:286-96.
[37] Kim I, Bae S, Kim J. Composition effect on high frequency properties of carbonyl-iron composites. *Materials Letters*. 2008;62(**17-18**):3043-6.

[38] Schrittesser B, Major Z, Filipcsei G. Characterization of the dynamic mechanical behavior of magneto – elastomers. *Journal of Physics: Conference Series*. 2009;149:012096.
[39] Ubaidillah U, Mazlan SA, Sutrisno J, Yahya I, Imaduddin F. Physicochemical Properties and Stress-Strain Compression Behaviors of a Waste based Magnetorheological Elastomers. *Scientia Iranica*. 2016;23(**3**):1144-59.
[40] Sapouna K. Modelling, characterization and development of new magnetorheological elastomers with enhanced vibration control performance Ph.D. thesis: University of Southampton; 2018.
[41] Oguro T, Endo H, Kikuchi T, Kawai M, Mitsumata T. Magnetic field gradient and sample size effect on magnetomechanical response for magnetic elastomers. *Reactive and Functional Polymers*. 2017;117:25-33.
[42] Oguro T, Sasaki S, Tsujiei Y, Kawai M, Mitsumata T, Kaneko T, et al. Sample size effect of magnetomechanical response for magnetic elastomers by using permanent magnets. *Journal of Nanomaterials*. 2017;2017.
[43] Ivaneyko D, Toshchevikov V, Saphiannikova M, Heinrich G. Mechanical properties of magneto-sensitive elastomers: unification of the continuum-mechanics and microscopic theoretical approaches. *Soft Matter*. 2014;10(**13**):2213-25.
[44] Martins A, Fereidooni A, Suleman A, Wickramasinghe VK. Test rig development and characterization of magnetorheological elastomers. 25th AIAA/AHS Adaptive Structures Conference2017. p. 0733.
[45] Bellelli A, Spaggiari A. Magneto-mechanical characterization of magnetorheological elastomers. *Journal of Intelligent Material Systems and Structures*. 2019;30(**17**):2534-43.
[46] Bellan C, Bossis G. Field dependence of viscoelastic properties of MR elastomers. *International Journal of Modern Physics B*. 2002;16:2447-53.
[47] Boczkowska A, Awietjan SF, Wroblewski R. Microstructure–property relationships of urethane magnetorheological elastomers. *Smart Materials and Structures*. 2007;16(**5**):1924-30.
[48] Fuchs A, Zhang Q, Elkins J, Gordaninejad F, Evrensel C. Development and characterization of magnetorheological elastomers. *Journal of Applied Polymer Science*. 2007;105(**5**):2497-508.
[49] Wang YF, He L, Yu WX, Yang X. Study on the magnetorheological effect of MR elastomer under shear-compression mode. Advanced Materials Research2011. p. 3018-23.
[50] Lerner A-MA. The design and implementation of a magnetorheological silicone composite state-switched absorber M.Sc. thesis: Georgia Institute of Technology; 2005.
[51] Sudhoff SD. Power magnetic devices: a multi-objective design approach. Hoboken, NJ, USA: Wiley; 2014.
[52] Rubber, vulcanized or thermoplastic - Determination of compression stress-strain properties. ISO 7743:2017; 2017.
[53] Standard test methods for rubber property—compression Set. ASTM D395 - 16; 2016.
[54] Yeadon WH, Yeadon AW. Handbook of small electric motors: McGraw-Hill New York; 2001.
[55] Kazimierczuk MK. High-frequency magnetic components. Hoboken, NJ, USA: Wiley; 2009.
[56] Ubaidillah, Sutrisno J, Purwanto A, Mazlan SA. Recent Progress on Magnetorheological Solids: Materials, Fabrication, Testing, and Applications. *Advanced Engineering Materials*. 2015;17(**5**):563-97.
[57] Li Y, Li J, Li W, Du H. A state-of-the-art review on magnetorheological elastomer devices. *Smart Materials and Structures*. 2014;23(**12**):123001.
[58] Leo DJ. Engineering analysis of smart material systems. Hoboken, NJ, USA: Wiley; 2007.

[59] Przybyłowicz PM, Szmidt T. Electromagnetic damping of a mechanical harmonic oscillator with the effect of magnetic hysteresis. *Journal of theoretical and applied mechanics*. 2009;47(**2**):259-73.
[60] Golnaraghi MF, Nakhaie Jazar G. Development and Analysis of a Simplified Nonlinear Model of a Hydraulic Engine Mount. *Journal of Vibration and Control*. 2001;7(**4**):495-526.
[61] Sadiku MN. Elements of electromagnetics. 6 ed. Oxford, U.K.: Oxford University Press; 2014.
[62] Hane Y, Nakamura K, Ohinata T, Arimatsu K. Reluctance Network Model of Three-Phase-Laminated-Core Variable Inductor Considering Magnetic Hysteresis Behavior. *IEEE Transactions on Magnetics*. 2019;55(**7**):1-6.
[63] Duan N, Xu W, Li Y, Wang S, Guo Y, Zhu J. Comparison of Limiting Loop Model and Elemental Operator Model for Magnetic Hysteresis of Ferromagnetic Materials. *IEEE Transactions on Magnetics*. 2017;53(**11**):1-4.
[64] Aydin U, Rasilo P, Martin F, Singh D, Daniel L, Belahcen A, et al. Modeling the Effect of Multiaxial Stress on Magnetic Hysteresis of Electrical Steel Sheets: A Comparison. *IEEE Transactions on Magnetics*. 2017;53(**6**):1-4.
[65] Batdorff MA. Transient analysis of electromagnets with emphasis on solid components, eddy currents, and driving circuitry Ph.D. thesis Electrical Engineering: Purdue University; 2010.
[66] Yamazaki K, Sakamoto Y. Electromagnetic Field Analysis Considering Reaction Field Caused by Eddy Currents and Hysteresis Phenomenon in Laminated Cores. *IEEE Transactions on Magnetics*. 2018;54(**3**):1-4.
[67] Do TA, Talleb H, Gensbittel A, Ren Z. 3-D Finite Element Analysis of Magnetoelectric Composites Accounting for Material Nonlinearity and Eddy Currents. *IEEE Transactions on Magnetics*. 2019;55(**10**):1-8.
[68] Gao Y, Araki Y, Dozono H, Muramatsu K, Guan W, Yuan J, et al. Modeling of Anomalous Eddy Current Losses Due to Movement of Domain Walls in Particles of a Soft Magnetic Composite. *IEEE Transactions on Magnetics*. 2020;56(**4**):1-4.
[69] Sneller AJ, Mann BP. On the nonlinear electromagnetic coupling between a coil and an oscillating magnet. *Journal of Physics D: Applied Physics*. 2010;43(**29**):295005.
[70] Xu X, Han Q, Chu F. Review of electromagnetic vibration in electrical machines. *Energies*. 2018;11(**7**):1779.
[71] Bae J-S, Hwang J-H, Park J-S, Kwag D-G. Modeling and experiments on eddy current damping caused by a permanent magnet in a conductive tube. *Journal of Mechanical Science and Technology*. 2009;23(**11**):3024-35.
[72] Popp KM, Kroger M, Li Wh, Zhang XZ, Kosasih PB. MRE Properties under Shear and Squeeze Modes and Applications. *Journal of Intelligent Material Systems and Structures*. 2009;21(**15**):1471-7.
[73] Wan Y, Xiong Y, Zhang S. Temperature effect on viscoelastic properties of anisotropic magnetorheological elastomers under compression. *Smart Materials and Structures*. 2018;28(**1**):015005.
[74] Fuchs A, Sutrisno J, Gordaninejad F, Caglar MB, Yanming L. Surface polymerization of iron particles for magnetorheological elastomers. *Journal of Applied Polymer Science*. 2010;117(**2**):934-42.
[75] Ubaidillah, Imaduddin F, Li Y, Mazlan SA, Sutrisno J, Koga T, et al. A new class of magnetorheological elastomers based on waste tire rubber and the characterization of their properties. *Smart Materials and Structures*. 2016;25(**11**):115002.

[76] Lee JY, Kumar V, Lee DJ. Compressive properties of magnetorheological elastomer with different magnetic fields and types of filler. *Polymers for Advanced Technologies*. 2019.
[77] Gong Q, Wu J, Gong X, Fan Y, Xia H. Smart polyurethane foam with magnetic field controlled modulus and anisotropic compression property. *RSC Advances*. 2013;3(**10**):3241-8.
[78] Zhu M, Yu M, Qi S, Fu J. Investigations on response time of magnetorheological elastomer under compression mode. *Smart Materials and Structures*. 2018;27(**5**):055017.
[79] Han Y, Mohla A, Huang X, Hong W, Faidley LE. Magnetostriction and Field Stiffening of Magneto-Active Elastomers. *International Journal of Applied Mechanics*. 2015;07(**01**):1550001.
[80] W.P. Fletcher ANG. Non-linearity in the dynamic properties of vulcanised rubber compounds. *Transactions of the Institution of the Rubber*. 1953;29:266-80.
[81] Payne AR, Whittaker RE. Low Strain Dynamic Properties of Filled Rubbers. *Rubber Chemistry and Technology*. 1971;44(**2**):440-78.
[82] Wollscheid D, Lion A. Predeformation- and frequency-dependent material behaviour of filler-reinforced rubber: Experiments, constitutive modelling and parameter identification. *International Journal of Solids and Structures*. 2013;50(**9**):1217-25.
[83] Diercks N, Johlitz M, Calipel J. The dynamic mullins effect: on the influence of the Mullins effect on dynamic moduli. *Proceedings of the Institution of Mechanical Engineers, Part L: Journal of Materials: Design and Applications*. 2016;230(**3**):705-16.
[84] Schubert G, Harrison P. Large-strain behaviour of magneto-rheological elastomers tested under uniaxial compression and tension, and pure shear deformations. *Polymer Testing*. 2015;42:122-34.
[85] Ahamed R, Choi S-B, Ferdaus MM. A state of art on magneto-rheological materials and their potential applications. *Journal of Intelligent Material Systems and Structures*. 2018;29(**10**):2051-95.
[86] Jalali A, Dianati H, Norouzi M, Vatandoost H, Ghatee M. A novel bi-directional shear mode magneto-rheological elastomer vibration isolator. *Journal of Intelligent Material Systems and Structures*. 2020;31(**17**):2002-19.
[87] Rubber, vulcanized or thermoplastic - Determination of dynamic properties - Part 1: General guidance.: ISO 4664-1; 2011.
[88] Brown R. Physical testing of rubber. Springer US: Springer Science & Business Media; 2006.
[89] Kim B-K, Youn S-K. A viscoelastic constitutive model of rubber under small oscillatory load superimposed on large static deformation. *Archive of Applied Mechanics*. 2001;71(**11**):748-63.
[90] Fan Y, Gong X, Xuan S, Zhang W, Zheng J, Jiang W. Interfacial friction damping properties in magnetorheological elastomers. *Smart Materials and Structures*. 2011;20(**3**):035007.
[91] Dickens J. Phase velocity of rubber element in vibration isolator under static load. *Journal of Sound and Vibration*. 2000;234(**1**):21-42.
[92] Liao G, Gong X, Xuan S. Magnetic Field-Induced Compressive Property of Magnetorheological Elastomer under High Strain Rate. *Industrial and Engineering Chemistry Research*. 2013;52(**25**):8445-53.
[93] Guelho I. Static and dynamic behavior of Rubbercork composite materials M.Sc. thesis Mechanical Engineering: University of Lisbon; 2011.
[94] Suphadon N. The viscoelastic properties of rubber under a complex loading Ph.D. thesis: Queen Mary, University of London; 2010.
[95] Payne A. Dynamic properties of vulcanised rubber 5: shape factors and functions in rubber engineering. *Technical Report No. 84, Research Association of British Rubber Manufacturers*. 1957.

[96] Payne A. Effect of shape on the static and dynamic stress–strain relationship of bonded rubber in compression. *Nature*. 1956;177(**4521**):1174.
[97] Standard Guide for Dynamic Testing of Vulcanized Rubber and Rubber-Like Materials Using Vibratory Methods. ASTM D5992-96; 2011.
[98] Ewoldt RH, Hosoi AE, McKinley GH. New measures for characterizing nonlinear viscoelasticity in large amplitude oscillatory shear. *Journal of Rheology*. 2008;52(**6**):1427-58.
[99] Meinecke E, Maksin S. Influence of large static deformation on the dynamic properties of polymers. *Colloid and Polymer Science*. 1980;258(**5**):556-63.
[100] Fukahori Y, Hon A, Jha V, Busfield J. Modified guth–gold equation for carbon black–filled rubbers. *Rubber Chemistry and Technology*. 2013;86(**2**):218-32.
[101] Westermann S, Kreitschmann M, Pyckhout-Hintzen W, Richter D, Straube E. Strain amplification effects in polymer networks. *Physica B: Condensed Matter*. 1997;234:306-7.
[102] Klüppel M, Meier J, Dämgen M. Modelling of stress softening and filler induced hysteresis of elastomer materials. *Constitutive models for rubber IV*. 2017:171.
[103] Hao D, Li D, Liao Y. A finite viscoelastic constitutive model for filled rubber-like materials. *International Journal of Solids and Structures*. 2015.
[104] Lejon J. On the frequency, dynamic strain amplitude, prestrain, temperature and magnetic field strength dependence of magneto-sensitive elastomers Ph.D. thesis: KTH Royal Institute of Technology; 2012.
[105] Feng J, Xuan S, Liu T, Ge L, Yan L, Zhou H, et al. The prestress-dependent mechanical response of magnetorheological elastomers. *Smart Materials and Structures*. 2015;24(**8**):085032.
[106] Wereley NM, Perez C, Choi YT. Strain-dependent dynamic compressive properties of magnetorheological elastomeric foams. *AIP Advances*. 2018;8(**5**):056721.
[107] Peng L, Li Z, Luo W, Li Y. Analysis of dynamic viscoelastic properties of chloroprene rubber considering pre-strain effect. *Materials Research Express*. 2019;6(**10**):105324.
[108] Xu Z, Gong X, Liao G, Chen X. An Active-damping-compensated Magnetorheological Elastomer Adaptive Tuned Vibration Absorber. *Journal of Intelligent Material Systems and Structures*. 2010;21(**10**):1039-47.
[109] Zhang WHLXZ. Adaptive tuned dynamic vibration absorbers working with MR elastomers. *Smart Structures and Systems*. 2009;5: 517-29.
[110] Hao D, Li D, Liao Y. A finite viscoelastic constitutive model for filled rubber-like materials. *International Journal of Solids and Structures*. 2015;64:232-45.
[111] Sadeghifar M, Sedaghati R, Jomaa W, Songmene V. Finite element analysis and response surface method for robust multi-performance optimization of radial turning of hard 300M steel. *International Journal of Advanced Manufacturing Technology*. 2018;94(**5**):2457-74.
[112] Winger J, Schümann M, Kupka A, Odenbach S. Influence of the particle size on the magnetorheological effect of magnetorheological elastomers. *Journal of Magnetism and Magnetic Materials*. 2019;481:176-82.
[113] Song H, Padalka O, Wereley N, Bell R. Impact of nanowire versus spherical microparticles in magnetorheological elastomer composites. 50th AIAA/ASME/ASCE/AHS/ASC Structures, Structural Dynamics, and Materials Conference2009. p. 2118.
[114] Davis LC. Model of magnetorheological elastomers. *Journal of Applied Physics*. 1999;85(**6**):3348.
[115] Woods B, Wereley N, Hoffmaster R, Nersessian N. Manufacture of bulk magnetorheological elastomers using vacuum assisted resin transfer molding. *International Journal of Modern Physics B*. 2007;21(**28n29**):5010-7.

[116] Ewoldt RH, Hosoi AE, McKinley GH. Nonlinear viscoelastic biomaterials: meaningful characterization and engineering inspiration. *Integrative and comparative biology*. 2009;49(**1**):40-50.
[117] Ulmer J, Hess W, Chirico V. The effects of carbon black on rubber hysteresis. *Rubber Chemistry and Technology*. 1974;47(**4**):729-57.
[118] Shuib RK, Pickering KL. Investigation and modelling of damping mechanisms of magnetorheological elastomers. *Journal of Applied Polymer Science*. 2016;133(**13**).
[119] Han Y, Hong W, Faidley LE. Field-stiffening effect of magneto-rheological elastomers. *International Journal of Solids and Structures*. 2013;50(**14–15**):2281-8.
[120] Snarskii AA, Shamonin M, Yuskevich P. Effect of Magnetic-Field-Induced Restructuring on the Elastic Properties of Magnetoactive Elastomers. *Journal of Magnetism and Magnetic Materials*. 2020:167392.
[121] Chen L, Jerrams S. A rheological model of the dynamic behavior of magnetorheological elastomers. *Journal of Applied Physics*. 2011;110(**1**):013513.
[122] Farshad M, Benine A. Magnetoactive elastomer composites. *Polymer Testing*. 2004;23(**3**):347-53.
[123] Boczkowska A, Awietjan SF. Urethane Magnetorheological Elastomers - Manufacturing, Microstructure and Properties. *Solid State Phenomena*. 2009;154:107-12.
[124] Song HJ, Wereley NM, Bell RC, Planinsek JL, Filer JA. Field dependent response of magnetorheological elastomers utilizing spherical Fe particles versus Fe nanowires. *Journal of Physics: Conference Series*. 2009;149:012097.
[125] Guðmundsson Í. A Feasibility Study of Magnetorheological Elastomers for a Potential Application in Prosthetic Devices 2011.
[126] Liao G, Gong X, Xuan S, Guo C, Zong L. Magnetic-Field-Induced Normal Force of Magnetorheological Elastomer under Compression Status. *Industrial and Engineering Chemistry Research*. 2012;51(**8**):3322-8.
[127] Slawinski G, Miedzińska D, Niezgoda T, Boczkowska A. Experimental Investigations of MREs Behavior under the Cyclic Load.In: Proceedings of Solid State Phenomena Conference. Conference, Conference 2012. p. 163-8.
[128] Guðmundsson FB. Preparation and Characterization of a Prototype Magnetorheological Elastomer for Application in Prosthetic Devices M.Sc. thesis Mechanical Engineering: University of Iceland; 2015.
[129] Ding JG, Qiao Z, Zhou CC. Study on the performance of magnetorheological elastomers and engineering application. *Materials Research Innovations*. 2015;19(**S8**):S8-168-S8-73.
[130] Hiptmair F, Major Z, Hasslacher R, Hild S. Design and application of permanent magnet flux sources for mechanical testing of magnetoactive elastomers at variable field directions. *Review of Scientific Instruments*. 2015;86(**8**):085107.
[131] Samal S, Vlach J, Kavan P. Improved mechanical properties of magneto rheological elastomeric composite with isotropic iron filler distribution. *Ciência & Tecnologia dos Materiais*. 2016;28(**2**):155-61.
[132] Kukla M, Górecki J, Malujda I, Talaśka K, Tarkowski P. The Determination of Mechanical Properties of Magnetorheological Elastomers (MREs). *Procedia Engineering*. 2017;177:324-30.
[133] Borin D, Stepanov G, Dohmen E. Hybrid magnetoactive elastomer with a soft matrix and mixed powder. *Archive of Applied Mechanics*. 2018:1-13.
[134] Brancati R, Di Massa G, Pagano S. Investigation on the Mechanical Properties of MRE Compounds. *Machines*. 2019;7(**2**):36.

[135] Zhao D, Zhao Z, Dai X, Wang S, Liu S, Liu Y. Study on mechanical properties of a novel polyurethane sponge magnetorheological elastomers in compressive mode. *Materials Research Express*. 2019;6(**11**):116101.
[136] Shi X, Liu S, Zhao D, Zhao Z, Cui J, Wang F. Effect of Electromagnetic Force on Dynamic Mechanical Properties of the Magnetorheological Elastomer Under Compression Mode. *Journal of Engineering Materials and Technology*. 2020;142(**2**).

APPENDIX A

Table A1 Summary of conditions employed in studies reporting compression mode characteristics of MREs.

Authors and year	Magnetic field (Tesla) [DC/AC]	(Pre-compression%), Strain %	Frequency or rate	Zero modulus (MPa) or stiffness (N/mm)
Bellan and Bossis [46], 2002	0-0.052 DC	4-5	5 Hz	4.1 Mpa
Farshad and Benine [122], 2004	0-0.180 DC	20	1mm/min	3.5 Mpa
Farshad and Le Roux [25], 2005	0-0.44 DC	30	1mm/min	0.427 Mpa
Boczkowska et al. [47], 2007	0-0.3 DC	1	5mm/min	0.16 Mpa
Fuchs et al. [48], 2007	0-0.4 DC	0.1-8	0.5-45 Hz	4 Mpa
Kallio et al. [6], 2007	0-0.87T DC	1-10	0.5-15 Hz	920 N/mm
Schrittesser et al. [38], 2009	0-0.440 DC	0.08-20	0.1-100	NR
Boczkowska and Awietjan [123], 2009	0-0.3 DC	0.1-45	5mm/min	NR
Popp et al. [72], 2009	0-0.155 DC	NR	48-85 Hz	0.182 Mpa
Song et al. [124], 2009	0-0.2 DC	1	1-20 Hz	0.2 Mpa
Fuchs et al. [74], 2010	0-0.62 DC	20	NR	NR
Koo et al. [20], 2010	0-0.6 DC	(5), 5	0.1-1 Hz	3 Mpa
Guðmundsson [125], 2011	0-0.56 DC	1-15	Static	5.9 Mpa
Gordaninejad et al. [17], 2012	0-1.6 DC	20	Static	0.67 Mpa
Liao et al. [126], 2012	0-1.1 DC	1-5	NR	NR
Slawinski et al. [127], 2012	0-0.3T DC	10-25	1	1 Mpa
Li and Sun [23], 2013	0-0.1T DC	0.5-5	0.1-100 Hz	2.6 Mpa
Gong et al. [77], 2013	0-1T DC	25	10mm/min	NR
Liao et al. [92], 2013	0-0.4 DC	1-14	3200-5600 Hz	4.09 Mpa

Authors and year	Magnetic field (Tesla) [DC/AC]	(Pre-compression%), Strain %	Frequency or rate	Zero modulus (MPa) or stiffness (N/mm)
Guðmundsson [128], 2015	0-0.7 DC	50	Static	4.66 Mpa
Schubert and Harrison [84], 2015	0-0.450T DC	50	10mm/min	2.05 Mpa
Ding et al. [129], 2015	0-0.8 DC	NR	1-10 Hz	0.35 Mpa
Hiptmair et al. [130], 2015	0-0.435 DC	1	0.1-25 Hz	0.208 Mpa
Samal et al. [131], 2016	0-0.5T DC	1.175	50 Hz	289 N/mm
Ubaidillah et al. [75], 2016	0-1.77T DC	20	1-16 Hz	3-23 Mpa
Ubaidillah et al. [39], 2016	0-2.4T DC	[1-10	1 Hz	6 Mpa
Kukla et al. [132], 2017	0-0.127 DC	10	0.04-0.5 Hz	3.9 Mpa
Martins et al. [44], 2017	0-0.6T DC	(6.5), 1.5	1-10 Hz	4000 N/mm
Vatandoost et al. [21], 2017	0-0.260 DC	(0), 2-14	[0.1-8 Hz	0.25 Mpa
Oguro et al. [42], 2017	0-420 DC	20	mm/min	0.441 MPa
Sapouna [40], 2018	0-0.5 DC	(2-10), 0.25-2	5 Hz	12 Mpa
Zhu et al. [78], 2018	NR	0.01-10	Static	NR
Agirre-Olabide and Elejabarrieta [27], 2018	0-0.085 DC	0.1-0.7	50-200 Hz	NR
Borin et al. [133], 2018	0-0.240	5	0.5	0.11-0.12 Mpa
Wan et al. [73], 2018	0-0.5 DC	1	1-60 Hz	23.5 Mpa
Bellelli and Spaggiari [45], 2019	0-0.2 DC	5-10	1 mm/min	4.1 Mpa
Lee et al. [26], 2019	0-0.3 DC	(3-18), up to 20	1 mm/minute	1 Mpa
Brancati [134], 2019	0-0.74 DC	up to 16.66	0.6 mm/min	600 N/mm
Zhao [135], 2019	NR	10	1-7 Hz	0.33 Mpa
Shi [136], 2020	0-1 DC	[8-10	1-5 Hz	510 N/mm

Table A2 Iron particles concentration, and shape factor of the MRE samples fabricated in reported studies of compression mode characteristics of MREs.

Authors and year	Shape factor $SF = \frac{D}{4h}$	Relative MR effect (%)	Particle Size(μm), Soft or Hard, fraction%	Isotropic/ Anisotropic
Bellan and Bossis [46], 2002	0.19	100	2, soft, 5-30 v	Both types
Farshad and Benine [122], 2004	0.25	20	3.8, soft, 27 v	Anisotropic
Farshad and Le Roux [25], 2005	0.25	101	3.8, soft, 80 w	Isotropic
Boczkowska et al. [47], 2007	0.2	100	6-9, soft, 1.5-33 w	Both types
Fuchs et al. [48], 2007	0.1875	500	3-7, soft, 50-70 w	Both types
Kallio et al. [6], 2007	0.625	11	3-5, soft, 30 v	Both types
Schrittesser et al. [38], 2009	0.25,1.04,1.56	35	4-8, soft, 10-30 w	Both types
Boczkowska and Awietjan [123], 2009	0.2	20	6-9, soft, 1.5-33 v	Both types
Popp et al. [72], 2009	0.83	77	5, soft, 60 w	Anisotropic
Song et al. [124], 2009	0.09	1170	6-10, soft, 10-70 w	Anisotropic
Fuchs et al. [74], 2010	5	17	3-7, soft, 70 w	Anisotropic
Koo et al. [20], 2010	0.5	35-38	10, soft, 30 v	Isotropic
Guðmundsson [125], 2011	0.31	25	7-9.5, soft, 27 v	Anisotropic
Gordaninejad et al. [17], 2012	0.375, 0.5, 0.75, 1.5	99	2-8, soft, 30-70 w	Anisotropic
Liao et al. [126], 2012	2.5	NR	6, soft, 80 w	Both types
Slawinski et al. [127], 2012	0.2	20	9, soft, 11.5 v	Both types
Li and Sun [23], 2013	0.26	10-15	15, soft, 10-30 v	Anisotropic
Gong et al. [77], 2013	0.25	NR	2-9, soft, 60-80 w	Both types
Liao et al. [92], 2013	2	22.7	2-9 soft, 60-80 w	Anisotropic
Guðmundsson [128], 2015	0.31	55	2-25, soft, 27 v	Both types

Authors and year	Shape factor $SF = \frac{D}{4h}$	Relative MR effect (%)	Particle Size(μm), Soft or Hard, fraction%	Isotropic/ Anisotropic
Schubert and Harrison [84], 2015	0.58	111	3.7-4.7, soft, 0-30 v	Both types
Ding et al. [129], 2015	NR	270	5, soft, 27 v	Anisotropic
Hiptmair et al. [130], 2015	0.1875	800	5, soft, 11.5 v	Both types
Samal et al. [131], 2016	0.25	12	50-150, soft, 30 v	Both types
Ubaidillah et al. [75], 2016	0.71	9-15	0.5-25, soft, 10-40 w	Isotropic
Ubaidillah et al. [39], 2016	0.75,1,1.5,3	15	0.5-25, soft, 10-40 w	Isotropic
Kukla et al. [132], 2017	0.25	24.6	6-9, soft, 33 v	Both types
Martins et al. [44], 2017	1.5	10	NR, soft, 30 v	Anisotropic
Vatandoost et al. [21], 2017	0.66	170	3-5, soft, 70 w	Isotropic
Oguro et al. [42], 2017	0.375, 0.5, 0.75, 1.5	50	7, soft, 28 w	Isotropic
Sapouna [40], 2018	0.34,0.56,1.17	35	(6, 220), soft, 30 v	Both types
Zhu et al. [78], 2018	2.5	NR	1-8, soft, 70 w	Both types
Agirre-Olabide and Elejabarrieta [27], 2018	0.25	8	1.25, soft, 0-30 v	Isotropic
Borin et al. [133], 2018	1.5	200	5, 35-55, soft-hard, overall: 40% v	Isotropic
Wan et al. [73], 2018	NR	33	5-9, soft, 30 v	Anisotropic
Bellelli and Spaggiari [45], 2019	1	16	45, soft, 20-80 w	Both types
Lee et al. [26], 2019	0.5	45	3-10, soft, 29-44 w	Anisotropic
Brancati [134], 2019	2.08	82	4-6, soft, 25 v	Anisotropic
Zhao [135], 2019	NR	36	8, soft, 20 v	Anisotropic
Shi [136], 2020	1	50	3-5, soft, 30 v	Anisotropic

NR - Not reported

APPENDIX B

Table B1 Specific data of the linear slope of the major axis and the area bounded by the stress-strain hysteresis characteristics of the isotropic and anisotropic MREs with particle volume fraction of 15% considering three level of static pre-strain.

	(B=0 mT)											
Frequency	Linear Slope of Major Axis (MPa)						Area Bounded by Hysteresis Loop (kN.m/m3 or KPa)					
	Isotropic			Anisotropic			Isotropic			Anisotropic		
	ε_p=6%	ε_p=11%	ε_p=21%	ε_p=6%	ε_p=11%	ε_p=21%	ε_p=6%	ε_p=11%	ε_p=21%	ε_p=6%	ε_p=11%	ε_p=21%
1 Hz	0.18	0.20	0.27	0.32	0.30	0.37	0.04	0.06	0.10	0.17	0.19	0.21
10 Hz	0.21	0.24	0.32	0.38	0.38	0.46	0.10	0.11	0.17	0.26	0.28	0.33
20 Hz	-	-	-	0.37	0.39	0.47	-	-	-	0.26	0.34	0.35
30 Hz	0.24	0.26	0.36	0.38	0.39	0.49	0.15	0.13	0.22	0.24	0.29	0.35
	(B=150 mT)											
	Isotropic			Anisotropic			Isotropic			Anisotropic		
	ε_p=6%	ε_p=11%	ε_p=21%	ε_p=6%	ε_p=11%	ε_p=21%	ε_p=6%	ε_p=11%	ε_p=21%	ε_p=6%	ε_p=11%	ε_p=21%
1 Hz	0.24	0.26	0.31	0.59	0.55	0.53	0.08	0.09	0.05	0.58	0.50	0.32
10 Hz	0.58	0.59	0.70	1.00	0.93	0.94	0.11	0.25	0.03	0.72	0.30	0.36
20 Hz	-	-	-	1.05	0.87	0.91	-	-	-	0.60	0.30	0.38
30 Hz	0.63	0.70	0.79	1.01	1.07	1.02	0.29	0.07	0.04	0.30	0.48	0.41
	(B=300 mT)											
	Isotropic			Anisotropic			Isotropic			Anisotropic		
	ε_p=6%	ε_p=11%	ε_p=21%	ε_p=6%	ε_p=11%	ε_p=21%	ε_p=6%	ε_p=11%	ε_p=21%	ε_p=6%	ε_p=11%	ε_p=21%
1 Hz	0.30	0.35	0.43	0.88	0.79	0.72	0.09	0.20	0.22	0.85	0.83	0.55
10 Hz	0.68	0.75	0.87	1.30	1.24	1.16	0.02	0.26	0.34	0.91	1.01	0.81
20 Hz	-	-	-	1.20	1.30	1.10	-	-	-	0.68	0.73	0.38
30 Hz	0.67	0.82	0.90	1.33	1.30	1.23	0.10	0.22	0.10	0.76	0.99	0.58
	(B=450 mT)											
	Isotropic			Anisotropic			Isotropic			Anisotropic		
	ε_p=6%	ε_p=11%	ε_p=21%	ε_p=6%	ε_p=11%	ε_p=21%	ε_p=6%	ε_p=11%	ε_p=21%	ε_p=6%	ε_p=11%	ε_p=21%
1 Hz	0.41	0.41	0.56	1.08	0.96	0.91	0.31	0.41	0.46	1.23	1.16	0.84

10 Hz	0.78	0.74	1.03	1.53	1.48	1.40	0.23	0.53	0.47	1.24	1.23	0.98
20 Hz	-	-	-	1.55	1.42	1.45	-	-	-	0.97	1.01	0.92
30 Hz	0.81	0.87	0.98	1.57	1.50	1.34	0.26	0.34	0.19	1.28	1.17	0.64
						(B=600 mT)						
	Isotropic			Anisotropic			Isotropic			Anisotropic		
	ε_p=6%	ε_p=11%	ε_p=21%	ε_p=6%	ε_p=11%	ε_p=21%	ε_p=6%	ε_p=11%	ε_p=21%	ε_p=6%	ε_p=11%	ε_p=21%
1 Hz	0.43	0.46	0.63	1.14	1.08	1.00	0.13	0.40	0.53	0.99	1.14	0.93
10 Hz	0.82	0.88	1.08	1.54	1.54	1.47	0.39	0.51	0.56	1.38	1.34	1.04
20 Hz	-	-	-	1.27	1.39	1.21	-	-	-	0.68	1.14	0.41
30 Hz	0.82	0.90	1.07	1.58	1.49	1.38	0.30	0.39	0.56	1.27	1.25	1.08
						(B=750 mT)						
	Isotropic			Anisotropic			Isotropic			Anisotropic		
	ε_p=6%	ε_p=11%	ε_p=21%	ε_p=6%	ε_p=11%	ε_p=21%	ε_p=6%	ε_p=11%	ε_p=21%	ε_p=6%	ε_p=11%	ε_p=21%
1 Hz	-	-	0.65	-	-	1.00	-	-	0.39	-	-	0.86
10 Hz	-	-	0.95	-	-	1.38	-	-	0.95	-	-	1.38
20 Hz	-	-	-	-	-	1.48	-	-	-	-	-	1.28
30 Hz	-	-	0.99	-	-	1.41	-	-	0.48	-	-	0.97

Table B2 Specific data of the linear slope of the major axis and the area bounded by the stress-strain hysteresis characteristics of the isotropic and anisotropic MREs with particle volume fraction of 30% considering three level of static pre-strain.

	(B=0 mT)											
Frequency	Linear Slope of Major Axis (MPa)						Area Bounded by Hysteresis Loop (kN.m/m3 or KPa)					
	Isotropic			Anisotropic			Isotropic			Anisotropic		
	ε_p=6%	ε_p=11%	ε_p=21%	ε_p=6%	ε_p=11%	ε_p=21%	ε_p=6%	ε_p=11%	ε_p=21%	ε_p=6%	ε_p=11%	ε_p=21%
1 Hz	0.22	0.44	0.62	0.80	0.74	1.08	0.13	0.20	0.32	0.42	0.52	0.79
10 Hz	0.22	0.52	0.75	0.96	0.90	1.25	0.15	0.28	0.47	0.66	0.75	0.95
20 Hz	0.46	0.64	1.24	0.80	0.84	1.16	0.27	0.38	0.71	0.52	0.66	0.85
30 Hz	0.58	0.55	0.88	0.85	0.85	1.13	0.30	0.31	0.59	0.58	0.74	0.87
	(B=150 mT)											
	Isotropic			Anisotropic			Isotropic			Anisotropic		
	ε_p=6%	ε_p=11%	ε_p=21%	ε_p=6%	ε_p=11%	ε_p=21%	ε_p=6%	ε_p=11%	ε_p=21%	ε_p=6%	ε_p=11%	ε_p=21%
1 Hz	0.51	0.69	0.90	1.24	1.11	1.33	0.34	0.46	0.58	1.05	1.06	1.18
10 Hz	0.82	1.14	1.38	1.68	1.57	1.78	0.44	0.34	0.73	1.60	1.37	1.34
20 Hz	0.90	1.08	1.62	1.67	1.55	1.80	0.31	0.23	0.67	1.42	1.31	1.45
30 Hz	1.00	1.13	1.40	1.57	1.69	1.72	0.02	0.40	0.67	1.18	1.54	1.42
	(B=300 mT)											
	Isotropic			Anisotropic			Isotropic			Anisotropic		
	ε_p=6%	ε_p=11%	ε_p=21%	ε_p=6%	ε_p=11%	ε_p=21%	ε_p=6%	ε_p=11%	ε_p=21%	ε_p=6%	ε_p=11%	ε_p=21%
1 Hz	1.00	1.11	1.35	1.74	1.58	1.72	0.70	0.98	1.18	1.77	1.85	1.90
10 Hz	1.51	1.72	2.00	2.38	2.31	2.42	0.86	1.29	1.61	2.68	2.56	2.28
20 Hz	1.21	1.57	1.88	2.25	2.22	2.35	0.36	0.82	0.92	2.21	2.26	2.05
30 Hz	1.46	1.68	1.98	2.33	2.22	2.32	0.63	1.23	1.27	2.23	2.64	2.19
	(B=450 mT)											
	Isotropic			Anisotropic			Isotropic			Anisotropic		
	ε_p=6%	ε_p=11%	ε_p=21%	ε_p=6%	ε_p=11%	ε_p=21%	ε_p=6%	ε_p=11%	ε_p=21%	ε_p=6%	ε_p=11%	ε_p=21%
1 Hz	1.44	1.51	1.81	2.21	2.02	2.20	1.28	1.53	1.84	2.41	2.51	2.63
10 Hz	2.02	2.19	2.64	3.02	2.85	2.78	1.51	1.92	2.29	3.54	3.30	2.93
20 Hz	1.80	2.13	2.57	3.05	2.78	2.95	1.03	1.52	1.65	3.20	3.15	3.08
30 Hz	1.93	2.10	2.60	2.93	2.55	2.84	1.38	1.70	1.94	3.14	3.16	2.79
	(B=600 mT)											
	Isotropic			Anisotropic			Isotropic			Anisotropic		

	ε_p=6%	ε_p=11%	ε_p=21%	ε_p=6%	ε_p=11%	ε_p=21%	ε_p=6%	ε_p=11%	ε_p=21%	ε_p=6%	ε_p=11%	ε_p=21%
1 Hz	1.72	1.81	2.18	2.39	2.18	2.47	1.32	1.74	2.21	2.58	2.83	3.00
10 Hz	2.32	2.43	3.05	3.29	3.04	3.17	1.90	2.14	2.74	4.05	3.57	3.24
20 Hz	1.95	2.46	2.83	3.16	2.98	2.97	1.14	1.93	1.79	3.21	3.46	2.94
30 Hz	2.11	2.33	2.74	3.12	2.92	3.16	1.70	2.13	2.40	3.66	3.73	3.47
						(B=750 mT)						
	Isotropic			Anisotropic			Isotropic			Anisotropic		
	ε_p=6%	ε_p=11%	ε_p=21%	ε_p=6%	ε_p=11%	ε_p=21%	ε_p=6%	ε_p=11%	ε_p=21%	ε_p=6%	ε_p=11%	ε_p=21%
1 Hz	-	-	2.08	2.62	2.37	2.58	-	-	2.18	2.88	2.62	3.12
10 Hz	-	-	3.17	3.49	3.14	3.23	-	-	3.22	4.44	3.59	3.59
20 Hz	-	-	3.29	3.01	2.87	3.37	-	-	2.61	3.20	3.19	3.43
30 Hz	-	-	2.90	3.08	3.01	3.25	-	-	2.54	3.43	3.44	3.37

"-": Not recorded

Table B3 Specific data of the linear slope of the major axis and the area bounded by the stress-strain hysteresis characteristics of the isotropic and anisotropic MREs with particle volume fraction of 45% considering three level of static pre-strain.

	(B=0 mT)											
Frequency	Linear Slope of Major Axis (MPa)						Area Bounded by Hysteresis Loop (kN.m/m3 or KPa)					
	Isotropic			Anisotropic			Isotropic			Anisotropic		
	ε_p=6%	ε_p=11%	ε_p=21%	ε_p=6%	ε_p=11%	ε_p=21%	ε_p=6%	ε_p=11%	ε_p=21%	ε_p=6%	ε_p=11%	ε_p=21%
1 Hz	0.17	0.84	1.43	1.33	1.50	2.26	0.08	0.58	1.03	0.83	1.44	1.90
10 Hz	1.07	2.24	5.02	1.49	1.60	2.42	0.74	1.42	3.10	0.95	1.48	2.15
20 Hz	-	-	-	1.48	1.45	2.32	-	-	-	1.09	1.32	2.12
30 Hz	1.21	1.95	3.43	1.23	1.22	1.93	0.80	1.35	2.51	0.86	1.10	1.76
	(B=150 mT)											
	Isotropic			Anisotropic			Isotropic			Anisotropic		
	ε_p=6%	ε_p=11%	ε_p=21%	ε_p=6%	ε_p=11%	ε_p=21%	ε_p=6%	ε_p=11%	ε_p=21%	ε_p=6%	ε_p=11%	ε_p=21%
1 Hz	0.85	1.62	2.00	2.42	2.32	2.86	0.89	1.86	2.27	2.87	3.21	3.13
10 Hz	1.91	3.02	5.29	2.85	2.93	3.52	1.49	2.21	3.99	2.69	3.30	3.96
20 Hz	-	-	-	2.65	2.64	3.30	-	-	-	2.99	3.18	3.80
30 Hz	2.03	3.06	4.90	2.17	2.40	2.97	1.43	2.51	4.05	2.02	2.91	3.52
	(B=300 mT)											
	Isotropic			Anisotropic			Isotropic			Anisotropic		
	ε_p=6%	ε_p=11%	ε_p=21%	ε_p=6%	ε_p=11%	ε_p=21%	ε_p=6%	ε_p=11%	ε_p=21%	ε_p=6%	ε_p=11%	ε_p=21%
1 Hz	2.11	2.61	3.16	3.83	3.47	3.95	2.53	3.57	4.57	5.15	5.82	5.48
10 Hz	3.21	4.38	6.62	4.09	4.37	5.60	2.80	4.75	5.96	5.19	6.00	7.14
20 Hz	-	-	-	3.96	4.43	4.73	-	-	-	5.37	6.33	6.62
30 Hz	3.40	4.65	6.7	3.21	3.71	4.55	3.03	4.91	6.59	4.13	5.55	6.12
	(B=450 mT)											
	Isotropic			Anisotropic			Isotropic			Anisotropic		
	ε_p=6%	ε_p=11%	ε_p=21%	ε_p=6%	ε_p=11%	ε_p=21%	ε_p=6%	ε_p=11%	ε_p=21%	ε_p=6%	ε_p=11%	ε_p=21%
1 Hz	3.35	3.65	4.71	4.30	4.52	5.14	4.50	5.70	6.60	6.15	8.36	7.91
10 Hz	4.32	5.99	8.39	5.60	5.88	6.72	4.55	6.56	8.02	7.49	8.45	8.86
20 Hz	-	-	-	5.05	5.16	6.70	-	-	-	7.64	8.24	9.05
30 Hz	4.54	5.89	8.46	4.58	4.93	5.74	4.92	6.55	8.33	6.23	7.13	7.99
	(B=600 mT)											
	Isotropic			Anisotropic			Isotropic			Anisotropic		

	ε_p=6%	ε_p=11%	ε_p=21%	ε_p=6%	ε_p=11%	ε_p=21%	ε_p=6%	ε_p=11%	ε_p=21%	ε_p=6%	ε_p=11%	ε_p=21%
1 Hz	4.01	4.41	5.09	5.35	5.78	6.05	5.47	6.47	8.21	8.08	9.33	9.43
10 Hz	5.36	6.85	9.38	6.81	6.92	8.08	5.75	7.79	9.42	8.75	10.51	10.81
20 Hz	-	-	-	6.52	6.68	7.52	-	-	-	9.12	9.15	9.92
30 Hz	5.65	6.71	9.55	5.98	5.73	7.01	5.81	7.20	9.65	7.89	8.69	9.51
	(B=750 mT)											
	Isotropic			Anisotropic			Isotropic			Anisotropic		
	ε_p=6%	ε_p=11%	ε_p=21%	ε_p=6%	ε_p=11%	ε_p=21%	ε_p=6%	ε_p=11%	ε_p=21%	ε_p=6%	ε_p=11%	ε_p=21%
1 Hz	4.43	4.80	5.70	5.75	6.15	7.10	6.29	6.83	8.45	8.33	10.40	10.21
10 Hz	6.00	7.63	10.04	7.07	7.48	8.81	6.30	8.34	10.54	9.48	9.90	11.47
20 Hz	-	-	-	6.58	6.47	8.32	-	-		9.39	9.62	10.63
30 Hz	5.72	7.37	10.19	5.85	6.46	7.70	5.87	7.71	10.15	7.69	9.19	10.33

"-": Not recorded

Table B4 Specific data of the pre-strain stiffening of the isotropic and anisotropic MREs with different particle volume fraction when pre-strain increased from 6% to 21%.

(B=0 mT)						
Frequency	ϕ=15%		ϕ=30%		ϕ=45%	
	Isotropic	Anisotropic	Isotropic	Anisotropic	Isotropic	Anisotropic
1 Hz	52.25	14.97	181.51	35.43	742.59	70.06
10 Hz	52.34	21.61	247.63	30.68	368.16	62.15
20 Hz	-	26.38	171.43	44.08	-	57.00
30 Hz	52.92	29.69	52.75	33.81	184.65	57.12
(B=150 mT)						
	Isotropic	Anisotropic	Isotropic	Anisotropic	Isotropic	Anisotropic
1 Hz	29.33	-10.47	77.58	6.74	134.34	17.86
10 Hz	20.93	-6.24	67.84	6.43	176.76	23.62
20 Hz	-	-13.37	79.13	7.68	-	24.64
30 Hz	26.24	1.38	39.57	9.31	141.11	36.88
(B=300 mT)						
	Isotropic	Anisotropic	Isotropic	Anisotropic	Isotropic	Anisotropic
1 Hz	42.12	-17.19	35.57	-1.01	50.07	3.14
10 Hz	28.47	-10.55	32.47	1.41	106.10	36.98
20 Hz	-	-8.63	55.54	4.55	-	19.50
30 Hz	33.16	-7.47	35.25	-0.67	97.08	41.72
(B=450 mT)						
	Isotropic	Anisotropic	Isotropic	Anisotropic	Isotropic	Anisotropic
1 Hz	38.99	-15.51	25.72	-0.29	40.38	19.51
10 Hz	31.74	-8.18	31.04	-7.96	93.73	20.16
20 Hz	-	-6.45	42.92	-3.08	-	32.63
30 Hz	21.40	-14.85	34.76	-3.17	86.43	25.28
(B=600 mT)						
	Isotropic	Anisotropic	Isotropic	Anisotropic	Isotropic	Anisotropic
1 Hz	45.86	-12.74	27.16	3.38	27.01	13.21
10 Hz	31.37	-4.77	31.46	-3.86	75.06	18.67
20 Hz	-	-4.66	45.25	-6.11	-	15.27
30 Hz	29.74	-12.37	29.84	1.29	68.91	17.14

	(B=750 mT)					
	Isotropic	Anisotropic	Isotropic	Anisotropic	Isotropic	Anisotropic
1 Hz	-	-	-	-1.22	28.51	23.38
10 Hz	-	-	-	-7.49	67.35	24.66
20 Hz	-	-	-	11.94	-	26.50
30 Hz	-	-	-	5.61	78.06	31.58

"-": Not recorded

Table B5 Specific data of the pre-strain dampening of the isotropic and anisotropic MREs with different particle volume fraction when pre-strain increased from 6% to 21%.

			(B=0 mT)			
Frequency	ϕ=15%		ϕ=30%		ϕ=45%	
	Isotropic	Anisotropic	Isotropic	Anisotropic	Isotropic	Anisotropic
1 Hz	135	27	137	74	1115	152
10 Hz	69	32	195	58	301	131
20 Hz	-	30	152	58	-	116
30 Hz	82	32	80	48	224	101
			(B=150 mT)			
	Isotropic	Anisotropic	Isotropic	Anisotropic	Isotropic	Anisotropic
1 Hz	-41	-46	68	4	155	10
10 Hz	-75	-48	71	-12	155	54
20 Hz	-	-38	127	1	-	39
30 Hz	-90	30	1675	22	165	75
			(B=300 mT)			
	Isotropic	Anisotropic	Isotropic	Anisotropic	Isotropic	Anisotropic
1 Hz	140	-34	61	-0.06	74	9
10 Hz	1638	-13	90	-11	110	33
20 Hz	-	-44	193	-10	-	33
30 Hz	-21	-26	111	-2	103	41
			(B=450 mT)			
	Isotropic	Anisotropic	Isotropic	Anisotropic	Isotropic	Anisotropic
1 Hz	51	-32	36	1	48	29
10 Hz	102	-24	51	-12	73	22
20 Hz	-	-10	63	-5	-	22
30 Hz	-30	-48	41	-11	60	27
			(B=600 mT)			
	Isotropic	Anisotropic	Isotropic	Anisotropic	Isotropic	Anisotropic
1 Hz	307	-6	63	9	49	18
10 Hz	47	-26	44	-16	63	22
20 Hz	-	-48	53	-9	-	19
30 Hz	98	-14	47	-5	59	26

	(B=750 mT)					
	Isotropic	Anisotropic	Isotropic	Anisotropic	Isotropic	Anisotropic
1 Hz	-	-	-	1.5	32	23
10 Hz	-	-	-	-7	60	19
20 Hz	-	-	-	9	-	20
30 Hz	-	-	-	-2	61	29

"-": Not recorded

Table B6 Specific data of the elastic and loss moduli of both types of the MREs with particle volume fraction of 15% considering three level of static pre-strain, loading frequency and magnetic flux density.

	(B=0 mT)											
Frequency	Elastic Modulus						Loss modulus					
	Isotropic			Anisotropic			Isotropic			Anisotropic		
	ε_p=6%	ε_p=11%	ε_p=21%	ε_p=6%	ε_p=11%	ε_p=21%	ε_p=6%	ε_p=11%	ε_p=21%	ε_p=6%	ε_p=11%	ε_p=21%
1 Hz	0.18	0.20	0.27	0.32	0.30	0.37	0.02	0.03	0.05	0.08	0.09	0.10
10 Hz	0.21	0.24	0.32	0.38	0.38	0.46	0.05	0.05	0.08	0.11	0.13	0.15
20 Hz	-	-	-	0.37	0.39	0.47	-	-	-	0.13	0.16	0.17
30 Hz	0.24	0.26	0.36	0.38	0.39	0.49	0.06	0.08	0.11	0.13	0.16	0.17
	(B=150 mT)											
	Isotropic			Anisotropic			Isotropic			Anisotropic		
	ε_p=6%	ε_p=11%	ε_p=21%	ε_p=6%	ε_p=11%	ε_p=21%	ε_p=6%	ε_p=11%	ε_p=21%	ε_p=6%	ε_p=11%	ε_p=21%
1 Hz	0.24	0.26	0.31	0.59	0.55	0.53	0.04	0.05	0.02	0.28	0.24	0.15
10 Hz	0.58	0.59	0.70	1.00	0.93	0.94	0.05	0.12	0.01	0.35	0.14	0.18
20 Hz	-	-	-	1.05	0.87	0.91	-	-	-	0.31	0.16	0.19
30 Hz	0.63	0.70	0.79	1.01	1.07	1.02	0.16	0.04	0.02	0.17	0.25	0.22
	(B=300 mT)											
	Isotropic			Anisotropic			Isotropic			Anisotropic		
	ε_p=6%	ε_p=11%	ε_p=21%	ε_p=6%	ε_p=11%	ε_p=21%	ε_p=6%	ε_p=11%	ε_p=21%	ε_p=6%	ε_p=11%	ε_p=21%
1 Hz	0.30	0.35	0.43	0.88	0.79	0.72	0.05	0.10	0.11	0.41	0.40	0.27
10 Hz	0.68	0.75	0.87	1.30	1.24	1.16	0.01	0.13	0.17	0.45	0.51	0.39
20 Hz	-	-	-	1.20	1.30	1.10	-	-	-	0.35	0.37	0.20
30 Hz	0.67	0.82	0.90	1.33	1.30	1.23	0.06	0.12	0.04	0.41	0.53	0.30
	(B=450 mT)											
	Isotropic			Anisotropic			Isotropic			Anisotropic		
	ε_p=6%	ε_p=11%	ε_p=21%	ε_p=6%	ε_p=11%	ε_p=21%	ε_p=6%	ε_p=11%	ε_p=21%	ε_p=6%	ε_p=11%	ε_p=21%
1 Hz	0.41	0.41	0.56	1.08	0.96	0.91	0.15	0.21	0.23	0.59	0.57	0.40
10 Hz	0.78	0.74	1.03	1.53	1.48	1.40	0.11	0.27	0.23	0.61	0.60	0.47
20 Hz	-	-	-	1.55	1.42	1.45	-	-	-	0.51	0.55	0.45
30 Hz	0.81	0.87	0.98	1.57	1.50	1.34	0.13	0.19	0.09	0.65	0.60	0.34
	(B=600 mT)											
	Isotropic			Anisotropic			Isotropic			Anisotropic		

	ε_p=6%	ε_p=11%	ε_p=21%	ε_p=6%	ε_p=11%	ε_p=21%	ε_p=6%	ε_p=11%	ε_p=21%	ε_p=6%	ε_p=11%	ε_p=21%
1 Hz	0.43	0.46	0.63	1.14	1.08	1.00	0.06	0.20	0.26	0.48	0.56	0.45
10 Hz	0.82	0.88	1.08	1.54	1.54	1.47	0.19	0.26	0.28	0.69	0.66	0.51
20 Hz	-	-	-	1.27	1.39	1.21	-	-	-	0.38	0.64	0.20
30 Hz	0.82	0.90	1.07	1.58	1.49	1.38	0.15	0.21	0.30	0.66	0.64	0.56
						(B=750 mT)						
	Isotropic			Anisotropic			Isotropic			Anisotropic		
	ε_p=6%	ε_p=11%	ε_p=21%	ε_p=6%	ε_p=11%	ε_p=21%	ε_p=6%	ε_p=11%	ε_p=21%	ε_p=6%	ε_p=11%	ε_p=21%
1 Hz	-	-	0.65	-	-	1.00	-	-	0.19	-	-	0.42
10 Hz	-	-	0.95	-	-	1.38	-	-	0.47	-	-	0.68
20 Hz	-	-	-	-	-	1.48	-	-	-	-	-	0.66
30 Hz	-	-	0.99	-	-	1.41	-	-	0.26	-	-	0.48

"-": Not recorded

Table B7 Specific data of the elastic and loss moduli of both types of the MREs with particle volume fraction of 30% considering three level of static pre-strain, loading frequency and magnetic flux density.

(B=0 mT)												
Frequency	Elastic Modulus (MPa)						Loss modulus (MPa)					
	Isotropic			Anisotropic			Isotropic			Anisotropic		
	ε_p=6%	ε_p=11%	ε_p=21%	ε_p=6%	ε_p=11%	ε_p=21%	ε_p=6%	ε_p=11%	ε_p=21%	ε_p=6%	ε_p=11%	ε_p=21%
1 Hz	0.22	0.44	0.62	0.80	0.74	1.08	0.07	0.1	0.16	0.22	0.27	0.38
10 Hz	0.22	0.52	0.75	0.96	0.90	1.25	0.08	0.14	0.24	0.31	0.38	0.49
20 Hz	0.46	0.64	1.24	0.80	0.84	1.16	0.15	0.20	0.37	0.30	0.35	0.48
30 Hz	0.58	0.55	0.88	0.85	0.85	1.13	0.17	0.19	0.30	0.32	0.39	0.48
(B=150 mT)												
	Isotropic			Anisotropic			Isotropic			Anisotropic		
	ε_p=6%	ε_p=11%	ε_p=21%	ε_p=6%	ε_p=11%	ε_p=21%	ε_p=6%	ε_p=11%	ε_p=21%	ε_p=6%	ε_p=11%	ε_p=21%
1 Hz	0.51	0.69	0.90	1.24	1.11	1.33	0.17	0.24	0.29	0.54	0.54	0.57
10 Hz	0.82	1.14	1.38	1.68	1.57	1.78	0.22	0.17	0.38	0.78	0.71	0.69
20 Hz	0.90	1.08	1.62	1.67	1.55	1.80	0.16	0.12	0.36	0.75	0.70	0.76
30 Hz	1.00	1.13	1.40	1.57	1.69	1.72	0.02	0.22	0.39	0.65	0.81	0.80
(B=300 mT)												
	Isotropic			Anisotropic			Isotropic			Anisotropic		
	ε_p=6%	ε_p=11%	ε_p=21%	ε_p=6%	ε_p=11%	ε_p=21%	ε_p=6%	ε_p=11%	ε_p=21%	ε_p=6%	ε_p=11%	ε_p=21%
1 Hz	1.00	1.11	1.35	1.74	1.58	1.72	0.36	0.50	0.58	0.92	0.94	0.92
10 Hz	1.51	1.72	2.00	2.38	2.31	2.42	0.44	0.66	0.84	1.31	1.30	1.17
20 Hz	1.21	1.57	1.88	2.25	2.22	2.35	0.17	0.45	0.50	1.21	1.21	1.10
30 Hz	1.46	1.68	1.98	2.33	2.22	2.32	0.34	0.65	0.71	1.24	1.44	1.21
(B=450 mT)												
	Isotropic			Anisotropic			Isotropic			Anisotropic		
	ε_p=6%	ε_p=11%	ε_p=21%	ε_p=6%	ε_p=11%	ε_p=21%	ε_p=6%	ε_p=11%	ε_p=21%	ε_p=6%	ε_p=11%	ε_p=21%
1 Hz	1.44	1.51	1.81	2.21	2.02	2.20	0.66	0.79	0.90	1.24	1.28	1.26
10 Hz	2.02	2.19	2.64	3.02	2.85	2.78	0.76	0.97	1.15	1.72	1.70	1.52
20 Hz	1.80	2.13	2.57	3.05	2.78	2.95	0.55	0.78	0.89	1.68	1.69	1.59
30 Hz	1.93	2.10	2.60	2.93	2.55	2.84	0.75	0.93	1.05	1.73	1.81	1.54
(B=600 mT)												
	Isotropic			Anisotropic			Isotropic			Anisotropic		

	ε_p=6%	ε_p=11%	ε_p=21%	ε_p=6%	ε_p=11%	ε_p=21%	ε_p=6%	ε_p=11%	ε_p=21%	ε_p=6%	ε_p=11%	ε_p=21%
1 Hz	1.72	1.81	2.18	2.39	2.18	2.47	0.69	0.89	1.12	1.32	1.45	1.44
10 Hz	2.32	2.43	3.05	3.29	3.04	3.17	0.96	1.13	1.39	1.96	1.88	1.65
20 Hz	1.95	2.46	2.83	3.16	2.98	2.97	0.63	1.01	0.95	1.73	1.89	1.58
30 Hz	2.11	2.33	2.74	3.12	2.92	3.16	0.93	1.14	1.36	2.00	2.02	1.90
	(B=750 mT)											
	Isotropic			Anisotropic			Isotropic			Anisotropic		
	ε_p=6%	ε_p=11%	ε_p=21%	ε_p=6%	ε_p=11%	ε_p=21%	ε_p=6%	ε_p=11%	ε_p=21%	ε_p=6%	ε_p=11%	ε_p=21%
1 Hz	-	-	2.08	2.62	2.37	2.58	-	-	1.16	1.46	1.35	1.49
10 Hz	-	-	3.17	3.49	3.14	3.23	-	-	1.62	2.03	1.86	1.88
20 Hz	-	-	3.29	3.01	2.87	3.37	-	-	1.40	1.71	1.70	1.87
30 Hz	-	-	2.90	3.08	3.01	3.25	-	-	1.42	1.91	1.91	1.88

"-": Not recorded

Table B8 Specific data of the elastic and loss moduli of both types of the MREs with particle volume fraction of 45% considering three level of static pre-strain, loading frequency and magnetic flux density.

	(B=0 mT)											
Frequency	Elastic Modulus						Loss modulus					
	Isotropic			Anisotropic			Isotropic			Anisotropic		
	ε_p=6%	ε_p=11%	ε_p=21%	ε_p=6%	ε_p=11%	ε_p=21%	ε_p=6%	ε_p=11%	ε_p=21%	ε_p=6%	ε_p=11%	ε_p=21%
1 Hz	0.17	0.84	1.43	1.33	1.50	2.26	0.04	0.31	0.53	0.40	0.69	1.00
10 Hz	1.07	2.24	5.02	1.49	1.60	2.42	0.39	0.75	1.58	0.50	0.75	1.15
20 Hz	-	-	-	1.48	1.45	2.32	-	-	-	0.52	0.72	1.12
30 Hz	1.21	1.95	3.43	1.23	1.22	1.93	0.44	0.77	1.43	0.49	0.60	0.98
	(B=150 mT)											
	Isotropic			Anisotropic			Isotropic			Anisotropic		
	ε_p=6%	ε_p=11%	ε_p=21%	ε_p=6%	ε_p=11%	ε_p=21%	ε_p=6%	ε_p=11%	ε_p=21%	ε_p=6%	ε_p=11%	ε_p=21%
1 Hz	0.85	1.62	2.00	2.42	2.32	2.86	0.47	0.97	1.19	1.49	1.56	1.64
10 Hz	1.91	3.02	5.29	2.85	2.93	3.52	0.81	1.18	2.06	1.32	1.67	2.04
20 Hz	-	-	-	2.65	2.64	3.30	-	-	-	1.47	1.79	2.04
30 Hz	2.03	3.06	4.90	2.17	2.40	2.97	0.85	1.40	2.26	1.15	1.63	2.02
	(B=300 mT)											
	Isotropic			Anisotropic			Isotropic			Anisotropic		
	ε_p=6%	ε_p=11%	ε_p=21%	ε_p=6%	ε_p=11%	ε_p=21%	ε_p=6%	ε_p=11%	ε_p=21%	ε_p=6%	ε_p=11%	ε_p=21%
1 Hz	2.11	2.61	3.16	3.83	3.47	3.95	1.36	1.89	2.36	2.64	2.76	2.87
10 Hz	3.21	4.38	6.62	4.09	4.37	5.60	1.45	2.51	3.05	2.64	3.16	3.50
20 Hz	-	-	-	3.96	4.43	4.73	-	-	-	2.64	3.26	3.52
30 Hz	3.40	4.65	6.7	3.21	3.71	4.55	1.82	2.69	3.70	2.41	3.09	3.40
	(B=450 mT)											
	Isotropic			Anisotropic			Isotropic			Anisotropic		
	ε_p=6%	ε_p=11%	ε_p=21%	ε_p=6%	ε_p=11%	ε_p=21%	ε_p=6%	ε_p=11%	ε_p=21%	ε_p=6%	ε_p=11%	ε_p=21%
1 Hz	3.35	3.65	4.71	4.30	4.52	5.14	2.33	3.03	3.45	3.15	4.05	4.06
10 Hz	4.32	5.99	8.39	5.60	5.88	6.72	2.34	3.37	4.04	3.78	4.36	4.60
20 Hz	-	-	-	5.05	5.16	6.70	-	-	-	3.88	4.48	4.73
30 Hz	4.54	5.89	8.46	4.58	4.93	5.74	2.92	3.72	4.68	3.58	4.12	4.53
	(B=600 mT)											
	Isotropic			Anisotropic			Isotropic			Anisotropic		

	ε_p=6%	ε_p=11%	ε_p=21%	ε_p=6%	ε_p=11%	ε_p=21%	ε_p=6%	ε_p=11%	ε_p=21%	ε_p=6%	ε_p=11%	ε_p=21%
1 Hz	4.01	4.41	5.09	5.35	5.78	6.05	2.88	3.45	4.29	4.16	4.46	4.93
10 Hz	5.36	6.85	9.38	6.81	6.92	8.08	3.00	4.06	4.89	4.52	5.34	5.51
20 Hz	-	-	-	6.52	6.68	7.52	-	-	-	4.52	4.98	5.36
30 Hz	5.65	6.71	9.55	5.98	5.73	7.01	3.42	4.29	5.42	4.31	4.92	5.44
	(B=750 mT)											
	Isotropic			Anisotropic			Isotropic			Anisotropic		
	ε_p=6%	ε_p=11%	ε_p=21%	ε_p=6%	ε_p=11%	ε_p=21%	ε_p=6%	ε_p=11%	ε_p=21%	ε_p=6%	ε_p=11%	ε_p=21%
1 Hz	4.43	4.80	5.70	5.75	6.15	7.10	3.30	3.63	4.35	4.25	5.03	5.22
10 Hz	6.00	7.63	10.04	7.07	7.48	8.81	3.35	4.21	5.36	4.88	5.21	5.79
20 Hz	-	-	-	6.58	6.47	8.32	-	-	-	4.85	5.21	5.83
30 Hz	5.72	7.37	10.19	5.85	6.46	7.70	3.56	4.43	5.72	4.46	4.99	5.75

"-": Not recorded

Table B9 Specific data of the relative MR effect in view of both elastic and loss factor of both types of the MREs with particle volume fraction of 15% considering three level of static pre-strain, loading frequency and magnetic flux density.

(B=150 mT)												
Frequency	Relative MR effect in view of elastic modulus ($MR_{\dot{E}}$)						Relative MR effect in view of loss factor (MR_{η})					
	Isotropic			Anisotropic			Isotropic			Anisotropic		
	ε_p=6%	ε_p=11%	ε_p=21%	ε_p=6%	ε_p=11%	ε_p=21%	ε_p=6%	ε_p=11%	ε_p=21%	ε_p=6%	ε_p=11%	ε_p=21%
1 Hz	33	31	13	83	81	42	110	54	-47	244	165	47
10 Hz	171	144	115	166	145	105	8.4	125	-84	207	1.5	20
20 Hz	-	-	-	184	123	95	-	-	-	143	-1	16
30 Hz	164	168	118	165	178	107	161	-50	-85	26	59	24
(B=300 mT)												
	Isotropic			Anisotropic			Isotropic			Anisotropic		
	ε_p=6%	ε_p=11%	ε_p=21%	ε_p=6%	ε_p=11%	ε_p=21%	ε_p=6%	ε_p=11%	ε_p=21%	ε_p=6%	ε_p=11%	ε_p=21%
1 Hz	69	80	58	170	164	94	131	225	135	400	337	159
10 Hz	218	212	168	247	226	155	-80	139	107	294	278	160
20 Hz	-	-		225	232	135	-	-	-	170	134	17
30 Hz	184	212	147	250	237	150	-9	57	-61	210	239	73
(B=450 mT)												
	Isotropic			Anisotropic			Isotropic			Anisotropic		
	ε_p=6%	ε_p=11%	ε_p=21%	ε_p=6%	ε_p=11%	ε_p=21%	ε_p=6%	ε_p=11%	ε_p=21%	ε_p=6%	ε_p=11%	ε_p=21%
1 Hz	127	109	108	233	220	145	676	597	397	619	520	286
10 Hz	268	210	218	307	289	208	130	391	174	433	345	208
20 Hz	-	-	-	320	263	211	-	-	-	295	252	173
30 Hz	240	233	170	314	289	172	119	150	-15	395	286	95
(B=600 mT)												
	Isotropic			Anisotropic			Isotropic			Anisotropic		
	ε_p=6%	ε_p=11%	ε_p=21%	ε_p=6%	ε_p=11%	ε_p=21%	ε_p=6%	ε_p=11%	ε_p=21%	ε_p=6%	ε_p=11%	ε_p=21%
1 Hz	141	136	131	251	258	167	223	571	460	483	504	333
10 Hz	286	265	233	311	304	222	289	368	237	498	393	236
20 Hz	-	-	-	245	256	160	-	-	-	199	310	21
30 Hz	247	245	194	316	287	182	149	180	171	398	313	223

	(B=750 mT)											
	Isotropic			Anisotropic			Isotropic			Anisotropic		
	ε_p=6%	ε_p=11%	ε_p=21%	ε_p=6%	ε_p=11%	ε_p=21%	ε_p=6%	ε_p=11%	ε_p=21%	ε_p=6%	ε_p=11%	ε_p=21%
1 Hz	-	-	138	-	-	168	-	-	317	-	-	302
10 Hz	-	-	192	-	-	202	-	-	461	-	-	349
20 Hz	-	-	-	-	-	219	-	-	-	-	-	294
30 Hz	-	-	172	-	-	188	-	-	134	-	-	178

"-": Not recorded

Table B10 Specific data of the relative MR effect in view of both elastic and loss factor of both types of the MREs with particle volume fraction of 30% considering three level of static pre-strain, loading frequency and magnetic flux density.

Frequency	Relative MR effect in view of elastic modulus ($MR_{\dot{E}}$)						Relative MR effect in view of loss factor (MR_{η})					
	Isotropic			Anisotropic			Isotropic			Anisotropic		
	ε_p=6%	ε_p=11%	ε_p=21%	ε_p=6%	ε_p=11%	ε_p=21%	ε_p=6%	ε_p=11%	ε_p=21%	ε_p=6%	ε_p=11%	ε_p=21%
(B=150 mT)												
1 Hz	130	58	45	56	49	23	154	136	80	150	103	50
10 Hz	280	119	83	75	74	42	179	23	62	154	88	41
20 Hz	99	69	31	108	84	55	7	-39	-4	151	99	59
30 Hz	74	106	59	86	100	52	-87	21	28	101	108	67
(B=300 mT)												
	Isotropic			Anisotropic			Isotropic			Anisotropic		
	ε_p=6%	ε_p=11%	ε_p=21%	ε_p=6%	ε_p=11%	ε_p=21%	ε_p=6%	ε_p=11%	ε_p=21%	ε_p=6%	ε_p=11%	ε_p=21%
1 Hz	351	153	117	118	112	59	428	405	258	323	248	142
10 Hz	597	231	166	149	156	93	447	366	253	326	247	141
20 Hz	166	145	52	181	164	104	17	129	36	304	247	130
30 Hz	153	207	124	176	162	105	100	251	134	284	272	154
(B=450 mT)												
	Isotropic			Anisotropic			Isotropic			Anisotropic		
	ε_p=6%	ε_p=11%	ε_p=21%	ε_p=6%	ε_p=11%	ε_p=21%	ε_p=6%	ε_p=11%	ε_p=21%	ε_p=6%	ε_p=11%	ε_p=21%
1 Hz	552	243	191	176	171	103	873	688	459	427	378	232
10 Hz	831	322	251	215	215	122	851	579	387	457	352	212
20 Hz	296	233	108	280	230	155	271	300	140	459	386	234
30 Hz	235	283	196	246	201	151	345	402	248	435	367	223
(B=600 mT)												
	Isotropic			Anisotropic			Isotropic			Anisotropic		
	ε_p=6%	ε_p=11%	ε_p=21%	ε_p=6%	ε_p=11%	ε_p=21%	ε_p=6%	ε_p=11%	ε_p=21%	ε_p=6%	ε_p=11%	ε_p=21%
1 Hz	676	313	250	199	193	129	909	792	591	509	439	281
10 Hz	973	368	306	243	236	153	1099	692	486	537	399	240
20 Hz	329	285	129	293	254	156	326	417	158	474	443	231
30 Hz	266	325	211	269	244	179	455	516	351	519	422	297

	(B=750 mT)											
	Isotropic			Anisotropic			Isotropic			Anisotropic		
	ε_p=6%	ε_p=11%	ε_p=21%	ε_p=6%	ε_p=11%	ε_p=21%	ε_p=6%	ε_p=11%	ε_p=21%	ε_p=6%	ε_p=11%	ε_p=21%
1 Hz	-	-	234	228	218	139	-	-	619	573	404	292
10 Hz	-	-	322	264	248	157	-	-	584	578	395	287
20 Hz	-	-	166	275	242	191	-	-	277	470	387	293
30 Hz	-	-	230	264	255	187	-	-	371	490	393	293

"-": Not recorded

Table B11 Specific data of the relative MR effect in view of both elastic and loss factor of both types of the MREs with particle volume fraction of 45% considering three level of static pre-strain, loading frequency and magnetic flux density.

(B=150 mT)												
Frequency	Relative MR effect in view of elastic modulus ($MR_{\dot{E}}$)						Relative MR effect in view of loss factor (MR_{η})					
	Isotropic			Anisotropic			Isotropic			Anisotropic		
	ε_p=6%	ε_p=11%	ε_p=21%	ε_p=6%	ε_p=11%	ε_p=21%	ε_p=6%	ε_p=11%	ε_p=21%	ε_p=6%	ε_p=11%	ε_p=21%
1 Hz	402	94	39	83	55	27	969	214	124	275	125	65
10 Hz	78	35	5	91	83	46	106	57	31	164	122	77
20 Hz	-	-	-	79	81	42	-	-	-	182	150	82
30 Hz	68	57	43	76	97	54	92	82	57	136	169	106
(B=300 mT)												
	Isotropic			Anisotropic			Isotropic			Anisotropic		
	ε_p=6%	ε_p=11%	ε_p=21%	ε_p=6%	ε_p=11%	ε_p=21%	ε_p=6%	ε_p=11%	ε_p=21%	ε_p=6%	ε_p=11%	ε_p=21%
1 Hz	1139	212	121	188	132	75	2997	510	343	566	298	187
10 Hz	199	96	32	174	173	132	270	233	93	428	320	204
20 Hz	-	-	-	168	205	104	-	-	-	408	355	214
30 Hz	182	139	96	161	205	135	313	248	158	394	411	247
(B=450 mT)												
	Isotropic			Anisotropic			Isotropic			Anisotropic		
	ε_p=6%	ε_p=11%	ε_p=21%	ε_p=6%	ε_p=11%	ε_p=21%	ε_p=6%	ε_p=11%	ε_p=21%	ε_p=6%	ε_p=11%	ε_p=21%
1 Hz	1874	337	229	224	202	128	5225	880	548	695	484	307
10 Hz	304	168	67	275	267	178	496	346	156	656	481	299
20 Hz	-	-	-	242	255	189	-	-	-	647	526	322
30 Hz	276	203	146	272	304	197	560	382	227	632	582	362
(B=600 mT)												
	Isotropic			Anisotropic			Isotropic			Anisotropic		
	ε_p=6%	ε_p=11%	ε_p=21%	ε_p=6%	ε_p=11%	ε_p=21%	ε_p=6%	ε_p=11%	ε_p=21%	ε_p=6%	ε_p=11%	ε_p=21%
1 Hz	2258	427	256	303	286	168	6465	1016	706	950	543	394
10 Hz	399	206	87	357	332	234	665	438	210	804	611	378
20 Hz	-	-	-	341	360	224	-	-	-	769	595	378
30 Hz	368	245	178	386	371	262	673	455	278	784	715	455

	(B=750 mT)											
	Isotropic			Anisotropic			Isotropic			Anisotropic		
	ε_p=6%	ε_p=11%	ε_p=21%	ε_p=6%	ε_p=11%	ε_p=21%	ε_p=6%	ε_p=11%	ε_p=21%	ε_p=6%	ε_p=11%	ε_p=21%
1 Hz	2509	475	298	333	311	214	7434	1076	717	972	624	423
10 Hz	459	241	100	374	367	265	752	459	240	876	593	402
20 Hz	-	-	-	345	345	259	-	-	-	833	627	420
30 Hz	374	279	197	376	430	298	705	473	299	813	726	487

"-": Not recorded

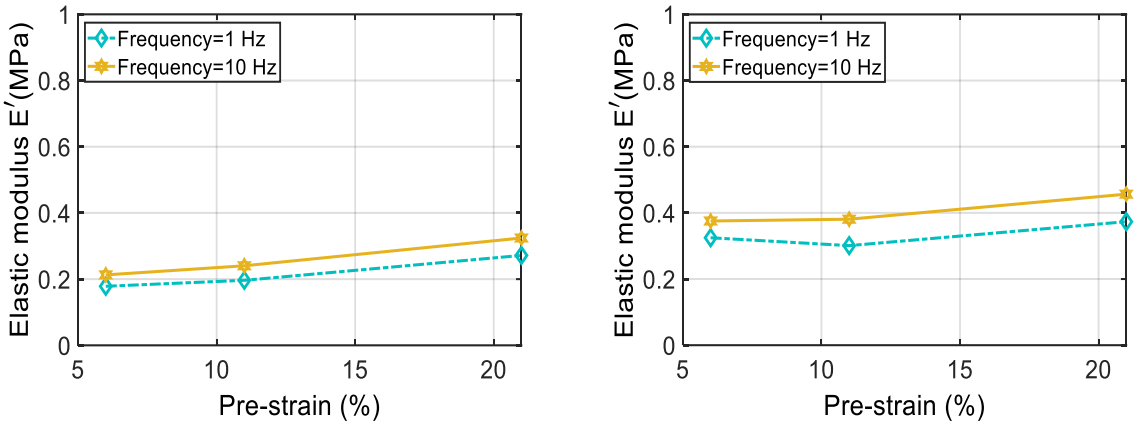

(a)

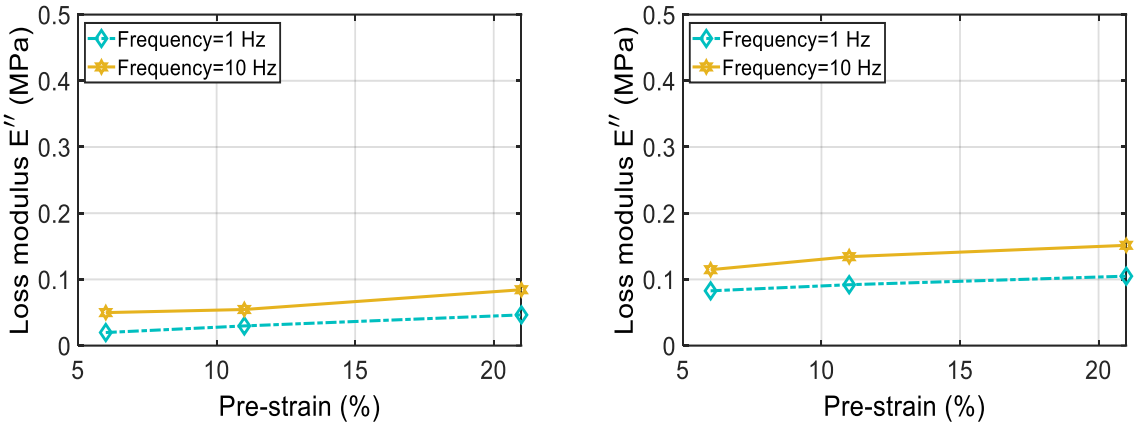

(b)

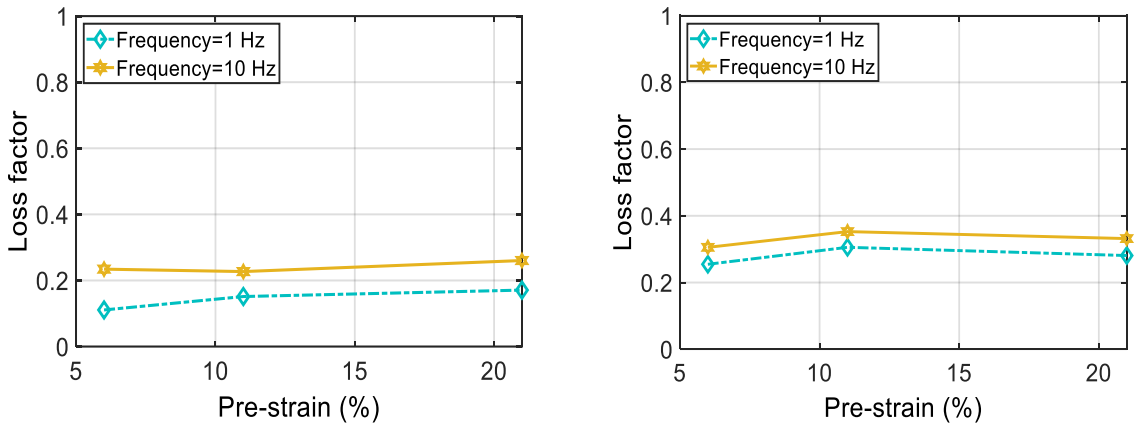

(c)

Figure B1 Effect of pre-strain on the compression mode elastic modulus (a), loss modulus (b), and loss factor (c) of the isotropic (left column) and anisotropic (right column) MREs with volume fraction of 15% under different excitation frequencies (ε_0=2.5%, and B=0 mT).

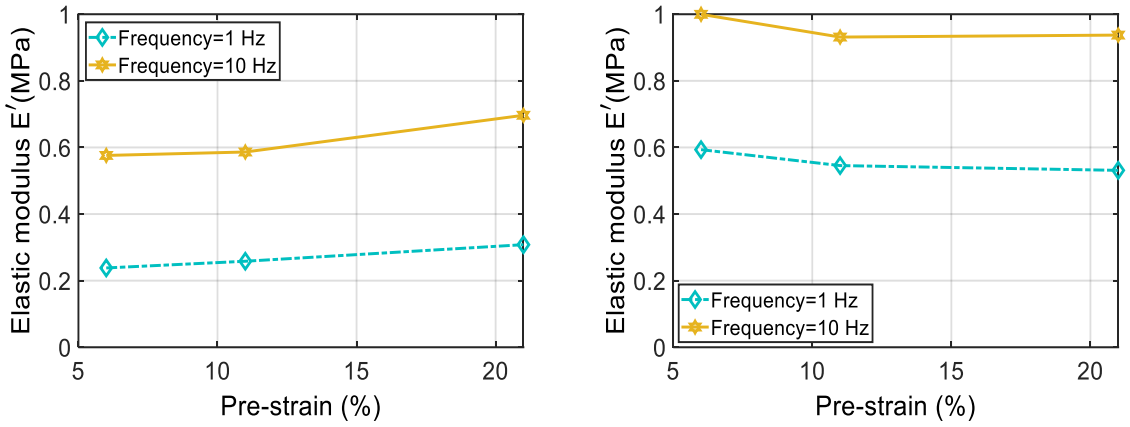

(a)

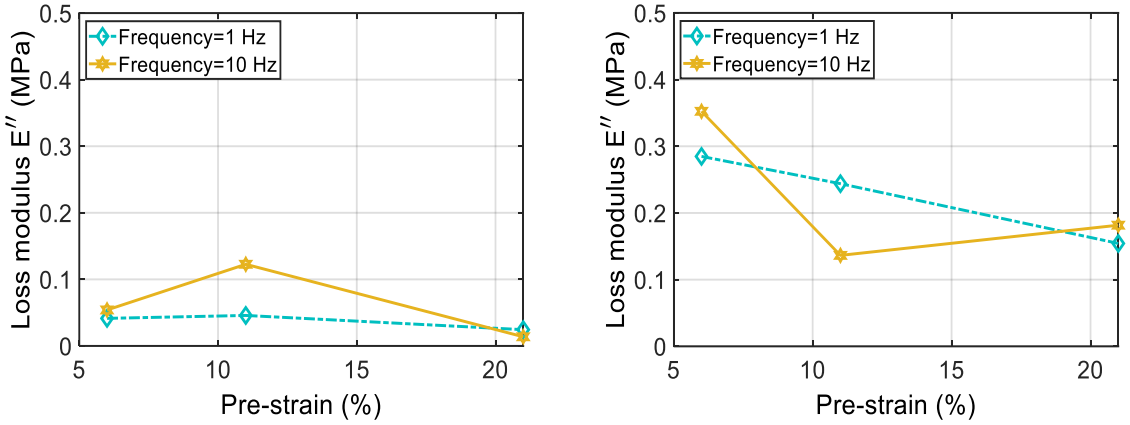

(b)

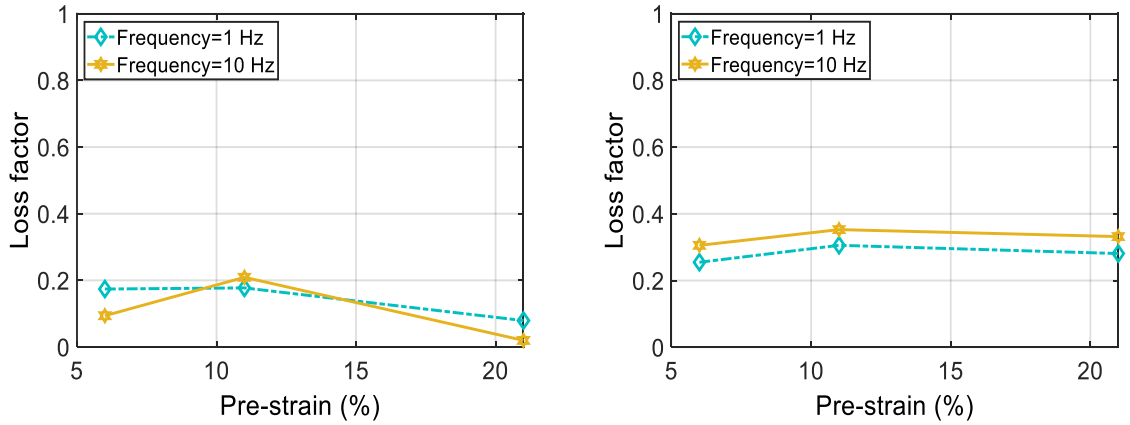

(c)

Figure B2 Effect of pre-strain on the compression mode elastic modulus (a), loss modulus (b), and loss factor (c) of the isotropic (left column) and anisotropic (right column) MREs with volume fraction of 15% under different excitation frequencies (ε_0=2.5%, and B=150 mT).

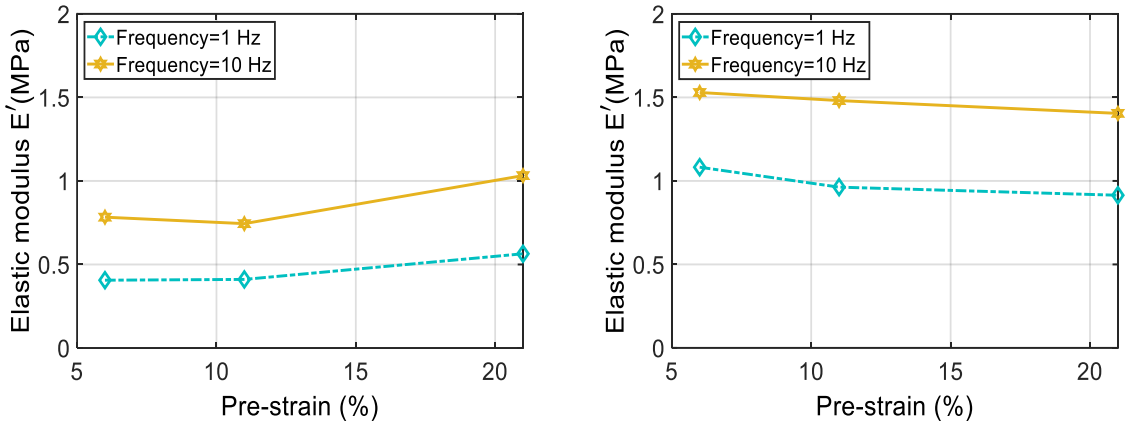

(a)

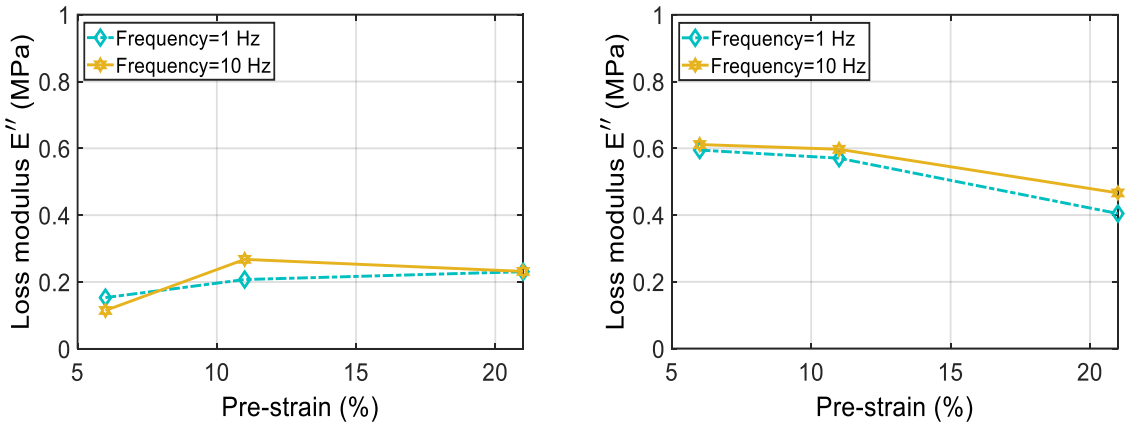

(b)

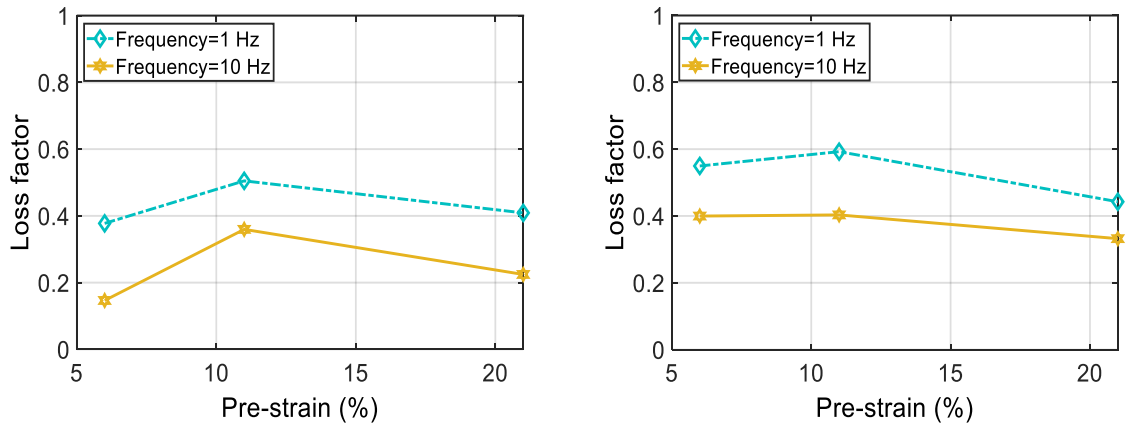

(c)

Figure B3 Effect of pre-strain on the compression mode elastic modulus (a), loss modulus (b), and loss factor (c) of the isotropic (left column) and anisotropic (right column) MREs with volume fraction of 15% under different excitation frequencies (ε_0=2.5%, and B=450 mT).

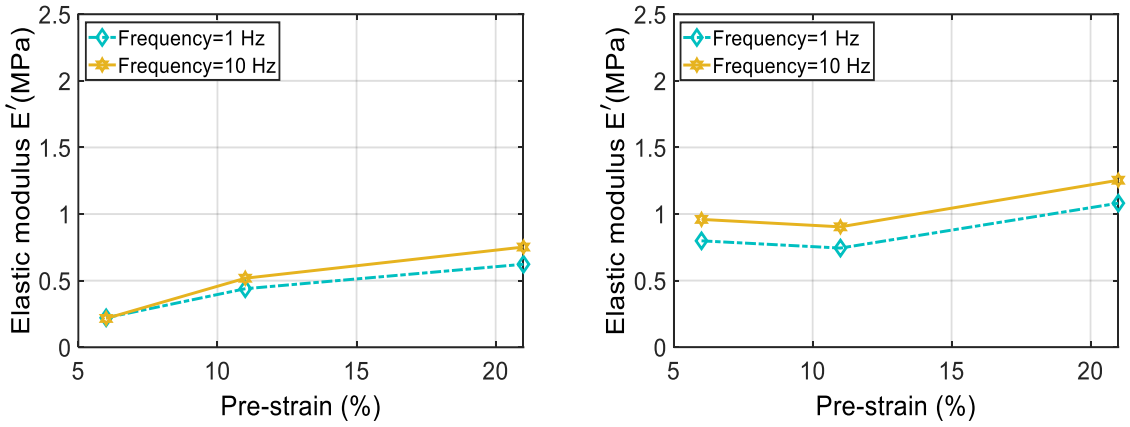

(a)

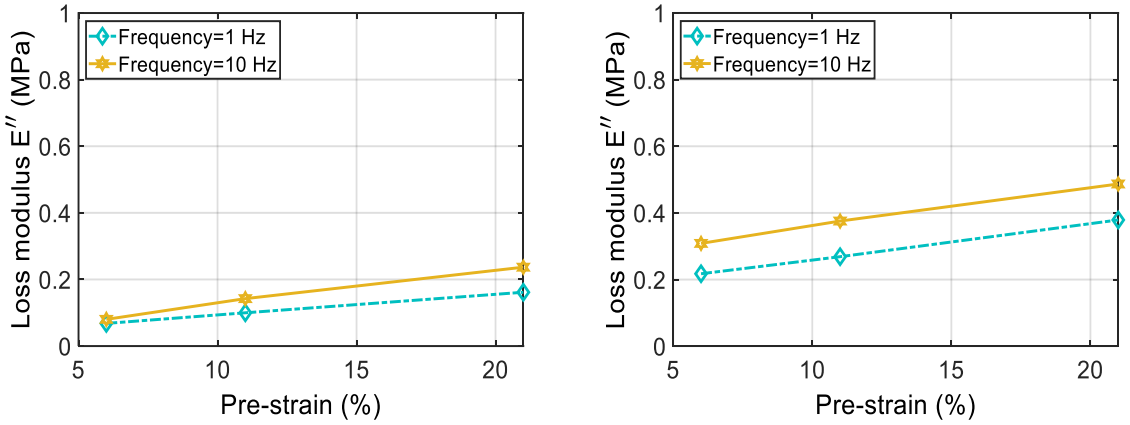

(b)

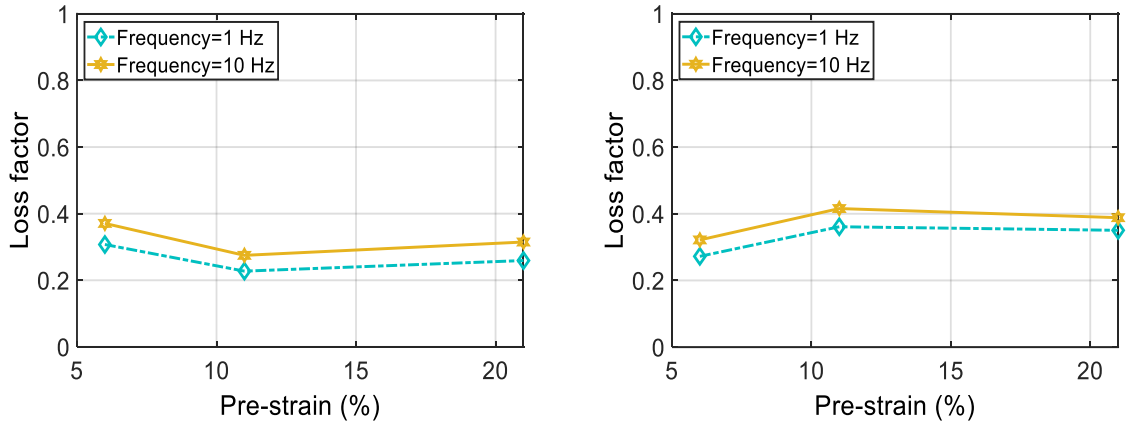

(c)

Figure B4 Effect of pre-strain on the compression mode elastic modulus (a), loss modulus (b), and loss factor (c) of the isotropic (left column) and anisotropic (right column) MREs with volume fraction of 30% under different excitation frequencies (ε_0=2.5%, and B=0 mT).

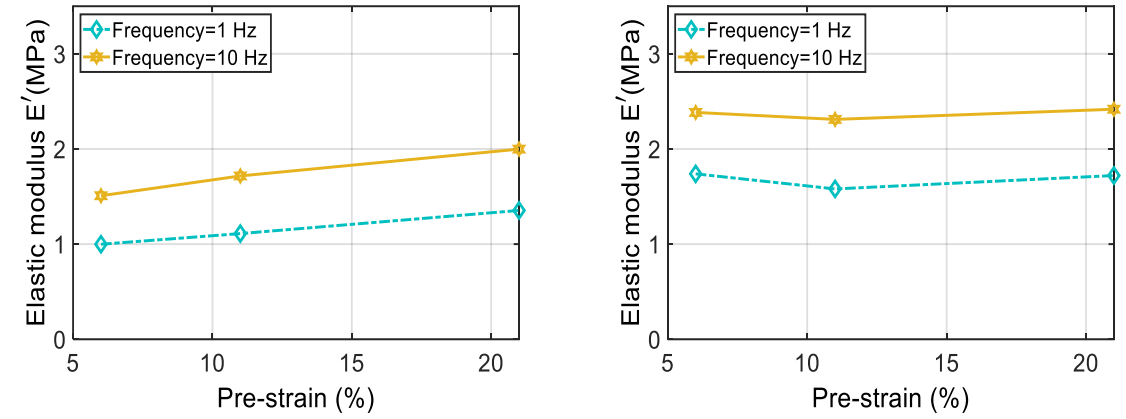

(a)

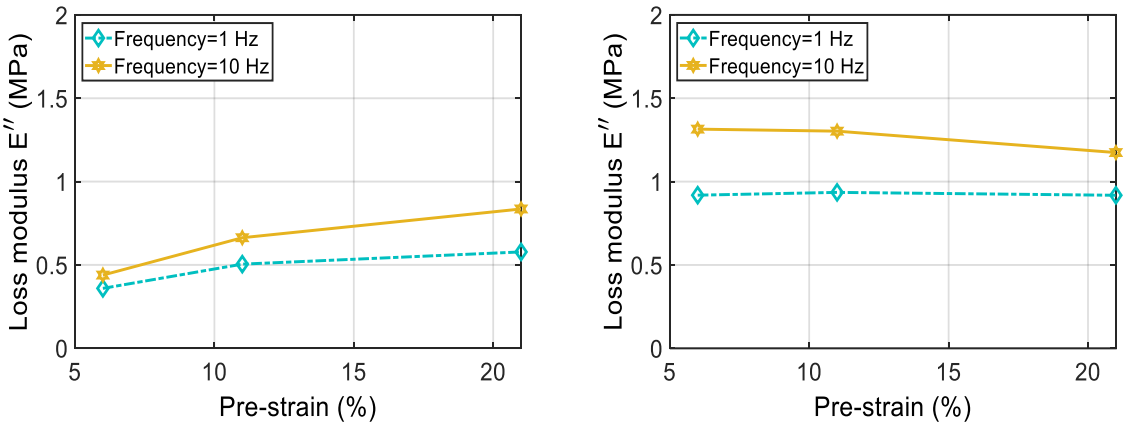

(b)

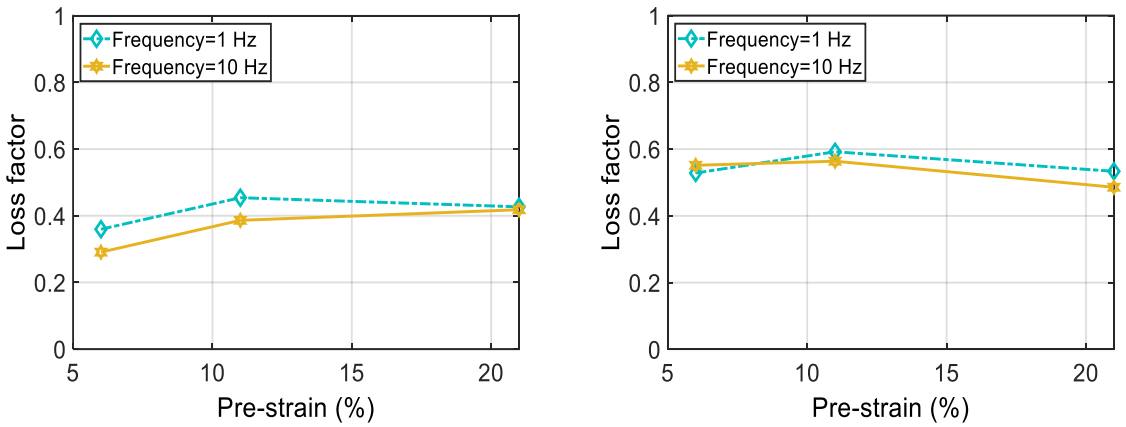

(c)

Figure B5 Effect of pre-strain on the compression mode elastic modulus (a), loss modulus (b), and loss factor (c) of the isotropic (left column) and anisotropic (right column) MREs with volume fraction of 30% under different excitation frequencies (ε_0=2.5%, and B=300 mT).

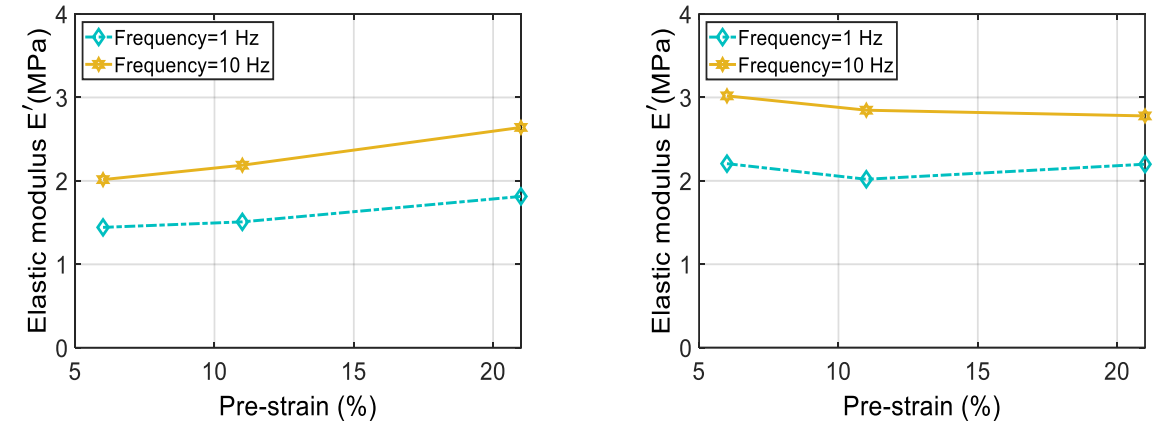

(a)

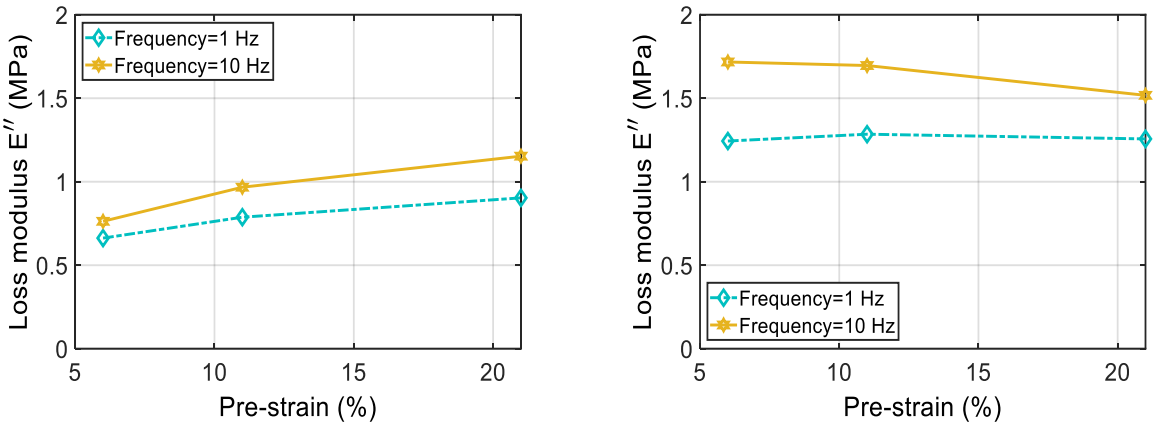

(b)

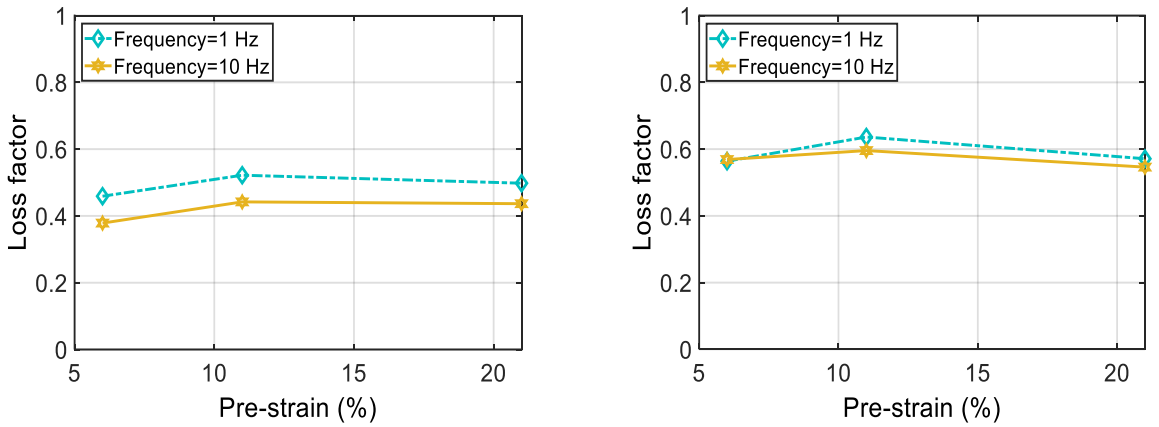

(c)

Figure B6 Effect of pre-strain on the compression mode elastic modulus (a), loss modulus (b), and loss factor (c) of the isotropic (left column) and anisotropic (right column) MREs with volume fraction of 30% under different excitation frequencies (ε_0=2.5%, and B=450 mT).

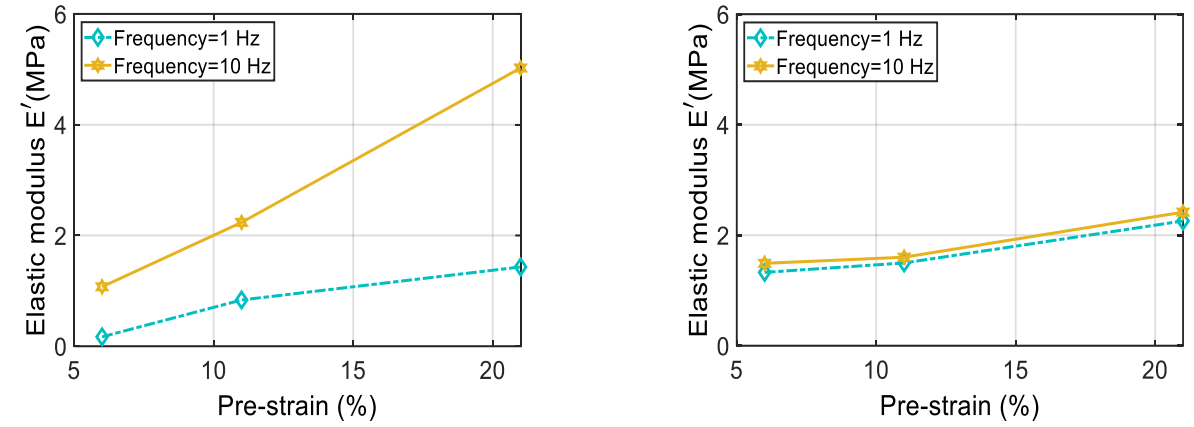

(a)

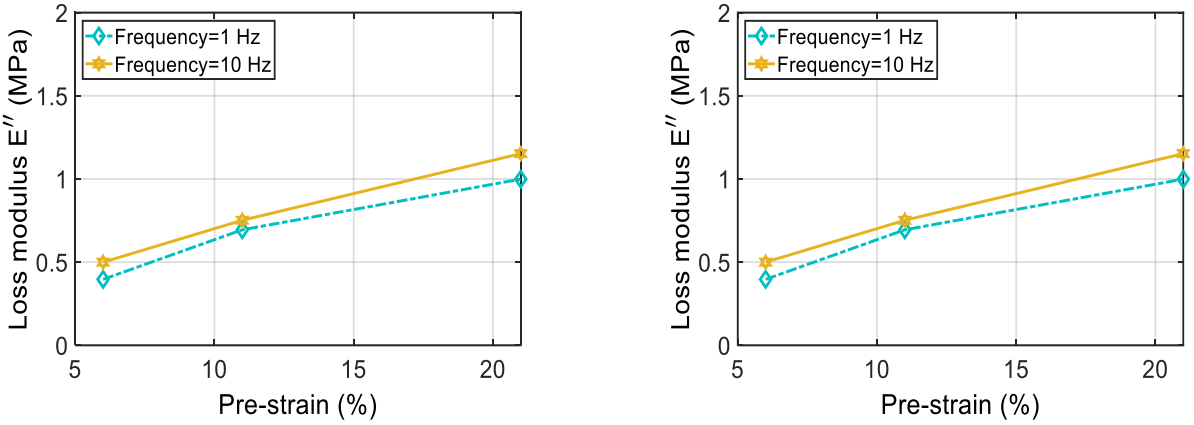

(b)

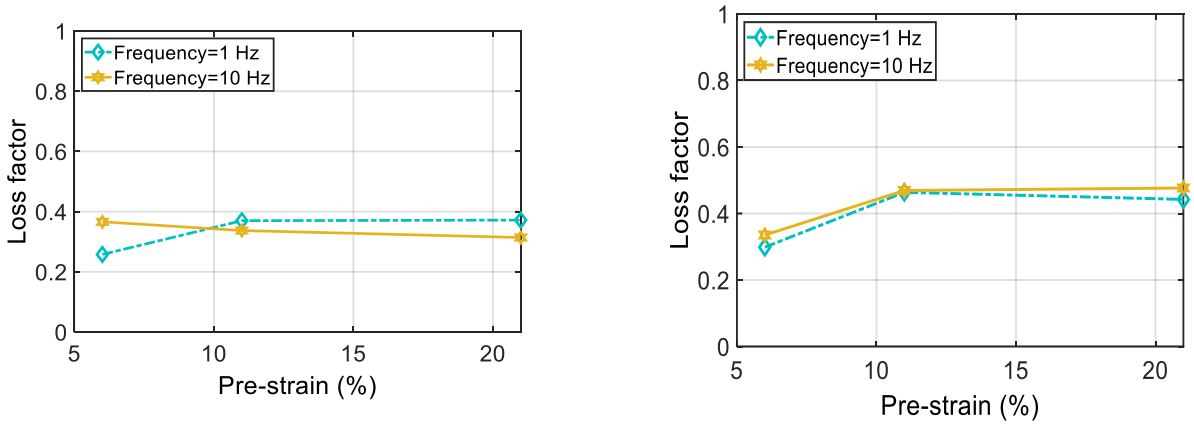

(c)

Figure B7 Effect of pre-strain on the compression mode elastic modulus (a), loss modulus (b), and loss factor (c) of the isotropic (left column) and anisotropic (right column) MREs with volume fraction of 45% under different excitation frequencies (ε_0=2.5%, and B=0 mT).

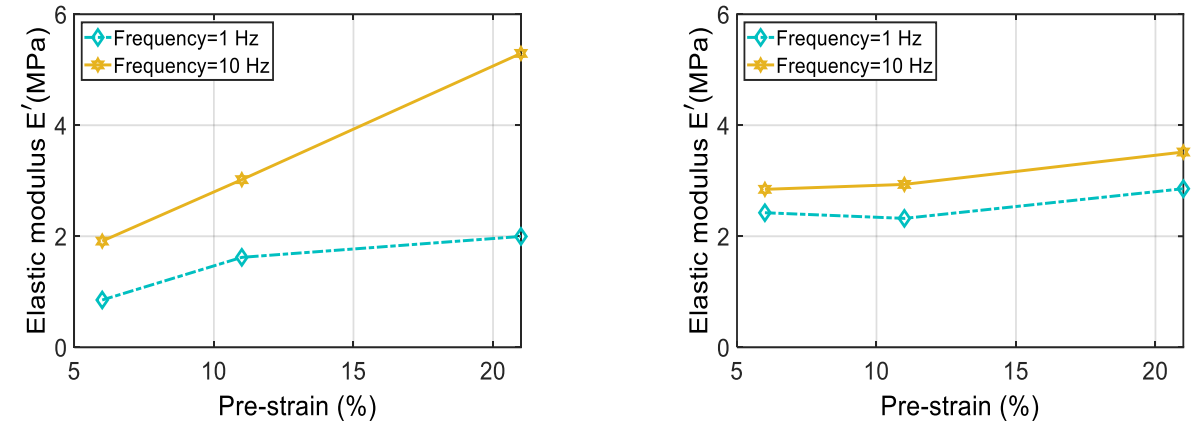

(a)

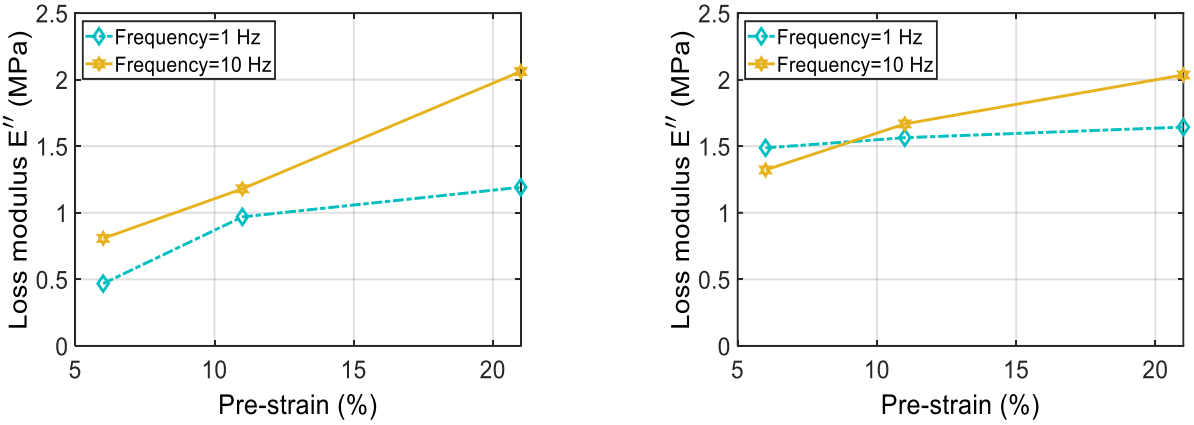

(b)

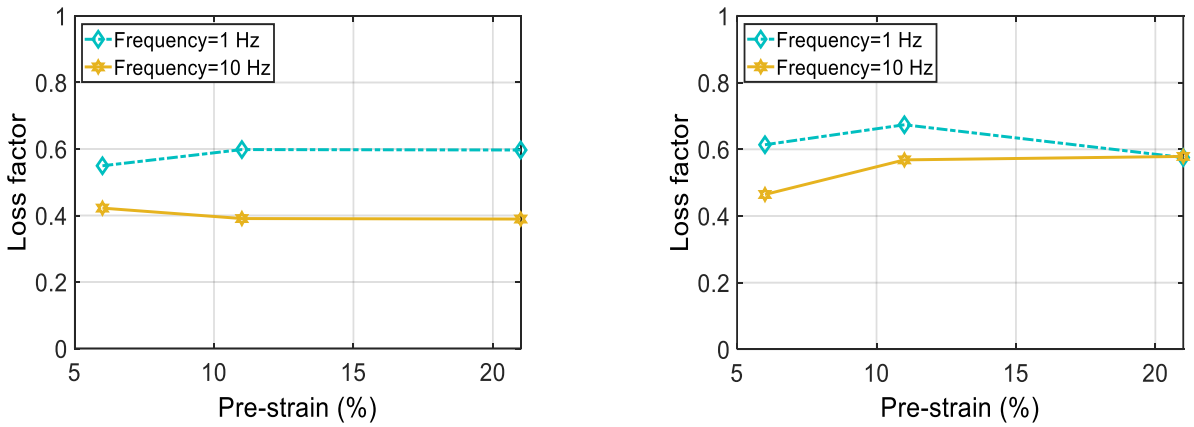

(c)

Figure B8 Effect of pre-strain on the compression mode elastic modulus (a), loss modulus (b), and loss factor (c) of the isotropic (left column) and anisotropic (right column) MREs with volume fraction of 45% under different excitation frequencies (ε_0=2.5%, and B=150 mT).

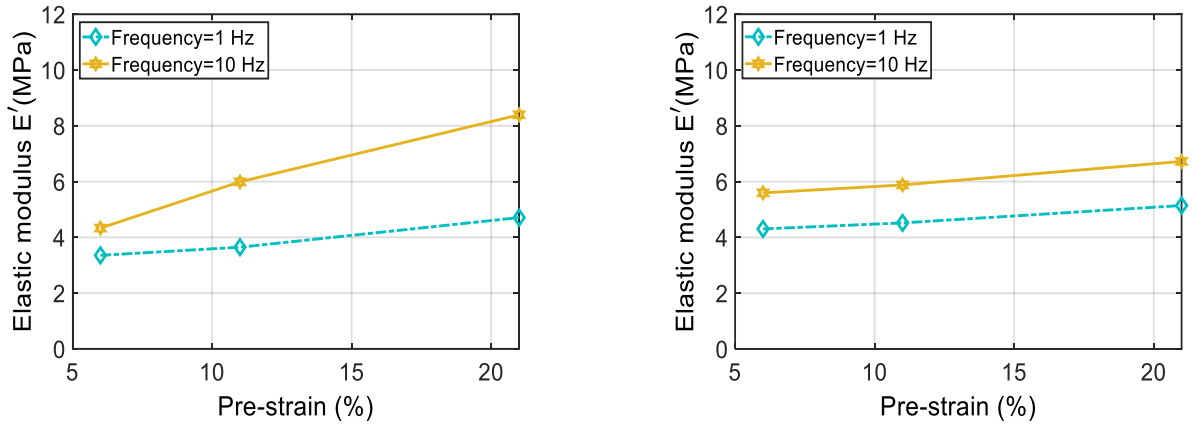

(a)

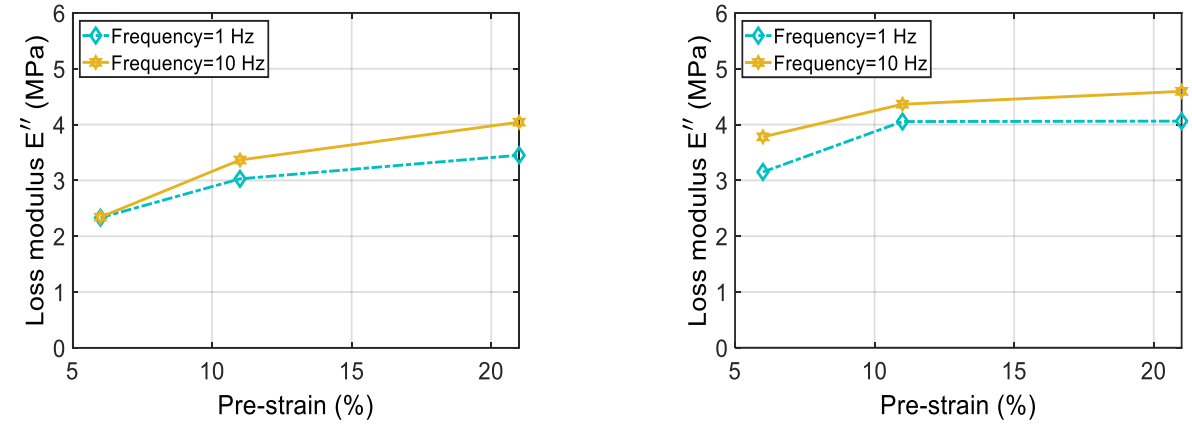

(b)

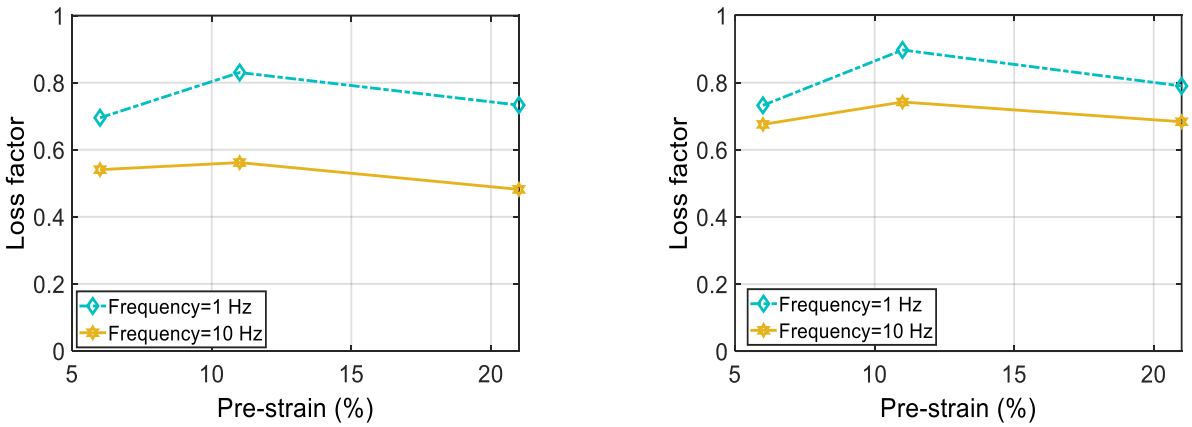

(c)

Figure B9 Effect of pre-strain on the compression mode elastic modulus (a), loss modulus (b), and loss factor (c) of the isotropic (left column) and anisotropic (right column) MREs with volume fraction of 45% under different excitation frequencies (ε_0=2.5%, and B=450 mT).

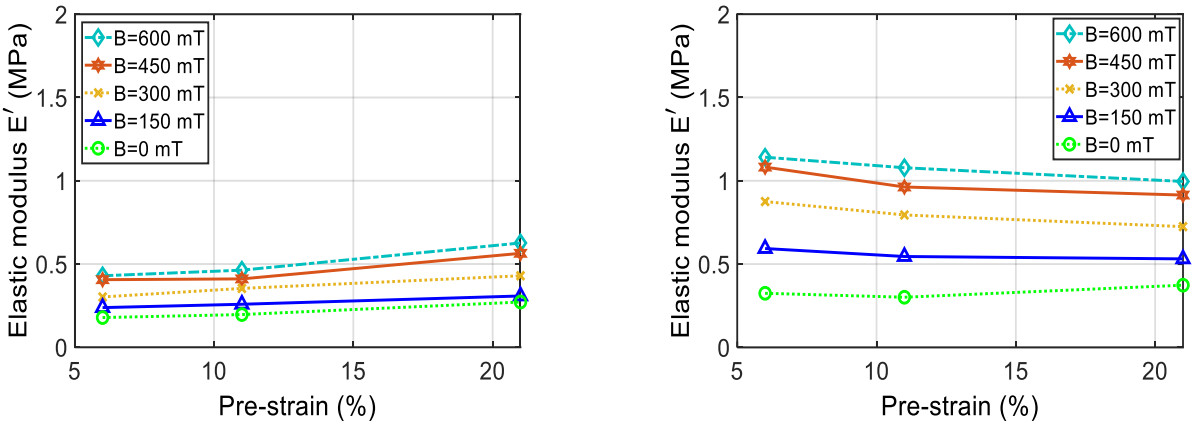

(a)

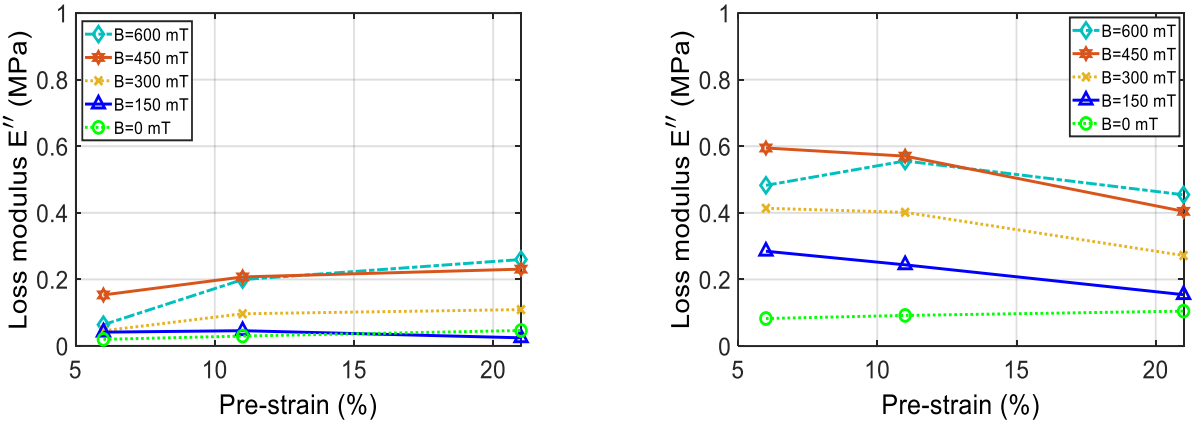

(b)

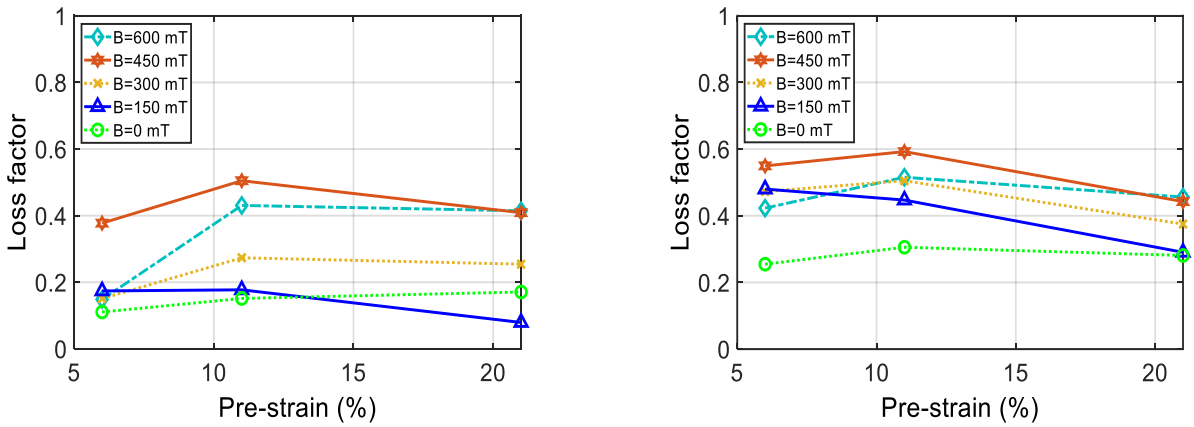

(c)

Figure B10 Effect of pre-strain on the compression mode elastic modulus (a), loss modulus (b), and loss factor (c) of isotropic (left column) and anisotropic (right column) MREs with volume fraction of 15% under different levels of magnetic flux density (ε_0=2.5%, f=1 Hz).

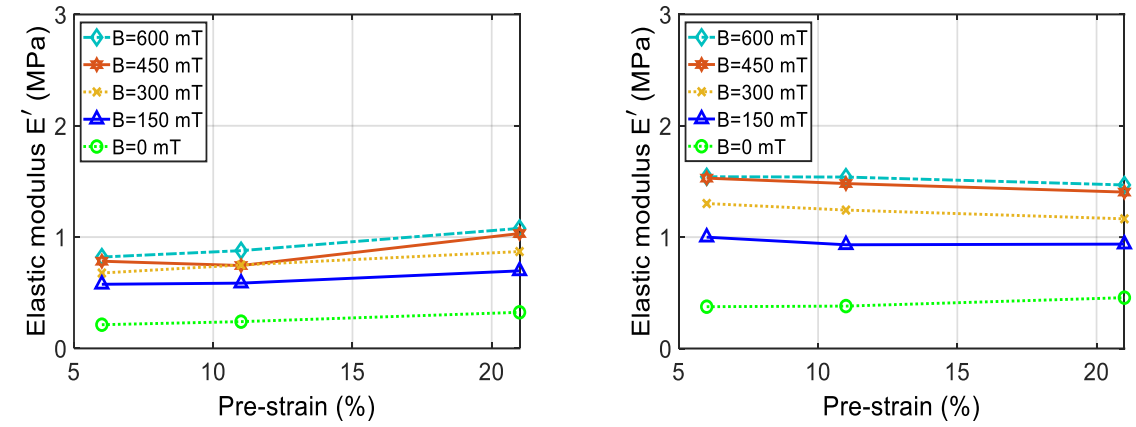

(a)

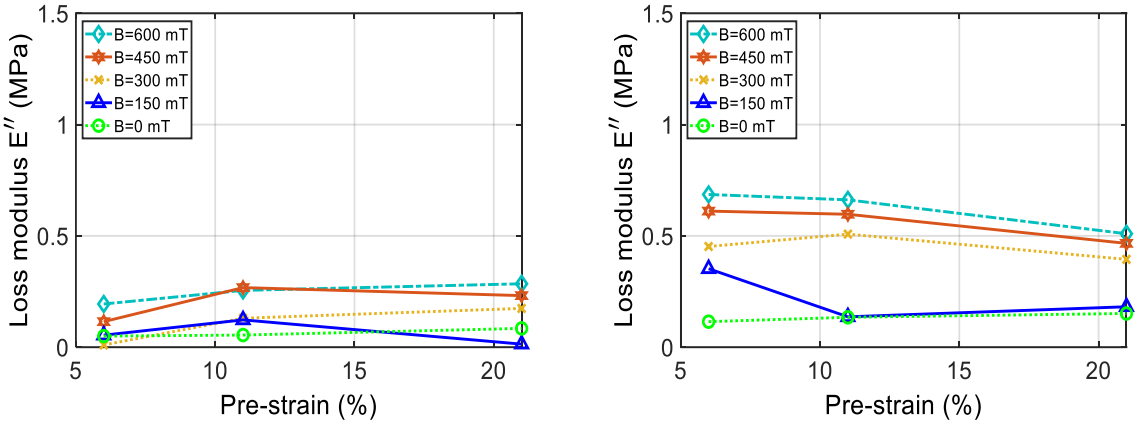

(b)

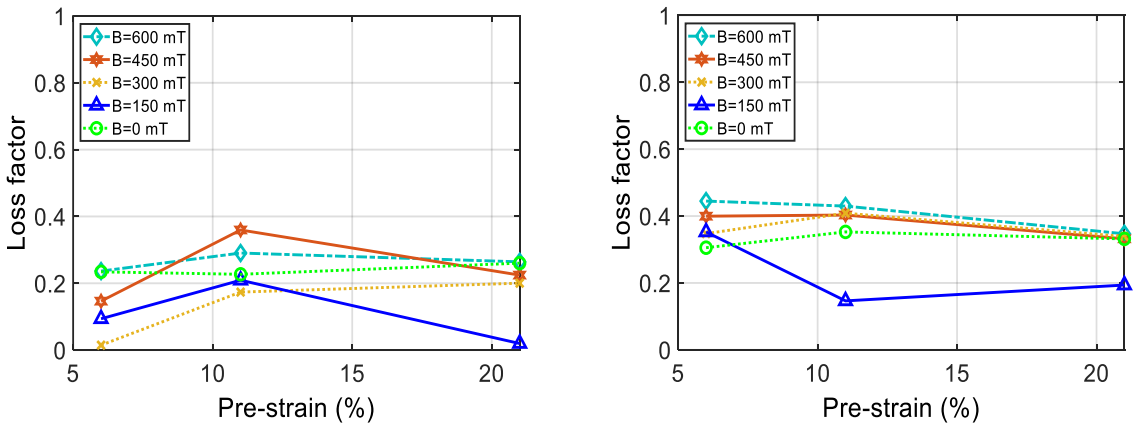

(c)

Figure B11 Effect of pre-strain on the compression mode elastic modulus (a), loss modulus (b), and loss factor (c) of isotropic (left column) and anisotropic (right column) MREs with volume fraction of 15% under different levels of magnetic flux density (ε_0=2.5%, f=10 Hz).

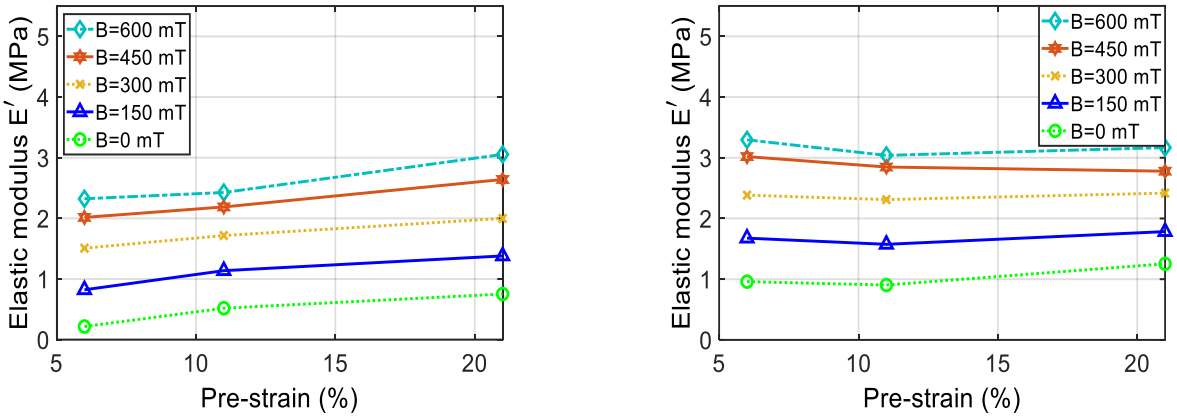

(a)

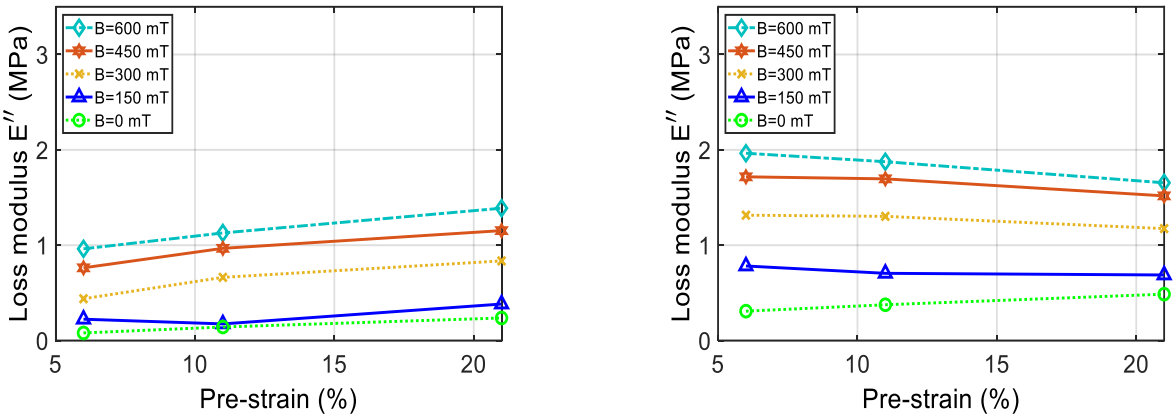

(b)

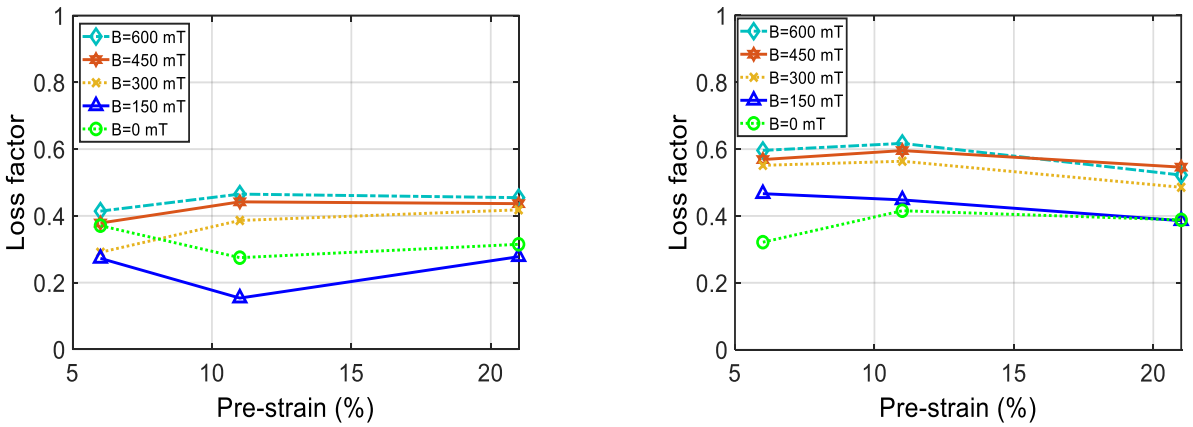

(c)

Figure B12. Effect of pre-strain on the compression mode elastic modulus (a), loss modulus (b), and loss factor (c) of isotropic (left column) and anisotropic (right column) MREs with volume fraction of 30% under different levels of magnetic flux density (ε_0=2.5%, f=10 Hz).

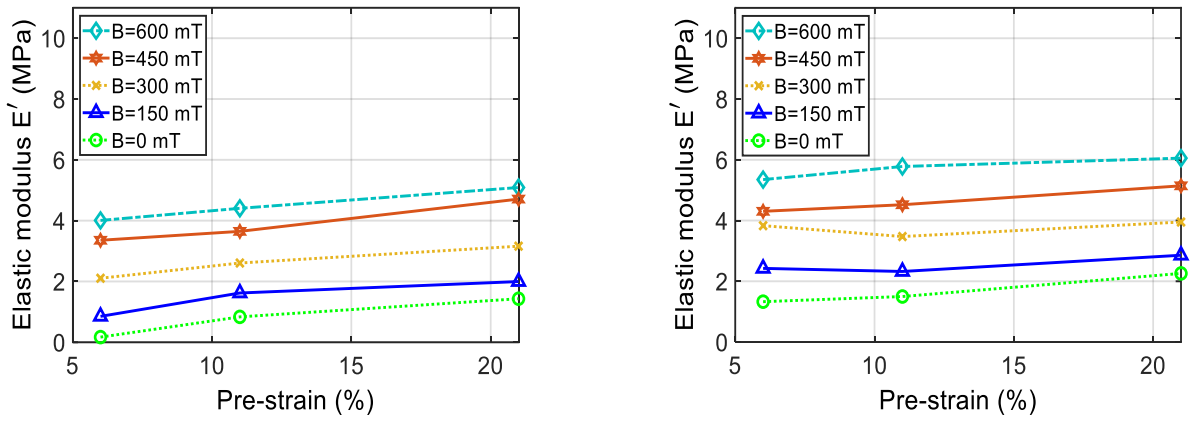

(a)

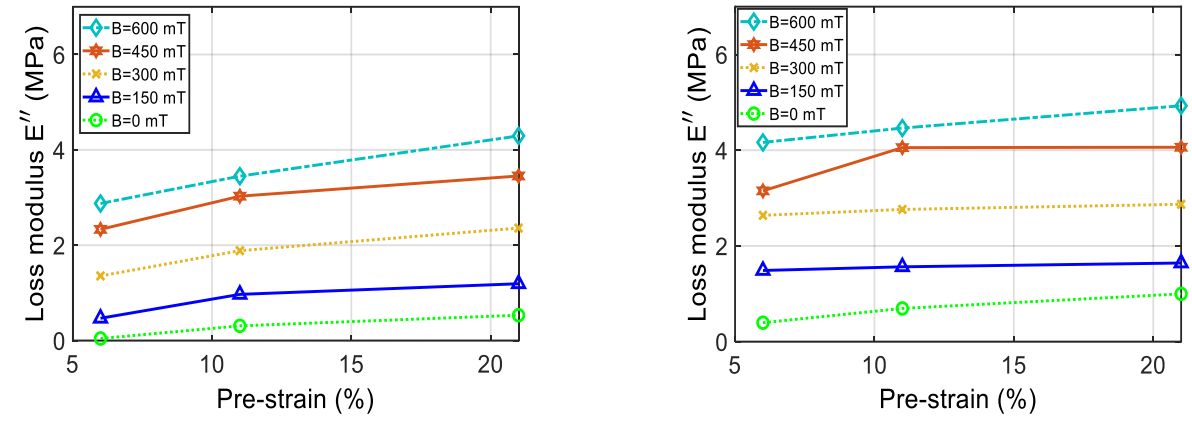

(b)

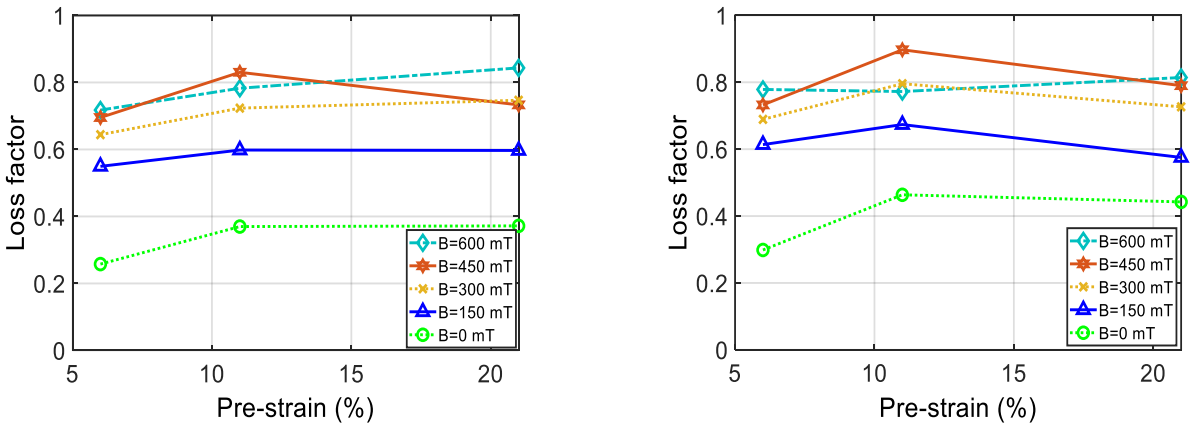

(c)

Figure B13 Effect of pre-strain on the compression mode elastic modulus (a), loss modulus (b), and loss factor (c) of isotropic (left column) and anisotropic (right column) MREs with volume fraction of 45% under different levels of magnetic flux density (ε_0=2.5%, f=1 Hz).

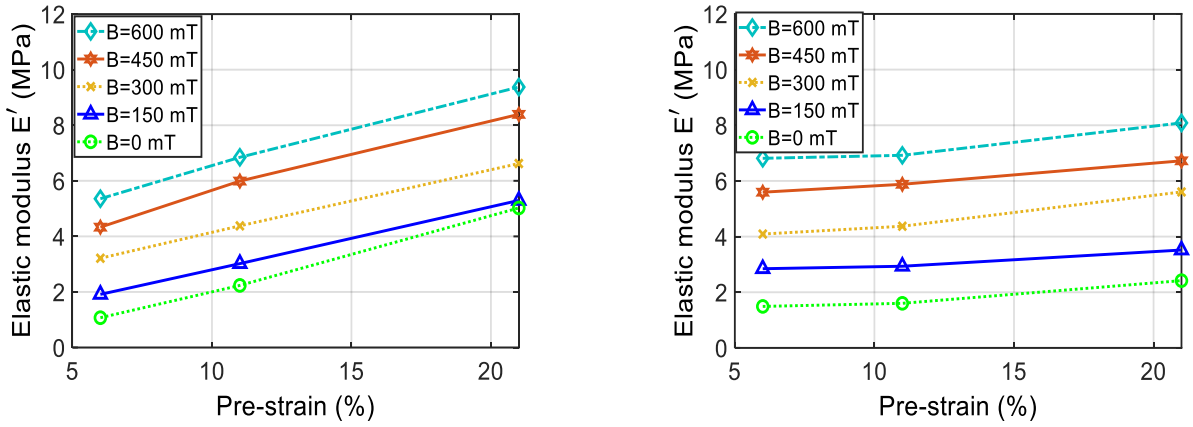

(a)

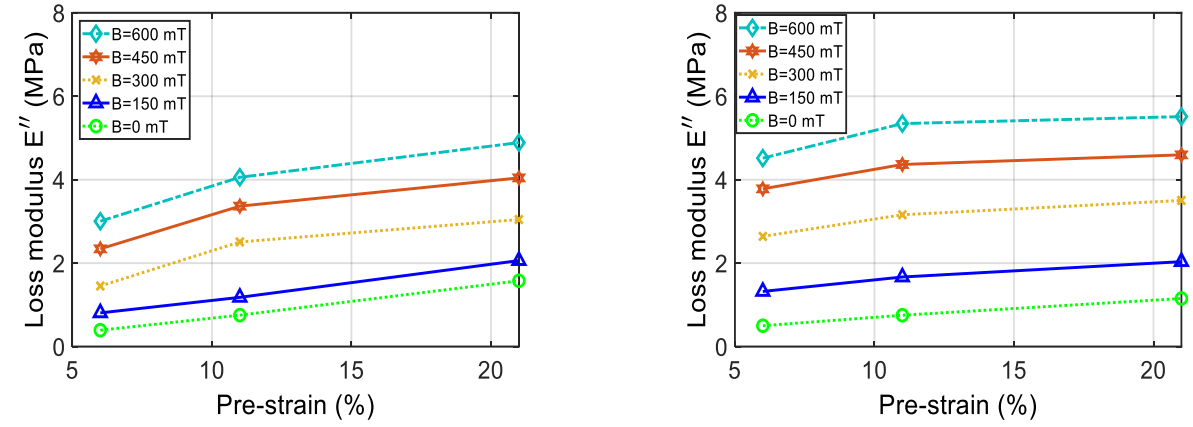

(b)

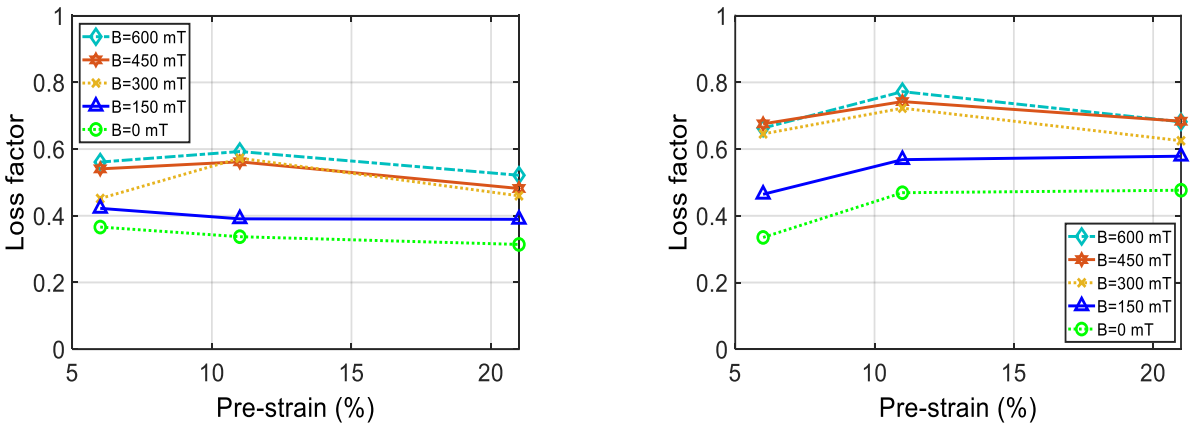

(c)

Figure B14 Effect of pre-strain on the compression mode elastic modulus (a), loss modulus (b), and loss factor (c) of isotropic (left column) and anisotropic (right column) MREs with volume fraction of 45% under different levels of magnetic flux density (ε_0=2.5%, f=10 Hz).

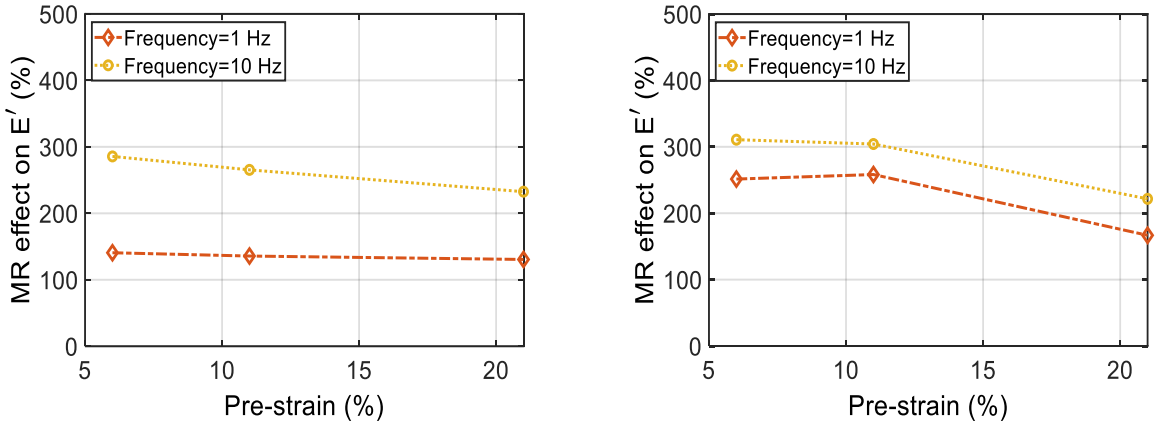

(a)

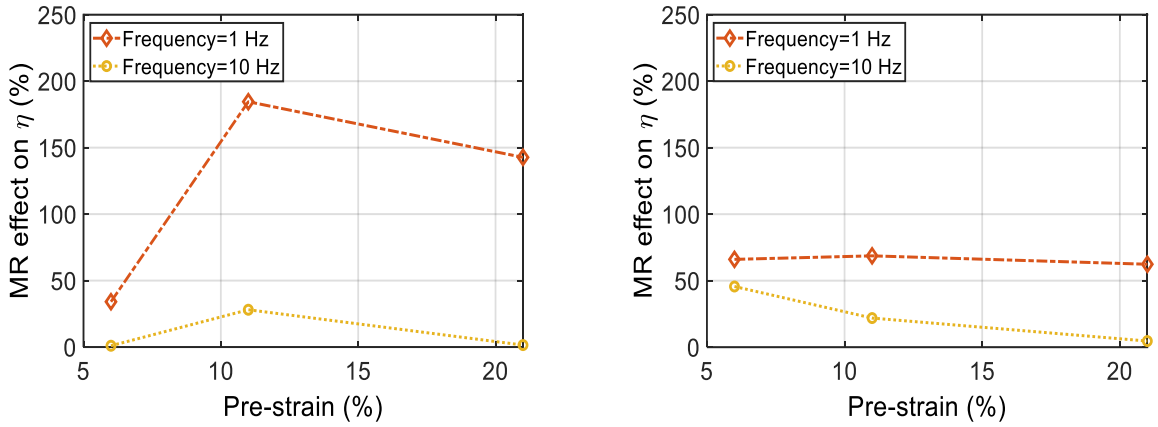

(b)

Figure B15 The effects of the pre-strain on the relative MR effect in view of elastic (a) and loss factor (b) of the isotropic (left column) and anisotropic (right column) MREs with 15% volume fraction under different excitation frequencies (ε_0=2.5%, and B= 600 mT).

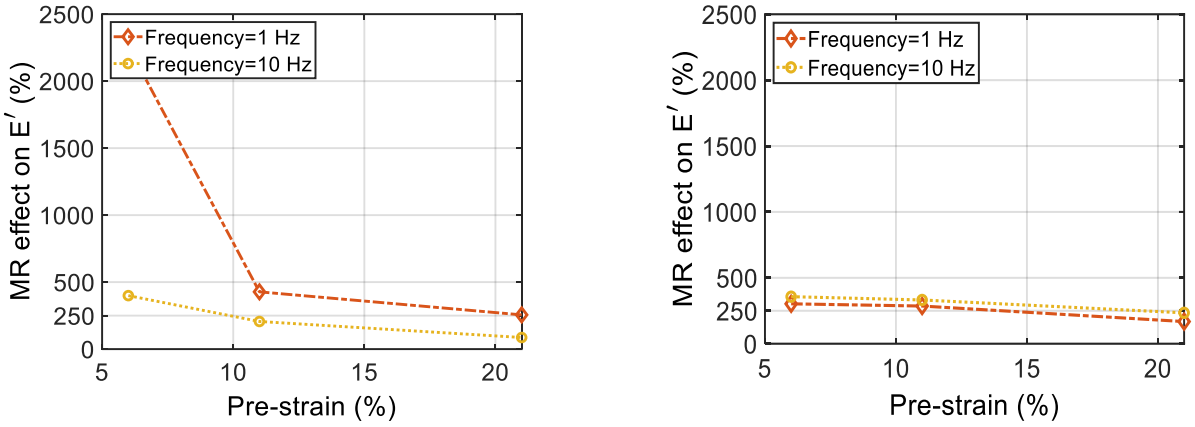

(a)

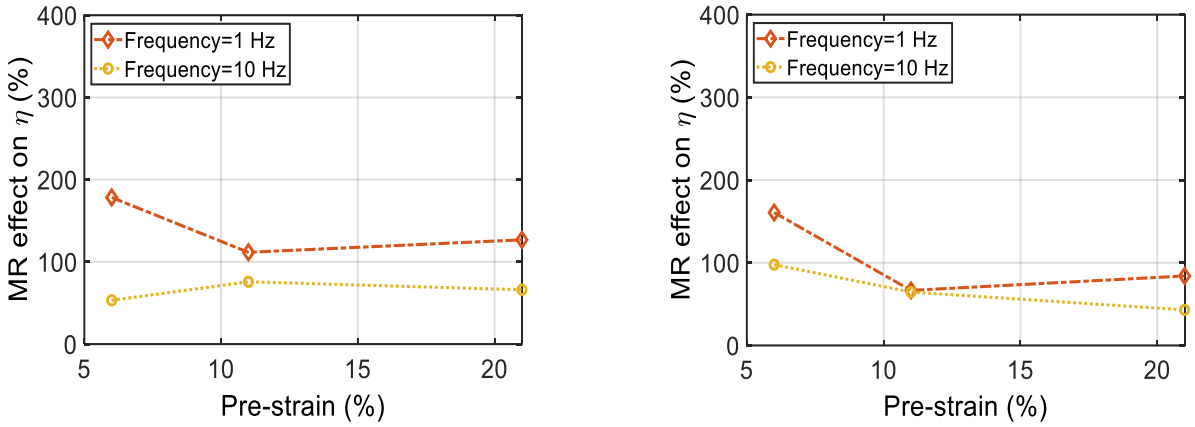

(b)

Figure B16 The effects of the pre-strain on the relative MR effect in view of elastic (a) and loss factor (b) of the isotropic (left column) and anisotropic (right column) MREs with 45% volume fraction under different excitation frequencies (ε_0=2.5%, and B= 600 mT).